In the IOCCG Report Series:

Reports and Monographs of the International Ocean-Colour Coordinating Group

An Affiliated Program of the Scientific Committee on Oceanic Research (SCOR)
An Associated Member of the (CEOS)

IOCCG Report Number 15, 2014

Phytoplankton Functional Types from Space

Edited by:
Shubha Sathyendranath (Plymouth Marine Laboratory)

Report of an IOCCG working group on Phytoplankton Functional Types, chaired by Shubha Sathyendranath and based on contributions from (in alphabetical order):

Jim Aiken, Séverine Alvain, Ray Barlow, Heather Bouman, Astrid Bracher, Robert J. W. Brewin, Annick Bricaud, Christopher W. Brown, Aurea M. Ciotti, Lesley Clementson, Susanne E. Craig, Emmanuel Devred, Nick Hardman-Mountford, Takafumi Hirata, Chuanmin Hu, Tihomir S. Kostadinov, Samantha Lavender, Hubert Loisel, Tim S. Moore, Jesus Morales, Cyril Moulin, Colleen B. Mouw, Anitha Nair, Dionysios Raitsos, Collin Roesler, Shubha Sathyendranath, Jamie D. Shutler, Heidi M. Sosik, Inia Soto, Venetia Stuart, Ajit Subramaniam and Julia Uitz.

Correct citation for this publication:

The International Ocean-Colour Coordinating Group (IOCCG) is an international group of experts in the field of satellite ocean colour, acting as a liaison and communication channel between users, managers and agencies in the ocean-colour arena.

The IOCCG is sponsored by Centre National d'Etudes Spatiales (CNES, France), Canadian Space Agency (CSA), Commonwealth Scientific and Industrial Research Organisation (CSIRO, Australia), Department of Fisheries and Oceans (Bedford Institute of Oceanography, Canada), European Space Agency (ESA), European Organisation for the Exploitation of Meteorological Satellites (EUMETSAT), Helmholtz Center Geesthacht (Germany), National Institute for Space Research (INPE, Brazil), Indian Space Research Organisation (ISRO), Japan Aerospace Exploration Agency (JAXA), Joint Research Centre (JRC, EC), Korea Institute of Ocean Science and Technology (KIOST), National Aeronautics and Space Administration (NASA, USA), National Centre for Earth Observation (NCEO, UK), National Oceanic and Atmospheric Administration (NOAA, USA), Scientific Committee on Oceanic Research (SCOR), and Second Institute of Oceanography (SIO), China.

http: //www.ioccg.org

Contents

<div style="border:1px solid #000; display:inline-block; padding:10px;">

Chapter 1

</div>

General Introduction

**Shubha Sathyendranath, Heidi M. Sosik, Jim Aiken, Séverine Alvain,
Ray Barlow, Lesley Clementson, Cyril Moulin, Nick Hardman-Mountford,
Takafumi Hirata, Jesus Morales, Anitha Nair, Colleen Mouw and
Venetia Stuart**

1.1 Background

Satellite-based remote sensing of ocean colour provides unique observational capability to biological oceanographers and other Earth observation scientists interested in processes that involve phytoplankton. No other observational strategy can provide synoptic views of upper ocean optical properties with such high spatial and temporal resolution (~1 km or better, daily or better) as well as high spatial and temporal extent (global scales, for years to decades).

Since the proof-of-concept Coastal Zone Color Scanner (CZCS) mission, the principal focus of ocean-colour research has been on retrieval of information about the content of chlorophyll-a, the major phytoplankton pigment in the upper ocean (e.g., Gordon et al., 1983). Whereas this focus continues to the present (Morel and Antoine 2000; O'Reilly et al., 1998; 2000) with chlorophyll concentration being by far the most utilised product from ocean-colour satellites, an evolving interest in retrieving other properties, including information on the composition of the phytoplankton community, has emerged in recent years. Note that the community may be described on the basis of their size structure, their taxonomic composition, or their functions.

This interest has paralleled the incorporation of the concept of phytoplankton functional types (PFTs) into studies of a range of ecological and biogeochemical problems, especially into modelling studies (Le Quéré et al., 2005; Hood et al., 2006). In this concept, each PFT represents a group of species aggregated according to distinct functional characteristics. Such approaches are receiving increasing attention because of the realization that capturing the role of phytoplankton in the global cycles of major and minor elements in the ocean (e.g., carbon, nitrogen, sulphur, iron) requires improved representation of their complex functionalities. The concurrent emergence of more complex property retrievals from ocean-colour data and of PFT-resolving conceptual and numerical models motivates this report.

Therefore, we have the following goals:

- ❖ to provide an overview of PFT concepts;
- ❖ to review current approaches for PFT retrieval from space;
- ❖ to present prospects for the future, including likely limitations; and
- ❖ to provide recommendations regarding mission characteristics, development of algorithms and validation studies.

In this chapter, we describe relevant terms and concepts, examine the relevance of the topic, discuss the contributions from remote sensing to the problem and highlight the need for complementary approaches to obtain the full picture.

1.2   What Do We Mean by a Functional Type?

The emerging use of the term "functional types" in biogeochemical models represents only a particular use of the term, which focuses specifically on the characteristic roles of organisms in biologically-mediated biogeochemical transformations. In a more general ecological context, a functional type or group represents an aggregation of organisms according to some well-defined property that sets a role or "function" for them in a system. This definition clearly lacks specificity, so there is no unique or universal interpretation (Reynolds et al. 2002): the choice of functions for consideration will depend on the question or problem of interest. For instance, in Nitrogen-Phytoplankton-Zooplankton (NPZ) models, P and Z can be taken to represent functional types, i.e., producers and consumers. This aggregation is acceptable for some applications, but may be too coarse or even inappropriate for others. Reynolds et al. (2002) propose that species in a functional group share "specialist adaptations and requirements" that differentiate them from other species. Which adaptations receive our attention would depend on the habitat or conditions under consideration, and on the particular problem being investigated.

These views echo earlier contributions in ecological studies, such as the definition of niches (Hutchinson, 1957) and the classic work of Root (1967) on ecological guilds. Root (1967) defined a guild as "a group of species that exploit the same class of environmental resources in a similar way", which is conceptually similar to the modern use of functional types. Various terms related to the concept of functional types are summarized in Box 1.1.

In keeping with these ideas and in the context of the global biogeochemical models mentioned above, a PFT or a phytoplankton biogeochemical class is often defined as a group of organisms (irrespective of taxonomic affiliation) that carry out a particular chemical process such as calcification, silicification, nitrogen fixation, or dimethyl sulfide production; these are also sometimes referred to as "biogeochemical guilds". Box 1.2 shows some important phytoplankton functional types from a biogeochemical perspective. Note that other functions may be used to describe the roles of non-phytoplankton groups, for example, denitrification and remineralization

(e.g., Hood et al., 2006).

Box 1.1: Functional Types and Related Terms

Functional Type:
The term emerges primarily from biogeochemical studies. A functional type is defined as a group of organisms that share common biogeochemical functions, but do not necessarily share a common phylogeny.

A Guild:
This term refers to a group of organisms that exploit a given environmental resource in a similar fashion (Root, 1967). The term, initially used in ecological studies dealing with competition, has in more recent years been used in the context of phytoplankton functions and ocean biogeochemistry (Hood et al., 2006).

A Trait:
A trait is a well-defined, measurable property of organisms, usually measured at the individual level, and used comparatively across species (McGill et al., 2006). Thus, a trait can be used to identify a functional type.

Functional Diversity:
This term represents responses of organisms to environmental change, at different time and space scales. The response may be to each other, or to the environment (Steele, 1991).

Ecological Niche:
According to Odum (1959), "The ecological niche of an organism depends not only on where it lives but also on what it does. By analogy, it may be said that the habitat is the organism's "address", and the niche is its "profession", biologically speaking." Hutchinson (1957) defined a niche as a region (n-dimensional hyper volume) in a multi-dimensional space of environmental factors that affect the welfare of a species. Note that Odum's definition of a niche emphasizes the organism's function, whereas the definition of Hutchinson emphasizes the habitats that a particular organism would tend to occupy.

Box 1.2:   Some Important Phytoplankton Functional Types

Nitrogen Fixers:

All phytoplankton require nitrogen for growth. Typically, phytoplankton are equipped to take up nitrogen in the form of nitrate, nitrite or ammonia. In the illuminated upper layer of the sea, these forms are often present at growth-limiting concentrations. A subset of phytoplankton, known as diazotrophs or nitrogen fixers, can overcome this limitation because they are able to utilize ("fix") nitrogen gas dissolved in seawater. They belong to the class of cyanobacteria or blue-green algae, and the most notable of these in open-ocean waters is the bloom-forming *Trichodesmium*.   However other cyanobacteria, either independently, or in symbiotic relationships with other types of phytoplankton, are also known to contribute to nitrogen fixation at sea (see brief review in Nair et al., 2008). When nitrogen fixation is high, the oceanic primary production may change from nitrogen-limited to phosphorus-limited, thus affecting the phosphorus cycle as well.
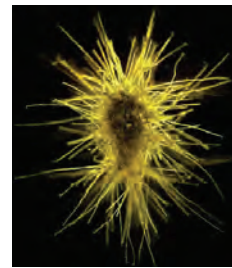
Trichodesmium colony ∼2 mm in diameter (Photo by Abby Heithoff ©WHOI, USA).

Calcifiers:

Calcifying phytoplankton produce calcium carbonate shells or coccoliths and are collectively referred to as coccolithophores. They belong to the class Prymnesiophyceae (Division Haptophyta, but note that not all Haptophytes are calcifiers). The chemical process involved in the formation of coccoliths ($Ca + 2HCO_3 \longrightarrow CaCO_3 + H_2O + CO_2$) removes dissolved bi-carbonate ion from the seawater, but increases dissolved CO_2 and thus decreases alkalinity. Globally, marine organisms (coccolithophores, foraminifera and other calcifiers) are estimated to produce between 0.6 and 1.2 GT calcite carbon per year. Some species (e.g., *Emiliania huxleyi*) can produce dense suspensions of coccoliths, that markedly change the reflectivity of the water, causing an impact on the underwater light regime and heat budget. See the *Emiliania huxleyi* webpage (www.soes.soton.ac.uk/staff/tt/) for details about the various properties and functions of coccolithophores.
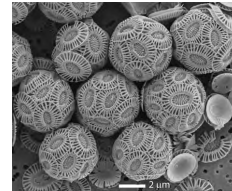
Emiliania huxleyi cells. Credit: Jeremy R. Young, University College London.

Silicifiers:

A class of phytoplankton (Bacillariophyceae), commonly known as diatoms, have silica frustules that surround and protect the cells. Their requirement for silica sets them apart from other phytoplankton. Diatoms are typically large-celled and this, combined with the presence of the silica frustules, makes them slightly negatively buoyant. They therefore tend to sink rapidly out of the surface layer of the ocean contributing to the transport of carbon, nitrogen and silica to deeper waters. Though diatoms are the major silicifiers in the ocean, some phytoplankton belonging to chrysophytes, silicoflagellates, and xanthophytes are also known to be silicifiers (Brownlee and Taylor, 2002).
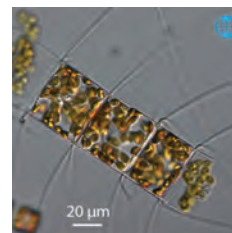
Diatom Chaetoceros teres (from planktonnet.awi.de, image author Alexandra).

Box 1.2 Continued

Size Classes:

Phytoplankton represent a continuum of sizes from ∼0.6 μm to species generating aggregates greater than 200 μm. This continuum of sizes has been broken down into broad size classes: pico- (0.2 - 2 μm), nano- (2 - 20 μm) and microphytoplankton (20 - 200 μm) (Sieburth et al., 1978). (Note: some authors use the term nanoplankton for the 5 to 20 μm size range and ultraphytoplankton for the 2 to 5 μm size range). These broad size classes occupy different physical and chemical niches based on their nutrient-uptake ability, light-harvesting efficiency, and sinking rate through the euphotic zone.

DMSP producers:

Many phytoplankton produce dimethyl sulfoniopropionate (DMSP), a precursor to dimethyl sulphide (DMS), which is a volatile organic compound. Various processes related to cell decay and grazing are implicated in the transformation of DMSP within the cell to DMS in the water. Some DMS escapes into the atmosphere and is responsible for the characteristic smell one often associates with seawater. Some phytoplankton belonging to the classes dinophyceae, haptophyceae (including coccolithophores), chrysophyceae, pelagophyceae and prasinophyceae are known to be DMS producers, with the intracellular concentration of the precursor DMSP reportedly highest in dinoflagellates and haptophytes (Sunda et al., 2002).

Neoceratium pentagonum (from `planktonnet.awi.de`*, image author Fatima Santos).*

For applications other than global biogeochemistry, different approaches to identifying functional types may be more appropriate. Various attempts have been made historically to characterize the structure of phytoplankton communities in the ocean (Margalef, 1967; Raymond, 1980; Smayda, 1980). The number of organisms, the relative abundance of species, their biological traits and functional roles have been used to describe phytoplankton community structure (Reynolds, 2006).

If we consider modification of the under-water light field as a phytoplankton function, then the relevant traits are the specific absorption and scattering properties of phytoplankton, and phytoplankton may be classified according to their optical characteristics. In fact, it has been recognised that optical properties of the upper ocean are affected by phytoplankton cell size (Yentsch and Phinney, 1989) because of the role particle size exerts on light scattering and absorption (e.g., Morel and Bricaud 1981; Stramski and Mobley, 1997; Ciotti et al., 1999; Loisel et al. 2006; Devred et al. 2006). Cell size has also been considered an important trait of plankton from ecological and biogeochemical perspectives (Sieburth et al., 1978) and ecological models have been developed to represent function according to cell size (Moloney and Field, 1991; Armstrong, 1999; Lima et al., 2002; Lima and Doney, 2004; Moore et al., 2004; Irwin et al., 2006). Even models that rely principally on biogeochemical roles as the basis for defining PFTs typically also have more generic size-based PFTs such as "picophytoplankton" (e.g., Lima and Doney, 2004; Le Quéré et al., 2005; Veldhuis and De Baar, 2005). From a purely ecological perspective, Reynolds et al.

(2002) emphasize characteristics such as nutrient-uptake affinity, light-harvesting efficiency, and motility as important for delineating functional groups of freshwater phytoplankton. Interestingly, some aspects of these characteristics can also be linked to cell size. Table 1.1 (from Nair et al. 2008) shows how traits of various functional types are related to their size.

Trait	Pico-autotrophs	Nitrogen-fixers	Calcifiers	Silicifiers	DMS-producers
Cell size (μm)	0.7-2.0	Variable	5-10	20-200	5
Light	High	High	Low	Low	High-Low
Nutrient required		N_2 gas	Calcium	Silica	
Iron	Low	High	High	High	High
Loss	Grazing	Viral lysis	Sinking	Sinking	Lysis, grazing
Bio-optical properties	High a_B^*	a_B^* high in UV, High b_{bB}^*	High b_{bB}^*	Low, flat a_B^*	?
Remote sensing	Yes	Yes	Yes	Yes	No

Table 1.1   Summary of the properties and requirements for growth (optical conditions and nutrient requirements) of different phytoplankton functional groups. Adapted from Nair et al. (2008), where a_B^* and b_{bB}^* represent the specific absorption and backscattering coefficients of phytoplankton, respectively. Nominal size ranges for different functional types are taken from Le Quéré et al. (2005).

It is not always straightforward to relate functionality with taxonomic affiliation. On the one hand, plankton belonging to various classes, over a wide range of cell sizes and pigment composition, may share a common function, such as production of DMSP. On the other hand, a single species may belong to more than one functional type. For example, the species *Emiliania huxleyi* may be classified as both a DMSP producer and a calcifier.

Functional groups, although often defined in ecological terms as a group of organisms that participate in similar biochemical processes (e.g., silicification or calcification), have been more traditionally defined as a group of organisms exhibiting similar physiological responses (light and nutrient utilization, for example) to the environment in which they exist. Margalef (1978) first introduced the concept of phytoplankton survival and seasonal succession being regulated by the physical forces experienced in temperate regions. In recent years, Margalef's framework has been refined (Cullen et al., 2002) to reflect new knowledge about the open ocean and picoplankton species such as *Prochlorococcus* spp., now widely accepted as the most abundant phytoplankton in oligotrophic waters (Chisholm et al., 1988), and about processes such as iron limitation in certain environments (Figure 1.1).

As noted above, the use of the PFT concept varies according to the scientific questions being considered and the observational capabilities available or required to address them. The range of approaches spans from categories related to phys-

Event-Scale Forcing —>
<— Succession

Low Turbulence and High Nutrients

LARGER CELLS
HIGHER BIOMASS
SLOWER TURNOVER
SELECTIVE PRESSURE
TO SEQUESTER NUTRIENTS
AND MINIMIZE LOSSES
(e.g., NOXIOUS/TOXIC BLOOMS)

Turbulence —>

Nutrients —>

Low Turbulence and Low Nutrients

High Turbulence and High Nutrients

SMALLER CELLS
HIGH TURNOVER
COMPETITION FOR NUTRIENTS
RETENTION BY RECYCLING
(MICROBIAL LOOP)

LARGER CELLS
HIGHER BIOMASS
TRANSIENT & SELF-LIMITING
SELECTION FOR
RAPID GROWTH
(DIATOMS)

LOW BIOMASS
SLOW TURNOVER
ADAPTATIONS FOR
EFFICIENT USE OF
LIGHT&NUTRIENTS
(HIGH-LATITUDE
"HNLC")

Turbulence —>

Nutrients —>

High Turbulence and Low Nutrients

Potential for Production and Export —>

Figure 1.1 Conceptual continuum of physical and chemical forces on phytoplankton distribution. Reproduced from Cullen et al. (2002), after the conceptual framework of Margalef (1978).

iological adaptations for dealing with environmental factors of relevance to all phytoplankton (e.g., light, nutrients, turbulence) to practical categories that can be quantified with a particular analytical technique (e.g., pigment types), to specialized adaptations relevant to narrowly defined phenomena (e.g., toxin-producing blooms). Thus, when adopting the concept of phytoplankton functional types, it is important to choose functional types that are clearly defined and selected to suit the problem at hand.

1.3 Distribution of Some Common Phytoplankton Groups

The pelagic environment, whether in coastal or open-ocean waters, is rarely comprised of a single algal class. Different algal groups adapt to environmental conditions such as high or low light, nutrient availability, temperature, and turbulence level (Aiken et al., 2008). For example, small-celled phytoplankton such as *Prochloro-*

coccus spp. (< 1 μm) are adapted to the high-light, oligotrophic, warm waters of the tropical and subtropical regions of the world's oceans, and are often most abundant in the deeper layers (100 – 200 m) of the water column, and generally are not found north or south of 40° latitude (Partensky et al., 1999; Post, 2006). *Prochlorococcus* is the only phytoplankton that has the divinyl derivatives of chlorophylls-a and -b, allowing for a greater capacity to utilize the blue light available deep in the euphotic zone (e.g., Sathyendranath and Platt, 2007). Studies have shown that the abundance of *Prochlorococcus* has been found to be negatively correlated with nutrient availability, suggesting that *Prochlorococcus* is unable to utilize NO_3^- in the same way as other phytoplankton (Moore et al., 1995; Cavender-Bares et al., 2001; McCarthy, 2002), perhaps explaining, at least partially, their geographic distribution being restricted to warmer waters. *Prochlorococcus* generally coexists with the picoplankton *Synechococcus* (1 – 2 μm), although the two occupy different niches within the water column (Zwirglmaier et al., 2007; 2008), often with *Synechococcus* occupying the surface and upper waters of the euphotic zone and *Prochlorococcus* the deeper waters (Partensky et al., 1999; Agustí, 2004).

In contrast to *Prochlorococcus*, large-celled diatoms, as an algal class, are found throughout the world's oceans and, due to their physiological traits, generally dominate in well mixed, high-nutrient waters such as found in the coastal regions off Peru and California (Bruland et al., 2001; 2005). Many species of diatoms, when in a nutrient-replete environment, continue to take up macronutrients (NO_3^-, PO_4^{3-}, and/or SiO_4) and some micronutrients (e.g., biologically-available Fe) beyond what is needed for immediate growth, often prolonging growth or blooms beyond the time when the euphotic zone is depleted of nutrients. This so-called "luxury uptake" strategy (Goldman et al., 1979), combined with high intrinsic growth rates, makes diatoms effective competitors in environments with episodic injection of nutrients. If the water column becomes more stable and stratifies, then the diatoms, once they have depleted their nutrient resources, will sink through the water column to the seabed.

Under stable conditions, common during the months of late spring and summer, the autotrophic flagellated phytoplankton (mainly dinoflagellates) tend to thrive. Dinoflagellates are motile algae and, in low energy environments, are able to regulate their position in the water column, occupying well-lit layers during the day to photosynthesize, and then descending at night to deeper waters to access higher nutrient concentrations (Eppley et al., 1968; Cullen, 1985; Lieberman et al., 1994; Smayda, 1997). While the water column remains stable, the dinoflagellates can out-compete other non-motile species by virtue of this migratory behaviour and sometimes form a near-monospecific phytoplankton community, sometimes resulting in harmful algal blooms or red tides.

Diazotrophic phytoplankton in the marine environment all belong to the cyanobacterial algal group, of which the most well-known and researched species is *Trichodesmium*. These phytoplankton thrive in the warm, high-light and nutrient-poor

conditions of oligotrophic waters in the tropical and subtropical regions of the world's oceans, often outcompeting other species by fixing nitrogen from the atmosphere. *Trichodesmium* can be found as individual filaments or in colonies, and under conditions of low wind stress and water-column stability, the colonies can form surface slicks covering many kilometres visible in ocean-colour images (Dupouy et al., 1988; 2000). The density of these surface slicks can modify light penetration to the euphotic zone. Gas vesicles within the *Trichodesmium* cells allow regulation of buoyancy such that the colonies can use vertical migration to maintain themselves in an optimum light field, often in a thin surface layer. *Trichodesmium* is not alone in contributing to nitrogen fixation, and recent work has emphasized the importance of unicellular cyanobacteria (Zehr et al., 2001; Moisander et al., 2010).

More recently, some diazotrophic cyanobacteria (i.e., *Richelia intracellularis*) have been observed in association with diatoms such as *Rhizosolenia* and *Hemiaulus* (Zehr et al., 2001). Another species of cyanobacteria, *Calothrix rhizosoleniae*, has been found to have a symbiotic relationship with *Chaetoceros* and *Bacteriastrum* spp. (Foster and Zehr, 2006), but more research is needed before generalizations about the distributions of such associations can be made.

Our understanding of distributions of different phytoplankton functional type and their evolution has to be linked to changes in the physical environment. For instance, in the Southern Ocean, the distribution of DMS producers such as *Phaeocystis* or silicifiers such as diatoms is related to the thickness of the mixed layer. Diatoms are found preferentially in shallow mixed layers that allow bloom development (Weber and El-Sayed, 1987; Jochem et al., 1995), whereas *Phaeocystis* usually prevails in regions of deep mixed layers (Arrigo et al., 1999; Goffart et al, 2000; Mangoni et al., 2004).

A key question in the context of climate variability is how the distribution of these functional types of phytoplankton might change, in response to modifications to the environmental conditions.

1.4   Why Study Phytoplankton Functional Types?

In the last few decades, our interest in phytoplankton processes found added impetus with the realization of their role in the global carbon cycle. Collectively, phytoplankton are responsible for fixing some 50 GT carbon into organic material by photosynthesis, also known as primary production (Longhurst et al., 1995; Antoine et al., 1996; Field et al., 1998; Behrenfeld et al., 2001). The magnitude of this process is comparable to net production by terrestrial plants at the global scale (Longhurst et al., 1995), and is several times greater than the anthropogenic carbon emission on an annual scale, which is estimated to be about 7 GT per annum (Sabine et al., 2004). Thus, phytoplankton play an important role in the global carbon cycle. In the context of climate change, there is increasing recognition that we need to

understand how phytoplankton may respond to changes, since variations in primary production could have major implications for the global carbon cycle (Sarmiento and Hughes, 1999). At the same time, we recognize that distinct phytoplankton groups affect the carbon cycle differently (Maier-Reimer, 1996; Bopp et al., 2005). Several studies have shown that total particulate carbon at the surface of the ocean and in the euphotic zone can be estimated from satellite data (Stamski et al., 1999; Loisel et al. 2002; Gardner et al., 2006; Stamski et al., 2008; Duforêt-Gaurier et al., 2010). Furthermore, Loisel et al. (2002) and Duforêt-Gaurier et al. (2010) showed that the ratio of particulate organic carbon to chlorophyll concentration varies with region and season. To the extent that these variations may be linked to phytoplankton community structure, it may be argued that we need to learn more about phytoplankton functional types, to understand variations in particulate organic carbon.

The fate of the carbon fixed by photosynthesis depends to some extent on the type of phytoplankton present. For example, small phytoplankton tend to have lower sinking rates, and hence may remain for a longer period in the surface mixed layer of the ocean. When they respire, or die, or are eaten by other organisms, they release carbon dioxide back into the mixed layer, which is in direct contact with the atmosphere. In contrast, larger cells have a higher chance of sinking out of the mixed layer and of even reaching the sea floor before they decompose, and the carbon associated with those cells may not come again in contact with the atmosphere for decades or centuries. Thus, to quantify the role of phytoplankton in the global carbon cycle, we need to understand not only the process of photosynthesis, but also the fate of the organic material produced. This simple example illustrates the importance of cell size in the carbon cycle. Other phytoplankton traits that link cell size to their ability to fix carbon include the chlorophyll-normalised production rates at saturating light levels (Bouman et al., 2005; Kameda and Ishizaka, 2005; Uitz et al., 2008; Brewin et al., 2010b), quantum efficiency (Aiken et al., 2008; Hirata et al., 2009) and growth rate (Marañón et al., 2013).

In addition to participating in primary production, some phytoplankton, notably the coccolithophores, form calcium carbonate plates known as coccoliths that surround their cells. The effect of this process is to change seawater alkalinity, and hence solubility of carbon dioxide in seawater, which in turn impacts the carbon cycle (Figure 1.2).

If the magnitude and variability in this process is to be understood, we need to know not only the amount of phytoplankton present in the water, but also the amount of coccolithophores present, and whether they are producing coccoliths.

One of the major threats now facing marine life is ocean acidification (Raven, 2005; Henderson, 2006; Doney et al., 2009). As anthropogenic carbon dioxide in the atmosphere increases, a significant fraction of it (25 – 30 %, Sabine et al., 2004; Canadell et al., 2007) finds its way into the ocean, since differences in the partial pressure of carbon dioxide across the air-sea interface typically favour a net transfer
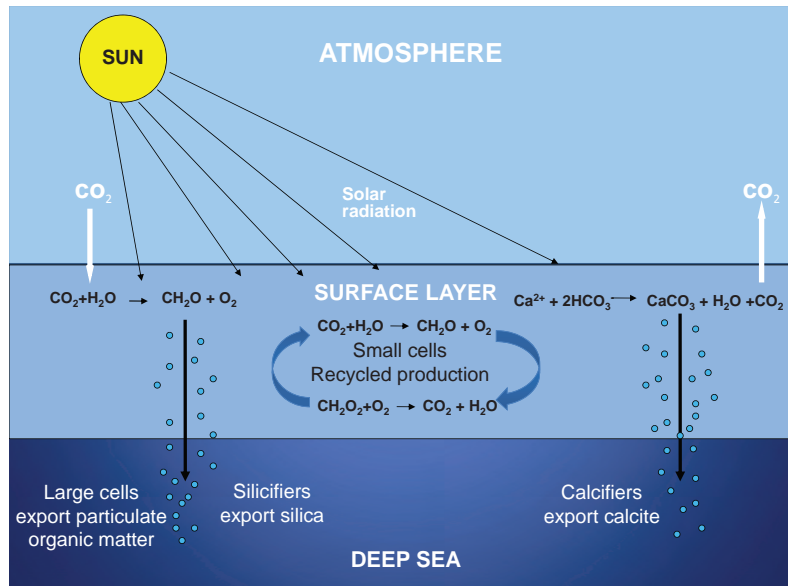
Figure 1.2 Production of organic and inorganic particulates by phytoplankton. Adapted from Rost and Riebesell (2004)

of carbon dioxide into the ocean. The oceans thus play a buffering role, decreasing the rate of accumulation of anthropogenic carbon dioxide in the atmosphere, and hence slowing the green-house effect. But this service provided by the oceans comes at a cost: as more and more carbon dioxide dissolves in the oceanic waters, it changes the pH of the water, making it more acidic (or more accurately, less alkaline). Many marine organisms have calcium carbonate components (such as skeletons, shells, corals, or coccoliths), and it has been shown under laboratory conditions that calcite formation by some marine phytoplankton may be reduced under high CO_2 conditions (e.g., Riebesell et al., 2000). When the pH of seawater moves away from a preferred value, it may threaten the ability of these organisms to complete their life cycle in a normal fashion, unless they are able to adapt to the changes. However, there is still much to be learned about species responses to a high-carbon-dioxide environment. Though it may be difficult to imagine an Earth without coral reefs, we now recognize that some corals may not be able to adapt to the rapid increase in ocean acidity. The fate of corals may be the most striking example of the threat to ocean life from ocean acidification, but the impact of acidification on microscopic life in the oceans may have a more profound effect on our lives through alteration of the carbon cycle. As noted above, coccolithophores have a role in the ocean as calcifiers, forming calcium carbonate liths, which on geological time scales have been important in carbon storage in deep-sea sediments. How would such organisms fare in a less alkaline ocean? To study the role of phytoplankton in the context of ocean acidification, and to appreciate their response to it, we can no longer treat all phytoplankton as a collective unit. Instead, we need to look at the calcifying

phytoplankton separately from the rest, again invoking the need to study functional types.

Phytoplankton are active not only in the cycling of carbon, but also of other elements, such as nitrogen and silica (Figure 1.2). In the process of primary production, phytoplankton take up not only carbon, but also nitrogen and other elements. All phytoplankton are able to take up nitrogen in one or more of the most biologically-utilisable forms: nitrate, nitrite and ammonia, with varying preferences for these different forms. But only some phytoplankton, notably certain species of cyanobacteria or blue-green algae, are able to take up nitrogen gas dissolved in seawater. Thus, to study the nitrogen cycle, we need to distinguish between nitrogen-fixing phytoplankton and the rest. On the other hand, diatoms form frustules made of silica, and are thus important players in the cycle of silica in the ocean, highlighting the need to distinguish silicifying phytoplankton from the rest in studies of the silica cycle.
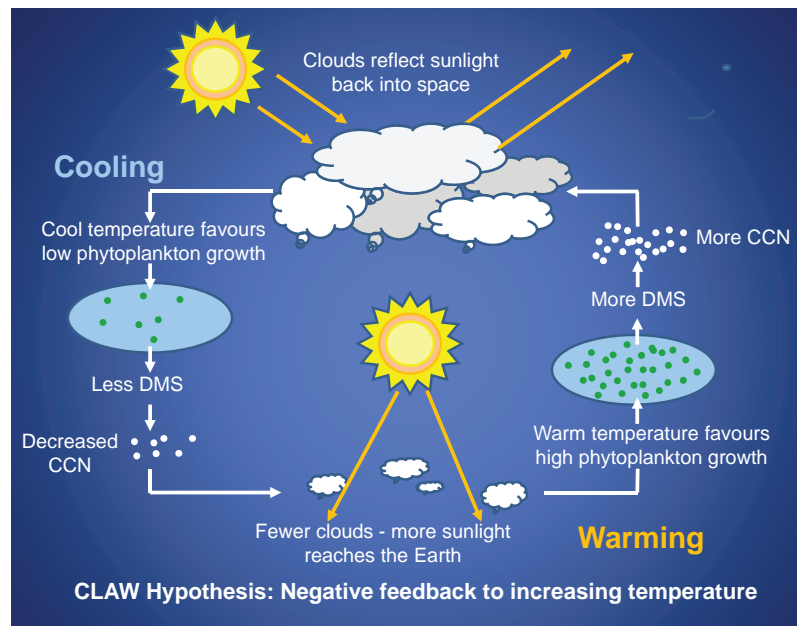
Figure 1.3 CLAW Hypothesis after Charleson et al. (1987): Negative feedback to increasing temperature. Figure adapted from Lucinda Spokes, Environmental Sciences, University of East Anglia, U.K.

The role of phytoplankton as an important natural source of reduced sulphur in the atmosphere also deserves our attention. Marine DMS emission from phytoplankton is estimated to contribute some 15×10^{12} to 35×10^{12} g S per year to the atmosphere (Kettle and Andreae, 2000; Simó, 2001; Lana et al. 2010). DMS influences the Earth's climate through the formation of sulphate aerosols. These aerosols serve as cloud-condensation nuclei, and the resultant clouds can reduce the sunlight reaching the sea surface, and also be a source of acid rain (Liss et al.,

1997). Krüger and Graßl (2011) reported that in the Southern Ocean, phytoplankton increase cloud albedo due to an increase of fine particles arising from DMS and possibly isoprene associated with phytoplankton, and decrease precipitation, because of delayed homogenous freezing by water particles. Charleson et al. (1987) posed the CLAW hypothesis (where the acronym CLAW is formed of the initials of the names of the four authors), which postulates that the DMS cycle may be a mechanism by which the temperature of the Earth is regulated (Figure 1.3). According to the hypothesis, increasing temperature would favour more primary production, and more phytoplankton would produce more DMS, hence contributing to increased cloud cover, which in turn would lead to a higher reflection of sunlight back into space, leading to a cooling effect. Under cooling conditions, the process would be reversed. More recently, Lovelock (2007) has proposed the Anti-CLAW hypothesis: increased temperature would increase stratification, thereby diminishing the supply of nutrients to the surface waters and hence primary production and DMS production (Figure 1.4). This would decrease cloud condensation nuclei, and hence cloud cover, and lead to further increase of temperature. In a recent review, Quinn and Bates (2011) have suggested that the relationship between biota and cloud-condensation nuclei is more complex than envisaged in the CLAW hypothesis. In the face of such opposing points of view, further research is needed to understand how the Earth functions as an interconnected system and the role of various phytoplankton functional types in the system, especially in the context of climate change.
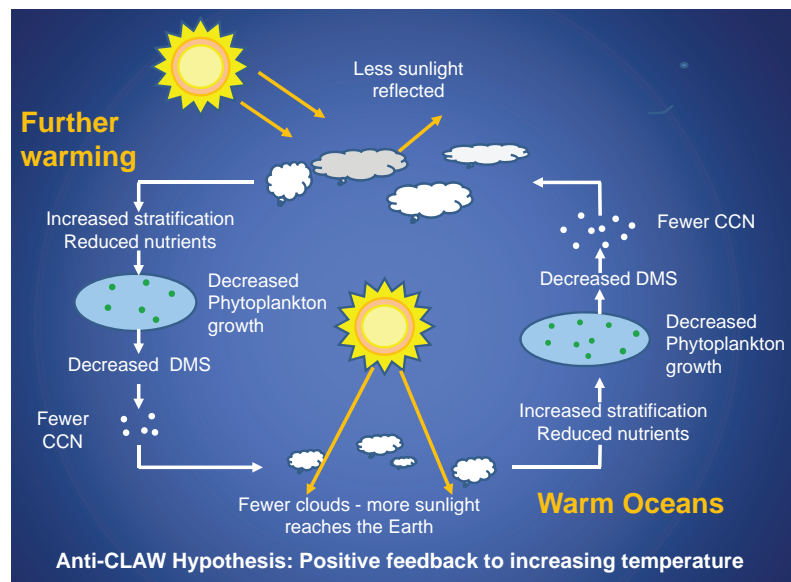
Figure 1.4 Anti-CLAW Hypothesis after Lovelock (2007): increased temperature increases stratification, diminishing the supply of nutrients to the surface waters and hence primary production and DMS production.

Humans rely on the oceans for food, especially high-protein food through fish-

eries and aquaculture. The fish in the oceans, on the other hand, depend ultimately on phytoplankton for their own food supply. Whereas it has long been recognized that availability of food is a limiting factor for growth of fish and shellfish in the oceans, there is now growing awareness that the type of phytoplankton available in the ocean may be an important factor that determines the energetics of different food webs and the type of fish that thrive in a given environment (Beaugrand, 2003; Beaugrand and Reid, 2003). For example, Cury et al. (2008) have suggested that, in the Benguela ecosystem, flagellates favour the growth of sardines, whereas diatoms favour the growth of anchovy. Thus, phytoplankton types are also relevant in studies of fish ecology, and hence are an important ingredient in efforts towards an ecosystem-based strategy for sustainable management of fisheries.

Certain types of phytoplankton, especially if they occur in very high concentrations, can have a negative impact on the environment, causing hypoxia (low-oxygen conditions), or producing toxins. Various dinoflagellates and diatoms have been implicated in such harmful algal blooms. For example, a diatom species *Pseudonitzchia multiseries* is known to produce the neurotoxin domoic acid. Shell fish filtering the phytoplankton concentrate the toxin many fold and human consumption of the contaminated shellfish can lead to serious health problems, or even fatalities (Lelong et al, 2012). Changing environmental conditions can result in increased prevalence and range of harmful algal blooms in coastal zones (Hallegraeff, 1993; Anderson, 2007), with implications for local and regional fisheries and potential feedback to climate systems.

From a more general ecosystem perspective, recognition of the intimate links between ecosystem function and diversity has led to renewed interest in understanding various aspects of marine biodiversity. Studying marine diversity at the species level at large scales remains an intractable problem for microscopic life in the oceans, because the thousands of species that exist in the ocean are not so readily analysed at large scales (though emerging genetic approaches provide some tantalizing glimpses of what might be possible in the future). Given the impracticalities of studying microscopic life at the species level in a dynamic environment that is vast and inaccessible, the approach of partitioning the phytoplankton into functional types provides an attractive, practical compromise in studies of marine diversity, where we probe diversity at the functional level instead of at the species level.

Thus, many reasons can be cited for our growing interest in studying phytoplankton functional types. The challenges inherent in developing and interpreting remotely-sensed PFT information may be outweighed by the imperative for better understanding of a range of ecological and biogeochemical processes with local- to global-scale relevance. Continued warming of the oceans, for example, has the potential to extend the geographic ranges of certain PFTs such as nitrogen fixers (e.g., *Trichodesmium*) and picoplankton (e.g., *Prochlorococcus* and *Synechococcus*), whereas increases in ocean acidity (associated with increases in atmospheric CO_2)

may impact calcifiers (e.g., *Emiliania huxleyi*) and their role in the carbon cycle (Doney, 2006; Orr et al., 2005). Implications and consequences of these kinds of changes cannot be adequately explored without PFT-resolving conceptual and numerical models.

As we see in the next section, recent developments in remote sensing provide a unique opportunity to study at least some phytoplankton functional types through analysis of ocean-colour data.

1.5 Why Study Phytoplankton Functional Types From Space?

Traditional approaches to interpretation of ocean-colour data are geared towards retrieval of the concentration of chlorophyll-a as an index of phytoplankton biomass. Standard chlorophyll algorithms (Morel and Antoine, 2000; O'Reilly et al., 2000) rely mostly on empirical relationships that use spectral band ratios of water-leaving radiance or radiance reflectance, typically in the blue-to-green portion of the spectrum. These algorithms are relatively simple to apply and are robust to a series of challenges including difficulties of implementing spectrally-resolved atmospheric correction or obtaining absolute calibration of space-based radiometers that is sustained over time. Inversion algorithms designed for routine retrieval of inherent optical properties (e.g., backscattering coefficients, absorption coefficients), in addition to chlorophyll concentration, are a noteworthy step away from empirical band ratio algorithms (e.g., Maritorena et al., 2002; Smyth et al., 2006), but are still designed to yield measures of total phytoplankton concentration. Most recently, there has been an expansion of research focused on retrieval of properties of the phytoplankton community, such as the dominant type, size structure, or simultaneous detection of multiple functional types.

Moving beyond chlorophyll retrieval to detecting phytoplankton types more directly from satellite data requires more complex interpretation and analysis of ocean-colour signals. Fortunately, it has been emerging over the years that some phytoplankton types are amenable to remote sensing. Many of these efforts have focused on specialized algorithms to detect a single taxon with distinctive optical characteristics known to affect water-leaving radiance signals detectable from space. Whereas validation of these approaches remains challenging, examples applied with some success include quantification from space of coccolithophorid blooms (Brown and Yoder, 1994; Iglesias-Rodríguez et al., 2002), near-surface *Trichodesmium* blooms (Subramaniam and Carpenter, 1994; Subramaniam et al., 2002; Westberry et al., 2005), cyanobacteria blooms (Hu et al., 2010b), diatom blooms (Sathyendranath et al., 2004b) and floating *Sargassum* (Gower and King, 2011). Some algorithms have also targeted a variety of phytoplankton (Alvain et al., 2005; Uitz et al. 2006; Aiken et al., 2007; Bracher et al., 2009). Interestingly, many taxa or types that are amenable to remote sensing are also "functional" types. For example, coccolithophorids are

calcifiers, *Trichodesmium* is an important bloom-forming cyanobacteria that belongs to the functional class of nitrogen-fixers, and diatoms are silicifiers.

In addition to phytoplankton biogeochemical classes, phytoplankton size classes have also been retrieved from satellite imagery. Some of these studies have used an estimate of phytoplankton abundance, such as chlorophyll concentration (Uitz et al., 2006; Brewin et al., 2010a; Hirata et al., 2011; Devred et al., 2011) or phytoplankton absorption (Hirata et al., 2008a), and their relationships with phytoplankton size. Other methods discriminate between phytoplankton types on the basis of their spectral optical signatures. These methods have focussed on either absorption (Ciotti and Bricaud, 2006; Devred et al., 2006; Uitz et al., 2008; Mouw and Yoder, 2010; Brewin et al., 2011a) or scattering characteristics (Loisel et al., 2006; Hirata et al., 2008a; Kostadinov et al., 2009). The scattering approaches are based on the total particle size distribution not differentiating phytoplankton from the total particle load. However, these scattering approaches employ a broad assumption that scattering particles in the open ocean are most likely phytoplankton. Alvain et al. (2008) and Bricaud et al. (2012) have studied PFTs over large expanses of the ocean during the SeaWiFS mission and explored biogeochemical implications of cell size.

Oceanographers today are familiar with routine accessibility of remotely-sensed chlorophyll images from sensors such as SeaWiFS, MODIS and MERIS, which can cover the globe on 1 – 2 day time scales. While the remote-sensing field has been progressing, the increasing capabilities of computers and conceptual developments have led to three-dimensional global circulation models being coupled with increasingly complex biogeochemical models. In some cases, these models extend well beyond three-box Nutrient–Phytoplankton–Zooplankton (NPZ) models, moving towards the class of models collectively known as Dynamic Green Ocean Models (DGOM, Le Quéré et al., 2005; Kishi et al., 2007) that strive towards more realistic representation of planktonic types and their functionalities (Gregg et al., 2003; Blackford et al., 2004; Le Quéré et al., 2005; Veldhuis and De Baar, 2005; Hood et al., 2006; Jin et al., 2006). More complex ecosystem models are justified by the need to resolve important ocean biogeochemical processes, many of which are mediated by specialized types of organisms (e.g., calcifiers, silicifiers, nitrogen fixers, see Figure 1.5). Spatially- and temporally-resolved information on relative abundance of these types of organisms is of great value for development and validation of these models, and satellite observations are used extensively for this purpose (e.g., Iglesias-Rodríguez et al., 2002; Gregg et al., 2003; Allen et al., 2010). Other observational strategies (e.g., ships, moorings) cannot approach the coverage and resolution of space-based sensors, so the motivation for retrieving PFT information is strong, even if it is established that remotely-sensed PFTs have coarse resolution and relatively large uncertainties. But of course, the usefulness of satellite-derived information would only increase if there is a quantitative understanding of the uncertainties associated with the products.

Remotely-sensed information can bring unique and essential information on the response of phytoplankton functional types to regional climatic events such as El Niño. For example, it is generally admitted that diatoms are not important contributors to phytoplankton biomass in the Equatorial Pacific region (Kobayashi and Takahashi, 2002; Dandonneau et al., 2004), but exceptional blooms have been reported in this area from *in situ* observations (Archer et al., 1997; Chavez et al., 1999) and their large spatial coverage has been recently observed using remote sensing (Alvain et al., 2008). Diatom blooms may occur when equatorial upwelling is intense and not limited to the coastal region, corresponding to a La Niña event, and give rise to massive exports of organic carbon to the bottom (Greene et al., 1991; Cavender-Bares et al., 1999).
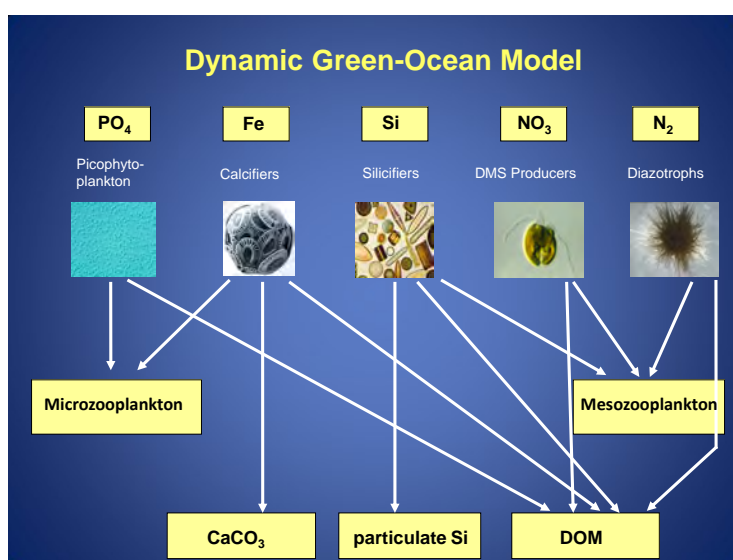
Figure 1.5 Dynamic Green Ocean Model (adapted from Aumont et al., 2003). Microzooplankton and mesozooplankton in the figure refer to two size classes of zooplankton in the model.

1.6 The Need for Complementary Approaches

A fundamental challenge in exploiting the PFT concept is that critical aspects of group function or characteristics associated with functional type affiliation cannot be observed directly at many important spatial and temporal scales. Laboratory- or field-based characterization of functional properties, combined with environmental characterization and taxon-specific identification in natural communities is a traditional approach (e.g., Root 1967; Reynolds et al., 2002), but one that is severely constrained by the labour-intensive nature of the methods and cost of access to study sites (e.g., ship time). For phytoplankton, microscopic analysis

and experimental incubations (e.g., C^{14} uptake, N^{15} transformation, etc.) remain the long-established standards for assessing composition and function. These approaches offer observational quality, accuracy, and functional resolution at the expense of space and time resolution (i.e., a few discrete samples), complementing remote-sensing approaches.

Some of the space and time limitations of these traditional methods can be offset with a variety of newer sampling and analysis strategies, each of which has different advantages and limitations. In almost all cases, a trade-off must be made between biological detail and spatio-temporal resolution of observations required to quantify PFT distributions in the ocean. Because many questions in biological oceanography depend at least as much on information regarding spatial and temporal variability as they do on biological detail, there are strong motivations to study PFT distributions derived from satellites, in spite of the limited scope for biological detail in these observations. Remote sensing approaches must be considered as part of this continuum of trade-offs between the quality and detail available from *in situ* observations and the extensive space and time scales accessible to remote sensing.

1.7   Concluding Remarks

The concept of phytoplankton functional types has emerged as a useful approach to classifying phytoplankton. It finds many applications in addressing some serious contemporary issues facing science and society. Its use is not without challenges, however. As noted earlier, there is no universally-accepted set of functional types, and the types used have to be carefully selected to suit the particular problem being addressed. It is important that the sum total of all functional types matches all phytoplankton under consideration. For example, if in a biogeochemical study, we classify phytoplankton as silicifiers, calcifiers, DMS-producers and nitrogen fixers, then there is danger that the study may neglect phytoplankton that do not contribute in any significant way to those functions, but may nevertheless be a significant contributor to, say primary production. Such considerations often lead to the adoption of a category of "other phytoplankton" in models, with no clear defining traits assigned them, but that are nevertheless necessary to close budgets on phytoplankton processes. Since this group is a collection of all phytoplankton that defy classification according to a set of traits, it is difficult to model their physiological processes. Our understanding of the diverse functions of phytoplankton is still growing, and as we recognize more functions, there will be a need to balance the desire to incorporate the increasing number of functional types in models against observational challenges of identifying and mapping them adequately. Modelling approaches to dealing with increasing functional diversity have been proposed, for example, using the complex adaptive systems theory and system of infinite

diversity, as in the work of Bruggemann and Kooijman (2007). But it is unlikely that remote-sensing approaches might be able to deal with anything but a few prominent functional types. As long as these challenges are explicitly addressed, the functional-type concept should continue to fill a real need to capture, in an economic fashion, the diversity in phytoplankton, and remote sensing should continue to be a useful tool to map them.

Remote sensing of phytoplankton functional types is an emerging field, whose potential is not fully realised, nor its limitations clearly established. In this report, we provide an overview of progress to date, examine the advantages and limitations of various methods, and outline suggestions for further development. The overview provided in this chapter is intended to set the stage for detailed considerations of remote-sensing applications in later chapters.

In the next chapter, we examine various *in situ* methods that exist for observing phytoplankton functional types, and how they relate to remote-sensing techniques. In the subsequent chapters, we review the theoretical and empirical bases for the existing and emerging remote-sensing approaches; assess knowledge about the limitations, assumptions, and likely accuracy or predictive skill of the approaches; provide some preliminary comparative analyses; and look towards future prospects with respect to algorithm development, validation studies, and new satellite missions.

In situ Methods of Measuring Phytoplankton Functional Types

Heidi M. Sosik, Shubha Sathyendranath, Julia Uitz, Heather Bouman and Anitha Nair

2.1   Introduction

Methods for identifying and characterizing phytoplankton in the field have progressed greatly, from the early approaches based on the light microscope, to the present use of satellite remote sensing. Many new tools have emerged to study phytoplankton in the sea in ways that complement microscopy. Advances include use of High Performance Liquid Chromatography (HPLC) to characterize pigments as chemical markers for phytoplankton groups, use of flow cytometry to characterize cells according to autofluorescence and light scattering properties, development of automated cell imaging techniques, and exploitation of molecular methods and gene sequencing approaches to characterize diversity. Optical properties of phytoplankton, such as absorption, scattering, and fluorescence excitation and emission spectra, have also been developed as tools for broadly classifying phytoplankton into different types. Furthermore, size classes of phytoplankton can be estimated in the field with successive filtration. In this chapter, various *in situ* methods for assessing phytoplankton types are summarized, along with their advantages and limitations. Some material in this chapter expands on that presented in Nair et al. (2008). We also examine how *in situ* data collected by the various methods can be related to satellite-based approaches, including prospects for developing and evaluating satellite algorithms.

2.2   Microscopy

Light microscopy is the traditional method for identifying phytoplankton, while the advent of epifluorescence and electron microscopy has significantly extended the capabilities for microscopic identification (e.g., Booth 1993; MacIsaac and Stockner, 1993). The microscope remains an essential tool for identifying many phytoplankton to the species level according to morphological features (Tomas, 1997). In some

methods, phytoplankton are collected on filters or mesh before identification and counting of cells. The inverted microscope or the Utermöhl method (Utermöhl, 1931) involves use of settling chambers to concentrate samples before microscopic analysis, an approach which is effective for many types of microphytoplankton (i.e., cell size >20 μm).

Despite the importance of microscopy, the method does have some general limitations. Most notably, it is time consuming and depends heavily on the expertise of the observer to discriminate taxa. Taxonomic identification is based on morphological characteristics, so it can be difficult even for experts to identify cells, if they have been damaged by handling. Pico- and nanophytoplankton (i.e., cell size < 2 μm and within the range 2-20 μm, respectively) are difficult to identify with light microscopy because of their small size and lack of distinctive morphological features. Epifluorescence microscopy, enabling discrimination of cells by fluorescence properties, is especially important for some characterization of picophytoplankton (e.g., *Prochlorococcus* versus *Synechococcus* versus picoeukaryotes), but still lacks sufficient resolution for many identification problems. This gap is filled by various types of electron microscopy (transmission and scanning), which are essential for discerning morphological differences among many pico- and nanophytoplankton, as well as fine details in larger cells such as species-specific frustule characteristics in diatoms. With these advanced methods, limitations are generally greater in terms of time, required expertise, and cost, such that relatively few samples can be analyzed and quantitative assessments of spatial and temporal variations in the ocean are prohibitive.

A further complication associated with microscopy is that samples are typically preserved for later analysis and the method of preservation used may not work equally well for all taxa, such that the results of enumeration may be biased. Though common microscopic methods tend to be effective for the identification and enumeration of large cells, an additional caveat is that even large cells may be easily missed, if they are rare in the sample.

For those who have never done it, it may be difficult to fully appreciate the magnitude of the task of identifying, counting, and measuring phytoplankton under a microscope. But some numbers, provided by Margalef (1994), drive home the point very tellingly. He reports that over a thirty-year period (1960 – 1991), he collected 1388 samples for phytoplankton analysis from the northwest Mediterranean. The total volume analysed with an inverted microscope at the end of the study was 5.1 litres of seawater. The total number of cells counted and measured for size was 194,983 and the total number of species identified was 353 (a high number, considering Sournia et al. (1991) report that only about 4,400 species of marine phytoplankton have been described globally). Of these, the most abundant species, *Chaetoceros curvisetus*, accounted for 11% of all counts. Notably, some 51 species were so rare they were each only encountered once during the entire study period. These figures demonstrate how impossibly difficult it would be to rely only on

microscopic analysis as a routine method for identifying phytoplankton types systematically at the global scale.

These challenges notwithstanding, there are notable efforts underway. For instance, phytoplankton species are counted routinely in samples collected with the Continuous Plankton Recorder (CPR). CPR sampling is done on surveys organised by the Sir Alistair Hardy Foundation for Marine Sciences and its sister organisations around the world (Reid et al., 2003b). It is important to note that the 270-μm mesh size used in the CPR and the microscopic method employed do bias these survey results towards larger phytoplankton (Richardson et al., 2006); though some cells much smaller than the mesh size can be trapped by the silk fibres of the CPR mesh and may be enumerated. Despite this limitation, CPR results have already provided means to evaluate aspects of some remote sensing algorithms for phytoplankton types (Brewin et al., 2011b).

When considering the goal of comparing microscopic estimates of phytoplankton types with satellite observations, some additional challenges emerge. Besides difficulties with identification and counting, it can be complicated to estimate biomass or biovolume from microscopic counts alone. Since many remote-sensing algorithms provide estimates of different phytoplankton types as absolute or relative contribution to pigment biomass, it is not straightforward to use microscope counts to evaluate algorithms; some assumptions must be made regarding chlorophyll content per cell or other conversion factors (see Brotas et al., 2013). Lastly, satellite observations provide information resolved to surface areas of hundreds of square meters, whereas microscopic counts are carried out on extremely small volumes (a few ml). This incompatibility of space scales makes it difficult to compare satellite observations and microscope counts directly, though the mismatch of space scales is not unique to microscopy and plagues all comparisons of *in situ* observations with satellite estimates.

2.3 Flow Cytometry

In contrast to manual microscopic methods, flow cytometers are renowned for the speed at which they are able to characterize phytoplankton in a water sample. For some three decades now, this method, adapted from medical tools designed for counting blood cells, has proven to be invaluable for the study of phytoplankton and even bacteria and viruses in the ocean (e.g., Yentsch and Horan, 1989; Olson and Chisholm, 1990; Reckermann and Colijn, 2000; Sosik et al., 2010). In flow cytometry, phytoplankton cells in a sample of seawater are forced individually through a small aperture into a light field. As a cell passes through the field, its optical properties such as fluorescence and scattering are measured (Figure 2.1a). A large number of cells are enumerated in this fashion in a short time ($>10^5$ cells per second) from water samples collected at sea.
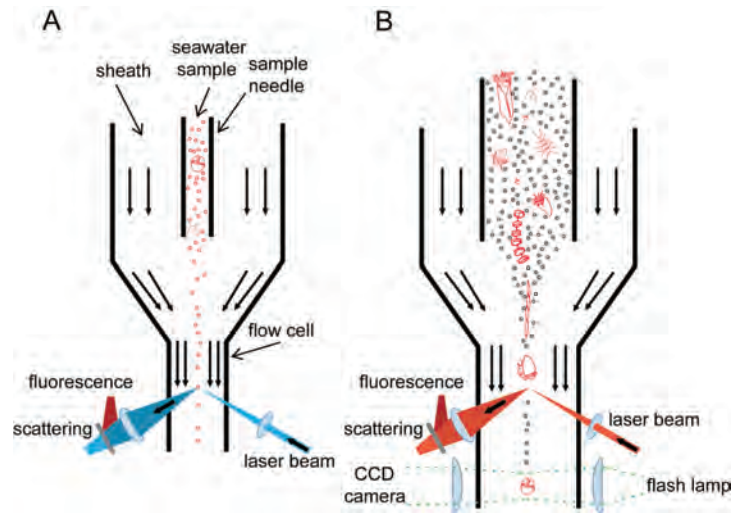
Figure 2.1 (a) Schematic representation of conventional flow cytometric analysis of individual phytoplankton cells in a seawater sample. As cells flow single file through a focused laser beam, the light they scatter or fluoresce is measured. Depending on the flow cytometer configuration, multiple scattering angles and fluorescence wavelength ranges may be measured. Typical flow cytometers are appropriate for enumerating and characterizing pico- and small nanophytoplankton. (b) High throughput customized flow cytometers enable characterization of microplankton, which are not only larger but also typically rarer, with the most detailed discrimination possible in systems that incorporate cell imaging (e.g., Olson and Sosik, 2007). An exposure flash and associated capture of a CCD camera frame are triggered by signals generated when the cell first passes through a laser beam. Only cells with signals above a threshold (represented here by those coloured red) trigger image capture, such that the abundant small cells (too small to identify with light microscopy) are not typically imaged.

Biomedical uses of flow cytometry usually involve treatment of cells with fluorescent dyes or probes prior to analysis, but the most common oceanographic applications entail measurement of untreated phytoplankton cells that naturally exhibit fluorescence associated with their photosynthetic pigments. Presence of chlorophyll fluorescence makes it possible to discriminate phytoplankton from other particles, and flow cytometric analysis permits enumeration, quantification of cell properties such as size and pigmentation, and some level of taxonomic, optical and/or sized-based discrimination (e.g., *Prochlorococcus*, *Synechococcus*, picoeukaryotes, pennate diatoms, coccolithophorids) (Olson et al., 1989; 1990b; Collier, 2000; Dubelaar and Jonker, 2000).

There are some important limitations of conventional flow cytometry. The approach provides much faster analysis of cells than microscopy, but the sample volumes are still small (from tens of μl to a few ml) and relatively few discrete samples can be processed compared with the space and time scales of change in the natural environment. Moreover, commercial instruments are typically optimized so

that analysis of small (pico- and nano-sized) phytoplankton is effective, but relatively rare and larger microplankton are missed or poorly characterized. At the same time, it is the case that many commercial flow cytometers lack sufficient sensitivity to detect the smallest, least fluorescent picophytoplankton typically encountered in open-ocean surface waters. So, there can be detection issues on both the small and the large ends of the phytoplankton size spectrum. Finally, the types of phytoplankton that can be discriminated on the basis of flow cytometric fluorescence and light scattering can be limited. Genera such as *Prochlorococcus* and *Synechococcus* can usually be unambiguously classified, but common analysis methods only permit other phytoplankton types to be characterized by size (estimated from light scattering).

Some of these limitations have been eased by recent advances. For instance, custom flow cytometers have been configured to increase sample volume throughput and dynamic range of signals so that larger, more rare cells can be characterized better (e.g., Dubelaar et al., 1989; Cavender-Bares et al., 1998; Green et al., 2003; Zubkov and Burkhill, 2006; Olson and Sosik, 2007). Others have been modified to increase sensitivity (e.g., Frankel et al., 1990; Olson et al., 1990a). Additional efforts have been focused on enhancing the ability to discriminate among cells types. An example is the use of fluorescence and light scattering pulse shapes to reveal aspects of cell (or chain) size and shape (Cunningham, 1990; Dubelaar and Gerritzen, 2000). Flow cytometry has also been combined with molecular probes for more refined analysis of taxonomic composition in phytoplankton (Biegala et al., 2003); however, this approach remains technically challenging and difficult to apply in a systematic manner for characterization of many phytoplankton types in diverse samples.

Important advances in flow cytometry have led to submersible instruments that can be programmed to sample automatically (Dubelaar and Gerritzen, 2000; Olson et al., 2003; Olson and Sosik, 2007), leading to long time series observations at a single point, and thus providing valuable information on phytoplankton dynamics (e.g., Sosik et al., 2003; Thyssen et al., 2008). These automated technologies can also be used for surveying during underway ship-based sampling to characterize spatial variability (e.g., Thyssen et al., 2009; Laney and Sosik, 2014).

The advent of imaging-in-flow cytometers is arguably the most important development for extending the level of taxonomic discrimination possible (Sieracki et al., 1998; Olson and Sosik, 2007). This method incorporates video imaging and effectively combines the speed and automation of flow cytometry with the strengths of light microscopy (Figure 2.1b). In current instruments, image resolution and quality is such that many microphytoplankton can be identified to genus or even species (Sosik and Olson, 2007; Poulton and Martin, 2010; Sosik et al., 2011), thus effectively overcoming the bias against detecting and discriminating large cells that limits conventional flow cytometry.

The combination of imaging-in-flow with automated cytometry introduces a new challenge because hundreds of thousands of cell images can be readily acquired and

must be analyzed and identified to provide new knowledge about spatial and temporal variability in phytoplankton types. While this type of automated measurement and analysis is a significant advance, it is important to note that the design and interpretation of automated image classifiers relies critically on the same human expertise in taxonomic identification that is inherent with manual microscopy. Fortunately, effective automated image analysis and taxonomic classification (machine learning) algorithms have been demonstrated (Sosik and Olson, 2007; Campbell et al., 2013). An additional advantage of automated image analysis is that it can provide quantitative estimates of biovolume on a cell-by-cell basis, so that variations in size and shape can be fully considered in natural assemblages (Sieracki et al., 1989; Moberg and Sosik, 2012). When coupled with automated classification, this approach can be used to produce taxon-specific biomass estimates (e.g., Laney and Sosik, 2014) that could be systematically compared with results from satellite algorithms.

2.4 HPLC Methods

Chromatographic analysis of pigments is probably the most common non-microscopic approach to phytoplankton community characterization (Jeffrey et al., 1997; Roy et al., 2011). High Performance Liquid Chromatography (HPLC), coupled with knowledge of taxon-specific pigment composition, can provide information on various phytoplankton classes that make up natural communities (e.g., Mackey et al., 1996) with less labour than microscopy. Phytoplankton pigments can be classified into three major groups: chlorophylls (a, b, and c), carotenoids (carotenes and their oxygenated derivatives, known as xanthophylls), and biliproteins (phycoerythrin, phycocyanin, and allophycocyanin). Chlorophyll-a, or more specifically, mono-vinyl chlorophyll-a, is ubiquitous and present in all phototrophic organisms, except *Prochlorococcus* which possesses the variant divinyl-chlorophyll-a. The distribution of all other pigments varies among taxa. Several pigments are restricted to specific taxa and, thus, can be used as marker pigments - also called diagnostic pigments, or pigment fingerprints - for those taxa (Jeffrey et al., 1997).

HPLC enables the separation, identification, and quantification of 25-50 pigments, depending on the method, in a single analysis (Figure 2.2). Briefly, pigment mixtures from samples introduced into a column are separated on the basis of their affinity to the chromatographic packing material contained in the column and the solvent stream moving through the column. Once separated, the eluted pigments pass through a detector for identification and quantification. HPLC offers the unique benefit that it simultaneously provides a comprehensive description of the phytoplankton community composition over the entire cell size spectrum, and an accurate determination of the chlorophyll-a concentration, the most widely used proxy for phytoplankton biomass. Although HPLC pigment determination provides

limited taxonomic resolution (compared with detailed microscopy), it allows useful interpretation at the class level. It also has the advantage of routine, relatively rapid analysis, without need for high-level training in algal taxonomy, and with less labour than microscopy.
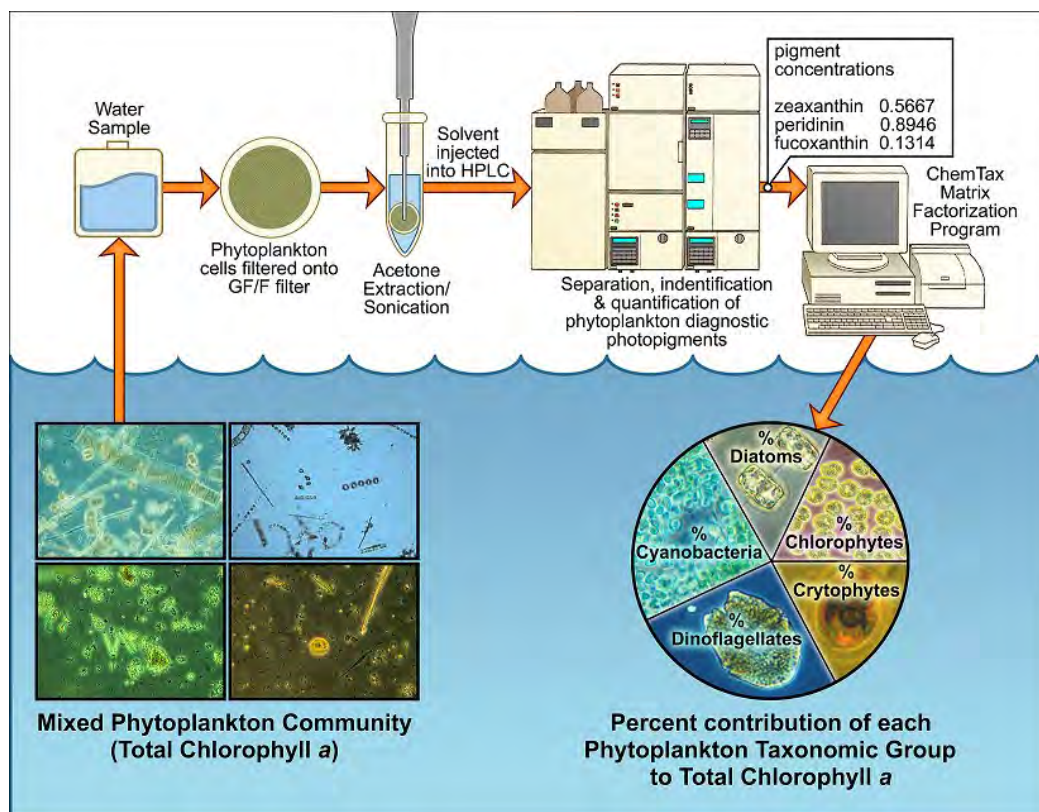
Figure 2.2 Schematic of HPLC analysis approach for characterizing phytoplankton community structure on the basis of pigment composition. Mixed species natural samples are filtered, then extracted and injected into the HPLC system, where individual pigments are separated and quantified. Taxonomic contributions to total chlorophyll-a can then be inferred from assumptions about diagnostic pigments and pigment ratios (Mackey et al., 1996). Figure credit: Alan Joyner and Hans Paerl (University of North Carolina-Chapel Hill, Institute of Marine Sciences).

A few pigments can be unambiguously assigned to a single phytoplankton class. For example, divinyl-chlorophyll-a and divinyl-chlorophyll-b are unique to *Prochlorococcus*, and alloxanthin to cryptophytes (see Table 2.1). However, interpretation of pigment data is not always straightforward, and is subject to uncertainties linked to biological and environmental sources of variability in pigment composition. In particular, some marker pigments are shared between several phytoplankton taxa, making the unambiguous identification of groups difficult (Table 2.2). Interpretation of pigment data may also be complicated by the presence of endosymbionts in some

Pigment	Taxonomic significance	Reference
Divinyl-chlorophyll-b	Prochlorophytes	Wright (2005)
Alloxanthin	Cryptophytes	Wright (2005)
Peridinin	Type-1 Dinoflagellates	Ornólfsdóttir et al.(2003)
Gyroxanthin diester	Type-2 Dinoflagellates	Ornólfsdóttir et al.(2003)
Prasinoxanthin	Type-3 Prasinophytes	Egeland et al. (1997)

Table 2.1 Unambiguous pigments and their associated phytoplankton group. Reproduced from Nair et al. (2008).

phytoplankton, such as cyanobacteria in diatoms, which give a mixed pigment signature (Hallegraeff and Jeffrey, 1984). The method is also susceptible to uncertainties linked to genetic and environmental sources of variability in pigment composition within classes (e.g., Irigoien et al., 2004; Llewellyn et al., 2005). Pigment composition within a particular group is influenced by numerous factors such as light (Goericke and Montoya, 1998), nitrogen (Sosik and Mitchell, 1991; Henriksen et al., 2002), or iron (Kosakowska et al., 2004), and varies with strains (Zapata et al., 2004). Nevertheless, and acknowledging these limitations, pigment concentrations provide a first-order estimate of total and group-specific phototrophic (chlorophyll-containing) biomass. This makes HPLC pigment analysis unique compared with other *in situ* techniques (e.g., microscopy, flow cytometry), which require conversion factors to estimate pigment biomass from cell density.

Pigment	Taxonomic significance
Fucoxanthin	**Diatoms**, Prymnesiophytes, Chrysophytes, Dinoflagellates
Peridinin	**Dinoflagellates**
19'-Hexanoyloxyfucoxanthin	**Prymnesiophytes**, Chrysophytes, Dinoflagellates
19'-Butanoyloxyfucoxanthin	**Pelagophytes**, Prymnesiophytes
Alloxanthin	**Cryptophytes**
Chlorophyll-b	**Chlorophytes**, Prasinophytes
Divinyl-chlorophyll-b	**Prochlorophytes**
Zeaxanthin	**Cyanobacteria**, Chlorophytes, Prasinophytes, Chrysophytes, Euglenophytes

Table 2.2 Major marker pigments used for classification of phytoplankton groups. The most commonly used pigment algal-class associations are in bold.

Various methods have been proposed to minimise these uncertainties and derive quantitative information on phytoplankton types from pigment data. Typically, selected marker pigments (Gieskes and Kraay, 1983; Letelier et al., 1993; Mackey et al,. 1996), or pigment groupings (also called pigment indices; Claustre, 1994; Vidussi et al., 2001), are used in conjunction with chlorophyll-a concentration to estimate the relative contribution of major phytoplankton groups (e.g., diatoms, prymnesiophytes,

cyanobacteria) or size classes (micro-, nano-, and picophytoplankton) (see Table 2.2). Although not definitive, such pigment approaches are recognized as valuable tools, and are commonly used for large-scale investigations of the distribution of dominant groups in the ocean (e.g., Barlow et al., 2004; Aiken et al., 2009; Ras et al., 2008).

HPLC measurements are now recognized as the standard for calibrating and validating satellite-derived chlorophyll-a concentration. Pigment analysis also has a useful role to play in validating satellite algorithms for mapping functional types of phytoplankton. Algorithms for distinguishing phytoplankton types from ocean-colour measurements are very different in their approaches. They focus either on taxonomy or size-based classification, and may yield either qualitative or quantitative information. These conceptual divergences make validation and comparison of algorithms difficult. In this regard, HPLC-derived pigment measurements are an effective validation method, since interpretation of pigment data has the potential to provide a range of information applicable to different algorithms. As described in subsequent chapters of this report, new applications of satellite-based observations (Uitz et al., 2006) are building on information contained in extensive HPLC-derived pigment databases, combined with empirical knowledge of relationships between pigment type and cell size (Vidussi et al., 2001), in an effort to expand accessible spatial and temporal scales. Use of HPLC measurements for comparison with satellite-derived products brings its own challenges, however. Such comparisons require the availability of extensive sets of *in situ* data, collected from a wide variety of oceanic regions and representative of long timescales. On the other hand, protocols for HPLC analyses may be optimized for different applications, with the consequence that data from different HPLC centers may not be fully comparable with each other (Hooker et al., 2005). The HPLC system is a specialised piece of equipment that requires highly-trained personnel to operate it, and the number of professional centres equipped to carry out HPLC analyses remains small. HPLC-based analysis is also limited to discrete samples that must be carefully stored and sample analysis is quite expensive (~US$50 to $150 per sample).

Many of these current drawbacks are minor and will certainly be addressed over the next few years. With the rapid advent of ocean-colour based algorithms for estimating biogeochemically-relevant products such as phytoplankton functional types (see Nair et al., 2008; McClain, 2009), a general interest is growing towards the merging of suitable databases, dedicated to calibration and validation activities. A major on-going effort has been invested into establishing and improving measurement protocols for HPLC pigment analysis (Bidigare et al., 2002), and conducting round-robin experiments involving several HPLC centres (Hooker et al., 2005). These exercises make it possible to quantify and understand propagation of methodological uncertainties originating from different sources within a data set (Claustre et al., 2004). They also enable important recommendations to be made as to how this information can be exploited for the study of phytoplankton types. Notably,

pigment indices (i.e., pigment sums or ratios), such as those proposed to derive phytoplankton size classes, have proven to be useful in minimizing uncertainties in large HPLC pigment databases derived from a diverse set of contributors (Claustre et al., 2004; Hooker et al., 2005).

2.5   Molecular Methods

Although the ecology and diversity of large phytoplankton, such as diatoms and dinoflagellates, have been relatively well studied with conventional light microscopy, much less is known regarding smaller phytoplankton, in particular those less than a few micrometers in diameter. Instead of identifying phytoplankton species from morphological characteristics of cells (phenotype), molecular methods exploit their genetic differences (genotype). The development of molecular tools to study the picophytoplankton, which includes all autotrophic cells less than 2-3 μm in diameter (Vaulot et al., 2008), has greatly enhanced our ability to identify rapidly not only the taxonomic affiliation of these tiny cells, but also their functional roles in marine ecosystems. Consistent with global pigment data, molecular datasets also show a dominance of haptophyte microalgae in the global ocean (Liu et al., 2009b). There is still a need, however, for a comparative study of size-fractionated HPLC pigment and molecular markers as tools to assess picophytoplankton community structure and abundance. Whereas molecular methods have been especially important in advancing knowledge about these small cells, the approaches also provide novel insight and expanded analysis capability for a wide range of phytoplankton groups (Medlin et al., 2010; Caron, 2013), especially harmful algae (Rhodes et al., 1998; Scholin et al., 2000; Bowers et al., 2006). Due to the cost and time required to design molecular probes, most have been designed to target a limited number of species, especially those which lack clear and reliable morphological features. Although molecular techniques are an extremely powerful and sensitive way of monitoring phytoplankton diversity in the marine environment, they all require access to molecular equipment and expertise.

DNA microarray technology allows the rapid processing of a large number of environmental samples with a range of molecular probes and hence is well suited for monitoring marine phytoplankton species (Schena et al., 1995). A microarray consists of DNA sequences that are attached to the surface of a silicon chip in an ordered array. The target nucleic acid is labeled with a fluorescent probe and the hybridization pattern is detected by the microarray scanner. Specific probes can be used for the detection of phytoplankton classes (Metfies and Medlin, 2004; Medlin et al., 2006) and harmful algal species (Ki and Han, 2006). Probe design requires the analysis of publicly-accessible databases (e.g., GENBANK) and specialized computer software. Although the number of sequences being deposited into these databases is steadily increasing, hybridization of probes with a non-target group may occur and

the specificity of probes should be routinely checked against sequence databases. Although the design and testing of microarrays requires a considerable investment (time and cost), it can be a powerful tool to monitor routinely the ecological dynamics of natural phytoplankton populations.

Fluorescent *in situ* hybridization (FISH) is a common culture-independent molecular technique for identification of a particular taxon or functional group in the marine environment. An oligonucleotide probe is designed to recognize and hybridize to complementary sequences that are unique to a specific phytoplankton group. In FISH, a fluorescent dye is covalently attached to the probe, and the cell fluorescence detected with epifluorescence microscopy. The advantage of FISH is that it provides directly the abundances of targeted groups (Simon et al., 1995), whereas most other molecular techniques are qualitative. The method also allows for the simultaneous labelling of multiple target groups. FISH has been used in the detection of algal classes (Simon et al., 1997; Eller et al., 2007) as well as harmful algae (Anderson, 1995; Anderson et al., 2005). The technique requires a trained individual to count cells with an epifluorescence microscope, though automated counting systems are available to increase sample throughput (Töbe et al., 2006). As is the case with the microarray method, once a probe is developed, its specificity to the target organism must be rigorously tested. A potential difficulty in using the method to assess the relative biomass of a particular functional group is that the preparation of the sample can result in cell loss.

Quantitative real-time polymerase chain reaction (qPCR) is another culture-independent approach used to detect and quantify the abundance of different phytoplankton species. This approach has been used to target toxic dinoflagellates in environmental samples (Bowers et al., 2000; Popels et al., 2003; Galluzzi et al., 2004; Touzet et al., 2009), as well as for spatial and temporal mapping of cyanobacterial (Johnson et al., 2006) and eukaryotic (Countway and Caron, 2006; Marie et al., 2006) assemblages. Since qPCR amplifies the genetic material in an environmental sample with a pair of oligonucleotide primers complementary to specific regions of DNA, it is highly sensitive. Both the expense of primer and probe design and the effort in testing them against sequences in large databases and local strains, mean that primers and probes have been designed for only a limited number of target organisms. Unlike FISH, only one species can be analyzed at a time using this method.

In addition to taxonomic affiliation, molecular probes can also be used to determine the biogeochemical function of particular cells. Since different ecotypes of *Prochlorococcus* are known to require different forms of nitrogen, genetic variability is readily linked to biogeochemical function (Moore et al., 2002; Rocap et al., 2003). One functional group that has been specifically targeted with molecular probes is the nitrogen fixers. Here, the gene responsible for nitrogen fixation (nifH) is targeted for the detection of nitrogen fixers in natural samples. With these molecular approaches microbiologists have found that the diversity of organisms carrying out nitrogen

fixation is far more extensive than previously thought, and that unicellular cyanobacteria may play an important role in the open ocean (Zehr et al., 2001; Mazard et al., 2004). But probes are not yet available for all functional groups.

Advances in environmental genomics and high-throughput sequencing techniques also promise to provide characterization of phytoplankton community structure and functional types that may have utility for evaluation of satellite-based approaches. These approaches can provide not only characterization of what taxa are present in environmental samples, but also what functional capabilities are associated with them (e.g., Coelho et al., 2013). Results from these approaches present many challenges with respect to producing metrics such as biomass proxies, but they provide unparalleled prospects to assess the biology, ecology, and physiology of whole communities. Very little work has been done to date, linking genetic information directly with satellite methods for detecting phytoplankton types.

2.6 Spectral Inherent Optical Properties of Phytoplankton

There is a long history of developing approaches to derive information about phytoplankton and other seawater constituents from measurements of spectrally-resolved inherent optical properties such as absorption and scattering (Sosik, 2008). Use of fluorescence characteristics is also discussed in the next section.

Since phytoplankton are photosynthetic organisms evolved to produce pigments that efficiently collect energy from sunlight for their survival, it may be expected that their influence on light absorption in the sea can be exploited to detect and characterize them. It is less obvious, but has nonetheless been known for a long time, that the absorption coefficient of phytoplankton varies not only with their pigmentation, but also with the size of their cells (Duysens, 1956; Kirk, 1975a,b; Morel and Bricaud, 1981). This size impact is such that the absorption spectra of large cells, when normalized to unit pigment concentration, appear low and spectrally flat, compared with the corresponding spectra of small cells, an effect often referred to as the flattening or pigment packaging effect (Figure 2.3a). Many algorithms have been proposed that exploit these differences in absorption spectra to infer information on phytoplankton size (Ciotti et al., 2002; Ciotti and Bricaud, 2006; Uitz et al., 2008; Brewin et al., 2010a; Devred et al., 2011; Organelli et al., 2013; Roy et al., 2013).

The spectral absorption characteristics of phytoplankton are further modulated by variations in their pigment composition (Sathyendranath et al., 1987; Hoepffner and Sathyendranath, 1991), with different accessory pigments exhibiting distinct absorption characteristics (Figure 2.3b) (Bidigare et al., 1990). Since the accessory pigment complement is characteristic of the type of phytoplankton present, there has been considerable interest in the use of absorption spectra to infer information about the underlying pigments. Such methods can be confounded, however, by
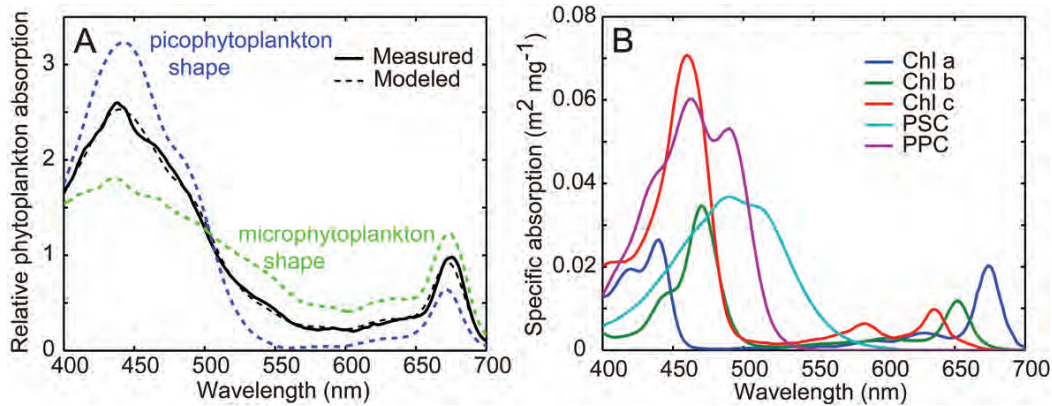
Figure 2.3 (a) Spectral absorption has a characteristic shape that is highly peaked for picophytoplankton and more flattened for microphytoplankton. An example phytoplankton community absorption spectrum from summertime surface waters at the Martha's Vineyard Coastal Observatory ("Measured") can be effectively represented by a linear mixture of 49% picophytoplankton and 51% microphytoplankton ("Modelled"), providing a means to characterize the size structure of the community on the basis of the influence on optical properties (Ciotti et al., 2002). (b) Example pigment specific absorption spectra for major categories of phytoplankton pigments, including chlorophylls-a, -b, and -c, plus two categories of carotenoids: photosynthetic (PSC) and photoprotective (PPC). These spectral differences can be exploited to infer pigment composition from the phytoplankton absorption spectrum. Spectra reproduced from Bidigare et al. (1990).

the flattening effect of cell size, such that absorption characteristics of the same accessory pigment may be different in small compared with larger cells. Furthermore, the absorption characteristics of pigment-protein complexes in the cell may differ from those of extracted pigments in isolation (Johnsen and Sakshaug, 2007). In spite of these difficulties, several methods have been developed, with some degree of success, to infer pigment complement from *in vivo* absorption spectra. Decomposition of spectra into Gaussian bands (Hoepffner and Sathyendranath, 1993; Lohrenz et al., 2003), spectral reconstruction (Bidigare et al., 1990; Babin et al., 1996; Allali et al., 1997), derivative analysis (Faust and Norris, 1985; Bidigare et al., 1989), multiple linear regression (Sathyendranath et al., 2005) and neural networks (Chazottes et al., 2006; Bricaud et al., 2007) have been used to estimate several pigments quantitatively from absorption.

Similar to absorption, the spectral backscattering, total scattering, total attenuation (sum of scattering and absorption), and pigment-specific backscattering are all known to vary with the size structure of the particles in seawater. This means there is potential to use these properties to infer particle size structure in the ocean (Boss et al., 2001a,b; Boss et al., 2004; Loisel et al., 2006; Hirata et al., 2008b; Kostadinov et al., 2009; 2010). But unlike absorption-based methods, scattering-based methods deal with the size structure of all particles, and not just phytoplankton. To infer

phytoplankton size structure from these estimates, one has to assume that either phytoplankton dominate the particle assemblages within their size range, or there is a prescribed relationship between phytoplankton and other particles.

As described in subsequent chapters, these distinctive optical properties also form the basis of remote-sensing algorithms for distinguishing different phytoplankton types from space.

2.7 Fluorescence Excitation and Emission Spectra of Phytoplankton

Absorption of photons by a substance leads to excitation of the material both electronically and vibrationally. In some substances, the subsequent vibrational relaxation of the electrons leads to emission of light, typically at a longer wavelength with less energy than that of the excitation photon. This phenomenon is called fluorescence. Spectrofluorometers are designed to measure fluorescence of a substance at a fixed wavelength when the excitation wavelength is changed systematically over a range of wavelengths (excitation spectrum), or to measure the emission over a range of wavelengths when the excitation wavelength is held constant (emission spectrum). These spectra are characteristic of the fluorescing substance, and hence spectrofluorometry is used in many fields for identifying and quantifying various substances.

In phytoplankton, chlorophyll-a and various biliproteins are known to fluoresce *in vivo*. Since the pigment composition of phytoplankton varies among taxonomic groups, their fluorescence properties also vary in ways that can be used to discriminate taxa (Yentsch and Yentsch, 1979; MacIntyre et al., 2010). Major differences in emission spectra make cryptophytes and cyanobacteria readily separable from other types of phytoplankton, while more subtle differences in excitation spectra can be used to separate chlorophytes and chromophytes (Figure 2.4)

Laboratory-based and *in situ* fluorometers of varying degrees of sophistication are available for monitoring phytoplankton at sea. The simplest of these, the Turner type of fluorometer, is the most common instrument for measuring total chlorophyll concentration at sea and in the laboratory: chlorophyll is extracted from phytoplankton using organic solvents, and the fluorescence emission by the sample at a fixed wavelength is measured in the instrument when excited by light at another fixed wavelength; and the results compared against a calibration curve established with standard chlorophyll (Holm-Hansen et al., 1965). Similarly, *in vivo* fluorescence meters are typical accessories now to CTD (conductivity, temperature and depth) instruments for continuous measurement of vertical structure in phytoplankton, and are becoming increasingly used on profiling floats, autonomous vehicles, moorings, and automated underway sampling systems on ships.

Inferring community structure from fluorescence requires more sophistication,

with multiple excitation and emission wavelengths being monitored. In fact, absorption and fluorescence properties of different phytoplankton pigments *in vitro* are at the heart of the HPLC technique as well. But interpretation of *in vivo* fluorescence signals from phytoplankton pigments is not straightforward: algal physiology (distribution of fluorescing pigments in photosystems I and II of phytoplankton), acclimation responses (plasticity in pigment ratios), function (photosynthesis), and ambient light conditions (quenching of fluorescence at high light levels) can affect the relationship between fluorescence strength and pigment concentration (e.g., IOCCG, 1999; Lutz et al., 2001; Sathyendranath et al., 2004a; Babin, 2005; Huot and Babin, 2010). Nonetheless, some success has been demonstrated in fluorescence-based discrimination of major groups in natural samples with instrumentation designed for use *in situ* or on shipboard (e.g., Beutler et al., 2002; Richardson et al., 2010; Chekalyuk et al., 2012). The distinct fluorescence emission characteristics associated with phycobiliproteins mean that discrimination of cryptophytes and cyanobacteria has been most effective, while the difficulty in separating groups such as diatoms and dinoflagellates from one another represents a major limitation of these approaches (e.g., Figure 2.4). Some resolution of this limitation may come from
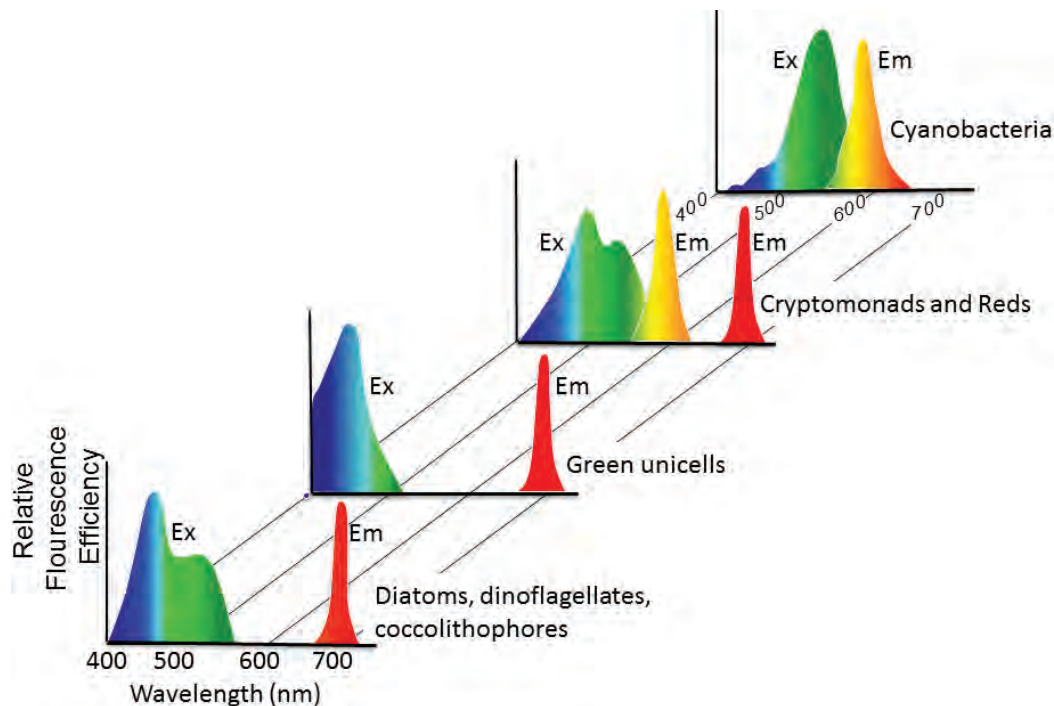
Figure 2.4 General characteristics of fluorescence excitation (Ex) and emission (Em) spectra for various groups of phytoplankton. Phytoplankton taxa with phycobiliproteins (cyanobacteria, cryptomonads) have distinctive emission peaks compared to other groups. Excitation spectra exhibit more subtle variations according to photosynthetic accessory pigment composition. Modified from Yentsch and Phinney (1985).

emerging approaches combining flow-through fluorescence analysis of individual cells with optical elements precisely designed to mimic linear discriminant functions that optimize fine separation between cell types (Pearl et al., 2013), though these techniques remain to be evaluated under a range of field conditions.

2.8 Phytoplankton Size Structure through Successive Filtration

A classic method for measuring the size structure of a phytoplankton community is by filtration of a sample of seawater through a selection of filters of known pore size. By measuring the chlorophyll-a concentration retained on each filter, the contribution from different size classes can be estimated. Though this is relatively straightforward in principle, the method is not without drawbacks: clogging of filters can retain cells of smaller size than the pores of the filter; flexible or elongated cells and cell breakage during filtration can lead to cells larger than the pore of the filter passing through. As with all approaches that rely on time-consuming manipulation of discrete samples, this method suffers from challenges in comparing results to the space scales relevant for satellite observations. Nonetheless, it is a valuable and direct approach for comparison and evaluation of other methods, such as use of marker pigments to infer information about phytoplankton size classes (e.g., Uitz et al., 2009; Brewin et al., 2014).

2.9 Concluding Remarks

Optical sensing of one type or another underlies most of the methods described above: microscopes rely on optical lenses and human eyes or cameras, HPLC techniques rely on detectors for absorption and fluorescence signals of phytoplankton pigments, flow cytometers incorporate photomultipliers or diodes to detect scattering and fluorescence properties of individual cells. Approaches that rely on optical properties have the potential to be incorporated with *in situ* technologies that do not require manipulation of samples in the laboratory, which ultimately can provide improved space-time coverage in assessing phytoplankton types in the sea.

Each of these methods has its own advantages and limitations, leading to the conclusion that use of any one method in isolation would result in characterization of phytoplankton communities that may be neither complete nor entirely unambiguous. Hence, approaches that combine information from various methodologies has promise in leading to more accurate and complete assessments.

The field methods can be compared with satellite observations with varying degrees of ease (Table 2.3). Methods that yield biomass estimates for phytoplankton types rather than their number densities, those that sample the whole assemblage

Table 2.3 Approaches for characterizing phytoplankton, with summaries of advantages, limitations, and relevance to advancing remote sensing applications.

Method	Advantages	Limitations	Relevance to Remote Sensing
Microscopy	- Only current method capable of identifying nearly all phytoplankton - Capital investment in equipment is low (at least for light microscopy) - Equipment maintenance is relatively straightforward	- Time consuming - Identification dependent on expert knowledge and subjective interpretation - Experts in phytoplankton taxonomy are increasingly rare - Assumptions required to convert to biovolume and biomass - Enumeration of small cells (picoplankton) requires the use of epifluorescence microscopy - Identification of small cells (picoplankton) to species level difficult - Sensitive to methods used to collect and concentrate cells - Preservation techniques do not work equally well for all taxa	- Assumptions required to link cell counts to estimates of pigment biomass - Small sample sizes lead to large uncertainties in contribution of rare cells, which can be large contributors to biomass (due to large cell size) - Cell counts have to be supplemented with cell size information to estimate phytoplankton size structure
Flow Cytometry	- Automatic and fast - Picoplankton are readily observed - Imaging in flow provides access to microplankton - Potential for optically estimated cell size - *In situ* tools available	- Specialized instruments required to assess entire phytoplankton size range - Identification is often possible only to the level of certain phytoplankton groups - Instrumentation is expensive and delicate; requires expert user	- Assumptions required to link cell counts to pigment biomass - Cell abundance and cell size information can be converted to group-specific biovolume or carbon biomass
HPLC	- Automatic and precise - Basis of chemotaxonomy	- Few unambiguous marker pigments - Sensitive to assumptions about pigment ratios - Uncertainty caused by intra-group variability in pigment ratios (e.g., with growth conditions) - Expensive - Few experts and facilities, globally - Comparison between laboratories confounded by differences in methodology (e.g., solvents, column materials) - No *in situ* tools	- Group-specific pigment biomass directly computed - Used extensively for development and validation of algorithms
Molecular Methods	- Taxa can be targeted with high degree of specificity - Particular functions can be targeted directly - *In situ* tools emerging	- Only a few probes now available - Method development and testing time consuming - Relatively expensive and requires specialized equipment - Assumptions required to convert to biomass or size structure	- Largely untested
Inherent Optical Properties	- Most methods are relatively simple and inexpensive - Many available tools, *in situ* and laboratory	- Assumptions required to convert between optical properties and biomass - Uncertainty in some methods caused by intra- and inter-group variability in optical properties (e.g., due to growth condition, taxonomy, etc.)	- Measurements directly linked to theoretical basis for remote sensing of phytoplankton
Fluorescence Excitation and Emission Spectra	- Simple and inexpensive method for extracted chlorophyll concentration - *In vivo* excitation and emission spectra useful for some group-specific assessment - Rapid and easy - *In situ* tools available	- Interpretation of *in vivo* fluorescence signal is complex and dependent on taxonomy and physiology - Assumptions required to convert *in vivo* signals to biomass - Uncertainty caused by intra-group variability in pigments and associated fluorescence	- Basis of most total phytoplankton biomass assessments - Used in active-passive remote sensing to detect phytoplankton types from laser-based remote sensing from aircraft - Solar-induced chlorophyll fluorescence is amenable to remote sensing
Successive Filtration	- Relatively simple	- Cell breakage and filter clogging can lead to inaccuracies - Practical constraints impose limits on the number of size classes that can be measured - Time consuming - No taxonomic information	- Most direct assessment of size-based biomass

rather than selected components, and those that make use of optical properties of phytoplankton may be the best candidates for comparison with satellite estimates.

For remote sensing, *in situ* observation must be "the truth" against which any algorithm is validated. Yet, as this review of available field and laboratory methods

emphasizes, none may be considered perfect for detection and quantification of phytoplankton types (Table 2.3). This presents a major challenge for developing and evaluating remote sensing approaches. In addition to the limitations associated with each of the methods, there is also the overarching challenge imposed by the differences in temporal and spatial scales between current capabilities for sea-truth and satellite-based measurements. Future prospects for expanded *in situ* sensors and deployment modes - emphasizing high resolution time series sites and numerous mobile platforms - will be welcome advances for addressing these problems.

<div style="border:1px solid #999; display:inline-block; padding:6px 14px; color:#2a5db0;">Chapter 3</div>

Detection of Dominant Algal Blooms by Remote Sensing

Chuanmin Hu, Shubha Sathyendranath, Jamie D. Shutler, Christopher W. Brown, Tim S. Moore, Susanne E. Craig, Inia Soto and Ajit Subramaniam

3.1 Introduction

The launch of the proof-of-concept Coastal Zone Color Scanner (CZCS) onboard the Nimbus-7 satellite in 1978 provided unprecedented data to study the biology of the oceans (Hovis et al., 1980). For the first time, chlorophyll-a concentrations in the surface ocean could be estimated at synoptic scales (Gordon et al., 1980; Smith and Baker, 1982), leading to improved understanding of the ocean's primary productivity and biogeochemistry (Mitchell, 1994). After about a 10-year gap, the Sea-viewing Wide Field-of-view Sensor (SeaWiFS) mission continued ocean-colour observations from 1997, followed by other sister missions such as the Moderate Resolution Imaging Spectroradiometer (on MODIS-Terra 2000, and -Aqua, 2002) and the Medium Resolution Imaging Spectrometer (MERIS, 2002 — 2012).

While the main goals of these missions were to determine the chlorophyll-a content and primary productivity the global oceans, recent efforts showed that it was also possible to map distributions of major phytoplankton functional types (PFTs) in the global open ocean (for example, Subramaniam et al., 2002; Sathyendranath et al., 2004b; Alvain et al., 2005; Ciotti and Bricaud, 2006; Cannizzaro et al., 2008; Nair et al., 2008; Raitsos et al., 2008; Brewin et al., 2010c; Mouw and Yoder, 2010; Moisan et al., 2012; 2013). Although most of these results are preliminary, they show great potential for studying biodiversity and bloom dynamics in the ocean.

The principle of detecting PFTs from space relies on their spectral differences in their contributions to remote sensing reflectance (R_{rs}, sr^{-1}), which in turn is determined by the spectral absorption (a, m^{-1}) and backscattering (b_b, m^{-1}) coefficients of the ocean (pure water and various particulate and dissolved matters):

$$R_{rs} = Gb_b/(a + b_b) = G(b_{bw} + b_{bp})/(a + b_{bw} + b_{bp})$$
$$= G(b_{bw} + b_{bp})/(a_w + a_B + a_d + a_g + b_{bw} + b_{bp}), \qquad (3.1)$$

where a is the sum of the individual absorption coefficients of water (a_w), phy-

toplankton pigments (a_B), coloured dissolved organic matter (a_g), and detrital particles (a_d). Here, G is a parameter related to the solar zenith angle and sensor viewing geometry. For simplicity the dependence on wavelength (λ) is omitted in the equation.

The algorithms to differentiate the PFTs make use of their different absorption and backscattering properties either implicitly (e.g., through empirical regression) or explicitly (e.g., through deriving the pigment-specific absorption). Whereas all these approaches can be found in the published literature, this chapter presents a brief summary and several examples on how to utilize the optical properties (R_{rs}, a, b_b) derived from remote sensing measurements to differentiate phytoplankton blooms. Some indirect methods that infer the distributions of PFTs from other satellite products, such as chlorophyll-a concentration, are also described. The objective is to demonstrate the current approaches of bloom differentiation and discuss their advantages and disadvantages, in the hope that improved methods may be developed from future satellite sensors equipped with more spectral bands at higher ground resolution.

3.2   Detection of Diatom Blooms

3.2.1   Background

Diatoms, typically large-celled organisms, incorporate silica that is used to form the characteristic frustules (a type of exoskeleton), which envelopes the diatom cells. Their large size as well as the presence of silica endows diatoms with a high sinking rate, facilitating the biological transport of organic material and silica to deep waters, or to the sediments. Since there is often a size-dependent relationship between prey and predators, the zooplankton that feed on diatoms tend to be different from those that rely on smaller phytoplankton cells, and these differences in the trophic structure can be transmitted all the way up the food chain. High turbulence and associated vertical mixing can counteract the sinking to some extent, and it is generally understood that diatom blooms are often associated with areas of high turbulence, which in turn are often associated with high vertical fluxes of nutrients. These properties set diatoms apart from other phytoplankton, and there is considerable interest in their distinct functional roles, from a biogeochemical perspective.

3.2.2   Distribution

Diatoms tend to dominate Spring blooms in temperate and high latitude areas, and can also be an important constituent of Autumn phytoplankton blooms. They are associated with upwelling areas, and in general with high-nutrient, high-turbulence,

low-light waters. Along a trophic gradient, they tend to dominate in high-chlorophyll waters (see also Chapter 1 of this report).

3.2.3   Optical traits

The absorption spectra of diatoms tend to be flat because of pigment packaging that typically occurs in large phytoplankton cells. As a result, the ratio of the absorption peak in the blue to that in the red is low for diatoms, compared with that of smaller cells. Their specific absorption coefficient (absorption coefficient at a given wavelength, normalized to the chlorophyll concentration in the sample) also tends to be different, being smaller than corresponding values for smaller cells. The optical traits of diatoms are further modulated by their pigment composition. Dierssen and Smith (2000) have reported that the diatoms tend to show less backscattering than other phytoplankton populations at similar concentrations.

3.2.4   Remote-sensing algorithms for identification and mapping of diatoms

The algorithms that have been proposed so far fall into three categories:
- ❖ Abundance-based methods
- ❖ Optical-trait-based methods
- ❖ Ecological approaches

Most of these models are described in other chapters of this report in different contexts, but they are mentioned here briefly for completeness. Algorithms types that are not detailed in the other chapters are described here at greater length.

3.2.4.1   Abundance-based methods

The simplest approach to map diatom distribution from space exploits the common occurrence and frequent dominance of diatoms in high-chlorophyll waters. In their implementation of this approach, Hirata et al. (2011), used *in situ* data on HPLC pigment composition of phytoplankton to estimate the fractional contribution of diatoms to total chlorophyll-a in any given sample. Such information collected from a large number of samples from diverse regions was used to plot the fraction of chlorophyll associated with diatoms as a function of total chlorophyll-a concentration in the sample. An empirical function was then fitted to the data to compute the diatom fraction as a function of chlorophyll-a concentration. According to their Table 2, fractional chlorophyll-a concentration [0.0 – 1.0] associated with diatoms (F_d) is computed from total chlorophyll-a (C_T) as:

$$F_d = [1.33 + exp(-3.98C_T + 0.20)]^{-1}, \qquad (3.2)$$

(where the model parameters are reported to two decimal points). Once this relationship is established, diatom concentration (in units of chlorophyll-a) can be

derived from satellite-based maps of chlorophyll-a. This method is also discussed in Chapter 5 that deals with algorithms that are designed to identify many functional types simultaneously.

Chapter 4 deals with algorithms designed to map size classes of phytoplankton. Of the typical size classes that are studied, microplankton (with diameters greater than 20 μm) have a close association with diatom algorithms, since microplankton are often made up of dinoflagellates and diatoms. In the absence of dinoflagellates, the microplankton component may be equated with diatoms. Many algorithms that deal with size classes are abundance based (see Chapter 4 for further details regarding such algorithms).

3.2.4.2 Optical-trait-based methods

Diatoms, being typically large-celled, have absorption spectra that are flattened relative to those of smaller cells. The distinctive characteristics of diatom absorption spectra have been exploited to discriminate them from other phytoplankton. In the method of Sathyendranath et al. (2004b) and Jackson et al. (2011), two versions of a spectrally-resolved reflectance model are implemented, one using absorption characteristics of diatoms and the other using that of non-diatoms. The underlying absorption models for diatoms and non-diatoms are based on simultaneous *in situ* measurements of absorption spectra and chlorophyll concentrations made in waters dominated by diatoms and non-diatoms. Relationships are then established between chlorophyll concentration and reflectance ratios at selected pairs of wavebands, for diatom and non-diatom models. These results are then applied to atmospherically-corrected remote-sensing reflectance values, which are used to compute chlorophyll concentration from two pairs of reflectance ratios (for diatom and non-diatom models). The difference between pairs of computations is then examined. If the percentage difference in the two chlorophyll values computed using the diatom model is less than the corresponding value for the non-diatom model, then the pixel is assigned to diatoms. Otherwise, the pixel in question is assumed to be dominated by non-diatoms. The method is represented schematically in Figure 3.1.

This method is designed to identify whether or not diatoms dominate phytoplankton populations in a particular location. Once this decision is made, the appropriate chlorophyll value can be assigned to the population. Also, if the results are cumulated for a finite period, say a week or a fortnight, then one can generate probability maps of diatom dominance for the area and for the period. This method is not designed to yield fractional contributions from diatoms to total chlorophyll-a in a single image. The method of Sathyendranath et al. (2004b) was developed for the North West Atlantic, using regional observations of phytoplankton absorption. Jackson et al. (2011) found that the optical properties of diatoms in the South East Pacific differed from those of the North West Atlantic, and that the use of regional observations of phytoplankton absorption in the reflectance model improved the
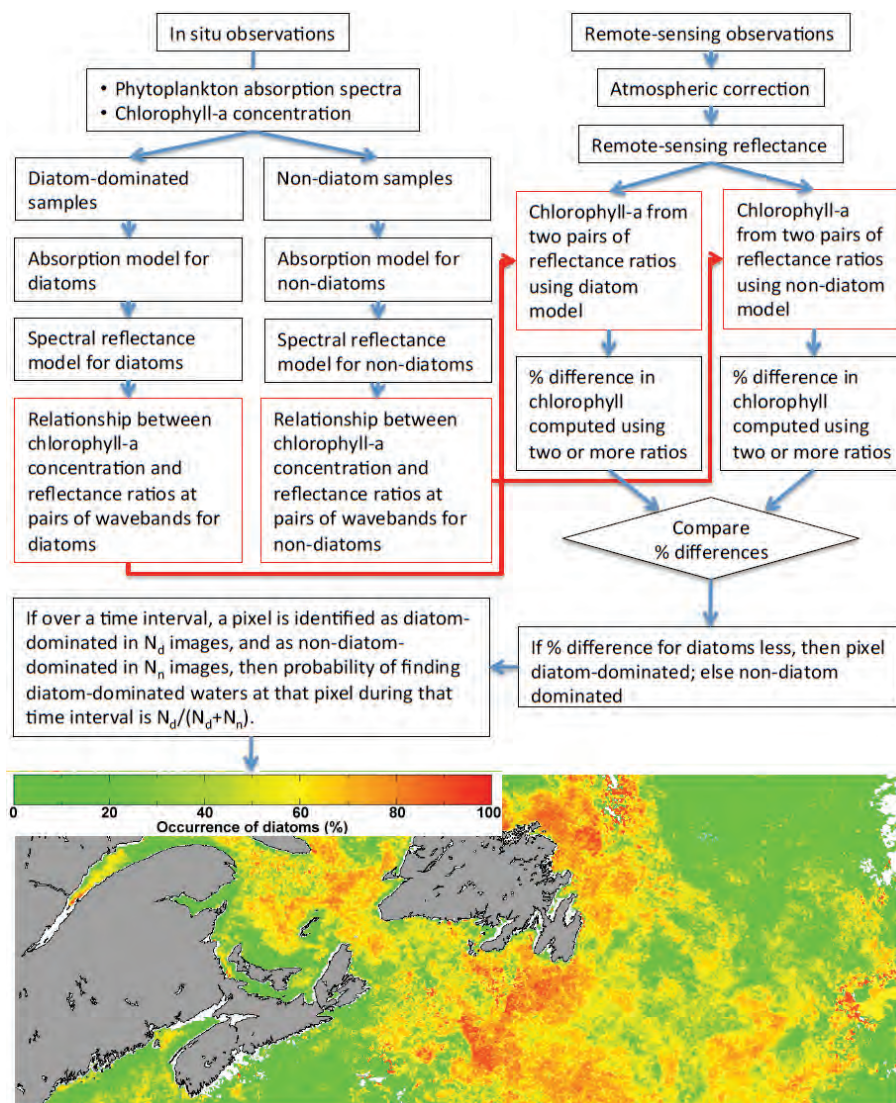
Figure 3.1 Schematic flow chart showing the remote sensing approaches and steps to classify diatom blooms.

performance of the regional model. The work of Jackson et al. (2011) points to a general note of caution: diatoms represent a large diversity of species with a broad range in size and a variety of cell shapes. As long as there are regional differences in the species composition of bloom-forming diatoms, the model would ideally be tuned for the region.

The optical traits of phytoplankton are also exploited in the differential optical absorption spectroscopy (DOAS) developed by Perner and Platt (1979) and adapted for phytoplankton applications by Bracher et al. (2009) and Sadeghi et al. (2012a). The method is applied to satellite data with very high spectral resolution (hyper-

spectral data) from the Scanning Imaging Absorption Spectrometer for Atmospheric Chartography (SCIAMACHY) onboard the ENVISAT satellite. The method is described in Chapter 5.

An alternative approach to exploiting the differences in the optical traits of diatoms for their identification is to examine observed differences in their reflectance spectra, as was done in the algorithm of Alvain et al. (2005). Using a large number of *in situ* pigment observations that provided information on diatom-dominated waters over a range of chlorophyll concentrations, they compared the corresponding reflectance spectra with those from non-diatom dominated waters and established statistical differences in the reflectance spectra that were then used to map diatom-dominated waters from satellite data. A theoretical underpinning for their method is provided in Alvain et al. (2012) and the full method (Alvain et al., 2005; 2012) is discussed in detail in Chapter 5 of this report.

As in the case of abundance-based models, there are algorithms for identification of size classes that are based on optical traits. Again, to the extent that microphytoplankton classes may be dominated by diatoms and not dinoflagellates, we can infer some information on diatom distribution from such algorithms (see Chapter 4 for details regarding these types of algorithms).

3.2.4.3 Ecological approaches

Another approach that has been used to map phytoplankton types from space is based on the ecological and geographical preferences of various phytoplankton types (e.g., Raitos et al., 2008). These authors used a number of satellite-derived inputs to map phytoplankton types, including chlorophyll and water-leaving radiance (at 555 nm) from ocean-colour data, along with the photosynthetically-active radiation (PAR) data provided by NASA, sea-surface temperature (SST) from the Advanced Very High Resolution Radiometer (AVHRR) and wind-stress data derived from satellite scatterometers. The radiance value served as a proxy for the backscattering coefficient, which is known to vary with phytoplankton type. The *in situ* data on phytoplankton types, from the Continuous Plankton Recorder (Reid et al., 2003a), were analyzed to determine dominant phytoplankton types in each sample using the *Z* factor standardized method. The data for the North Atlantic Ocean yielded over 3000 match-up data points between the years 1997 and 2003, and were complemented with information on the geographic location (latitude and longitude) of the sample. The data were processed using a probabilistic neural network to associate patterns of *in situ* data (including location) with dominant phytoplankton types. Once the neural network is established, the probabilistic distributions of the phytoplankton types are mapped using the satellite data and the locations as inputs. The method was used to map areas dominated by diatoms, dinoflagellates, coccolithophores or silicoflagellates. More recently, Palacz et al. (2013) have also used an ecological approach to map phytoplankton types. See Chapter 5 for further

details on ecological approaches.

3.3 Detection of Coccolithophore Blooms

3.3.1 Background

Coccolithophores are marine phytoplankton that form external calcium carbonate ($CaCO_3$) scales or platelets (coccoliths) and are abundant at both high and low latitudes where they can form large blooms (Beaufort et al., 2008). They are considered to be major calcifiers in the open ocean and play a key role in the oceanic carbon cycle (Iglesias-Rodriguez et al., 2002; Balch et al., 2005). As with all phytoplankton, coccolithophores consume carbon dioxide (CO_2) during photosynthesis and release CO_2 during respiration, yet they also generate CO_2 when they produce coccoliths. This pelagic calcification counter-acts the CO_2 uptake related to their fixation of carbon during primary production (Harlay et al., 2010). As a consequence, their presence affects the air-to-sea CO_2 flux and the oceanic CO_2 sink in a complex manner (Shutler et al., 2013). Sedimentation of their coccoliths also constitutes a major regional input to carbonate sediments, which serves as the largest reservoir of carbon on Earth (Iglesias-Rodriguez et al., 2002). These phytoplankton are also linked to the generation of dimethyl sulphide (DMS) gas (Keller et al., 1989; Keller, 1989). Once ventilated to the atmosphere, DMS is oxidized to a variety of compounds, including sulfate aerosols. These aerosols contribute to the pool of cloud-condensation nuclei (Steinke et al., 2002; Marandino et al., 2008) and affect the Earth's radiation budget (and thus climate) by scattering sunlight and influencing cloud physics and albedo. The DMS-derived sulfate aerosols can also react with rain droplets to produce acid rain. Consequently, coccolithophores are considered to play an important role in oceanic carbon and sulphur cycles and they are able to influence our climate. Furthermore, these phytoplankton may be sensitive to (and be important indicators of) climate change (Smyth et al., 2004; Winter et al., 2013) and ocean acidification (Tyrrell, 2008).

Of the numerous coccolithophores that live in the sun–lit layers of the world's oceans, the cosmopolitan species *Emiliania huxleyi*, when present at high concentrations (blooms) in the surface layer, can profoundly impact the optical properties of the upper ocean (Balch et al., 1991; Tyrrell et al., 1999; Holligan et al., 1993), making them visible to the naked eye and from Earth observation (EO). They occur predominantly during the spring and summer months (Tyrrell and Merico, 2004), although the remains from previous blooms may be visible at the surface during winter months, due to re-suspension within the water column from storm mixing (Broerse et al., 2003). In the later stages of growth these phytoplankton shed their coccoliths, turning the water a milky or turquoise-white colour (Holligan et al., 1983; Merico et al., 2003; Smyth et al., 2004). These conditions are easily discernible from satellite ocean-colour data owing to their high reflectance across the visible

spectrum. This unique characteristic allows the study of their frequency and distribution by satellite EO (Brown and Yoder, 1994; Cokacar et al., 2001; Merico et al., 2003; Smyth et al., 2004; Shutler et al., 2013). This characteristic also means that their presence can distort spectral band ratio EO ocean-colour chlorophyll-a estimations and certain atmospheric correction algorithms (Gordon et al., 1988; Balch et al., 1989). Consequently, data locations deemed to contain coccolithophore bloom are routinely masked from NASA ocean-colour chlorophyll-a retrievals. Due to the large spatial extent over which these blooms occur, EO data provide a useful tool for mapping their aerial extent. Methods to detect and map these blooms from space have concentrated on spectral approaches of varying complexity (Groom and Holligan, 1987; Brown and Yoder, 1994; Brown and Podesta, 1997; Brown, 2000; Cokacar et al., 2001; Gordon et al., 2001; Shutler et al., 2010; Moore et al., 2012).
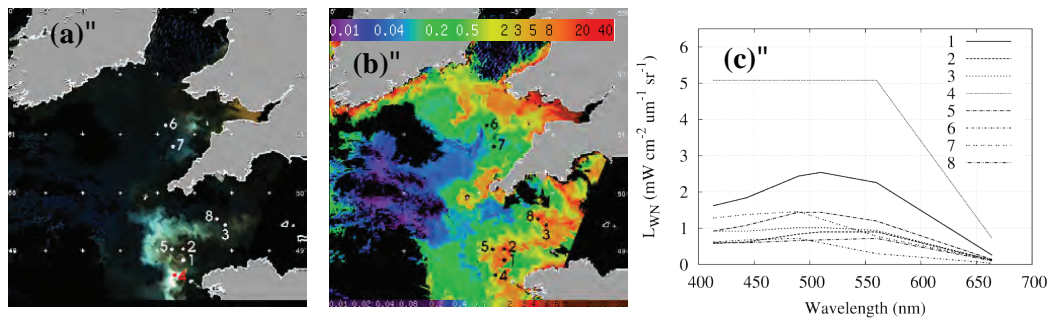
Figure 3.2 Example MERIS data on 20 June 2003 1124 UTC off the West English Channel. The area of interest is from 48 to 52°N and 10 to 2°W. The a) MERIS three-band pseudo true-colour image from combining three L_{wN} bands (560, 490 and 443 nm), b) MERIS Algal 1 chlorophyll-a (units mg m^{-3}) scene with positions of eight study sites labelled, c) normalised water leaving radiance spectra for each of the eight sites labelled in a) and b).

In this section we define a bloom as a phytoplankton concentration leading to a spectral reflectance that is greater than the characteristic background reflectance for a particular region. When studying coccolithophores using Earth observation these concentrations are likely to be principally detached coccoliths, with some coccospheres (coccolithophore cells). Figure 3.2a shows a MERIS pseudo-true colour image and Figure 3.2b shows a chlorophyll-a scene of the Celtic sea in 2004; both images are labeled with eight locations. The normalized water leaving radiance spectra for each of these eight different locations are plotted in Figure 3.2c (these spectra have been constructed using eight of the MERIS bands). The spectral response for point 4 indicates that the spectral signal in this image element (or pixel) is dominated by coccolithophores as it shows a high (saturated) and spectrally flat response across all visible wavebands. From looking at Figure 3.2a it is apparent that position 4 is located within the white area of a coccolithophore bloom (i.e. white indicates a spectrally flat and high response across all wavelengths). In contrast, points 1–3 and 5–8 exhibit a range of different spectral responses (Figure 3.2c) with

much lower signals, and likely represent a combination of other phytoplankton species, coloured dissolved material, or suspended particulates.

3.3.2 Detection using Earth observation

The earliest approach developed to detect these phytoplankton from EO uses data from the AVHRR sensors orbiting the Earth from 1982 to present. This sensor is carried onboard the NOAA series of satellites and the longevity of this data record provides the means to study coccolithophores blooms over a time series extending over 30+ years, with global coverage. However, due to lower detector gain and sensitivity in the AVHRR channel of interest (channel 1, 580 – 680 nm), this method is only able to detect very intense coccolithophore blooms. This approach, originally developed by Groom and Holligan (1987), and more recently refined by Smyth et al. (2004), has been used successfully to detect the presence of coccolithophores in the north Atlantic (Trees et al., 1992; Holligan et al., 1993), the Barents Sea (Smyth et al., 2004) and various other subpolar waters (Uz et al., 2013). However, due to the reduced sensitivity, it is difficult to determine the full extent of surface blooms using this approach, and regions of less intense blooms (i.e., the full extent of any perimeters) are not detected.

A more complete description of the spatial extent of *E. huxleyi* blooms is possible by using data from dedicated ocean-colour radiometric sensors, such as SeaWiFS, MODIS and MERIS. The simplest approach to detect these phytoplankton groups using visible spectrum sensors is to examine the normalized water leaving radiance data, $L_{wN}(\lambda)$ (or equivalent $R_{rs}(\lambda)$), from a single spectral band. Due to the ability of coccolithophores to scatter light at all wavelengths, any band in the visible spectrum can potentially be used, but typically a band in the green part of the spectrum, e.g., $L_{wN}(555)$, is employed. This simplistic approach enables the identification of these phytoplankton under the assumption that no other highly scattering particulates are present in the water. For example, this approach has been used as a proxy to study coccolithophore blooms in the waters south of Iceland (Raitsos et al., 2006). Similarly, by producing a composite image using three spectral bands of normalized water leaving radiance data, regions of suspected coccolithophores can be identified by their characteristic relatively flat spectral response, i.e., coccolithophore blooms appear white. For MODIS, such a composite would use 547, 443 and 412 nm data as the three layers of a pseudo-true-colour image. A more advanced species-specific approach was developed for CZCS data (Brown and Yoder, 1994) and later updated for SeaWiFS (Brown, 2000; Cokacar et al., 2001). This empirical approach is based on thresholding the spectral response across a combination of three spectral bands, and provides a species-specific description of bloom extent. The algorithm was developed using an *in situ* dataset collected in the North Atlantic. Due to the spectral similarity between bands, this approach has also been successfully applied to MODIS. Consequently, it is used within the standard NASA data processing chain (and the

NASA SeaDAS tool) for both SeaWiFS and MODIS data.

The presence of spectrally-mimicking conditions, such as re-suspended sediments, may cause problems with this approach and can produce false indications of blooms (Brown and Yoder, 1994; Broerse et al., 2003). This causes significant problems when the algorithm is applied to blooms in certain shelf seas and coastal zones, particularly in lower latitudes, which are often characterised by high concentrations of reflective suspended particulates. This characteristic is especially prevalent during winter months, creating problems when studying annual trends or long time series. Work by Shutler et al. (2010) attempts to overcome this shortfall through exploiting temporal correlation to reduce the effects of the background signals. Through analyzing a time series of data, a statistical description of the region is generated. This allows anomalous regions (i.e., suspected coccolithophore blooms) to be separated from the background variations (i.e., suspended particulates from river outflows and mixing). By applying the spectral approach of Brown and Yoder (1994) to only those regions that are anomalous, the number of false positives can be reduced. Whilst considerably reducing the number of false positives, this technique does involve a computation overhead. The approaches of Brown and Yoder (1994) and Shutler et al. (2010) yield similar results in open-ocean waters, under the assumption that all suspended particles are due to coccolithophores. However, the generation and analysis of long time series of coccolithophore blooms in coastal regions will require the approach of Shutler et al. (2010). In theory, the approaches of Brown and Yoder (1994) and Shutler et al. (2010) are also applicable to MERIS data, yet to date this approach for MERIS data has not been investigated. No explicit algorithm for detecting coccolithophores has been included in the standard ESA MERIS data processing chain. However, regions exhibiting high levels of scattering in the visible spectrum are labelled by the MERIS atmospheric correction algorithm (Aiken and Moore, 2000). In the open ocean, these regions are likely to be blooms of coccolithophores.

The only approach to date that has been applied to SeaWiFS, MODIS and MERIS data is that of Moore et al. (2012). This approach combines an optical water type (OWT) approach with that of the spectral classifier of Brown and Yoder (1994). In the OWT scheme, mean reflectance vectors for coccolithophore blooms were developed from Brown and Yoder (1994) classified pixels (i.e., NASA level 2 flagged pixels) in SeaWiFS data. These vectors were then added to the NOMAD-based OWT vectors (Moore et al., 2009) and filled a 'missing class' specific to coccolithophore blooms, and thus provided a new coccolithophore bloom water type. Applying these techniques to SeaWiFS, MODIS and MERIS data provides the means to study coccolithophores blooms over a >13 year (1997 onwards) global time series. The work of Shutler et al. (2010; 2013) and Moore et al. (2012) include results from applying a selection of these algorithms over multiple year time series of the North Atlantic and global oceans respectively.

Determining the concentration of detached coccoliths and calcite is also possible

from EO data using two methods, both of which are based upon the backscatter coefficient at 547 nm, i.e., $b_b(547)$. The 2-band method uses a look-up-table (LUT) to estimate $b_b(547)$ based on the remote sensing reflectances in the blue and green bands (Gordon and Balch, 1999; Balch et al., 2005). The 3-band method employs a model that uses reflectances at $L_{wN}(667)$, $L_{wN}(748)$ and $L_{wN}(869)$ to estimate $b_b(547)$ (Gordon et al., 2001). Both methods return similar results for moderate to high concentrations, whereas the 2-band method performs better at low calcite concentrations. The standard NASA processing (and the SeaDAS tools) for SeaWiFS and MODIS data combines the two approaches (Gordon and Balch, 1999 and Gordon et al., 2001) into a single blended algorithm. If the 2-band methods fails, the 3-band method is used to retrieve the estimate. The existence of other suspended particulates reduces its performance, so care must be taken when applying this algorithm in coastal waters.
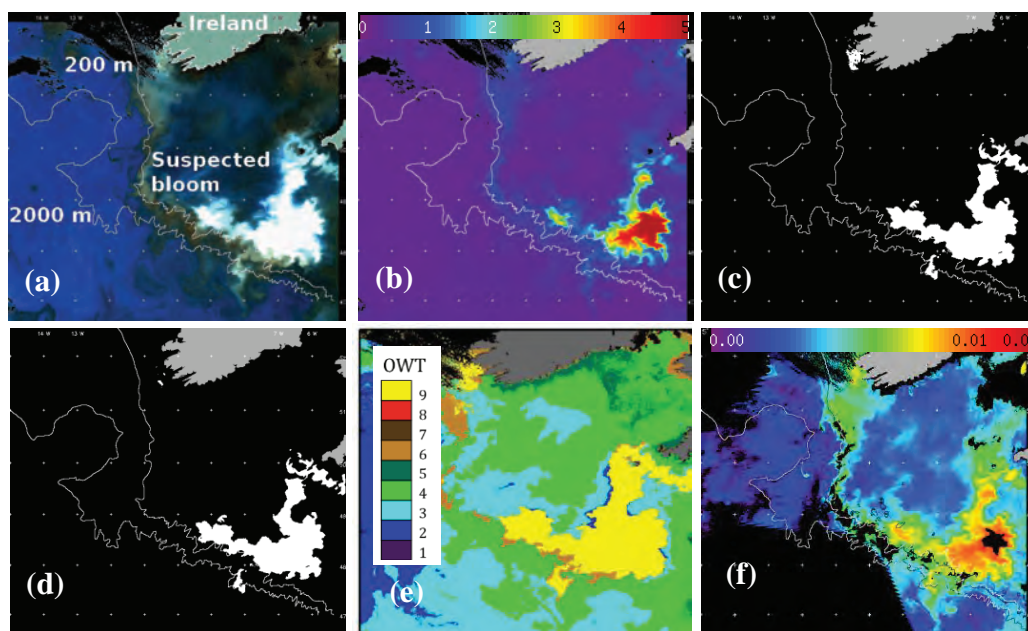
Figure 3.3 Example scene of a coccolithophore bloom on 15 June 2004 with land shown in grey (SeaWiFS at 1348 UTC and MODIS-Aqua at 1335 UTC). a) SeaWiFS L_{wN} three-band pseudo true-colour composite (555, 490 and 443 nm), b) SeaWiFS $L_{wN}(555)$ response (units mW cm^{-2} sr^{-1} μm^{-1}), c) applying the approach of Brown and Yoder (1994) to SeaWiFS data, d) applying the approach of Shutler et al., (2010) to SeaWiFS data, e) applying the OWT approach of Moore et al. (2012) to SeaWiFS data and f) the combined two and three band calcite concentration result using Gordon et al. (2001) and Gordon and Balch (1999) as applied to MODIS-Aqua data (units moles m^{-3}).

Figure 3.3 shows examples of using the seven different approaches to study a coccolithophore bloom in the Celtic sea on 15 June 2004. Figure 3.3a shows a SeaWiFS L_{wN} three-band pseudo-true colour image, which clearly shows a large

region of white illustrating a spectrally flat signal across all visible wavelengths. Figure 3.3b shows the L_{wN} at the 555 nm spectral band; Figure 3.3c shows the output of the Brown and Yoder (1994) algorithm for the SeaWiFS scene, Figure 3.3d shows the result of Shutler et al. (2010) for the same SeaWiFS scene, and Figure 3.3e shows detection using the OWT approach of Moore et al. (2012) on SeaWiFS data. Figures 3.3b and 3.3c are comparable as this scene was captured during the northern hemisphere summer when these waters are stratified. Figure 3.3f shows the estimated calcite concentration using the combined approach of Gordon and Balch (1999) and Gordon et al. (2001) applied to MODIS-Aqua data. The region of missing (black) pixels within the bloom in Figure 3.3f is due to the MODIS-Aqua 547 nm band saturating due to the intense scattering of light.
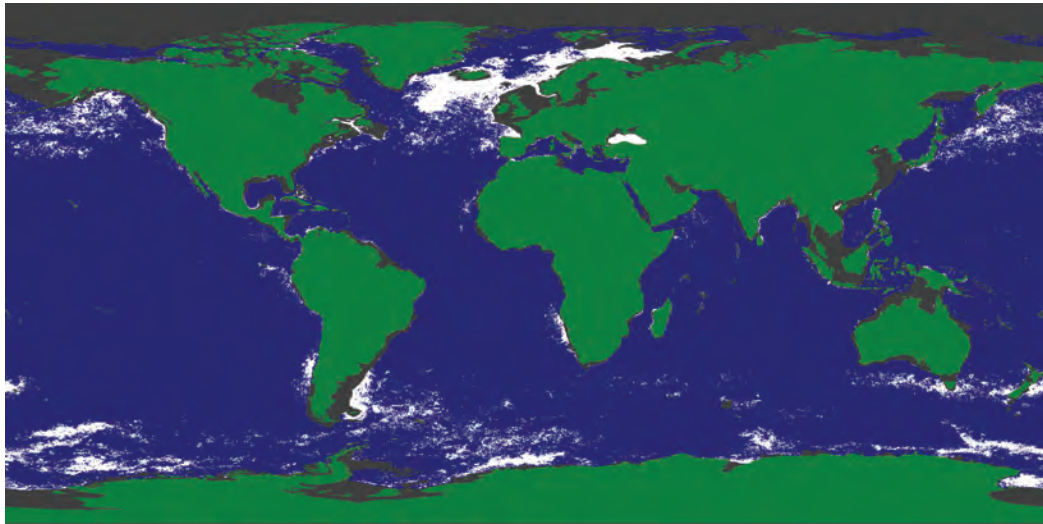
Figure 3.4 Composite of classified coccolithophore blooms in SeaWiFS imagery dating from October 1997 to September 2009 using the approach of Brown and Yoder (1994) with the updated spectral criteria in Brown (2000). The coccolithophore bloom class is white, the non coccolithophore bloom class is blue, and land is green. Grey indicates areas where waters are less than 200 meters deep, where the algorithm is prone to errors, and lacking image coverage.

Figure 3.4 shows all the regions identified as coccolithophore blooms in the global oceans between 1997 – 2009, as detected by the approach of Brown and Yoder (1994) using the updated spectral criteria (Brown, 2000). Regions of water depth of less than 200 m have been masked in grey. As MODIS instruments and the most recent VIIRS instrument continue the ocean-colour observations from the SeaWiFS era, time-series of similar maps will provide unprecedented information on the formation, evolution, and dynamics of coccolithophore blooms on both global and regional scales.

3.4 Detection of *Karenia brevis* and *K. mikimotoi* Blooms

3.4.1 Background

The dinoflagellate *Karenia brevis* forms massive harmful algal blooms (HABs) nearly annually in the Gulf of Mexico (Tester and Steidinger, 1997; Magaña et al., 2003; Walsh et al., 2006). These blooms, which are commonly referred to as "red tides", produce brevetoxin, a neurotoxin responsible for neurotoxic shellfish poisoning, massive fish kills, marine animal mortality, and when aerosolised in sea spray, respiratory irritation in humans and other mammals (Steidinger, 2009). As a result of these potential effects, *K. brevis* blooms have enormous economic implications in the form of fisheries and tourism-related losses for all five of the adjacent Gulf coast states (Anderson et al., 2000).

The dinoflagellate *Karenia mikimotoi* is a high biomass HAB species that has been identified in harmful concentrations in European waters and the coastal waters of New Zealand (Faust and Gulledge 2002; Haywood et al. 2004; Rhodes et al. 2004; Davidson et al. 2009). This dinoflagellate can be commonly present within the marine flora at relatively low densities, but when the conditions allow, it can bloom sporadically in high densities. These blooms can result in mortality of farmed fish and other marine animals through the production of haemolytic cytotoxins (Satake et al., 2005) and the hypoxic conditions often created by high cell densities (Tangen, 1977). Traditionally, coastal management agencies and researchers have relied on analyses of discrete water samples to detect and assess *K. brevis* and *K. mikimotoi* blooms. The samples are usually acquired from nearshore waters, and the analyses include microscopic cell counts, toxin analyses and determination of chlorophyll-a concentration. However, these approaches are time consuming, labour intensive, and spatially and temporally limited. As a result, data collected in this way are often susceptible to considerable spatial bias and are ultimately inadequate in terms of providing timely warnings of bloom events for coastal management agencies (Cannizzaro et al., 2008). The challenge, therefore, has been to develop monitoring systems with sufficiently high temporal and spatial resolution that permit the accurate and timely identification of *K. brevis* blooms and provide the means to monitor bloom development and transport. As *K. brevis* and *K. mikimotoi* blooms strongly modulate the colour of surface waters (Carder and Steward, 1985), measurement of ocean optical properties, either *in situ* or from space-based platforms, may provide a robust means to reveal synoptic patterns in bloom formation and transport at various temporal and spatial scales (Steidinger and Haddad, 1981; Cullen et al., 1997; Tester and Stumpf, 1998; Schofield et al., 1999; Kirkpatrick et al., 2000; Stumpf, 2001; Miller et al., 2006; Stumpf et al., 2009; Davidson et al., 2009; Shutler et al., 2012; Kurekin et al., 2014).

3.4.2 *K. brevis* bloom detection

Measurement of the spectral absorption properties of phytoplankton may allow HAB detection since phytoplankton species often possess taxon-specific pigments (Hoepffner and Sathyendranath, 1993; Johnsen et al., 1994). However, due to similarities in the absorption spectra of phytoplankton pigments and pigment packaging effects, absorption based discrimination amongst species can be challenging (Garver et al., 1994). This is particularly true of *K. brevis*, which lacks the light harvesting pigment, peridinin, normally associated with dinoflagellates. Instead, it contains fucoxanthin, a pigment common to many algal groups such as diatoms, prymnesiophytes and chlorophytes (Jeffrey and Vesk, 1997). The only pigment unique to *K. brevis* is gyroxanthin diester that absorbs light in the same spectral region as many carotenoids (Millie et al., 1995; Millie et al., 1997), but may impart sufficient uniqueness to *K. brevis* absorption spectra to allow discrimination from other species (Millie et al., 1997; Kirkpatrick et al., 2000; Craig et al., 2006). This property has been exploited to develop an approach whereby the fourth derivatives of a mixed phytoplankton assemblage absorption spectrum and a reference *K. brevis* absorption spectrum are calculated to enhance minor spectral inflections, then their similarity to each other is quantified by means of a similarity index (Millie et al., 1997; Kirkpatrick et al., 2000; Craig et al., 2006). The magnitude of the similarity index (SI) is then examined for correlation with proxies of *K. brevis* biomass. Kirkpatrick et al. (2000) and Robbins et al. (2006) used a liquid waveguide capillary attached to a spectrometer deployed on various *in situ* platforms to measure the hyperspectral phytoplankton absorption coefficient ($a_B(\lambda)$ m^{-1}). This was then used to calculate an SI to allow the identification and tracking of *K. brevis* blooms. Craig et al. (2006) derived $a_B(\lambda)$ from *in situ* hyperspectral $R_{rs}(\lambda)$ using an inversion algorithm (Lee et al., 2002) and found a strong correlation between *K. brevis* cell counts and the magnitude of the SI (Figure 3.5a), thereby demonstrating the potential of apparent optical property measurements for this approach. A sensitivity analysis also showed that the approach was affected by CDOM and *K. brevis* cell concentrations (Craig et al., 2006). These methods rely on hyperspectral data to reveal the subtle spectral inflections imparted by the *K. brevis* pigment complement, and so, are not suitable for use with multispectral sensors.

Other approaches for optically detecting *K. brevis* focus on methodologies that are suitable for use with the multispectral data provided by current satellite sensors. Steidinger and Haddad (1981) demonstrated the first use of satellites for detecting *K. brevis* blooms using the CZCS sensor, and subsequently satellite remote sensing has been proposed as a means of detecting, monitoring and characterising the location and extent of HABs (Cullen et al., 1997; Tester and Stumpf, 1998; Schofield et al., 1999). Stumpf et al. (2003) developed the chlorophyll anomaly approach, and this method, along with other ancillary data, forms the basis of the operational product currently in use by the US National Oceanic and Atmospheric Administration (NOAA)

$r^2 = 0.743$
N = 23

Similarity Index

log cells ml^{-1}

$< 10^3$
$10^3 - 10^4$
$10^4 - 10^5$
$> 10^5$

Morel (1988)
upper + lower
optimal

K. brevis flag

$b_{bp}(550)$ (m^{-1})

bloom edge

Chl (mg m^{-3})
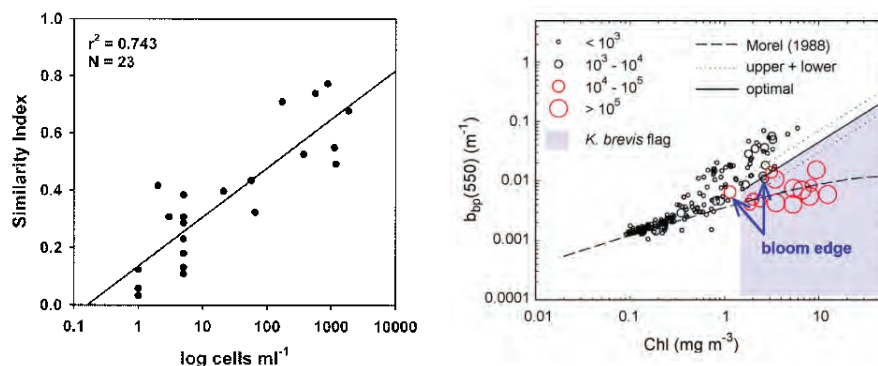
Figure 3.5 (a) Surface *K. brevis* cell concentration versus SI magnitude (Craig et al., 2006); (b) Relationship between Chlorophyll and $b_{bp}(550)$ for the 10 ECOHAB cruises between 2000 and 2001 on the central west Florida Shelf. Symbol size increases with increasing *K. brevis* cell concentration (cells l^{-1}). Upper and lower threshold functions (dotted lines) for separating *K. brevis* bloom ($>10^4$ cells l^{-1}) and non-*K. brevis* bloom ($<10^4$ cells l^{-1}) data were generated using chlorophyll-specific particulate backscattering coefficients, equal to 0.007 m^2 mg^{-1} and 0.003 m^2 mg^{-1} respectively. The solid line represents the optimal threshold function, generated using = 0.0045 m^2 mg^{-1}. The shaded area represents the classification criteria (Chl $\geq$ 1.5 mg m^{-3} and $\leq$ 0.0045 m^2 mg^{-1}) for determining *K. brevis* blooms. An empirical relationship determined for Case 1 waters (Morel, 1988) (dashed line) is also shown. Arrows point to misclassified data points (8000 and 13,000 cells l^{-1}) that were located on the edge of a bloom (Cannizzaro et al., 2009).

(http://tidesandcurrents.noaa.gov/hab/). Stumpf and colleagues (2003) defined an anomaly to flag for *K. brevis* as the difference in chlorophyll concentrations between a single image and a 60-day running mean ending two weeks before the image. An anomaly of >1 mg m^{-3} corresponding to a potential bloom of >1 $\times10^5$ cells l^{-1} and associated with major fish kills (Steidinger et al., 1998), was considered indicative of *K. brevis*. However, this cell concentration is more than an order of magnitude greater than the current regulatory guideline of >0.5 $\times$ 10^4 cells l^{-1} for shellfish bed closure (NSSP, 2011). Hu et al. (2008) conducted an analysis of SeaWiFS imagery spanning 1998 – 2003 from the west Florida Shelf using the chlorophyll anomaly method and found that *K. brevis* blooms, confirmed by *in situ* cell counts, were correctly identified. However, they also found that, despite the absence of widespread reports of red tides by local fishermen, the method indicated ~1000 km^2 anomaly areas between the 10 and 50 m isobaths nearly every day. This was the case even when only the late summer-fall period recommended by Stumpf et al. (2003) was considered, and optically complex regions were omitted from the analysis. Unfortunately, most of the patches flagged as possible *K. brevis* blooms did not have corresponding *in situ* cell counts for validation. However, it seems unlikely that these persistent features were always caused by *K. brevis*. Rather, it is possible that, in at least some of these instances, the anomalies are false positives caused by confounding factors such high CDOM concentration or

enhanced reflectance due to bottom reflection or benthic resuspension. Additionally, persistent elevated chlorophyll-a that results from prolonged blooms can give rise to zero-valued anomalies (i.e., no change in chlorophyll-a above the 60-day mean) thereby resulting in false negative flagging. However, the method is effective in identifying "new" blooms (Tomlinson et al., 2004; Hu et al., 2008; Tomlinson et al., 2009).

To overcome some of these difficulties (zero-valued anomalies, bottom reflection and benthic re-suspension), the approach of Shutler et al. (2012), taking into account the temporal evolution of *K. mikimotoi* blooms, may be adopted. Alternatively, Hu and colleagues (2005) combined enhanced RGB (ERGB) images and MODIS fluorescence line height (FLH) to detect and track a *K. brevis* bloom in the West Florida Shelf. ERGB images are composites constructed from imagery at 551, 488 and 443 nm, and reveal dark features associated with high absorption due to Chl and/or CDOM, and bright features associated with bottom reflection and/or sediment resuspension. FLH utilises red wavelengths (667, 678, 748 nm) to detect solar-stimulated chlorophyll fluorescence (Letelier and Abbott, 1996). The relationship between chlorophyll-a and FLH is complex due to variability in fluorescence quantum yield caused by taxonomic differences, phytoplankton physiology and light exposure history (Kiefer, 1973; Letelier and Abbott, 1996). Nonetheless, over the west Florida Shelf, Hu et al. (2005) established a robust relationship between FLH and chlorophyll-a that yielded superior estimates of chlorophyll-a compared with standard SeaWiFS band-ratio chlorophyll-a. With this relationship, they were able to use FLH to differentiate between dark ERGB features produced by high chlorophyll-a and those produced by high CDOM, thereby providing superior and more accurate feature identification than chlorophyll-a imagery. However, this technique was not developed for automatic detection and requires visual image interpretation.

Previous modelling and *in situ* studies of the optical properties of *K. brevis* have shown that it exhibits lower backscattering per unit chlorophyll compared to other species due to its relatively large size (20-40 μm) and low index of refraction (Carder and Steward, 1985; Mahoney, 2003; Schofield et al., 2006). Consistent with these findings, an *in situ* study by Cannizzaro et al. (2008) showed that *K. brevis* blooms had 3–20 times lower particulate backscattering coefficients at 550 nm ($b_{bp}(550)$) than diatom dominated waters at similar chlorophyll concentrations, and that this led to 3-4 times lower $R_{rs}(\lambda)$. Cannizzaro and colleagues (2008; 2009) also postulated that the lower $b_{bp}(550)$ may be due to a paucity of sub-micron detrital particles caused by either reduced grazing pressure due to cellular toxicity, or the inability of *K. brevis* to outcompete rapidly-growing diatoms in high backscattering, detritus rich coastal waters. Based on these findings, they developed a set of criteria for detection of *K. brevis* blooms: 1) Chl-a >1.5 mg m^{-3} 2) Chl-a:$b_{bp}(550) < 0.0045$ m^2 mg^{-1}, as defined for case 1 waters by Morel (1988) (Figure 3.5b). This approach was found to be suitable for both *in situ* and satellite based measurements of ocean colour, but false positives were sometimes obtained when CDOM absorption at 443

nm was two times or greater than $a_B(443)$ and when the water was very turbid.

To overcome the difficulties associated with obtaining accurate chlorophyll-a estimates in optically complex waters, Cannizzaro et al. (2008) proposed the use of FLH (Figure 3.6). This technique provided the ability to avoid erroneously high estimates of chlorophyll-a often associated with high CDOM concentrations and so reduce misclassifications of *K. brevis* blooms. Hu et al. (2008) implemented the Chl-a:b_{bp}(550) technique using SeaWiFs imagery on the west Florida Shelf, and found that its performance was less satisfactory than the *in situ* scenarios described by Cannizzaro et al. (2008; 2009), and speculated that this may be due to uncertainties in the SeaWiFS-derived chlorophyll-a and backscattering products. Carvalho et al. (2011) conducted a comparison of three *K. brevis* detection algorithms on the cen-
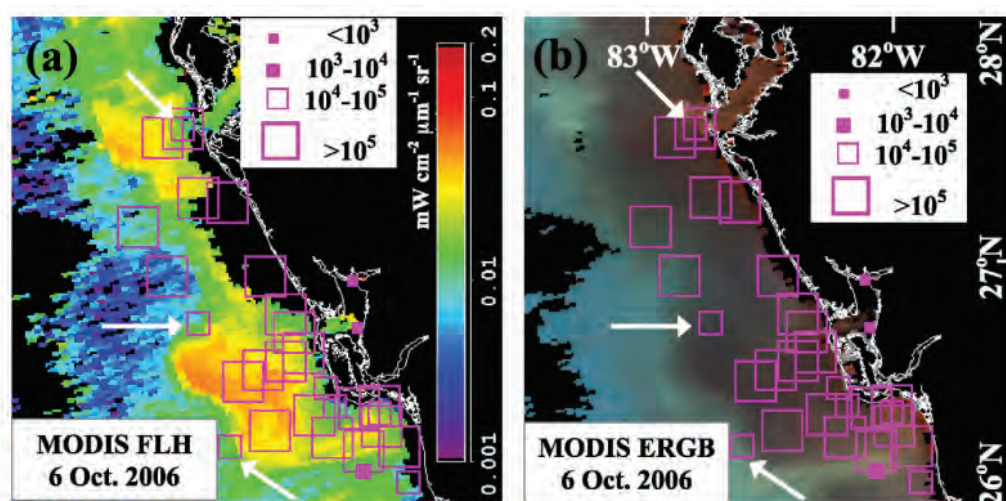
Figure 3.6 MODIS-Aqua (a) fluorescence line height (FLH) (mW cm^{-2} μm^{-1} sr^{-2}) and (b) enhanced RGB (ERGB) composite imagery of the central west Florida Shelf (26–28 °N) for 6 October 2006. Overlaid on both images are *K. brevis* cell concentrations (cells l^{-1}) (2–6 October 2006) sorted into four groups: <10^3, 10^3–10^4, 10^4–10^5, and >10^5. The white arrows indicate false negative classification events when the *K. brevis* bloom classification criteria were applied to the October 2006 data (Cannizzaro et al., 2009).

tral west Florida shelf using, for the first time, MODIS-Aqua data spanning a 4-year period. The algorithms tested were the Stumpf et al. (2003) NOAA operational algorithm, Chl-a:b_{bp}(550) Cannizzaro et al. (2008), and a new approach they named the empirical approach. Their empirical approach essentially retained the methodology of Cannizarro et al. (2008) but replaced b_{bp}(550) by water-leaving radiance, L_w(550), reasoning that L_w is a lower order processing product and subject to less IOP algorithm-associated uncertainty. They found that the operational method had an elevated frequency of false-negative cases (i.e., low accuracy in detecting known blooms), so decided to further compare only the Cannizzaro et al. (2008) and empirical methods by optimisation via sensitivity analyses. Following optimisation,

both algorithms were found to perform similarly.

Tomlinson et al. (2009) suggested that the low backscattering and detrital absorption in *K. brevis* blooms may affect the spectral curvature of reflectance in the blue region of the spectrum. Based on this, they developed a technique using the spectral shape around 490 nm to differentiate *K. brevis* blooms from other blooms. They concluded that, when used in an ensemble approach along with the Stumpf et al. (2003) chlorophyll-a anomaly and Cannizzaro et al. (2008) algorithms, it could increase the user accuracy (i.e., number of confirmed positives/number of satellite positives) by ~30–50%. Amin et al. (2009) proposed a technique called the Red Band Difference (RBD). This takes advantage of the fact that, due to the low backscattering properties of *K. brevis*, fluorescence dominates the water-leaving signal in the red region of the spectrum producing a more pronounced red peak than non-*K. brevis* blooms. However, modelling exercises showed that the RBD for *K. brevis* blooms was not sufficiently unique to distinguish it from other blooms, and a second metric of *K. brevis*, the *K. brevis* bloom index (KBBI), was introduced, which, when combined with the RBD and a method to account for non-zero reflectance in the near infrared from turbid waters, resulted in improved *K. brevis* identification. They note, however, that to overcome noise in the imagery, an RBD threshold equivalent to a chlorophyll-a concentration of ~5 mg m^{-3} is required, potentially excluding many instances of *K. brevis* blooms.

Most recently, Soto (2013) conducted an extensive evaluation, optimisation and intercomparison of six published *K. brevis* detection techniques: 1) chlorophyll-a anomaly (Stumpf et al., 2003), 2) spectral shape (Tomlinson et al., 2009), 3) b_{bp}:Chl-a ratio (Cannizzaro et al., 2008; 2009; Hu et al., 2011), 4) RBD-KBBI (Amin et al., 2009), 5) a modification of the Carvalho et al. (2010) approach, but using $R_{rs}(\lambda)(555)$ instead of $L_w(555)$, and 6) a multi-algorithm method proposed by Carvalho et al. (2010). The techniques were implemented on the west Florida Shelf and it was found that, after optimisation of the thresholds, the success of each of the approaches in correctly identifying *K. brevis* blooms was significantly improved. Furthermore, they developed a new and straightforward approach that utilised only FLH and $R_{rs}(\lambda)(555)$. This approach performed similarly to the most successful of the other six techniques (RBD-KBBI), but is significantly easier to implement with existing satellite products and allows for easier adjustment of the thresholds based on the needs of the user. Several other methods for satellite detection of *K. brevis* blooms such as image segmentation (Zhang, 2002), artificial intelligence approaches, and a combination of techniques (Carvalho et al., 2010), have been proposed and complement the approaches discussed herein.

3.4.3 *K. mikimotoi* bloom detection

A number of the approaches that have been developed for detecting and monitoring *K. mikimotoi* are similar to those developed for *K. brevis*. As with *K. brevis* there are

two distinct approaches: algal (or biomass) concentration-based and those that are spectrally based.

As already discussed for *K. brevis*, in situations where the HABs dominate the biomass, algorithms that detect new increases (or anomalous increases) in chlorophyll-a are effective tools for identification. Through the use of background subtraction, (the process of removing a mean background signal to identify regions of interest) an algal anomaly can be detected. However, many approaches using simple background subtraction regimes to detect high biomass blooms are region specific or require tuning (e.g., Stumpf et al. 2003; Miller et al. 2006; Davidson et al., 2009). Phytoplankton blooms will typically last several weeks so care must also be taken to ensure that the bloom of interest does not dominate the background image, thus meaning that it will not be detected by background subtraction technique. More recent work has exploited the statistical analysis of temporal data to aid detection (Shutler et al., 2012). This work provides a region-independent approach that is able to follow seasonal trends and avoids the need for specific tuning. The approach was originally developed to detect blooms of harmless coccolithophores (Shutler et al., 2010) and was later applied to *K. mikimotoi* (Shutler et al., 2012). The approach was shown to achieve a correct classification rate of 68% (false alarm rate of 0.24, N=25) on a small database of *in situ* samples.

As already mentioned, blooms of *K. mikimotoi* can significantly alter the colour of surface waters. Miller et al. (2006) exploited this characteristic and used multivariate classification as an objective means to discriminate between harmful (*K. mikimotoi* and cyanobacteria) and harmless algae in SeaWiFS data. The approach produces maps of HAB likelihood, rather than distinct regions of HABs and non-HABs. Miller then used the approach to monitor the dynamics of a number of different bloom instances. In order to estimate the constituents of the surface water, along with $R_{rs}(\lambda)$ data they used an inversion scheme to estimate the inherent optical properties (IOP). This approach was also applied to MERIS data (Shutler et al., 2005) and used to aid the study of a large *K. mikimotoi* bloom that occurred in Scottish waters in 2006 (Davidson et al., 2009); the bloom resulted in damage to the fish gills of farmed fish and extensive mortalities of benthic organisms. More recently Kurekin et al., (2014) further developed the approach to study *K. mikimotoi* and *Phaeocystis globosa* and its application to both MERIS and MODIS data. The approach was shown to correctly identify 89% of *Phaeocystis globosa* HABs in the southern North Sea and 88% of *K. mikimotoi* blooms in the western English Channel.

3.4.4 Summary

All of the approaches discussed above have been shown, to a greater or lesser degree, to be useful in the identification of *K. brevis* and/or *K. mikimotoi* blooms, and demonstrate unambiguously the role of ocean colour in detection, management and mitigation of HABs. In most cases, the approaches require careful, contextual

interpretation by skilled users to be most effective, but recent work has refined and simplified the methods making true automation more likely. The new generation of geostationary satellites such the South Korean GOCI (Geostationary Ocean Color Imager) and the proposed GEO-CAPE (NASA) sensors will offer multispectral to hyperspectral measurements at timescales ranging from hours to decades and will, undoubtedly, greatly enhance the capabilities of remote sensing to detect HABs.

3.5 Detection of *Trichodesmium* Blooms

3.5.1 Background

Trichodesmium spp., a charismatic marine cyanobacterium, is well known to form large surface blooms that can cover 100's of thousands of kilometers and can be observed from space-based sensors. This nitrogen fixer has been shown to play an important role in global and regional nitrogen and carbon cycles (Capone et al., 1997; Gruber and Sarmiento, 1997; Karl et al., 1997). On continental shelves such as the west Florida shelf, *Trichodesmium* blooms can serve as a significant nitrogen source for toxic *Karenia brevis* blooms (Walsh and Steidinger, 2001). Accurate assessment of *Trichodesmium* blooms on global and regional scales can thus improve our understanding of nitrogen and carbon cycles as well as our capacity to forecast toxic blooms.

3.5.2 Bloom detection

The first report in the literature of a direct observation of *Trichodesmium* is the photograph taken from the Space Shuttle of a massive bloom of this organism in the Capricorn Channel (Kuchler and Jupp, 1988). To identify and quantify a specific species of bacteria from space, the organism needs to have characteristic properties that can be remotely sensed. Phototrophic bacteria such as cyanobacteria carry auxiliary pigments including phycoeryrthin (PEB) and phycocyanin (PC) that have unique optical properties (e.g., Figure 3.7). Researchers (Subramaniam and Carpenter, 1994; Bracher et al., 2009) have proposed techniques that exploit changes in absorption of light due to the presence of these pigments to identify and quantify cyanobacteria such as the filamentous, non-heterocystous *Trichodesmium* spp. However, it should be noted that Garver et al. (1994) analyzed about 400 *in situ* absorption spectra and concluded that more than 99% of the variance in the absorption spectra of particulate matter was related to the amount of material, and only a very small signal (less than 0.5%) was related to the presence of auxiliary pigments. In other words, they concluded that, for typical conditions (non-mono species, non-bloom, organism that are heterogeneously mixed through the upper water column), it was unlikely that ocean-colour remote sensing would be able to uniquely identify particular phytoplankton groups. Morel (1997) analyzed optical
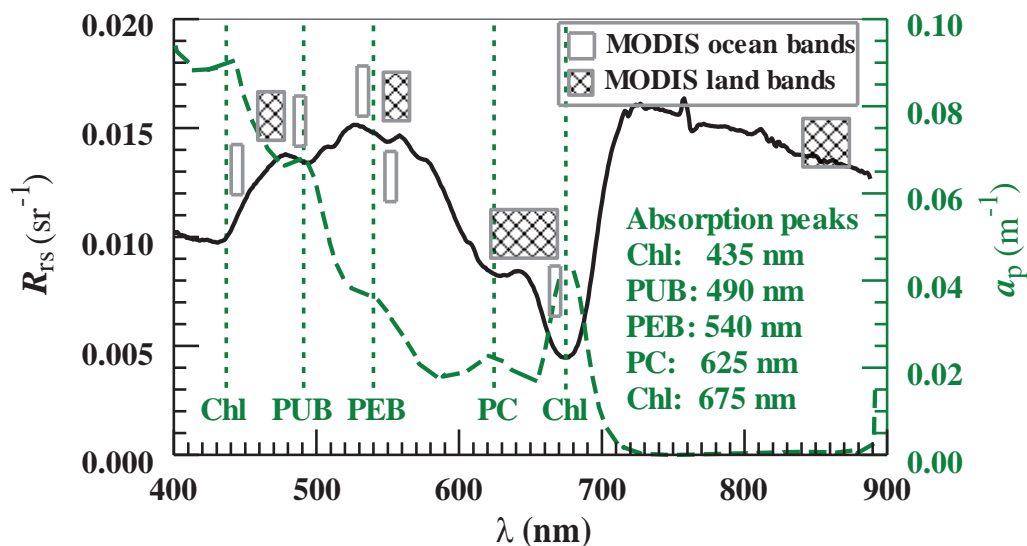
Figure 3.7 Spectra of remote sensing reflectance (R_{rs}) and absorption coefficient (a_p) measured from *Trichodesmium* mats off the west coast of Florida. The vertical dashed lines denote the local absorption maxima due to Chl (chlorophyll-a), PUB (phycourobilin), PEB (phycoerythrobilin), and PC (phycocyanin). The empty and filled rectangles show the positions and bandwidths of the MODIS bands. The 10-nm ocean bands centered at 443, 488, 531, 551, and 667 nm have 1-km nadir resolutions. The land bands at 469 (459 – 479), 555 (545 – 565), 645 (620 – 670), and 859 (841 – 876) nm have spatial resolutions of 500, 500, 250, and 250 m, respectively. Local reflectance maxima are found at 478, 528, and 558 nm, while local reflectance minima are found at 490 and 550 nm. Figure adapted from Hu et al. (2010a).

data collected during a dense bloom (3×10^8 cells per liter) of *Synechococcus*, a cyanobacterium that contains PEB, and contributed to over half the chlorophyll concentration. He concluded that it would be "illusory to expect more than the possibility of producing an index or a flag indicating the presence of PEB bearing organisms" from ocean-colour sensors.

Trichodesmium has several unique attributes that has allowed for its unique identification under specific conditions: 1) in addition to its absorption characteristics due to the presence of PEB, it also contains gas vesicles that scatter light making surface blooms of this organism "brighter". Indeed, senescing blooms of this organism have been described as silvery grey in colour (Devassy et al., 1978); 2) Water molecules absorb strongly in the red/near infrared region of the spectrum and the optical signature of sub-surface blooms in this region of the spectrum are lost due to this absorption by water. However, the gas vesicles in *Trichodesmium* cause it to accumulate at the surface as a microlayer above the water (Villareal and Carpenter, 2003) creating a high reflectance in the near infrared – so high that surface blooms of *Trichodesmium* often get classified as clouds in standard satellite data processing routines. This high reflectance of surface blooms of *Trichodesmium* was exploited

by Subramaniam et al. (1999) to detect this organism using the visible and infrared bands of the AVHRR sensor. Capone et al. (1998) used the same technique to map a bloom of *Trichodesmium* in the Arabian Sea that covered an area greater than 2 million square kilometers.

The first use of ocean-colour satellites to map *Trichodesmium* was shown by Dupouy et al. (1988) who used CZCS imagery to map a massive bloom of *Trichodesmium* in the waters off New Caledonia. Subramaniam and Carpenter (1994) developed an empirical algorithm based on the bright reflectance and potential changes in reflectance due to presence of phycoerythrin. The first optical model for estimating the remote sensing reflectance of *Trichodesmium* for developing remote sensing algorithms was developed by Borstad et al. (1989). Tassan (1995) used a three-component optical model to determine the minimum concentration of *Trichodesmium* needed to identify this organism from space. Subramaniam et al. (1999) developed an optical model that was based on *Trichodesmium*-specific measurements of absorption and backscatter. They used the combination of the absorption, fluorescence, and scattering properties of *Trichodesmium* in addition to the high infrared reflectance to develop satellite algorithms for its detection and quantification with SeaWiFS data (Subramaniam et al., 2002). They concluded that widespread use of this algorithm was not feasible because of the challenges of spatial resolution of the satellite. Since *Trichodesmium* slicks are often very heterogeneous in their spatial distribution, it was very difficult to use standard globally applicable algorithms. Westberry et al. (2005) used a semi-analytical model to produce global maps of this organism and analyze its occurrence on a global basis, where the optical signatures of *Trichodesmium* blooms could be identified for waters with chlorophyll-a concentrations greater than 0.8 mg m^{-3}.

The Maximum Chlorophyll Index (MCI) approach of Gower et al. (2005; 2008) has also been used to detect and track surface slicks of *Trichodesmium*. The MCI detects the local reflectance peak around 709 nm for intense phytoplankton blooms, so the identified blooms are not *Trichodesmium* specific. In contrast, Hu et al. (2010a) used a Floating Algae Index (FAI) to first identify surface mats of blooms, and then used reflectance spectral curvatures in the blue-green wavelengths to differentiate *Trichodesmium* blooms from other blooms (e.g., Figure 3.8). Indeed, because of the *Trichodesmium*-specific pigments such as PUB and PEB, *Trichodesmium* bloom mats showed unique spectral curvatures that can be differentiated from other bright features such as coccolithophore blooms (Figure 3.8) or *Sargassum* blooms (Hu et al., 2010a). Application of this approach successfully identified a massive *Trichodesmium* bloom south of Fiji Island (Figure 3.9a). However, such an approach is limited to blooms only when they form surface mats that result in elevated "red-edge" reflectance in the near-infrared. Likewise, a similar approach developed for the Great Barrier reef region (McKinna et al., 2011) worked well only for surface mats of *Trichodesmium* blooms. In contrast, the approach of Dupouy et al. (2011) developed for the South Western Tropic Pacific examined the radiance anomaly in
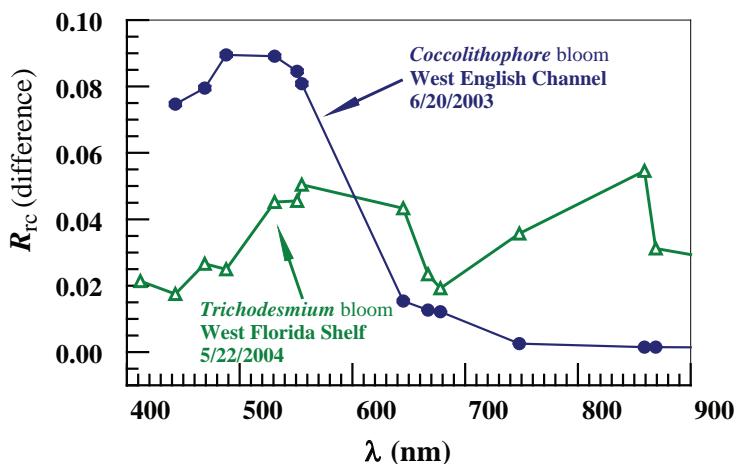
Figure 3.8 MODIS-Aqua reflectance difference spectra of a *Trichodesmium* bloom on the west Florida shelf and a Coccolithophore bloom off the West English Channel (same as in Figure 3.2). Note the spectral curvatures between 469 nm and 555 nm (i.e., the low-high-low-high-low-high features) due to the *Trichodesmium*-specific pigments. In contrast, the coccolithophore spectrum does not show such curvatures.

the visible wavelengths relative to waters without *Trichodesmium* blooms. This approach does not rely on the elevated reflectance in the NIR, and therefore may be applicable for blooms where *Trichodesmium* cells are mixed in the water column.
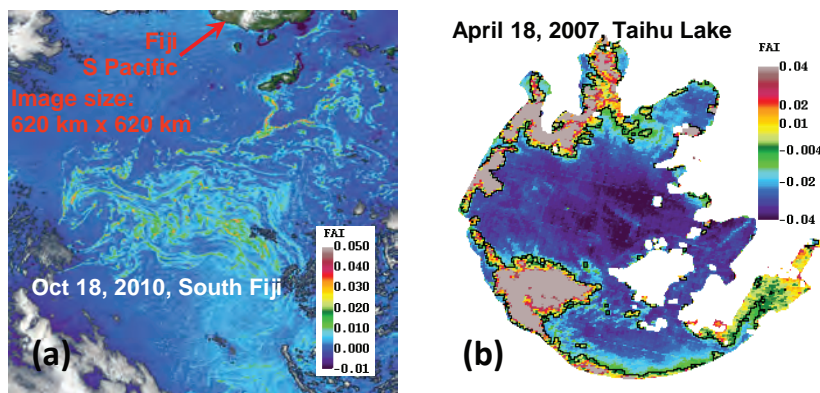
Figure 3.9   (a) MODIS-Aqua FAI image showing a *Trichodesmium* bloom south of Fiji Island in the South Pacific on 18 October 2010. The bloom showed spectral curvatures in the blue-green wavelengths similar to those shown in Fig. 3.8; (b) MODIS-Aqua FAI image showing a cyanobacteria bloom of *Microcystis aeruginosa* in Taihu Lake, China (a shallow, freshwater lake of about 2300 km^2 centered around 31.2°N, 120.2°E.

3.5.3   Other cyanobacterial blooms

Various types of cyanobacterial blooms other than *Trichodesmium* have been reported in both marine and fresh waters. Whether they can be differentiated from space depends upon whether they exhibit spectral signatures that can be detected by the remote sensors at specific spectral, spatial, and radiometric resolutions. Below are two examples of such cyanobacterial blooms.

3.5.3.1   *Nodularia* blooms in the Baltic Sea

Each summer during upper water column warming, a sequence of cyanobacterial blooms occur in the Baltic Ocean, usually culminating in a major bloom of *Nodularia spumigena*. *Nodularia*, a nitrogen fixing cyanobacteria, is also associated with nodularin, a hepatotoxin (Sivonen et al., 1989) and beta methyl amino alanine (BMAA), a neurotoxic amino acid (Cox et al., 2005). Kahru et al. (1993) showed that surface blooms of these organisms can be detected using the AVHRR sensor and compiled a time series of images to explore the factors that contribute to the formation and transport of these blooms (Kahru et al., 2000), yet the algorithm to detect the bloom was based on the *a priori* knowledge that *Nodularia spumigena* is the dominant bloom species. Based on field-measured optical properties, Metsamaa et al. (2006) showed signatures around 630 and 650 nm in the modelled reflectance spectra, which may be useful for developing remote sensing algorithms for intense blooms (chlorophyll >8 – 10 mg m^{-3}).

3.5.3.2   *Microcystis* blooms in lakes

Simis et al. (2007) developed a technique for quantifying concentrations of phycocyanin, the marker pigment for freshwater cyanobacteria, and found that their algorithm could allow for assessment of cyanobacterial risk to water quality and public health following the World Health Organization guidelines (WHO, 2003) in about 70% of the cases they considered. Budd et al. (2001b) exploited the enhanced scattering of light by surface blooms of the toxic cyanobacterium *Microcystis* to map blooms of this organism using visible band channels on the AVHRR and Landsat Thematic Mapper (TM) sensors. Using this combination, Budd et al. (2001a) constructed a time series of satellite-based turbidity maps for Lake Erie from 1987 to 1993, representing the period from before to after the establishment of zebra mussels (*Dreissena polymorpha*) in these waters. Similarly, using the MODIS FAI to capture the elevated reflectance in the NIR when blooms of *Microcystis aeruginosa* form surface mats (Figure 3.9b), Hu et al. (2010b) established a 10-year time-series of bloom characteristics for Taihu Lake of China to study bloom seasonality and inter-annual changes. Similar to the Baltic case, however, these bloom detection algorithms require *a priori* knowledge of the bloom type in the specific study regions.

3.6   Detection of *Ulva prolifera* Blooms

3.6.1   Background

Green tides of macroalgae blooms have been reported in the world's oceans (e.g., Fletcher, 1996; Blomster et al, 2002; Nelson et al. 2003; Merceron et al., 2007), but it was not until summer 2008 when a massive bloom of the macroalgae *Ulva prolifera* in the Yellow Sea off Qingdao, China, caught wide international attention from both the research community and the public (Hu and He, 2008). Since then, several targeted studies attempted to determine the bloom's origin, cause, temporal evolution, and ecological consequences (Lü and Qiao, 2008; Sun et al., 2008; Liu et al., 2009a; Hu et al., 2010c). Although *Ulva prolifera* may serve as an important habitat for marine animals and can be utilized as fertilizers, it also represents a marine hazard for transportation. Excessive *Ulva prolifera* may cause a beach nuisance and is a burden to local management (Hu and He, 2008; He et al., 2011). Satellite remote sensing has been used to study the extent and distribution of the green macroalgae blooms. In particular, Hu et al. (2010c) used MODIS and Landsat time series to demonstrate that the *Ulva prolifera* blooms in the Yellow Sea and East China Sea are recurrent and they related to local seaweed aquaculture. The principle to detect these blooms from space is briefly discussed below.
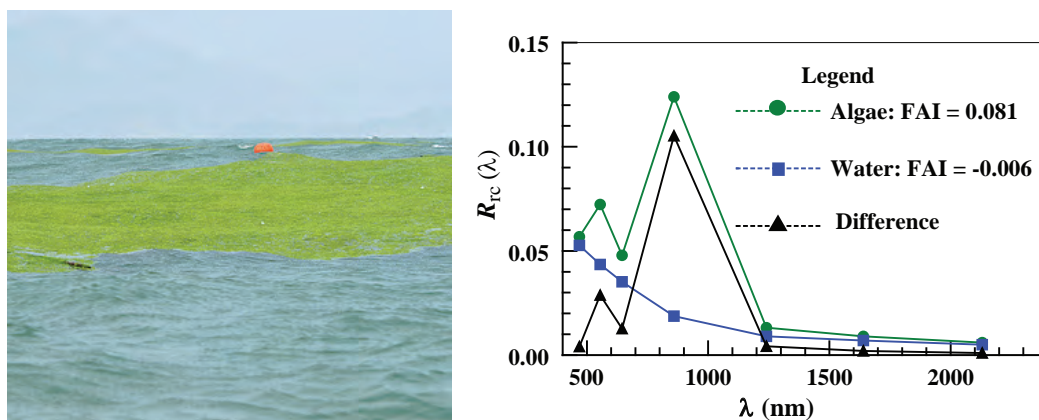
Figure 3.10   *Ulva prolifera* bloom off Qingdao, China. (b) MODIS reflectance of *Ulva prolifera* bloom and bloom-free water. Also shown is their difference spectrum. Note the reflectance peak at 859 nm, which forms the basis to use FAI for bloom detection (Hu, 2009).

The individual multi-cell *Ulva prolifera* are thin filaments that can grow to one meter in length. Their aggregation can make them appear as surface vegetation (Figure 3.10a), and therefore detectable in satellite imagery (Figure 3.10b). Most algorithms to differentiate phytoplankton functional groups rely on visible wavelengths (Nair et al., 2008). However, atmospheric interference, especially for the Yellow Sea, may induce unexpected errors in these wavelengths. This is because that the

interference is estimated from longer wavelengths in the near-infrared or shortwave-infrared and then extrapolated to the visible. In contrast, reflectance data in the near-IR derived from satellite measurements are less prone to the extrapolation-induced errors. Indeed, *Ulva prolifera* blooms show elevated reflectance in the near-IR, which can be used to differentiate them from the bloom-free background water.

3.6.2   Bloom detection

Based on the above argument, the traditional way to quantify surface vegetation, through a Normalized Difference Vegetation Index (NDVI), was used to detect *Ulva prolifera* blooms (Hu and He, 2008). However, NDVI is very sensitive to changes in observing conditions such as variable aerosols and solar/viewing geometry. Using model simulations and satellite data product comparison, Hu (2009) showed that the relative reflectance height in the near-IR is relatively stable against these variable conditions. Thus, similar to the concept of the MODIS fluorescence line height (FLH, Letelier and Abott, 1996) and MODIS maximum chlorophyll index (MCI, Gower et al., 2005), a floating algae index (FAI) was introduced to detect and quantify the surface area of *Ulva prolifera* blooms (Hu, 2009). The FAI is defined as the difference between MODIS Rayleigh corrected reflectance (R_{rc}) at 859-nm and a baseline formed linearly between R_{rc} at 645 nm and 1240 nm. The baseline subtraction provides a simple and practical means to correct atmospheric effects due to aerosol scattering, thus making bloom features comparable under different observing conditions.

The linear design of the FAI makes it simple to estimate surface area of a bloom from mixed pixels. Using statistics and visual examination to determine the FAI threshold values for 0% and 100% pixel coverage, respectively, Hu et al. (2010c) estimated that MODIS 250-m resolution data could be used to detect algae slicks >5 m wide when the length is greater than several pixels. This preliminary estimate is dependent on the sensor's sensitivity and therefore should not be generalized for other sensors.

While the details on the spectral shape of *Ulva prolifera* surface slicks/patches and application of FAI to document the 10-year occurrence of the algae blooms in the Yellow Sea and East China Sea can be found elsewhere (Hu, 2009; Hu et al., 2010c), Figure 3.11 shows two MODIS FAI images obtained on 21 June 2010 in coastal waters off Qingdao. R_{rc} spectra from the identified slicks show elevated R_{rc} in the near-IR, indicating floating vegetation. Given the fact that *Ulva prolifera* blooms are recurrent in this region, one may conclude that these surface floating features are the green macroalgae, *Ulva prolifera*. Note that the two images were collected only three hours apart from MODIS/Terra and MODIS/Aqua, respectively. The two wide-swath (about 2330-km) satellite instruments not only increase the chance of cloud-free observations, but also complement each other to potentially estimate the movement, direction and speed of these surface floating features.
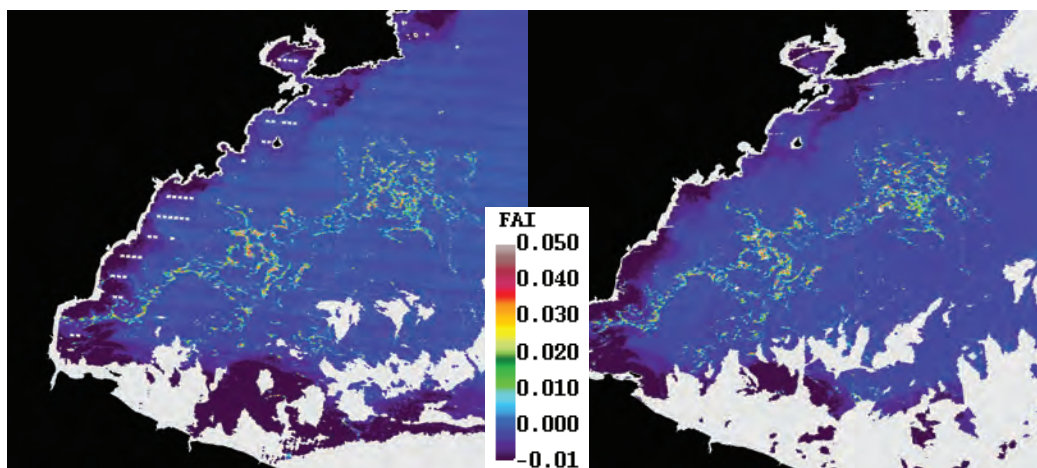
Figure 3.11   MODIS FAI images on 21 June 2010 showing an *Ulva prolifera* bloom off Qingdao, China in the Yellow Sea (about 200 x 200 km centered around 36°N, 120°E). The *Ulva prolifera* aggregation on the surface makes them appear as surface vegetation slicks and patches, which can be identified and quantified using the FAI (Hu, 2009; Hu et al., 2010c).

The FAI approach has limitations. First, because of water's strong absorption in the near-IR, submerged blooms do not show elevated reflectance in the near-IR, and therefore cannot be identified using FAI imagery. This shortcoming may limit the ability to detect a bloom in its early stage. Further, FAI does not distinguish the spectral differences (except in the near-IR) from various bloom types. In principle, FAI detects the R_{rc} peak in the near-IR and therefore can be used to identify any suspicious features that show near-IR peaks, such as *Trichodesmium* blooms and *Sargassum* spp. macroalgae (Subramaniam et al., 2002; Gower et al., 2006). For the same reason, FAI cannot distinguish them spectrally. The ability of using FAI to detect *Ulva prolifera* in the Yellow Sea and East China Sea relies on the *a priori* knowledge that these green macroalgae blooms are recurrent. In an unknown environment, the ability to differentiate algae types is limited. However, once the suspicious features are delineated in FAI imagery, Hu et al. (2010b) showed that the spectral curvatures in the blue-green wavelengths can be used to differentiate *Trichodesmium* from *Sargassum* in the Gulf of Mexico. The approach to combine FAI and other spectral information to differentiate other phytoplankton groups, especially in other parts of the world's oceans, remains to be tested. Nevertheless, the simple design of the FAI makes it straightforward to implement for many existing and planned satellite instruments at various spatial resolutions (e.g., MODIS, Landsat, Suomi NPP/VIIRS), and time-series studies using FAI imagery may reveal previously unknown oceanographic phenomena and processes.

3.7 Detection of *Sargassum* spp. Blooms

3.7.1 Background

The brown macroalgae, *Sargassum* spp., has two holopelagic species, *Sargassum natans* and *Sargassum fluitans*, both characterized by numerous blades, a thallus, and air bladders that form surface mats or "weak lines" on the ocean surface at convergence zones (Ryther, 1956; Figure 3.12a). The macroalgae provides important
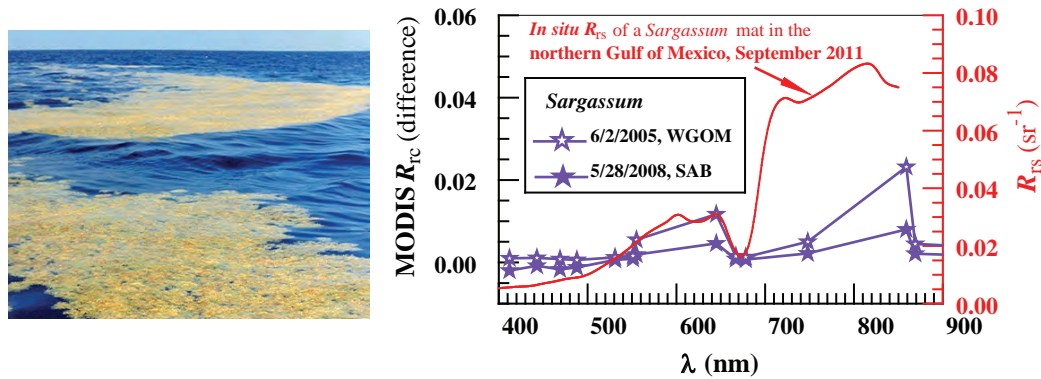
Figure 3.12 (a) Pelagic *Sargassum* mats in the Gulf of Mexico (GOM). (b) MODIS reflectance of *Sargassum* lines in the western GOM and South Atlantic Bight. Also shown is a R_{rs} spectrum collected from a *Sargassum* mat in the northern GOM in September 2011. Note the elevated reflectance around 600 nm in both MODIS and *in situ* spectra. The major difference between MODIS and *in situ* spectra in the NIR wavelengths is primarily due to the mixed MODIS pixels.

habitat (food, shade, shelter from predators) to a variety of marine animals including fish, shrimp, crabs, and several threatened species of turtles (South Atlantic Fishery Management Council, 2002; Rooker et al., 2006; Witherington et al., 2012). Accurate knowledge of *Sargassum* occurrence and their biomass distributions can help plan field surveys to study these marine organisms and their associated ecosystem. *Sargassum* may also play an important role in marine primary productivity, thus contributing to carbon cycling (Gower et al., 2006). *Sargassum* may affect local biogeochemistry through nutrient remineralization, enhanced coloured dissolved organic matter, and bacteria activities (Laptointe, 1995; Zepp et al., 2008). *Sargassum* can also be a natural source of fertilizer for dune plants which help to stabilize coastal dune systems from erosion (Tsoar, 2005; Anthony et al., 2006). On the other hand, excessive *Sargassum* on the beach represents a nuisance and a health hazard, and they often need to be physically removed. Many beaches around the GOM and in the southern Caribbean suffer from *Sargassum* deposition on a regular basis (e.g., Gower et al., 2013). Timely information on the occurrence of *Sargassum* blooms is useful for both research and management such as implementation of harvesting policy, equipment rental for beaching cleaning, and guidance on recreational fishing. Time series of *Sargassum* abundance and distributions can help understand their

origin, evolution, and transport among various marginal seas, as such information is currently limited despite a handful of remote sensing studies (Gower and King, 2011; Gower et al., 2013).

3.7.2 Bloom detection

Similar to other surface floating vegetation, *Sargassum* shows elevated reflectance in the NIR (the red-edge reflectance, see *in situ* R_{rs} spectrum in Figure 3.12b). In addition to this feature, the reflectance around 600 nm is also elevated; this is why *Sargassum* mats often appear brownish. While the red-edge reflectance is not unique to *Sargassum* (e.g., other organisms such as *Ulva prolifera* and cyanobacteria may also show elevated NIR reflectance), the elevated reflectance around 600 nm might be useful in differentiating brown *Sargassum* from other types of macroalgae (e.g., the green macroalgae *Ulva prolifera*) or microalgae (e.g., cyanobacteria).

Based on the principle of red-edge reflectance and several assumptions, Gower et al. (2006), perhaps the first remote sensing-based *Sargassum* study, used MERIS and MODIS to detect and quantify *Sargassum* in the Gulf of Mexico. Specifically, the reflectance red edge at the 709-nm MERIS band (300-m resolution) was examined, and elevated reflectance was assumed to be caused by *Sargassum* surface aggregations. The elevated reflectance in the NIR also caused negative MODIS FLH values, which were used (together with some *a priori* knowledge of the ocean environment) as an indicator of floating *Sargassum* mats. The concept has been extended to MODIS data to form the FAI (Hu, 2009) to examine the elevated reflectance at 859-nm (250-m resolution) to detect *Sargassum* and other floating materials. This is because the 859-nm MODIS band (designed for land use) does not saturate over bright targets and it has higher spatial resolution than the 1-km ocean bands.

Figure 3.13a shows a MODIS-Terra FAI image collected east of Bermuda, where elongated line features can be clearly visualized. Although there is no strictly concurrent ground truth data on the same day, local reports for the same period indicated that these lines could be *Sargassum* slicks. Application of this approach to MODIS data over the Gulf of Mexico, the Sargasso Sea, and the central Atlantic Ocean showed success in detecting floating algae lines in many images, which formed the basis to establish time-series data for statistical analysis. Indeed, Gower and King (2011) and Gower et al. (2013) used MERIS time-series data to document spatial distributions of *Sargassum* abundance and their temporal changes in the Gulf of Mexico and Atlantic. The addition of MODIS data may provide complementary results to refine the interpretations, as the MODIS swath width is twice as wide as that of MERIS, and furthermore there are two MODIS instruments in orbit.

Both MODIS and MERIS are limited by their coarse resolutions when detecting surface features. Hu et al. (2010c) proposed that macroalgae slicks of <5 m wide could not be detected by the MODIS 250-m data at current MODIS signal-to-noise ratio (SNR). However, the simple design of FAI could be extended to other higher-
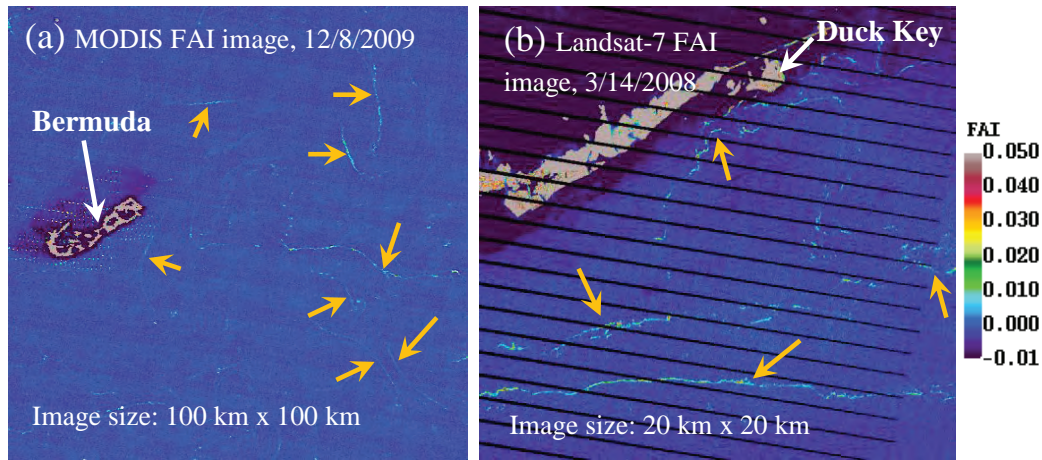
Figure 3.13 MODIS and Landsat FAI images (250- and 30-m resolutions, respectively) showing *Sargassum*-like features in the Sargasso Sea near Bermuda at 32.30°N, 64.77°W (a) and in the Florida Strait near Duck Key at 24.77°N 80.91°W (b). Some of the prominent features are annotated with brown arrows. Note that the slicks shown in (b) cannot be detected by MODIS on the same day due to the coarser resolution of MODIS.

resolution sensors such as Landsat TM or ETM+ (30-m) as long as the sensor has three spectral bands in the red, NIR, and shortwave infrared (SWIR) wavelengths (Hu, 2009). Figure 3.13b shows a Landsat-7 EMT+ FAI image, where surface lines of floating algae, thought to be *Sargassum*, could be visualized. The global availability of Landsat data series, in particular with the recently launched Landsat-8, will greatly facilitate regional studies of *Sargassum* distributions and their movement patterns.

3.8   Summary and Discussion

Through demonstration of several examples, this chapter presents the basic principles and algorithms in remote sensing detection of several dominant phytoplankton functional types including diatoms, coccolithophores, *Karenia brevis*, *Karenia mikimotoi*, *Trichodesmium*, *Ulva prolifera*, and *Sargassum*. Most of these types can be found globally, while *Ulva prolifera* and *Sargassum* have only been reported regionally. The algorithms shown here can be summarized as follows:

❖ Diatoms: based on the differences between pigment absorption spectra between diatoms and other phytoplankton types.

❖ Coccolithophores: based on the elevated reflectance in the visible spectrum (particularly in the blue-green wavelengths) and on band ratios.

❖ *Karenia brevis*: based on chlorophyll-specific high biomass (anomaly) detection, chlorophyll-specific backscattering efficiency, spectral shape in the blue-green wavelengths, or band ratios in the red and NIR.

❖ *Karenia mikimotoi*: based on chlorophyll-specific high biomass (anomaly)

detection or its spectral shape.

❖ *Trichodesmium*: based on absorption features of *Trichodesmium*-specific pigments and on the red-edge reflectance

❖ *Ulva prolifera*: based on the red-edge reflectance of the floating macroalgae

❖ *Sargassum* - based on the red-edge reflectance of the floating algae.

The demonstrations showed successful examples, yet there are limitations in all algorithms and there is much room for further improvement. On the algorithm accuracy, except for the case of *Trichodesmium* where the spectral shapes show unique features that can be distinguished from other phytoplankton types, most of these algorithms require *a priori* information on the ocean environment. For example, without knowing the location of the image, it would be very difficult to tell whether the red-edge reflectance is caused by *Ulva prolifera* or by *Sargassum*. Likewise, the spectral characteristics of *Karenia brevis*, and *Karenia mikimotoi* are not expected to be unique on a global basis, where other phytoplankton types (e.g., other toxic blooms or waters containing mixed phytoplankton populations) may be falsely detected as *K. brevis* or *K. mikimotoi* blooms. Similarly, sediment plumes from rivers or the re-suspension due to storms of historical coccoliths can cause false positives when attempting the detection of coccolithophore blooms. Likewise, if other non-diatom phytoplankton have similar pigment absorption properties to diatoms in other marginal seas, it would be difficult to differentiate diatoms from others. In the future, the algorithms should be tested in other regions with more cases, where more spectral bands are analyzed to rule out other look-alike (spectrally similar) features.

Another limitation is how to quantify the bloom biomass or chlorophyll concentrations. Except for the case of diatoms, one *K. mikimotoi* approach and one coccolithophore approach, most of the algorithms only show the presence or absence of a certain bloom. This is primarily due to the difficulties in sampling the blooms and matching the satellite observations. *K. brevis* blooms are known to be very patchy, where concentrations of the phytoplankton cells can change by orders of magnitude within hundreds of meters. In this case, it is extremely difficult to match the field samples with large satellite pixels. Likewise, blooms of *Trichodesmium*, *Ulva prolifera*, and *Sargassum* are also very patchy, creating difficulties in validating satellite algorithms. In addition, it is difficult to determine the biomass or chlorophyll concentration per bloom area to relate to surface reflectance, as the presence of a boat often disturbs the bloom environment. Even though the bloom could be sampled accurately in the field, satellite pixels are often mixed with bloom features and bloom-free water, thus requiring appropriate algorithm to un-mix the pixels. Gower et al. (2006) and Gower and King (2011) estimated *Sargassum* biomass based on several crude assumptions, yet these assumptions require field validation. Likewise, the assumption used in Hu et al. (2010c) on the biomass of *Ulva prolifera* per unit area also needs field validation. Clearly, the immediate need in the future is to develop improved sampling techniques to develop algorithms to quantify the

bloom intensity.

Except for the case of diatoms, coccolithophores, and *Trichodesmium* cells mixed in the water column, the detection limit of floating mats of *Trichodesmium*, *Ulva prolifera*, and *Sargassum* is unknown due to the sampling difficulty as mentioned above. This is in addition to the spatial resolution restrictions as shown in Figure 3.13b. The detection limit is also a function of the sensor's spatial resolution and SNR, which varies among sensors. Thus, in addition to developing improved sampling techniques, it is necessary to study and compare sensor performance for their ability to detect and quantify the various blooms.

Despite the above limitations, it is clear that the algorithms worked well on the case studies outlined here. Indeed, with some *a priori* knowledge of the ocean environment and availability of global ocean-colour data and Landsat data, it is possible to establish remote sensing systems to assess and monitor blooms on a quasi-operational fashion in different ocean regions. In the absence of validated algorithms to estimate biomass or chlorophyll-a concentrations, the relative patterns in space and time based on educated assumptions can still provide critical information on the spatial and temporal changes of these biologically and ecologically important marine organisms.

Detection of Phytoplankton Size Structure by Remote Sensing

Robert J.W. Brewin, Shubha Sathyendranath, Annick Bricaud, Aurea Ciotti, Emmanuel Devred, Takafumi Hirata, Tihomir S. Kostadinov, Hubert Loisel, Colleen B. Mouw and Julia Uitz

4.1   Introduction

For many ecological and biogeochemical processes, the size of phytoplankton is a good indicator of its functional role (Sieburth et al., 1978). For example, nutrient uptake, light absorption, sinking rate and export are all influenced by cell size (McCave, 1975; Eppley and Peterson, 1979; Morel and Bricaud, 1981; Prieur and Sathyendranath, 1981; Probyn, 1985; Michaels and Silver, 1988; Sunda and Huntsman, 1997; Boyd and Newton, 1999; Laws et al., 2000; Bricaud et al., 2004; Guidi et al., 2009). Cell size also influences phytoplankton physiology (Platt and Denman, 1976; Geider et al., 1986; Chisholm, 1992; Raven, 1998), metabolic rates (Platt and Denman, 1977; 1978) and the marine food web (Maloney and Field, 1991; Legendre and LeFevre, 1991; Parsons and Lalli, 2002). Partitioning phytoplankton according to size offers an integrative approach to describing phytoplankton function and structure in relation to key marine biogeochemical cycles (Le Quéré et al., 2005; Marañón, 2009). Many phytoplankton types classified according to their biogeochemical function may also be approximately partitioned according to their size (Table 4.1). Thus, to a first-order approximation, a size-based classification is suitable for categorising phytoplankton functional groups.

Many large-scale marine biogeochemical models adopt a size-based classification (e.g., Aumont et al., 2003; Blackford et al., 2004; Kishi et al., 2007; Marinov et al., 2010) and require measurements of phytoplankton size for validation and model improvement. In the past, this has typically relied on *in situ* measurements. Owing to the spatial-temporal sampling advantages of remote sensing over conventional *in situ* measurements, there has been an increasing effort to extract information on phytoplankton size structure using satellite ocean-colour observations.

In open-ocean waters (Case 1 waters according to Morel and Prieur, 1977), variations in sea surface reflectance are driven primarily by the abundance of

Table 4.1 Phytoplankton taxonomic groups, important elements and compounds that play a distinctive role in the related biogeochemical cycles, and typical size classes of the taxonomic groups (adapted from Hirata and Brewin, 2009). See also Le Quéré et al., 2005; Nair et al., 2008 and Chapter 1 of this report.

Taxonomic group	Biogeochemical elements and compounds	Typical Cell Size
Diatoms	Si	Micro (> 20 μm)
Dinoflagellates	DMS	Micro (>20 μm)
Haptophytes	$CaCO_3$, DMS	Nano (2-20 μm)
Cyanobacteria	N_2	Pico (<2 μm)

Si = Silica, DMS = dimethyl sulfide, $CaCO_3$ = calcium carbonate, N_2 = nitrogen gas

phytoplankton, with co-varying influence (at least to a first-order, Siegel et al., 2005) from detritus and yellow substances. However, changes in abundance are also typically accompanied by modifications in the size structure of the phytoplankton community (Yentsch and Phinney, 1989; Ciotti et al., 1999). The challenge here is to use ocean-colour data to estimate not just phytoplankton abundance, but also additional information on the size structure of phytoplankton present. Current approaches that detect phytoplankton size from satellite data in Case 1 waters may be partitioned into two categories: abundance-based approaches (uni-variate) and spectral-based approaches (multi-variate).

4.2 Abundance-Based Approaches

Abundance-based approaches rely on observed relationships between some measure of abundance of phytoplankton and their size structure. Such methods typically assume that information on the size-structure of phytoplankton is latent in the satellite-derived bio-optical fields, such that large phytoplankton cells, generally associated with high biomass, typically dominate in eutrophic regions (e.g., upwelling areas), whereas small phytoplankton cells, usually associated with low biomass, generally prevail in oligotrophic areas such as the subtropical gyres (Chisholm, 1992; Platt et al., 2005; Aiken et al., 2009). Within this general class of approaches, differences exist in the implementation, as detailed below.

4.2.1 Size-classes based on discrete trophic classes

Uitz et al. (2006) used the near-surface chlorophyll-a concentration to infer the column-integrated phytoplankton biomass and vertical distribution of three phy-

toplankton size classes (pico-, nano- and microphytoplankton). They analysed an extensive set of algal pigment data determined by high performance liquid chromatography (HPLC), comprising about 2400 vertical pigment profiles collected in various trophic regimes encountered in the open ocean (Case-1 waters exclusively). For each *in situ* sample, the fractional contribution of each size class to the total chlorophyll concentration was derived from pigment data, using specific biomarker pigments (Vidussi et al., 2001; Uitz et al., 2006).

In situ data were partitioned into stratified and mixed waters based on the ratio of the euphotic depth (Z_p) to the mixed-layer depth (Z_m) at the sampling station. Nine trophic categories (S1-S9) were identified in stratified waters and five in mixed waters (M1-M5), based on class intervals in surface chlorophyll concentration. For each category, an associated mean size structure was determined from the *in situ* HPLC data (vertical composition and column integrated chlorophyll concentration). Therefore, given information on the surface chlorophyll-a concentration, Z_p and Z_m, the chlorophyll biomass and vertical distribution of the three phytoplankton size classes can be estimated.

The method is illustrated here given information on satellite-derived surface chlorophyll (O'Reilly et al., 1998), euphotic depth (Morel et al., 2007), and a global climatology of mixed layer depth (de Boyer Montégut et al., 2004). Figure 4.1 shows a flow diagram of the Uitz et al., (2006) approach, which may in fact be used in a continuous manner across discrete trophic categories, by interpolating between the mean chlorophyll values associated with each of the trophic categories, as was done when generating the size-class maps in Figure 4.1. The Uitz et al., (2006) approach was the first method to provide quantitative information on the phytoplankton community composition within the entire euphotic zone, rather than just the surface layer as observed from satellite.

Ranges in phytoplankton abundance have been used also by other authors to demarcate waters dominated by different phytoplankton size classes. For example, Aiken et al. (2007) showed that waters dominated by different size classes of phytoplankton had ranges in chlorophyll concentration and in phytoplankton absorption coefficients that differed from each other, and used this information to map waters dominated by different phytoplankton size classes in the Benguela upwelling region. Similarly, Hirata et al. (2008a) proposed that ranges in phytoplankton absorption coefficient at a single wavelength could be used to identify at the global scale, waters dominated by different size classes of phytoplankton. Unlike the method of Uitz et al. (2006), the methods of Aiken et al. (2007) and Hirata et al. (2008a) are designed to identify dominant size classes at a satellite pixel, and not the fractional contribution of each size class to total chlorophyll biomass.
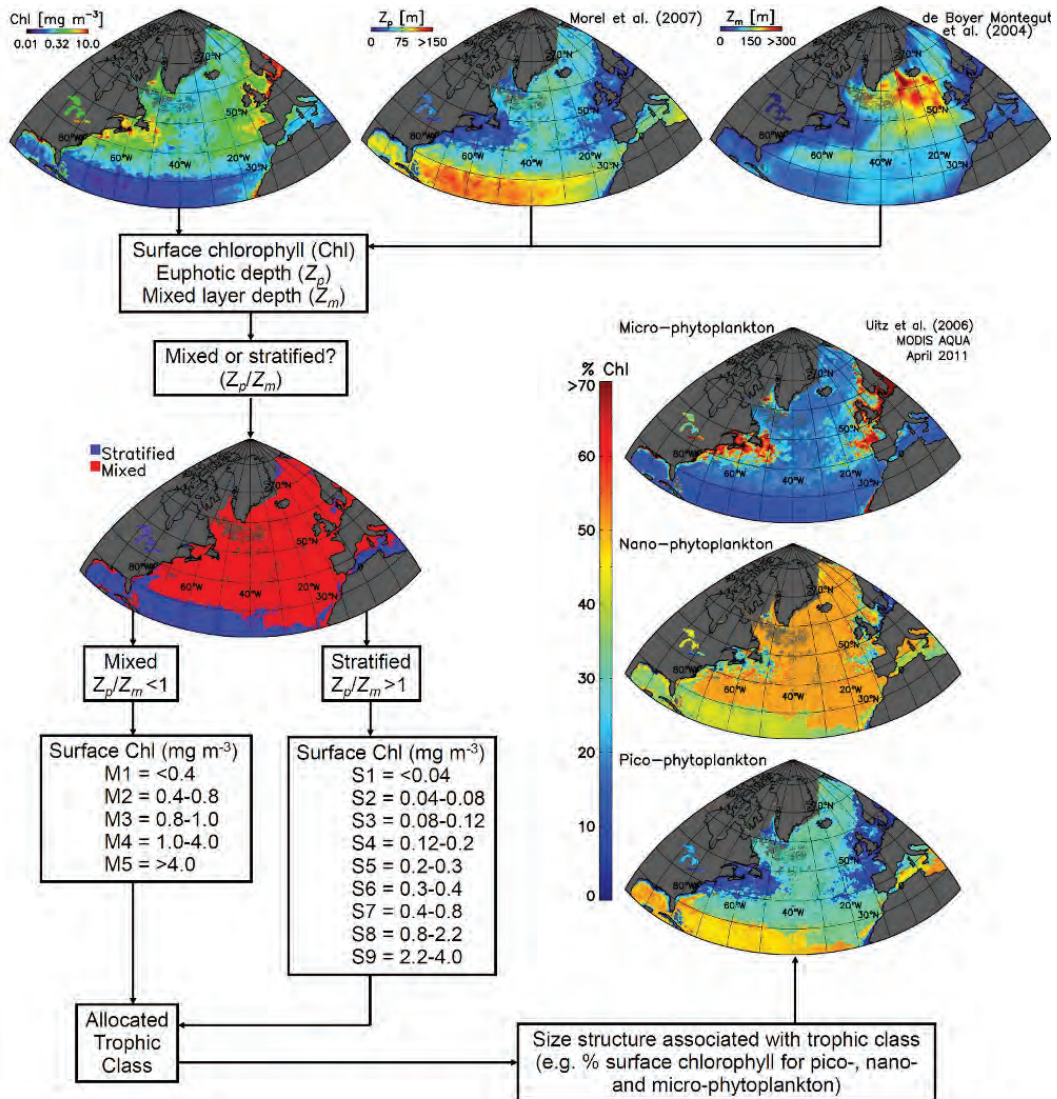
Figure 4.1 Flow diagram showing the application of the Uitz et al. (2006) approach. Method illustrated using a mapped Level 3 monthly chlorophyll image from MODIS-Aqua for April 2011.

4.2.2 Phytoplankton size classes based on a continuum of abundance measures

The methods presented in this section make use of a continuum of abundance measures to infer the size structure of phytoplankton in the ocean, rather than discrete class intervals, as was the case in the previous section.

Brewin et al. (2010a) proposed a simple model designed to estimate the chlorophyll concentrations of three phytoplankton size classes (pico- $<2\mu$m, nano- 2-20μm and microphytoplankton $>20\mu$m) as a continuous function of total chlorophyll con-

centration. The model is based on the work of Sathyendranath et al. (2001) and assumes small cells are incapable of growing beyond a particular chlorophyll concentration, with an upper limit imposed possibly from a combination of bottom-up (e.g., nutrient control) and top-down (e.g., grazing) processes, and that, beyond this value, chlorophyll is added to a system solely by the addition of larger size classes of phytoplankton (Raimbault et al., 1988; Chisholm, 1992).

The model can be expressed through two simple exponential equations, such that the chlorophyll concentrations of the combined pico-nanophytoplankton population ($C_{p,n}$), cells <20μm, and the picophytoplankton population (C_p), cells <2μm, can be expressed according to:

$$C_{p,n} = C_{p,n}^m[1 - \exp(-S_{p,n}C)], \tag{4.1}$$

and

$$C_p = C_p^m[1 - \exp(-S_pC)], \tag{4.2}$$

where the total chlorophyll-a concentration is represented as C [mg m^{-3}], the subscripts p and n refer to picophytoplankton and nanophytoplankton respectively, $C_{p,n}^m$ and C_p^m are the asymptotic maximum values for the associated size classes (<20μm and <2μm respectively) and $S_{p,n}$ and S_p determines the increase in size-fractionated chlorophyll (<20μm and <2μm respectively) with increasing total chlorophyll-a (C). The chlorophyll concentration of nanophytoplankton (C_n) and microphytoplankton (C_m) can then be calculated according to:

$$C_n = C_{p,n} - C_p, \tag{4.3}$$

and

$$C_m = C - C_{p,n}. \tag{4.4}$$

The percentage of each phytoplankton size class to the total chlorophyll concentration (P_m, P_n and P_p) can then be calculated by dividing the size-specific chlorophyll concentrations (C_p, C_n and C_m) by the total chlorophyll concentration (C) and multiplying by 100.

The unknown parameters of Eqs. 4.1 – 4.4 ($C_{p,n}^m$, C_p^m, $S_{p,n}$ and S_p) can be computed if we know the total chlorophyll concentration (C), the chlorophyll concentrations of the combined pico-nanophytoplankton population ($C_{p,n}$) and the picophytoplankton population (C_p), using an appropriate fitting procedure (e.g., least-square fit). The concentrations $C_{p,n}$ and C_p can be estimated using specific biomarker pigments following Uitz et al. (2006), with further refinements (e.g., Brewin et al., 2010a; Hirata et al., 2011; Devred et al., 2011), or alternatively by use of size-fractionation. Once these parameters are established, the chlorophyll concentrations of each size class can be computed directly from total chlorophyll, and hence from any satellite-based estimate of chlorophyll (Figure 4.2).

Brewin et al. (2010a) established their model parameters from an analysis of a large database of HPLC pigment data in the Atlantic Ocean. Devred et al.
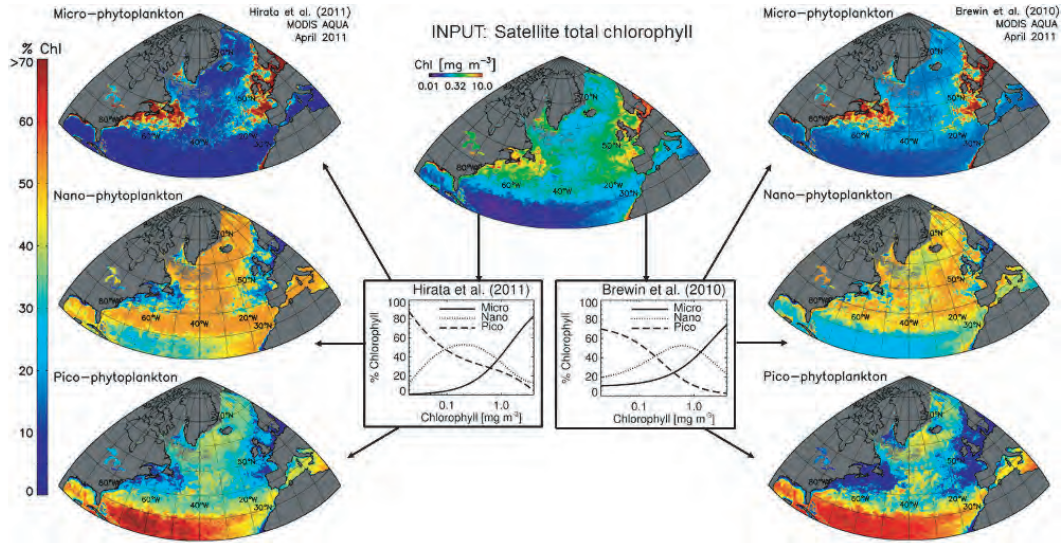
Figure 4.2 Diagram showing the application of the models of Hirata et al. (2011) (left) and Brewin et al. (2010a) (right) to satellite data. Methods are illustrated using a mapped Level 3 monthly chlorophyll image from MODIS-Aqua for April 2011.

(2011) derived the parameters of Eqs. 4.1-4.4 using large datasets comprising of phytoplankton absorption and chlorophyll data, though they did not use their results to implement an abundance-based method (see section 4.3.1.2 for discussion on the spectral-based Devred et al. (2011) model). The underlying models of Brewin et al. (2010a) and Devred et al. (2011) are the same (see Sathyendranath et al., 2001) but the model parameters differ from each other (Table 4.2), because of methodological differences in the implementation, and in the datasets used (see legend of Table 4.2).

As the chlorophyll concentration tends towards zero, the derivative of Eqs. 4.1 and 4.2 can be expressed according to:

$$\left. \frac{dC_{p,n}}{dC} \right|_{C \to 0} = S_{p,n} C_{p,n}^m, \tag{4.5}$$

and

$$\left. \frac{dC_p}{dC} \right|_{C \to 0} = S_p C_p^m, \tag{4.6}$$

respectively. In the Devred et al. (2011) approach, in order to help obtain model parameters solely from phytoplankton absorption and chlorophyll data, the assumption is made that as the chlorophyll concentration tends towards zero there is no contribution from large cells, and hence $C = C_p$ and the products of $S_{p,n} C_{p,n}^m$ and $S_p C_p^m$ are equal to one. This assumption is not made in the Brewin et al. (2010a) model as HPLC data is used to fit the equations, but unlike Devred et al. (2011), the model of Brewin et al. (2010a) is constrained by uncertainty in deriving information on size classes from HPLC data (or alternatively size-fractionated filtration).

Table 4.2 Parameter values for Eqs. 4.1 – 4.6 provided from Brewin et al. (2010a) for the Atlantic Ocean (Atlantic Meridional Transect HPLC data), Brewin et al. (2011a) from the NOMAD HPLC dataset version 1.3, Brewin et al. (2012) from the Indian Ocean and Devred et al. (2011) using chlorophyll and absorption data from the NW Atlantic and NOMAD.

Study	Parameters for Eqs. 4.1 – 4.6					
	$C_{p,n}^m$ *	$S_{p,n}$	C_p^m *	S_p	$C_{p,n}^m S_{p,n}$	$C_p^m S_p$
Brewin et al. (2010a)	1.057	0.851	0.107	6.801	0.900	0.728
Brewin et al. (2011a)	0.775	1.152	0.146	5.118	0.893	0.747
Brewin et al. (2012)	0.937	1.033	0.170	4.804	0.968	0.817
Devred et al. (2011)	0.546	1.830	0.148	6.765	1.000	1.000

* denotes units in $\mathrm{mg\,m^{-3}}$

Similarly, Hirata et al. (2011) proposed a number of empirical equations to estimate the fractional contribution of three phytoplankton size classes (pico- <2μm, nano- 2-20μm and microphytoplankton >20μm) and seven phytoplankton functional groups (diatoms, dinoflagellates, green algae, haptophytes, pico-eukaryotes, prokaryotes and *Prochlorococcus sp.*) to the total chlorophyll concentration in a satellite pixel. They expressed the percentage (P) of each size class in the total chlorophyll concentration as:

$$P_m \quad = \quad [0.912 + \exp(-2.733 \cdot \log_{10}(C) + 0.400)]^{-1} \cdot 100, \qquad (4.7)$$

$$\begin{aligned} P_p \quad = \quad & (-[0.153 + \exp(1.031 \cdot \log_{10}(C) - 1.558)]^{-1} \qquad (4.8) \\ & -1.860 \cdot \log_{10}(C) + 2.995) \cdot 100, \end{aligned}$$

and

$$P_n \quad = \quad 100 - P_m - P_p, \qquad (4.9)$$

where P_m, P_n and P_p are the percentages of chlorophyll for micro-, nano- and picophytoplankton respectively. The model parameters in Eqs. 4.7 to 4.9 were estimated using a large database of HPLC measurements (including data from the Atlantic Meridional Transect (AMT); the Beagle cruise; the NASA SeaBASS and NOMAD databases; the SEEDS II iron enrichment experiment; the Japanese Fisheries Research Agency; and the Oshoro-Maru cruise by Hokkaido University). Using the total chlorophyll concentration from ocean colour as input, the percentage contribution of each size class can be computed as illustrated in Figure 4.2.
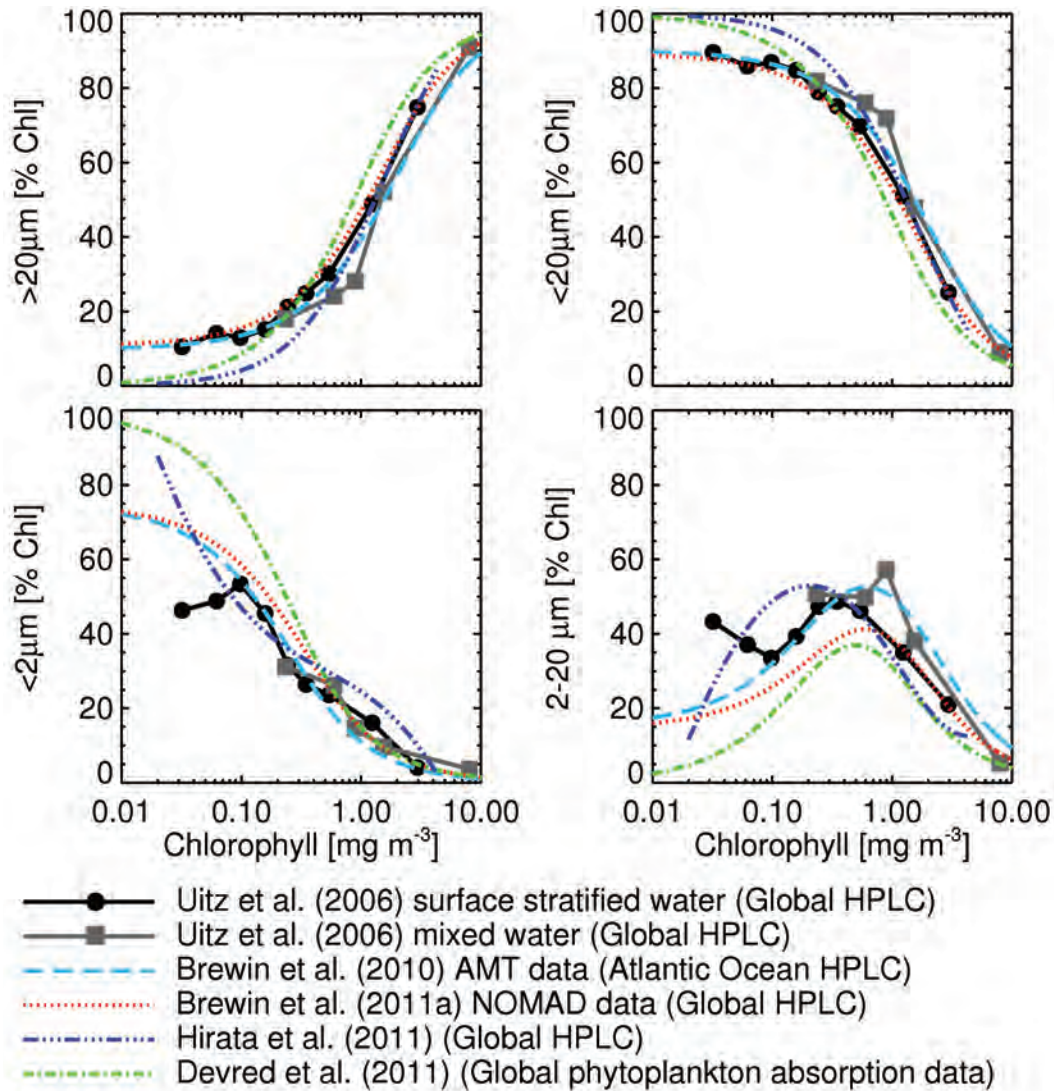
Figure 4.3 Comparison of methods that propose patterns of change in the size structure with a change in chlorophyll.

4.2.3 Comparison of abundance-based methods

Three of the abundance-based approaches presented above (Uitz et al., 2006; Brewin et al., 2010a; Hirata et al., 2011) are designed to estimate fractions of size classes in a given chlorophyll concentration. Of these, the method of Uitz et al. (2006) assigns size classes according to a finite number of trophic statuses defined on the basis of surface chlorophyll and on whether or not the euphotic zone may be treated as stratified or mixed. The methods of Brewin et al. (2010a) and Hirata et al. (2011) are both based only on chlorophyll concentration, but differ from each other in the functional relationships assigned to relate total chlorophyll concentration to partial

chlorophyll concentrations associated with the size classes. The equations used by Brewin et al. (2010a), and also Devred et al. (2011), emerge from an underlying conceptual model (Sathyendranath at al., 2001) on how phytoplankton populations change with chlorophyll concentration, whereas the equations of Hirata et al. (2011) are purely empirical, and are not constrained by an underlying model. Note that the Devred et al. (2011) model is not included in the comparison of abundance-based methods as it is classified as a spectral-based approach (see section 4.3.1.2).

These differences notwithstanding, all three approaches assume change in size structure with a change in chlorophyll. These patterns are compared in Figure 4.3. In general, all three approaches are consistent in that the percentage of large cells (>20μm) to total chlorophyll increases monotonically as a function of total chlorophyll-a and that of small cells (<2μm and <20μm) decreases monotonically. Furthermore, the fraction of nanophytoplankton (2-20μm) to total chlorophyll appears to display a uni-modal relationship with increasing chlorophyll. The relationships developed using diagnostic pigment analysis of HPLC data are in qualitative agreement with those proposed by Devred et al. (2011) using phytoplankton absorption and chlorophyll measurements (Figure 4.3).

Table 4.3 Differences in the use of diagnostic pigments to infer size structure from Uitz et al. (2006), Brewin et al. (2010a) and Hirata et al. (2011). Micro >20μm, Nano 2-20μm and Pico <2μm.

Diagnostic Pigment	Taxonomic group	Uitz et al. (2006)	Brewin et al. (2010a)	Hirata et al. (2011)
Fucoxanthin	Diatoms	Micro	Micro	Micro/Nano
Peridinin	Dinoflagellates	Micro	Micro	Micro
19'-Hex-fucoxanthin	Prymnesiophytes	Nano	Nano/Pico	Nano/Pico
19'-But-fucoxanthin	Pelagophytes	Nano	Nano	Nano
Alloxanthin	Cryptophytes	Nano	Nano	Nano
Zeaxanthin	Cyanobacteria, Prochlorophytes	Pico	Pico	Pico
Total chlorophyll-b*	Chlorophytes, Prochlorophytes	Pico	Pico	Nano

* Total chlorophyll-b = chlorophyll-b + divinyl-chlorophyll-b

One of the sources of deviations among methods of Uitz et al. (2006), Brewin et al. (2010a) and Hirata et al. (2011) could be different diagnostic pigment methods adopted in each approach (Table 4.3). Brewin et al. (2010a) and Hirata et al. (2011) adapted the method proposed by Vidussi et al. (2001) and Uitz et al. (2006). The Brewin et al. (2010a) approach introduces an empirical pico-eukaryote adjustment that partly attributes 19'-Hexanoyloxyfucoxanthin to the pico-size class in low chlorophyll waters. Its effect can be observed in Figure 4.3 as the model of Brewin

et al. (2010a) produces higher estimates of picophytoplankton percent chlorophyll, and lower estimates of nanophytoplankton percent chlorophyll, when compared with Uitz et al. (2006) at low chlorophyll concentrations. The model of Hirata et al. (2011) introduced a further adjustment, attributing a portion of the fucoxanthin pigment to the nano-size class (also see the adjustment proposed by Devred et al., 2011), as fucoxanthin can occur in both micro- and nano-sized phytoplankton. The impact of this modification is probably responsible for the differences observed in Figure 4.3 at low chlorophyll concentrations (<0.2 mg m^{-3}) as the model of Hirata et al. (2011) produces higher estimates of nanophytoplankton percent chlorophyll (between 0.04 to 0.2 mg m^{-3} chlorophyll) and lower estimates of microphytoplankton percent chlorophyll, when compared with Brewin et al. (2010a). Another source of the differences between curves in Figure 4.3 could be the spatial and temporal differences in *in situ* data used to parameterise each approach.

The observed differences in the patterns of change in the size structure with a change in chlorophyll between models (Figure 4.3) are further exemplified when mapping the differences between each approach to a monthly satellite composite of the North Atlantic (Figure 4.4).
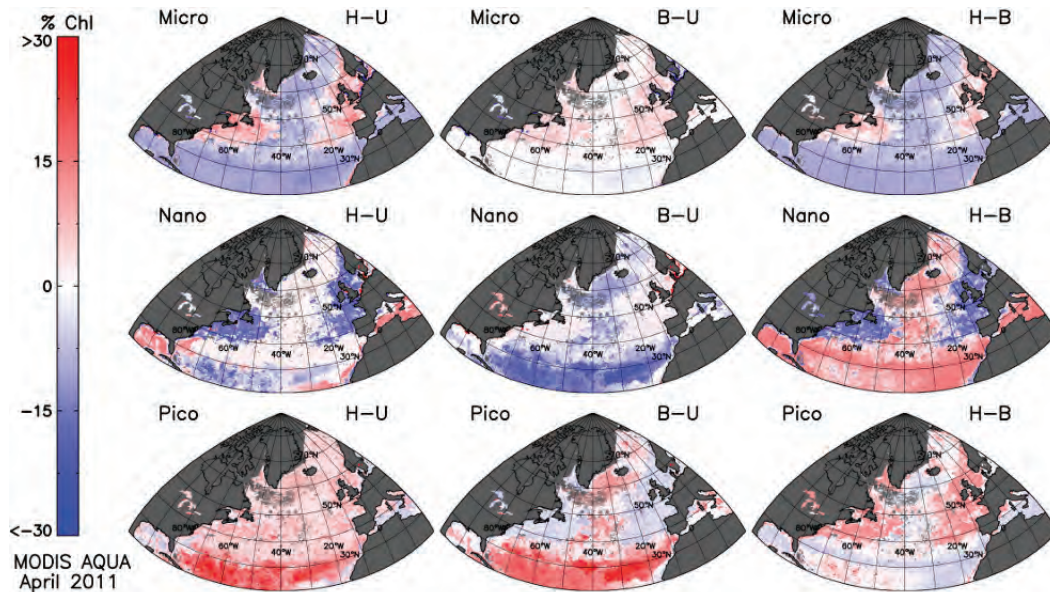
Figure 4.4 Comparison of abundance-based models for a Level 3, MODIS-Aqua composite of April 2011. H-U refers to the model results of Hirata et al. (2011) minus the results of Uitz et al. (2006); B-U refers to the model results of Brewin et al. (2010a) minus the results of Uitz et al. (2006); and H-B refers to the model results of Hirata et al. (2011) minus the results of Brewin et al. (2010a).

4.3 Spectral-Based Approaches

Spectral-based approaches utilise optical characteristics of phytoplankton or total particulate matter that vary as a function of size. To see how this might be done, let us begin with a brief examination of the relationship between ocean colour and inherent optical properties. Reflectance at the sea surface, at wavelength λ, can be related to the absorption (a) and backscattering coefficients (b_b) according to:

$$R_{rs}(\lambda) = G\frac{b_b(\lambda)}{a(\lambda) + b_b(\lambda)}, \tag{4.10}$$

where G is a dimensionless parameter that varies with sun-zenith angle and shape of the volume-scattering function. The absorption coefficient (a) can be partitioned into the sum of contributions from pure sea-water (a_w), phytoplankton (a_B) and combined non-algal particles and dissolved substances (a_{dg}) such that:

$$a(\lambda) = a_w(\lambda) + a_B(\lambda) + a_{dg}(\lambda). \tag{4.11}$$

The absorption by non-algal particles and dissolved substances are often combined in a remote sensing context, as they display similar spectral shapes (Carder et al. 1991; Nelson et al., 1998). Similarly, the backscattering coefficient can be expressed as:

$$b_b(\lambda) = b_{bw}(\lambda) + b_{bp}(\lambda), \tag{4.12}$$

where $b_{bw}(\lambda)$ represents back-scattering by pure seawater, and $b_{bp}(\lambda)$ refers to the backscattering from particulate matter, including both phytoplankton and detrital matter. In Case 1 waters, phytoplankton may directly or indirectly influence all non-water components of Eqs. 4.11 and 4.12 (a_B, a_{dg} and b_{bp}), but explicit optical information about the phytoplankton is only contained in the inherent optical properties (IOPs) directly determined by phytoplankton (a_B and to a lesser extent b_{bp}). Spectral-based approaches can therefore be partitioned into those that use distinct optical signatures of a_B (absorption approaches) or b_{bp} (backscattering approaches). In contrast to absorption approaches, the backscattering approaches provide information on the size of the whole particulate assemblage and not only on phytoplankton cells. There is currently no method to partition the contribution of b_{bp} by phytoplankton and non-algal particles using satellite data.

Approaches that utilise spectral information about either absorption or backscattering have been implemented using inversion methods, where the satellite reflectance is inverted to obtain information on size structure. One way to develop inversion methods is to use a forward model to simulate reflectance values where the IOPs are varied according to the size structure of the phytoplankton, from which a look-up-table is produced for comparison with the satellite reflectance to obtain information on size structure.

4.3.1 Absorption spectral-based approaches

Spectral-based approaches that use phytoplankton absorption (a_B) rely on size-dependent changes in the spectral shape of a_B or changes in the chlorophyll-specific absorption coefficient (a_B^*). It has been well established that small phytoplankton display a higher a_B^* at blue wavelengths and more pronounced peaks when compared with large phytoplankton cells (Duysens 1956; Morel and Bricaud, 1981; Sathyendranath et al., 1987). Such signatures have been used to develop absorption-based approaches for identifying size structure in phytoplankton communities from satellite data.

4.3.1.1 Two size classes of phytoplankton

Making use of size-fractioned phytoplankton absorption spectra (pico <2μm, ultra 2-5μm, nano 5-20μm and micro >2μm) and microscopic analyses from a variety of natural sea-water surface samples, Ciotti et al. (2002) suggested that a size parameter could be retrieved from the phytoplankton absorption coefficient normalised by its spectral mean for the 400–700 nm range, hereafter denoted $\underline{a}_B(\lambda)$. They found that more than 80% of the variability in $\underline{a}_B(\lambda)$ could be explained by the dominant size class and developed a two-component model that related $\underline{a}_B(\lambda)$ of a sample to the size structure of the phytoplankton. In their model, $\underline{a}_B(\lambda)$ is assumed to vary linearly between two possible extremes, which were represented by the smallest and the largest cells in their dataset. A dimensionless size factor (S_f) varying between 0 (100% microphytoplankton) and 1 (100% picophytoplankton) is used, such that:

$$\underline{a}_B(\lambda) = [S_f \underline{a}_{B,pico}(\lambda)] + [(1 - S_f)\underline{a}_{B,micro}(\lambda)], \tag{4.13}$$

where $\underline{a}_{B,pico}(\lambda)$ and $\underline{a}_{B,micro}(\lambda)$ represent the spectral shapes of pico- and microphytoplankton respectively. Ciotti and Bricaud (2006) partitioned the total absorption (a), derived from satellite data using the model of Loisel and Stramski (2000) and Loisel and Poteau (2006), into a_B and a_{dg} using either analytical decomposition or non-linear optimisation (Ciotti and Bricaud, 2006; Bricaud et al. 2012). The phytoplankton size factor (S_f) and the slope of the exponential decrease of a_{dg} with wavelength (S_{dg}) was obtained assuming:

$$
\begin{aligned}
a(\lambda) \;=\; & a_w(\lambda) + a_B(505)([S_f \underline{a}_{B,pico}(\lambda)] + [(1 - S_f)\underline{a}_{B,micro}(\lambda)]) \\
& + a_{dg}(443)\exp[-S_{dg}(\lambda - 443)].
\end{aligned}
\tag{4.14}
$$

The known parameters of the above equation are $a_B(505)$, $\underline{a}_{B,pico}(\lambda)$, $\underline{a}_{B,micro}(\lambda)$ and $a_w(\lambda)$. Phytoplankton absorption at 505 nm is estimated as a power function of chlorophyll (Bricaud et al., 1998) using a standard chlorophyll algorithm (e.g., NASA OC4) prior to the inversion. The retrieved parameters in the approach include S_f, $a_{dg}(443)$ and S_{dg}. Note that this approach allows a pixel-by-pixel retrieval of S_{dg} for

the very first time. Bricaud et al. (2012) successfully applied this approach to 12 years of SeaWiFS data and analysed spatial-temporal variations in phytoplankton size, as indexed by S_f, at global and regional scales.

Using the Ciotti et al. (2002) model, Mouw and Yoder (2010) developed an approach to estimate the fraction of microphytoplankton in the phytoplankton assemblage in a satellite pixel by application of a forward ocean-colour model. Using the HYDROLIGHT software (Mobley and Sundman, 2006), remote sensing reflectances ($R_{rs}(\lambda)$) were modelled using inherent optical properties (Figure 4.5). The phytoplankton absorption coefficient ($a_B(\lambda)$) was modelled as a function of chlorophyll and the chlorophyll-specific absorption coefficients for micro- and picophytoplankton derived from Ciotti et al. (2002) and Ciotti and Bricaud (2006), respectively. A size factor for microphytoplankton (S_{fm}), the inverse of the S_f parameter developed by Ciotti et al. (2002) ($S_{fm} = 1 - S_f$), was used to vary the chlorophyll-specific absorption coefficient between pico- and microphytoplankton. An ensemble of simulations was run varying S_{fm}, $a_{dg}(443)$ and chlorophyll concentration (C) within realistic bounds found across the global ocean. The result was a look-up table (LUT) of simulated $R_{rs}^{LUT}(\lambda)$, C, S_{fm} and $a_{dg}(443)$.

In their method, Mouw and Yoder (2010) first estimated chlorophyll and $a_{dg}(443)$ from satellite data using the GSM model (Maritorena et al., 2002). These values were then used to narrow the search-space of the simulated LUT. The satellite-retrieved remote-sensing reflectances ($R_{rs}^{SAT}(\lambda)$), adjusted so as to be equivalent to $R_{rs}^{LUT}(\lambda)$, were then compared with corresponding values in the LUT. The closest match between the adjusted and simulated values was determined and the associated S_{fm} assigned to that pixel. A schematic diagram showing the application of the approach of Mouw and Yoder (2010) is provided in Figure 4.5.

Devred et al. (2006) extended the two-population absorption model of Sathyendranath et al. (2001) to obtain the chlorophyll-specific absorption coefficients ($a_B^*(\lambda)$) for two component size classes. Their model estimates $a_B(\lambda)$ as a function of chlorophyll assuming the assemblages of the two sizes vary as the chlorophyll concentration changes, such that:

$$a_B(\lambda) = C_{p,n}^m [a_{p,n}^*(\lambda) - a_m^*(\lambda)][1 - \exp(-S_{p,n}C)] + a_m^*(\lambda)C, \qquad (4.15)$$

where $C_{p,n}^m$ represents the chlorophyll-maximum for small cells, $S_{p,n}$ determines the increase in small-celled chlorophyll with increasing total chlorophyll-a (C), and $a_{p,n}^*(\lambda)$ and $a_m^*(\lambda)$ represent chlorophyll-specific absorption coefficients of small- and large-celled populations, respectively. These parameters were derived directly from the absorption and chlorophyll data, assuming that small cells dominate at low chlorophyll concentrations. Devred et al. (2006) used $a_m^*(440)=0.05$ (m^2 [mgC]$^{-1}$) as an arbitrary threshold value to distinguish between populations dominated by small (pico- and nanophytoplankton) and large (microphytoplankton) populations, and demonstrated a good correlation between size structure inferred from absorption characteristics and those estimated independently using HPLC pigment analysis.

Figure 4.5 Schematic diagram showing the application of the approach of Mouw and Yoder (2010).

Significant seasonal and regional changes in $a_{p,n}^*(\lambda)$ and $a_m^*(\lambda)$ were identified, related to changes in species composition.

4.3.1.2 Three size classes of phytoplankton

Using a large database of absorption and HPLC data, and making use of relationships between HPLC diagnostic pigments and size structure (Vidussi et al., 2001; Uitz et al., 2006), Uitz et al. (2008) computed chlorophyll-specific absorption coefficients for pico- ($a_p^*(\lambda)$), nano- ($a_n^*(\lambda)$) and microphytoplankton ($a_m^*(\lambda)$), and modelled changes in these coefficients with depth-related changes in irradiance, such that:

$$a_B^*(\lambda) = \frac{1}{C} \sum_{i=1}^{3} C_i a_i^*(\lambda) \exp\left(-R_i \frac{z}{Z_p}\right), \tag{4.16}$$

where i = {pico-, nano- and microphytoplankton} and R_i represent the slopes describing the variations in the chlorophyll-specific absorption coefficients for the three size classes along the vertical z/Z_p axis (z = depth and Z_p = euphotic depth). The model was coupled to the abundance-based method of Uitz et al. (2006), and together with additional size-specific phytophysiological parameters (Uitz et al., 2008), used to compute size-fractionated primary production at regional and global scales (Silió-Calzada et al., 2008; Uitz et al., 2009; 2010; 2012).

Making use of HPLC data and the pigment size-class model of Brewin et al. (2010a) (see Eqs. 4.1 – 4.4), Brewin et al. (2011a) extended the two-component model of Sathyendranath et al. (2001) and Devred et al. (2006) to three-components, such that:

$$
\begin{aligned}
a_B(\lambda) \quad = \quad & a_p^*(\lambda)C_p^m[1 - \exp(-S_p C)] + \\
& a_n^*(\lambda)\{C_{p,n}^m[1 - \exp(-S_{p,n}C)] - C_p^m[1 - \exp(-S_p C)]\} + \\
& a_m^*(\lambda)\{C - C_{p,n}^m[1 - \exp(-S_{p,n}C)]\},
\end{aligned}
\tag{4.17}
$$

where the pico- and the nanophytoplankton components are split into two components, and $a_p^*(\lambda)$ and $a_n^*(\lambda)$ represent the chlorophyll-specific absorption coefficients of pico- and nanophytoplankton respectively, and S_p determines the rate of change in the chlorophyll concentration associated with picophytoplankton, with change in total chlorophyll concentration. The three terms in Eq. 4.17 represent the contributions to absorption at wavelength (λ) from each of the three size classes.

To solve the above equation, Brewin et al. (2011a) used a database of corresponding phytoplankton absorption and HPLC pigment data (Werdell and Bailey, 2005). The parameters $C_{p,n}^m$, C_p^m, $S_{p,n}$ and S_p were first obtained using the pigment-based model of Brewin et al. (2010a) (see Eqs. 4.1 – 4.4), and then Eq. 4.17 was fitted to the phytoplankton absorption and chlorophyll data to obtain the chlorophyll-specific absorption coefficients for pico- ($a_p^*(\lambda)$), nano- ($a_n^*(\lambda)$) and microphytoplankton ($a_m^*(\lambda)$). They used the model to map the absorption at 443 nm from the three size

classes, using Eq. 4.17 along with satellite-derived chlorophyll values (O'Reilly et al., 1998).

Devred et al. (2011) solved Eq. 4.17 by successive two-step application of the two-component model of Sathyendranath et al. (2001) and Devred et al. (2006), such that, $a_p^*(\lambda)$, $a_n^*(\lambda)$ and $a_m^*(\lambda)$ were derived directly from the absorption and chlorophyll data. The method was then integrated into the model of Sathyendranath and Platt (1997), incorporating Raman Scattering (Sathyendranath and Platt, 1998), to compute the chlorophyll concentrations of the three size classes directly from remote-sensing reflectances, using non-linear optimisation. Computed size-fractionated chlorophyll compared well with independent estimates using HPLC pigment data.

4.3.1.3   Comparison of spectral approaches based on absorption

Figure 4.6 shows spectral values of chlorophyll-specific phytoplankton absorption coefficients for pico-, nano- and microphytoplankton from a number of studies. In general, the coefficients display some consistency, such that at blue wavelengths picophytoplankton has higher chlorophyll-specific absorption coefficients than the nanophytoplankton size class, which are higher than those of the microphytoplankton size class. Furthermore, picophytoplankton generally displays sharper peaks in absorption than the nano-size class, and the microphytoplankton size class displays the flattest spectral shape.

Despite this consistency, some differences are also evident in Figure 4.6. A probable cause is differences in the methods by which the coefficients were derived. For instance, the Uitz et al. (2008) and the Brewin et al. (2011a) methods made use of HPLC data, Ciotti et al. (2002) made use of filtered size-fractioned phytoplankton absorption data, and Devred et al. (2006; 2011) used phytoplankton absorption and chlorophyll data. There are also considerable spatio-temporal differences in the datasets used in each study. The chlorophyll-specific phytoplankton absorption coefficient and its associated spectral shape are influenced not only by phytoplankton size structure, but also the physiological state of the phytoplankton and changes in the growth environment (Johnsen et al., 1994). Differences in phytoplankton species within size-classes are also likely contributors to the discrepancies between coefficients presented in Figure 4.6. It remains to be evaluated how sensitive the spectral-based absorption approaches are to variations as shown in Figure 4.6.

To evaluate the sensitivity of blue-green reflectance ratios (typically used to estimate chlorophyll empirically from satellite data) to the differences in the chlorophyll-specific phytoplankton absorption coefficients of the different size classes, a simple Case 1 optical model was developed (Figure 4.7). In this model, the IOPs are modelled as a function of chlorophyll: a_d and a_g are modelled following Bricaud et al. (2010) and Morel (2009); a_w is taken from Pope and Fry (1997); b_{bp} is modelled following Huot et al. (2008); and b_{bw} is estimated from Zhang and Hu (2009) and Zhang et al. (2009). The phytoplankton absorption coefficient (a_B) was estimated as a product of
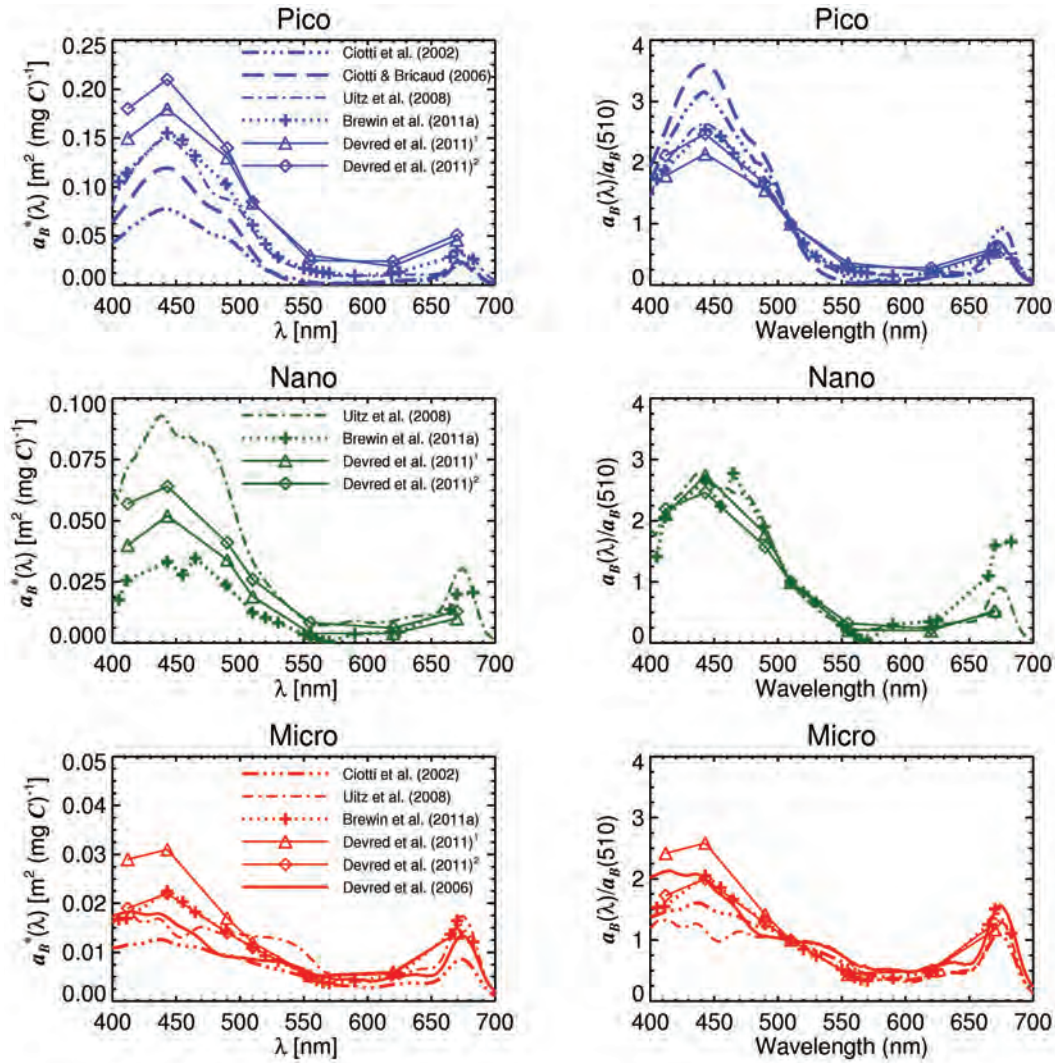
Figure 4.6 Chlorophyll-specific phytoplankton absorption coefficients and spectral shapes of phytoplankton absorption coefficients for three size classes, estimated from some studies. For the Devred et al. (2011) study, the super-script 1 refers to coefficients derived using data from the North-West Atlantic and super-script 2 data from the NOMAD database. For the Uitz et al. (2008) study, surface spectra are shown and z/Z_p in Eq. 4.16 is set to zero.

the chlorophyll-specific phytoplankton absorption coefficient (a_B^*) and chlorophyll concentration. Having computed a and b_b, remote-sensing reflectance (R_{rs}) was estimated at a number of wavelengths following Gordon et al. (1988). A number of simulations were run for each size class by varying a_B^* among values shown in Figure 4.6. The maximum band ratio ($R_{rs}(443) > R_{rs}(490) > R_{rs}(510)/R_{rs}(555)$) for each simulation was then plotted as a function of chlorophyll (Figure 4.7) with the empirical OC4v6 algorithm O'Reilly et al. (1998) superimposed.

Consistent with Dierssen (2010), the general shape of the OC4v6 algorithm was retrieved for each simulation, with high blue-green reflectance-ratios at low chlorophyll concentrations and low blue-green reflectance-ratios at high chlorophyll concentrations. The amplitude and shape of the trend line, however, varied according to the size structure. At lower chlorophyll concentrations, the OC4v6 algorithm was closer to the picophytoplankton simulations, but at higher chlorophyll concentrations it was closer to the nano- and microphytoplankton simulations. The results highlight the fact that information on the absorption properties of phytoplankton size is implicit in the empirical OC4v6 algorithm (Dierssen, 2010). Both *in situ* and modelling studies, however, have shown that empirical algorithms such as the OC4v6, can overestimate chlorophyll concentration in waters where specific IOP values are higher than average and vice versa (Loisel et al. 2010; Mouw et al., 2012). For instance, as shown in Figure 4.7 at a chlorophyll concentration of $1\,\mathrm{mg\,m^{-3}}$, if a picophytoplankton population dominates, with a higher than average $a_B^*(443)$ typically observed at $1\,\mathrm{mg\,m^{-3}}$, chlorophyll would be overestimated using the OC4v6 algorithm. Studies have shown that species-dependant algorithms can result in better estimates of chlorophyll when compared with standard empirical algorithms (Sathyendranath et al., 2004b; Alvain et al., 2006).

For our test case (Figure 4.7), the relationships between the blue-green reflectance-ratios and chlorophyll concentration display consistency for each size class. For a given chlorophyll concentration, the blue-green reflectance-ratio of picophytoplankton is always lower than that of nanophytoplankton, which is lower than that of the microphytoplankton size class, regardless of whether values from the studies of Ciotti and Bricaud (2006), Uitz et al. (2008), Brewin et al. (2011a) or Devred et al. (2011) were used.
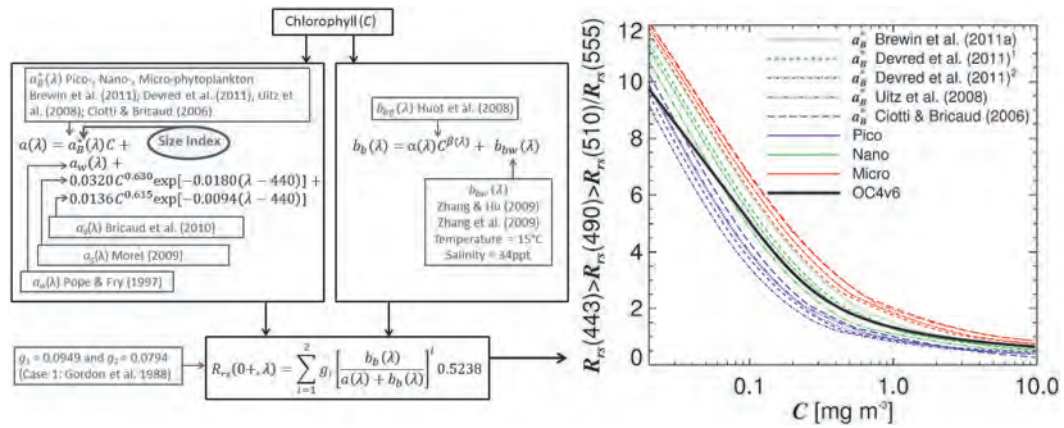
Figure 4.7 An example of the expected variation in the ratio of blue-to-green reflectance caused by varying the chlorophyll-specific phytoplankton absorption coefficients of three size classes of phytoplankton from a number of different studies shown in Figure 4.6.

4.3.2 Backscattering approaches

Backscattering approaches differ from absorption-based approaches as they provide size estimates for the whole particulate pool and not just for phytoplankton. To link the size-structure of the whole particulate pool with the size-structure of the phytoplankton assumes that either the ocean particulate assemblage is predominately biogenic, or that there exists some natural covariation between the size distributions of phytoplankton and that of non-algal particles.

Spectral-based approaches that use the particle backscattering coefficient (b_{bp}) to derive information on size structure typically rely on the assumption that small particles have enhanced backscattering towards shorter wavelengths, whereas larger particles tend to have a flatter backscattering spectrum. Morel (1973) showed that the spectral dependency of scattering is sensitive to the shape of the particle size distribution (PSD), using theoretical calculations. Using field data, Reynolds et al. (2001) observed that the spectral dependency of b_{bp} expressed as a power function with exponent γ increases with the relative contribution of small sized particles to the total particle assemblage (see also Ulloa et al., 1994). Their equation is represented as Eq. 4.18 below, where λ_0 is the reference wavelength.

$$b_{bp}(\lambda) = b_{bp}(\lambda_0) \left(\frac{\lambda}{\lambda_0} \right)^{-\gamma}. \tag{4.18}$$

Using Mie scattering calculations, Ulloa et al. (1994) and Wozniak and Stramski (2004) found that, as the slope of the PSD increases, so does the spectral slope of b_{bp} (γ). Therefore, γ may provide an index of the proportion of small-sized and larger particles in the total particle assemblage, and potentially information on the slope of the PSD, with higher γ values indicating a steeper slope of the PSD and vice versa.

Loisel et al. (2006) applied an inverse optical model (Loisel and Stramski, 2000; Loisel and Poteau, 2006) to derive the particulate backscattering coefficient (b_{bp}) at three wavelengths. Once b_{bp} is obtained at the three wavelengths using the Loisel and Poteau (2006) model, Loisel et al. (2006) computed γ as the slope of the linear regression between $\log[b_{bp}(\lambda)]$ and $\log[(\lambda)]$. Application of the model to satellite imagery demonstrated a general decrease in γ from oligotrophic to eutrophic regimes, with higher values of γ (> 2) in oligotrophic waters where smaller phytoplankton dominate, and lower values of γ (~ 0) in more eutrophic waters where larger phytoplankton dominate. This is consistent with the expectation that small particles have enhanced backscattering at shorter wavelengths and that the spectral shape of back-scattering by large particles is flatter. An inverse correlation between chlorophyll and γ was noted, but with significant spatial and temporal variation.

Kostadinov et al. (2009) assumed that the PSD can be approximated by a linear function in log space (the classical power-law or Junge-type distribution), with

parameters ξ, the slope, and N_0, the particle number concentration for a given reference diameter D_0, such that:

$$N(D) = N_0 \left(\frac{D}{D_0}\right)^{-\xi},$$

(4.19)

where $N(D)$ is the number of particles per volume of seawater normalised by the size bin width and D is the particle diameter. Based on simulations using Mie theory, a look-up table (LUT) was generated of γ and corresponding values of ξ and $\log_{10}(b_{bp}(440)/N_o)$. Using satellite remote-sensing reflectance, γ and $b_{bp}(440)$ were computed using the model of Loisel and Poteau (2006), on a pixel-by-pixel basis. Corresponding values of ξ and N_o were then estimated from the LUT. Then, ξ and N_o were used to estimate the particle number and volume concentrations of pico-, nano- and micro-sized particles by integration of Eq. 4.19 between certain size diameter limits. A schematic diagram of the method of Kostadinov et al. (2009) is provided in Figure 4.8.

Kostadinov et al. (2009) provide a detailed description of assumptions and uncertainties in their approach and highlight the fact that highest uncertainty is expected in very productive regions. Furthermore, when retrieving information on particle size-structure, the assumption is made that relative proportions of biovolume are roughly constant across size classes. The Kostadinov et al. (2009) approach was validated against HPLC data (Kostadinov et al., 2010) which indicated pigment-based pico-, nano- and micro-sized phytoplankton correspond approximately to pico-, nano- and micro-particles derived from backscattering. The approach has been applied to 10-years of satellite measurements to investigate seasonal and inter-annual variations in phytoplankton size structure (Kostadinov et al., 2010). Results indicate that, whereas spatial patterns in log-transformed chlorophyll and ξ exhibit a marked inverse correlation ($r = -0.88$ for waters deeper than 200m), trends in ξ and particle-size classes, and their relationships with the El Niño Southern Oscillation, may behave differently to that of chlorophyll, emphasising a need to capture additional information beyond chlorophyll, for use in ocean ecosystem characterisation.

Using data from the Benguela (eastern boundary current system) in South Africa, Hirata et al. (2008b) developed a model that retrieves ξ, and then linked it to the dominant phytoplankton size class. Using Lorenz-Mie light scattering theory, the ratio of b_{bp} at two wavelengths (λ_1 and λ_2) can be tied to ξ and γ assuming that:

$$\frac{b_{bp}(\lambda_1)}{b_{bp}(\lambda_2)} = \left(\frac{\lambda_1}{\lambda_2}\right)^{-\xi+3} = \left(\frac{\lambda_1}{\lambda_2}\right)^{-\gamma},$$

(4.20)

where $\gamma = \xi - 3$ (Morel, 1973). Equation 4.20 shows that it is the relative spectral variation of $b_{bp}(\lambda)$ at a pair of wavelengths that is required to estimate ξ rather than the absolute magnitude of $b_{bp}(\lambda)$. The Lorenz-Mie approach also highlights the direct
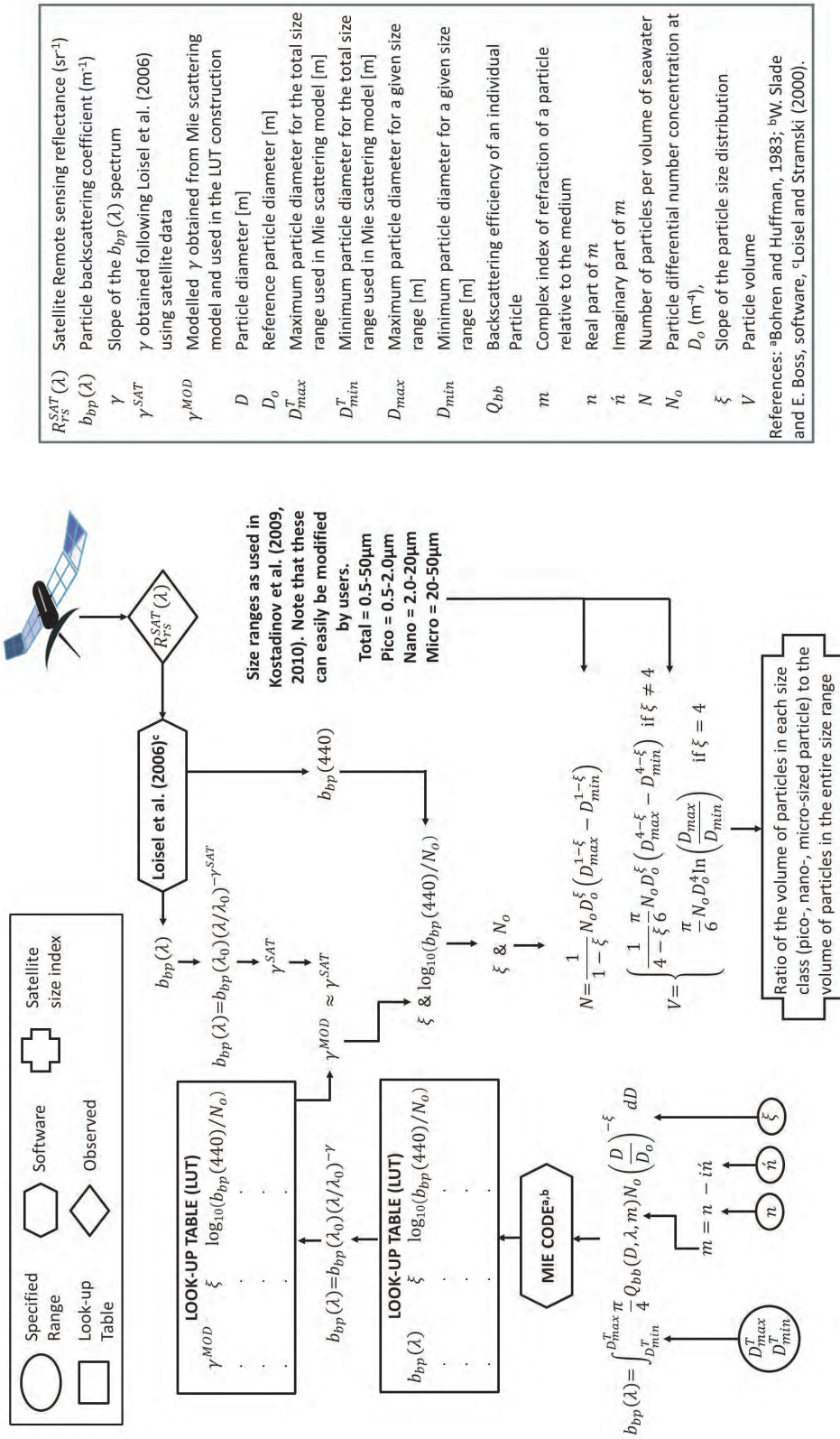
$R_{rs}^{SAT}(\lambda)$	Satellite Remote sensing reflectance (sr⁻¹)
$b_{bp}(\lambda)$	Particle backscattering coefficient (m⁻¹)
γ	Slope of the $b_{bp}(\lambda)$ spectrum
γ^{SAT}	γ obtained following Loisel et al. (2006) using satellite data
γ^{MOD}	Modelled γ obtained from Mie scattering model and used in the LUT construction
D	Particle diameter [m]
D_o	Reference particle diameter [m]
D_{max}^T	Maximum particle diameter for the total size range used in Mie scattering model [m]
D_{min}^T	Minimum particle diameter for the total size range used in Mie scattering model [m]
D_{max}	Maximum particle diameter for a given size range [m]
D_{min}	Minimum particle diameter for a given size range [m]
Q_{bb}	Backscattering efficiency of an individual Particle
m	Complex index of refraction of a particle relative to the medium
n	Real part of m
$\acute{n}$	Imaginary part of m
N	Number of particles per volume of seawater
N_o	Particle differential number concentration at D_o (m⁻⁴),
ξ	Slope of the particle size distribution.
V	Particle volume

References: [a]Bohren and Huffman, 1983; [b]W. Slade and E. Boss, software, [c]Loisel and Stramski (2000).

Legend:
- Specified Range
- Software
- Look-up Table
- Satellite size index
- Observed

Size ranges as used in Kostadinov et al. (2009, 2010). Note that these can easily be modified by users.
Total = 0.5-50µm
Pico = 0.5-2.0µm
Nano = 2.0-20µm
Micro = 20-50µm

Loisel et al. (2006)[c]

$b_{bp}(\lambda)$

$b_{bp}(\lambda) = b_{bp}(\lambda_0)(\lambda/\lambda_0)^{-\gamma^{SAT}}$

γ^{SAT}

$\gamma^{MOD} \approx \gamma^{SAT}$

LOOK-UP TABLE (LUT)

$\gamma^{MOD} \quad \xi \quad \log_{10}(b_{bp}(440)/N_o)$

$b_{bp}(\lambda) = b_{bp}(\lambda_0)(\lambda/\lambda_0)^{-\gamma}$

LOOK-UP TABLE (LUT)

$b_{bp}(\lambda) \quad \xi \quad \log_{10}(b_{bp}(440)/N_o)$

MIE CODE[a,b]

$m = n - i\acute{n}$

$b_{bp}(\lambda) = \int_{D_{min}^T}^{D_{max}^T} \frac{\pi}{4} Q_{bb}(D,\lambda,m) N_o \left(\frac{D}{D_o}\right)^{-\xi} dD$

$b_{bp}(440)$

ξ & $\log_{10}(b_{bp}(440)/N_o)$

ξ & N_o

$N = \frac{1}{1-\xi} N_o D_o^\xi \left(D_{max}^{1-\xi} - D_{min}^{1-\xi}\right)$

$V = \begin{cases} \frac{1}{4-\xi}\frac{\pi}{6} N_o D_o^\xi \left(D_{max}^{4-\xi} - D_{min}^{4-\xi}\right) & \text{if } \xi \neq 4 \\ \frac{\pi}{6} N_o D_o^4 \ln\left(\frac{D_{max}}{D_{min}}\right) & \text{if } \xi = 4 \end{cases}$

Ratio of the volume of particles in each size class (pico-, nano-, micro-sized particle) to the volume of particles in the entire size range

Figure 4.8 Schematic diagram showing the application of the approach of Kostadinov et al. (2009) to satellite data.

relationship between γ and ξ. However, the full Mie calculations show deviations from this simple relationship, especially for low values of ξ (e.g., see Figure 1 in Kostadinov et al., 2009). Using *in situ* data, Hirata et al. (2008b) showed that γ_t (the spectral dependency of b_b, not of b_{bp}) may be related to γ according to $\gamma = 0.562\gamma_t - 0.220$. Then ξ was estimated as:

$$\xi = 0.562\gamma_t + 2.780. \tag{4.21}$$

Hirata et al. (2008b) also used a relationship between ocean-colour reflectance ratio and γ_t. The ocean-colour reflectance can be expressed as:

$$R_{rs}(\lambda) = tF(\lambda)\frac{b_b(\lambda)}{a(\lambda)}, \tag{4.22}$$

where t and $F(\lambda)$ are the transmittance function between air-sea interface and the bidirectional reflectance function, respectively. When t has no significant wavelength dependency (Austin, 1974), the ocean-colour reflectance ratio can be expressed as:

$$\frac{R_{rs}(\lambda_1)}{R_{rs}(\lambda_2)} = \delta(\lambda_1,\lambda_2)\frac{b_b(\lambda_1)}{b_b(\lambda_2)} = \delta(\lambda_1,\lambda_2)\left(\frac{\lambda_1}{\lambda_2}\right)^{-\gamma_t}, \tag{4.23}$$

where $\delta(\lambda_1,\lambda_2)$ is $[F(\lambda_1)a(\lambda_2)]/[F(\lambda_2)a(\lambda_1)]$. For the wavelength pair $\lambda_1 = 490\,\text{nm}$ and $\lambda_2 = 555\,\text{nm}$, Hirata et al. (2008b) found a mean value of $\delta(\lambda_1,\lambda_2)^{-1}$ of 1.003, with a standard deviation of 0.291, based on an analysis of *in situ* data (NOMAD version 2.0). Substitution of Eq. 4.21 into 4.23 (assuming $\delta(\lambda_1,\lambda_2)$ is constant), gives:

$$\xi = A_1 \cdot \log\left(\frac{R_{rs}(\lambda_1)}{R_{rs}(\lambda_2)}\right) + A_0, \tag{4.24}$$

where A_1 and A_0 are empirically-determinable coefficients. Eq. 4.24 suggests that ξ may be derived from a simple ocean-colour ratio. Note that ξ derived using Eq. 4.24 is highly correlated with chlorophyll estimated from a simple ocean-colour ratio (O'Reilly et al., 1998). Hirata et al. (2008b) showed that for the Benguela study area $A_0 = 2.5311$ and $A_1 = 1.4480$ when using satellite $R_{rs}(\lambda)$. They then identified the dominant phytoplankton size classes using threshold values of ξ derived from *in situ* data ($\xi <2.38$ for microphytoplankton, $\xi >2.38$ and <3.53 for nanophytoplankton, and $\xi >3.53$ for picophytoplankton).

Figure 4.9 shows maps of (a) ξ, (b) the dominant phytoplankton size classes estimated using the backscattering approach of Hirata et al. (2008b) and (c) the absorption approach of Hirata et al. (2008a), for the Benguela upwelling system using SeaWiFS data for December 2005. It is clear that the dominant phytoplankton size classes derived from both approaches (backscattering and absorption) agree well.
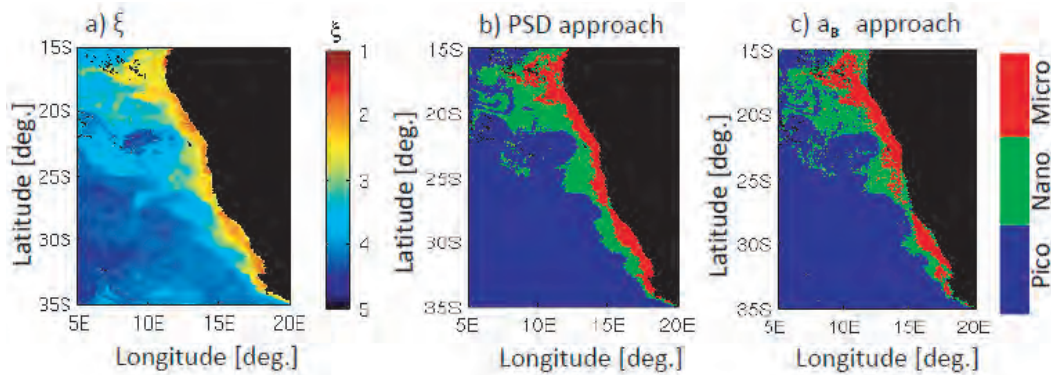
Figure 4.9 SeaWiFS-derived variables for December 2005: a) Junge parameter ξ, b) phytoplankton size classes using the backscattering and PSD approach following Hirata et al. (2008b), and c) phytoplankton size classes using the absorption approach (a_B) following Hirata et al. (2008a). Higher values of ξ (approximately 5) indicate abundance of smaller particles, and lower values (toward 1) indicate larger particles.

4.3.2.1 Comparison of spectral approaches based on backscattering

The spectral approaches based on backscattering of Loisel et al. (2006) and Kostadinov et al. (2009) differ in their conceptual framework from that of Hirata et al. (2008b). Loisel et al. (2006) estimate γ using an inversion model and relate it qualitatively to small and large particles in the ocean. The method of Kostadinov et al. (2009) builds on the work of Loisel et al. (2006), and using Mie theory, relates γ quantitatively to parameters of the particle size distribution (PSD), such as the slope (ξ) and the particle number concentration (N_o) for a given reference diameter (D_o), to compute the particle volume concentrations of three size classes of particles. Alternatively, Hirata et al. (2008b) empirically relate the slope of the PSD (ξ) to a simple blue-green ocean-colour band-ratio. These differences notwithstanding, all three approaches link a change in particle size structure to a change in the spectral slope of $b_{bp}(\lambda)$ (γ), and assume that particle populations dominated by small particles have a relatively high value of γ and ξ and the inverse for particle populations dominated by large particles.

To evaluate the sensitivity of blue-green reflectance ratios to the differences in values of γ associated with small and large particles, a simple Case 1 optical model was developed (Figure 4.10), similar to that of Figure 4.7. In this model, the IOPs are modelled as a function of chlorophyll: a_d and a_g are modelled following Bricaud et al. (2010) and Morel (2009); a_B modelled as a power-function of chlorophyll following Bricaud et al. (1995); a_w is taken from Pope and Fry (1997); $b_{bp}(550)$ is modelled following Huot et al. (2008); and b_{bw} is estimated from Zhang and Hu (2009) and Zhang et al. (2009). Using different values of γ, the spectral shape of b_{bp} is then set to environments expected of small-cell dominated populations ($\gamma \sim 2$) and environments dominated by large-cell populations ($\gamma \sim -1$). Having computed

a and b_b, remote sensing reflectance (R_{rs}) was estimated at a number of wavelengths following Gordon et al. (1988) for the different values of γ. A maximum band ratio ($R_{rs}(443) > R_{rs}(490) > R_{rs}(510)/R_{rs}(555)$) for each simulation was then plotted as a function of chlorophyll (Figure 4.10) with the empirical OC4v6 algorithm (O'Reilly et al., 1998) superimposed.
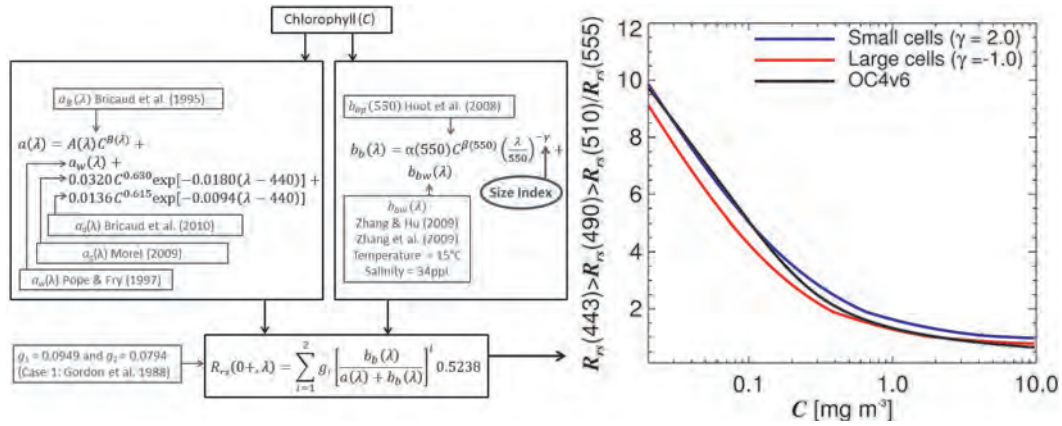
Figure 4.10 An example of the expected variation in the ratio of blue-to-green reflectance caused by varying typical values of γ for small and large particles.

Consistent with Figure 4.7, the general shape of the OC4v6 algorithm was retrieved for each simulation (Figure 4.10). However, the location of the trend line varied according to the chosen γ value. At lower chlorophyll, the OC4v6 algorithm was closer to the model results for environments dominated by small cells ($\gamma \sim 2$), whereas, at higher chlorophyll the OC4v6 algorithm was closer to that of environments dominated by large cells ($\gamma \sim -1$), indicating that information on the backscattering properties of the size classes are also implicitly built into the empirical OC4v6 algorithm.

4.4   Discussion

4.4.1   Spectral-based approaches: absorption or backscattering?

Spectral-based models shown in this chapter are based on the spectral characteristics of either the phytoplankton absorption coefficient, or the particle backscattering coefficient. There are advantages and disadvantages to using either index.

The advantage of using spectral characteristics of the phytoplankton absorption coefficient, in comparison with the particle backscattering coefficient, is that it can be solely tied to the phytoplankton, whereas, the particle backscattering coefficient is influenced by all particles (organic or inorganic) in addition to phytoplankton. Whereas some studies have attempted to partition the influence of these components on b_{bp} using Mie scattering theory (Stramski and Keifer, 1991), there is currently

no method available using satellite data. Some have argued that phytoplankton are responsible for only a small fraction of backscattering by particles, as they are large with respect to the wavelengths of visible light and their refractive index is similar to seawater (Stramski and Keifer, 1991). However, numerous evidences, based on theoretical and experimental studies, have suggested that phytoplankton-sized particles may contribute more to backscattering than previously predicted (Bohren and Singham, 1991; Bricaud et al., 1992; Kitchen and Zaneveld, 1992; Vaillancourt et al., 2004; Clavano et al., 2007; Bernard et al. 2009; Dall'Olmo et al., 2009; Whitmire et al., 2010; Martinez-Vicente et al., 2012).

On the other hand, the shape of the phytoplankton absorption coefficient is influenced by light and nutrient-driven changes in intracellular pigment concentrations, whereas, the particle backscattering coefficient is less sensitive to physiological variability in the phytoplankton. Making use of bio-optical models tuned to the Chukchi and Bering Sea shelf region, Fujiwara et al. (2011) used information on both the shape of the phytoplankton absorption coefficient and the shape of the particle backscattering coefficient, as input to a multi-linear regression to determine the fraction of small and large celled phytoplankton in Artic waters. They found model performance improved when using both pieces of information.

4.4.2 Advantages and disadvantages of abundance-based and spectral-based approaches

As highlighted in Figures 4.7 and 4.10, empirical relationships that tie the chlorophyll concentration to the ratio of blue to green reflectance, implicitly contain information on the size structure of the phytoplankton. Abundance-based approaches essentially expose these underlying relationships. They are easy to implement offering a simple method to reveal the expected size structure of the phytoplankton at a given pixel, based on *in situ* correlations between size structure and phytoplankton abundance. The model of Hirata et al. (2008b) could also fall under the abundance-based category, considering it uses a blue-to-green reflectance ratio to estimate the slope of the particle size distribution which is empirically related to size structure. Abundance-based approaches have been used in primary production models to provide synoptic estimates of size-fractionated primary production using satellite data (Silió-Calzada et al., 2008; Uitz et al., 2008; 2009; 2010; 2012; Hirata et al., 2009; Brewin et al., 2010b).

A disadvantage of abundance-based approaches is that they are indirect methods for detecting phytoplankton size structure. They rely on observed patterns of change in the size structure with a change in abundance. They would fail to distinguish between blooms of different types of phytoplankton with the same abundance. Variability in optical properties of phytoplankton within size-classes according to temperature, nutrient and light regimes may introduce additional classification errors. Furthermore, considering that abundance-based methods rely

on observed relationships between size structure and abundance, and considering that these relationships maybe subject to change (e.g., climate change), abundance-based approaches are less suitable for long-term analysis as they require on-going recalibration with *in situ* observations.

In comparison with abundance-based approaches, spectral-based approaches are more direct, as they rely on observing distinct optical signatures. They are therefore more suitable for long-term analysis. Unlike abundance-based approaches, they are also capable of detecting changes in size structure independent of phytoplankton concentration.

A disadvantage of spectral-based approaches is that the optical signatures on which they depend can be small and easily confounded with noise (Garver et al., 1994). Accurately exploiting the spectral characteristics of different phytoplankton size classes to identify and distinguish among them may not always be successful. Problems with spectral-based approaches can also occur when trying to discriminate different phytoplankton size classes with similar optical signatures. Furthermore, as with abundance-based approaches, variability in optical properties of phytoplankton within size-classes according to temperature, nutrient and light regimes, may also introduce additional classification errors in absorption-based approaches.

An initial intercomparison of abundance-based and spectral-based approaches indicated that they may perform with similar accuracy (Brewin et al., 2011b). However, uncertainties in the intercomparison procedure and data sources (both *in situ* and satellite) suggest that improved availability of *in situ* observations is required to draw more definitive conclusions. Continuing international intercomparison efforts are currently underway (Hirata et al., 2012).

Figure 4.11 shows a hierarchical classification of models used for phytoplankton size-class detection as described in this chapter. The models become progressively more complex and complete from the upper to the lower level of the flow diagram. Pending future international intercomparison efforts (Hirata et al., 2012), there is currently little evidence to indicate which approach gives the best performance. It is likely that models perform differently under contrasting conditions and environments, hence the need to tailor models for specific applications or for specific regions. The choice of model, whether abundance-based or spectral-based (using absorption or backscattering approaches), should depend very much on the scientific question being addressed.

The glossary box in the figure contains:

Symbol	Definition
$R_{rs}(\lambda)$	Remote sensing reflectance (sr^{-1})
$L_w(\lambda)$	Water-leaving radiance (uW cm^{-2} nm^{-1} sr^{-1})
C	Chlorophyll-a concentration (mg m^{-3})
ξ	Junge slope of the particle size distribution
$b_b(\lambda)$	Backscattering coefficient (m^{-1})
$b_{bp}(\lambda)$	Backscattering coefficient of particles (m^{-1})
$b_{bw}(\lambda)$	Backscattering of seawater (m^{-1})
γ	Spectral dependency of $b_{bp}(\lambda)$
$a(\lambda)$	Total absorption coefficient (m^{-1})
$a_B(\lambda)$	Phytoplankton absorption coefficient (m^{-1})
$a_{dg}(\lambda)$	Detritus + dissolved absorption coefficient (m^{-1})
$a_w(\lambda)$	Seawater absorption coefficient (m^{-1})
$a_B^*(\lambda)$	Chlorophyll-specific $a_B(\lambda)$ (m^2 [mg Chl-a]$^{-1}$)

References: [1]Uitz et al. (2006), [2]Hirata et al. (2008), [3]Brewin et al. (2010), [4]Hirata et al. (2011), [5]Hirata et al. (2008b), [6]Loisel et al. (2006), [7]Kostadinov et al. (2009), [8]Ciotti & Bricaud (2006), [9]Ciotti et al. (2002), [10]Mouw & Yoder (2010), [11]Devred et al. (2011).

Figure 4.11 A hierarchical classification of models used for phytoplankton size-class detection. The models become progressively more complex and complete as we move from the upper to the lower level of the flow diagram.

4.4.3 Novel and future methods

In this chapter, methods for detecting phytoplankton size structure have been partitioned into abundance-based and spectral-based approaches. This classification is by no means exhaustive. Advanced statistical approaches have been applied to optical data to extract additional information on phytoplankton such as size structure. Such methods include self-organising maps, multi-layered perceptrons and neural-networks (Chazottes et al., 2006; 2007; Bricaud et al. 2007).

Raitsos et al. (2008) used combined bio-optical and other information (including chlorophyll concentration, water-leaving radiance, sea-surface temperature (SST), photosynthetic available radiation, wind stress and geographic and temporal location) as input to a neural-network to map the distribution of diatoms, dinoflagellates, silicoflagellates and coccolithophores. The phytoplankton types were grouped into size-classes and included in a size-class intercomparison (Brewin et al., 2011b) yielding reasonable results. Barnes et al. (2011) used information on remotely-sensed SST as well as chlorophyll concentration as input to an empirical model to estimate information about the phytoplankton community in relation to its size structure, such as the median phytoplankton cell weight and the slope and intercept of the size spectra.

Pan et al. (2010b) developed empirical algorithms based on reflectance ratios to approximate key phytoplankton pigment concentrations (e.g., fucoxanthin and zeaxanthin) in the northeast coast of the United States. Using these empirical algorithms coupled to CHEMTAX analysis, the distributions of different phytoplankton communities were mapped using satellite observations (Pan et al. 2010a). Such an approach could be applied to HPLC-based size class classification methods, to map size-class distributions using satellite observations. Roy et al. (2010) developed an approach that used the *in vivo* absorption coefficient of phytoplankton cells per unit chlorophyll concentration, to derive the average size of the phytoplankton population analytically. Their model computes the average cell size for a sample, given the phytoplankton absorption coefficient at 676 nm and the chlorophyll concentration. The method is easy to apply as an operational tool for *in situ* measurements and has the potential for application to remote sensing of ocean-colour data.

Most of the theoretical models that underpin our understanding of the effect of size on inherent optical properties are based on the assumption that the suspended particles in the ocean, including phytoplankton, can be modelled as homogenous spheres. But refinements to such models have been explored Kitchen and Zaneveld (1992). For example, Bernard et al. (2007; 2009) investigated the optical properties of algal cells using two-layered spherical geometry. Two-layered models were used to examine effects of varying cellular geometry, chloroplast volume and complex index of reflection on optical efficiency factors. The approach was then extended to poly-dispersed populations using equivalent size distribution models to demonstrate variability in simulated inherent optical properties for phytoplankton assemblages

of changing dominant cell size and functional type. The study indicated that the combined use of equivalent size distributions with heterogeneous geometry can be used to establish a quantitative formulation between single particle optics, size structure and assemblage-specific IOPs, and has potential for application to ocean colour.

A recurrent problem in using ocean-colour data to extract information on phytoplankton or particle size structure is the limited number of wavelengths available to address the problem, compared with the number of model parameters that are to be retrieved. The development of hyperspectral remote sensing is expected to alleviate this problem significantly. Hyperspectral remote sensing may allow for monitoring additional spectral features characteristic of phytoplankton communities that are indistinguishable though current multi-spectral sensors. Lubac et al. (2008) used *in situ* hyperspectral and multispectral data to investigate the feasibility of detecting *Phaeocystis globosa* in coastal waters. They found that, whereas it is feasible to detect *Phaeocystis globosa* using multispectral data, additional information about CDOM concentration should be included. By analysing the second derivative of R_{rs} using hyperspectral data, which was found to be closely related to a_B^* of *Phaeocystis globosa* as well as its relative biomass, additional information about CDOM concentration was not required, as the second derivative was not effected by the characteristic exponential function associated with CDOM.

4.5   Summary

In this chapter a number of approaches designed to detect phytoplankton size structure have been illustrated. Such approaches were partitioned into abundance-based methods, that rely on observed relationships between some measure of abundance of phytoplankton and their size structure, and spectral-based methods, that utilise optical characteristics of phytoplankton or total particulate matter that vary as a function of size.

Abundance-based methods were partitioned into those that rely on discrete trophic classes and those that estimate phytoplankton size structure based on a continuum of abundance measures. Despite their conceptual differences, abundance-based methods essentially assume a change in size structure with a change in chlorophyll (or possibly other measures of abundance, such as total phytoplankton absorption coefficient at a specific wavelength), with large cells dominating at high concentrations and small cells at low concentrations. Differences between abundance-based approaches can be partly explained by the differences in the methods and *in situ* data used for model parameterisation.

Spectral-based methods can be partitioned into those that use distinct optical signatures of the phytoplankton absorption coefficient or the particle backscattering coefficient. Absorption-based spectral approaches have been proposed to detect

two and three size classes, and despite some conceptual differences, essentially rely on the assumption that small cells have a higher chlorophyll-specific absorption coefficient at blue wavelengths and more pronounced peaks when compared with larger phytoplankton. Backscattering spectral-based approaches typically rely of the assumption that smaller particles have enhanced backscattering at blue wavelengths whereas large particles display a relatively flat backscattering spectrum.

Similarities and differences between abundance-based and spectral-based approaches were investigated in this chapter, as were advantages and disadvantages of each method. The classification into abundance-based and spectral-based methods is by no means clear cut, and we have highlighted some other novel approaches that are likely to gain in strength with the development of hyperspectral satellite data.

Remote Sensing Algorithms for Multiple Phytoplankton Types

Shubha Sathyendranath, Severine Alvain, Astrid Bracher, Takafumi Hirata, Samantha Lavender, Dionysios Raitsos and Collin Roesler

5.1 Introduction

This chapter is devoted to algorithms that are designed to deal with detection and mapping of multiple phytoplankton types using satellite data. The chapter describes a number of approaches that differ from each other from a technical perspective, as well as in the nature of the products.

One of the methods is based on observed differences in the anomalies of reflectance spectra with changes in the dominant type of phytoplankton present in the water. Another makes use of differential absorption spectra of phytoplankton types. This approach exploits hyperspectral satellite data, and a novelty of the method is that it deals with the total signal received by the satellite, without going through an atmospheric correction algorithm first to isolate the ocean signal. Methods based on Artificial Neural Networks are presented, which make use of data from multiple satellites, including ocean-colour sensors, and map the phytoplankton types on the basis of their environmental preferences. Abundance-based methods are also available for mapping multiple phytoplankton types that infer phytoplankton types from measures of abundance derived from ocean-colour data. Algorithms based on forward modelling of remote-sensing reflectance that accounts for the distinctive inherent optical properties of different phytoplankton types, combined with statistical inversion methods to identify the contributions of the component types from observed reflectance spectra have also been proposed.

Of all these algorithms, the abundance-based methods and the environmental approaches can be classified as indirect methods, in the sense that the distributions of phytoplankton types are inferred, and not detected directly from any remotely-sensed signal that sets each phytoplankton type apart from everything else. According to this criterion, the other methods can be treated as direct methods.

Some of these algorithms are designed to identify dominant phytoplankton types, whereas some of the others are capable of identifying the relative contributions

from multiple types. Some are based on pigment concentrations as measure of abundance of phytoplankton populations, whereas others are based on cell counts.

5.2 Statistical Methods Based on Spectral Anomaly

As seen in Chapter 1 and elsewhere in this report, various phytoplankton species in the ocean have different types and proportions of accessory pigments, resulting in slightly different absorption spectra. Furthermore, phytoplankton types are also distinguished often by their cell sizes and refractive indices that affect their absorption and backscattering efficiency. All these changes lead to modifications of the reflectance spectrum that are type-specific. When such differences exist, anomalies in remote-sensing reflectance (R_{rs}) spectra can be associated in a systematic manner with the dominant phytoplankton type present, and particular features in the anomaly spectra can then be associated directly with the phytoplankton types. This information can then form the basis of remote-sensing algorithms for identifying those phytoplankton types. The approach is illustrated using the work of Alvain et al. (2005; 2008), which goes by the acronym PHYSAT (see http://log.univ-littoral.fr/Physat: IDDN.FR.001.330003.000.S.P.2012.000.30300).

Since the method is based on direct empirical comparison of information on community structure with anomalies in R_{rs}, it is particularly important to assemble an exhaustive *in situ* dataset that is representative of all possible cases to which the method is applied.

5.2.1 Establishing a global *in situ* dataset for satellite match-ups

The first step is to collect the pertinent *in situ* measurements with biological information rich enough to indicate the dominant species, and numerous enough to allow a statistical approach using ocean-colour measurements made by satellite at the same time and place. The samples should be representative of a wide range of climatic conditions and geographic locations. For PHYSAT, the requisite data were first collected by sampling along a commercial sea route: A German shipping company agreed to host an oceanographer on board one of its ships, the *Contship London*, to collect water samples on each of its voyages from Le Havre (France) to Noumea (New Caledonia). This was the origin of the GeP&CO project (Geochemistry, Phytoplankton and Color of the Ocean; Dandonneau et al., 2004). This long sea route crossed most conditions that can be encountered in the world ocean (except the polar and subpolar regions) and included the North Atlantic with its spring phytoplankton bloom, the East coast of North America, the Caribbean Sea and Gulf of Panama, the Equatorial Pacific with abundant nutrients but no iron, the South Pacific anticyclonic gyre where plankton is scarce, and Temperate waters near New Zealand and the Tasman Sea.

Routine measurements of about 20 pigments enabled most phytoplankton groups, with known pigment signatures, to be identified. GeP&CO consisted of 12 campaigns, one per trimester from November 1999 to August 2002 (see `http://www.lodyc.jussieu.fr/gepco/`). This database was used to establish the first version of PHYSAT (2005; 2008). More recently, a new calibration and validation exercise was undertaken, with additional *in situ* measurements, some of which were acquired in the Austral Ocean (NOMAD dataset: `http://oceancolor.gsfc.nasa.gov/`, ICOTA and OISO campaigns, see Alvain et al., 2012). However, due to the requirement for very clear sky conditions, only 12% of the *in situ* measurements could be matched with coincident and co-located satellite measurements. This underlines the need to collect field data, whenever possible, covering large spatial and seasonal domains. This is crucial in developing an appropriate match-up database that would ensure good calibration of validation of remote-sensing algorithms such as PHYSAT.

5.2.2 Removing the effect of chlorophyll concentration

Once sufficient *in situ* information is available, it can be used in empirical models to identify specific features in the coincident remotely-sensed measurements. However, for studying the impact of phytoplankton community structure on R_{rs}, it is important that these effects are distinguished from the effect of changes in abundance of phytoplankton (as indexed by chlorophyll concentration).

The first step in the algorithm development is to establish a statistical model of average spectra of marine reflectances (R_{rs}) from satellite observations (Alvain et al., 2005), which serves as a reference against which individual reflectance spectra are compared. The average spectra were generated as a function of chlorophyll-a concentration, using a large number of reflectance data corresponding to a range of chlorophyll concentrations, which were then binned in small chlorophyll intervals between 0.04 and 4 mg m^{-3} (see Figure 1 in Alvain et al., 2005 for the reference set for SeaWiFS. LUT for other sensors are available on the PHYSAT web page `http://log.univ-littoral.fr/Alvain,195`). Note that the mean signal must be computed for each satellite sensor to account for the sensor-specific differences in the R_{rs} signal, and that the reference set is generated independently of the match-up dataset described above. This set of spectra is used as a reference set against which observations are compared.

Next, each R_{rs} spectrum from the match-up data set is paired with the reference spectrum for the corresponding chlorophyll concentration. Then, the reflectance value from the match-up dataset at each wavelength is normalised by the corresponding value from the paired reference set, to identify spectrally-resolved radiance anomalies, R_a.

Because the reference spectra used to normalize the observations change with the chlorophyll concentration, it is important to use consistent chlorophyll algorithms to establish the reference spectra and to estimate the chlorophyll concentration

in the match-up dataset. For example, the SeaWiFS reference spectra cannot be used to normalize MODIS reflectance spectra because the chlorophyll algorithms used in the standard processing of data from the two sensors are not the same. Note, however, that anomalies of the reflectance are independent of chlorophyll concentration by virtue of the normalization, and so should be independent of the bio-optical algorithm.

5.2.3 Reflectance anomalies and phytoplankton types

Comparison of the reflectance anomalies with the pigments in the match-up database reveal systematic differences in the anomalies that correspond with changes in the phytoplankton type (see Figure 5.1):
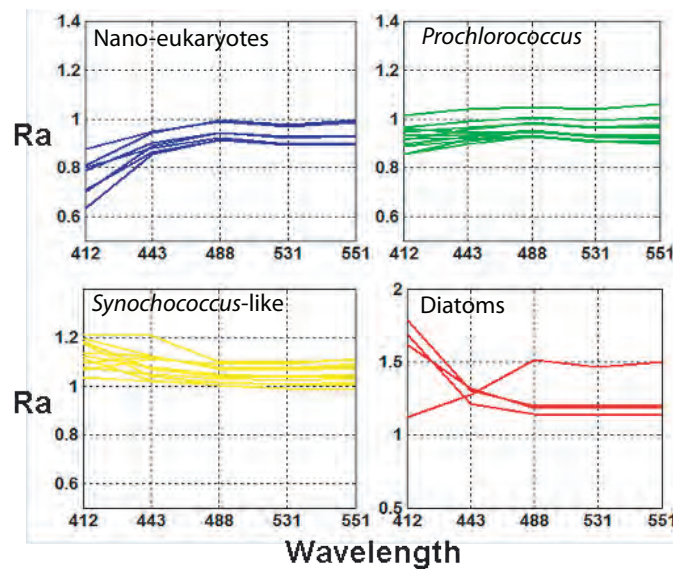
Figure 5.1 Anomalies in MODIS-Aqua reflectance spectra used to identify four phytoplankton types (see Ben Mustapha et al., 2013). Results are based on the use of Self Organising Maps to characterize the types. If the anomaly spectrum from a pixel is within a range defined by the mean value of the anomaly spectrum for a particular phytoplankton type ± one standard deviation, then that pixel is assigned to that particular phytoplankton type.

❖ The lowest negative spectral anomalies corresponded with abundant concentrations of 19'hexanoyloxyfucoxanthin, a pigment found in haptophytes (considered as nano-eukaryotes).

❖ Waters with relatively abundant divinyl-chlorophyll-a, which exists only in the genus *Prochlorococcus*, were characterized by anomalies (R_a) slightly lower than one.

❖ Observations with slightly positive anomalies had a high zeaxanthin-to-divinyl-chlorophyll-a ratio. Zeaxanthin is characteristic of photosynthetic cyanobac-

teria belonging to both *Synechococcus* and *Prochlorococcus* genera, whereas divinyl-chlorophyll-a is present only in *Prochlorococcus*. Therefore, a high zeaxanthin/total-chlorophyll-a ratio which is also associated with a limited divinyl-chlorophyll-a/total-chlorophyll-a ratio can be used to identify samples dominated by *Synechococcus*.

❖ Finally, the highest positive spectral anomalies (R_a markedly greater than 1.2) were found for observations with especially high fucoxanthin content, a pigment which is characteristic of diatoms. Note that, with some exceptions (e.g., diatoms), the shapes of the anomaly spectra also appear to change with phytoplankton types, in addition to changes in the magnitude.

These results suggest that dominant phytoplankton functional types can be identified by remote sensing once sufficient *in situ* information is available to characterise shapes and amplitudes of R_a at a range of chlorophyll-a concentrations (Alvain et al., 2005). The capability to characterise the R_a spectra for various phytoplankton has been recently improved (Ben Mustapha et al., 2013) using Self Organizing Maps (SOM) (Kohenen, 1984). This allows the characterisation of a larger portion of the *in situ* dataset and the identification of a wider range of R_a spectra than was possible earlier. The improved method (Ben Mustapha et al., 2013) allows the classification of twice the number of pixels than the initial method published by Alvain et al. (2005).

5.2.4 Implementation of the method

Since the implementation of the method requires information provided by satellites (marine reflectance spectra and chlorophyll concentration), it can be applied to data from any ocean-colour satellite. A data processing chain has been established to identify the dominant phytoplankton group in a given pixel, and to map global distributions of the groups discussed above.

The first step is to discard all pixels with an aerosol optical thickness greater than 0.15 or with chlorophyll-a concentration outside the 0.04 to 4 mg m^{-3} range. For each remaining valid pixel, the normalization is applied to derive spectral anomalies given chlorophyll-a and R_{rs} at the five chosen wavelengths of MODIS or SeaWiFS (between 400 and 600 nm). The anomaly spectrum is then compared with the means of the R_a spectra for each of the four phytoplankton types shown in Figure 5.1. If the R_a spectrum from the sample is within the mean plus or minus one standard deviation of the mean R_a spectrum for a particular phytoplankton type, then that pixel is identified as being dominated by that phytoplankton group. Pixels with R_a spectra that cannot be classified as one of the phytoplankton groups are still considered valid and are assigned to an additional group of "unidentified phytoplankton assemblages".

A monthly synthesis product from PHYSAT is presented in Figure 5.2. To generate this product, daily maps of phytoplankton groups at a resolution of 1/12°

were used to produce monthly maps by selecting, for each pixel, the phytoplankton type that was dominant for at least half of the days when data were available. The PHYSAT database and further information is available at `http://log.univ-littoral.fr/Physat`.
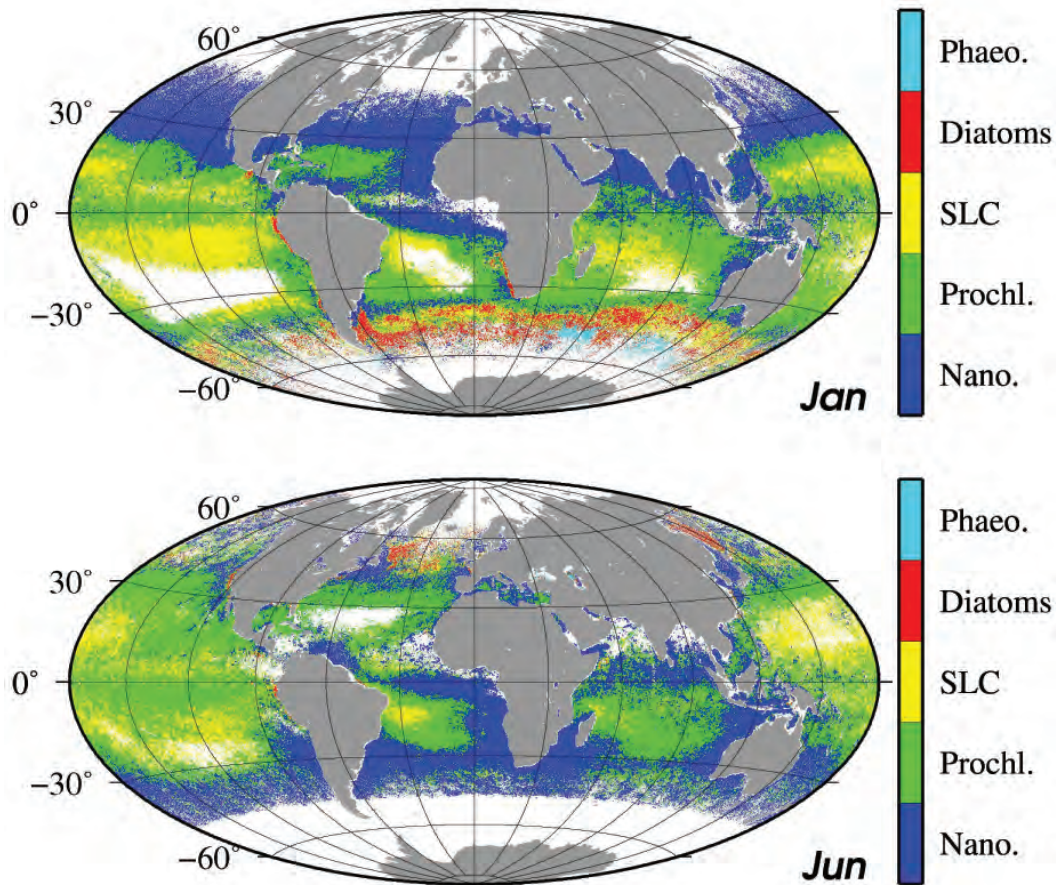
Figure 5.2 Monthly climatology (SeaWiFS data, 1998 – 2010) of the dominant phytoplankton groups (nano-eukaryotes, *Prochlorococcus*, *Synechococcus*-like cyanobacteria (SLC), diatoms and *Phaeocystis*-like, see Alvain et al., 2008) for January (top) and June (bottom). White colour represents areas where remotely-sensed measurements were either not available or not usable according to the algorithm criteria, or where dominant phytoplankton types were not identified.

Patterns shown in Figure 5.2 are in good agreement with previous knowledge of the distribution of phytoplankton groups. A validation exercise (Alvain et al., 2012) has shown that these results are satisfactory for diatoms and nano-eukaryotes with 73% and 82% successful identification, respectively. A decrease in success rates was observed for *Prochlorococcus* and *Synechococcus*-like cyanobacteria (SLC) (61 and 57%, respectively, with incorrect identification mainly associated with a confusion between the two groups). This result was anticipated since these two groups show

similar R_a characteristics and geographical distribution.

The results from this approach have been used to study the distribution of phytoplankton groups and their forcing by (sub)-mesoscale ocean circulation (D'Ovidio et al., 2010; De Monte et al., 2013). In addition, they have been used to validate biogeochemical models of the global ocean (Bopp et al., 2005), and in studies examining links between atmospheric compounds and phytoplankton groups (Colomb et al., 2009; Arnold et al., 2010; Belviso et al., 2012). Furthermore, these products have been used to study the influence of climate on marine ecosystems (Demarcq et al., 2011; Masotti et al., 2011; Alvain et al., 2013).

5.2.5 A theoretical explanation for PHYSAT

Although the method was developed as an empirical, statistical method, recent studies have provided a theoretical underpinning for the method. In a recent study (Alvain et al., 2012) radiative transfer simulations (Hydrolight: Mobley, 1994) were used to provide a theoretical basis for the features in the radiance anomalies identified in the PHYSAT method. Sensitivity analyses were performed to assess the impact of the variability in specific phytoplankton absorption, absorption by coloured dissolved organic matter, and particle backscattering. The shape and amplitude of the spectra of the theoretically-computed anomalies for three phytoplankton groups considered in the algorithm (diatoms, nano-eukaryotes and picoplanktonic cyanobacteria) were in good agreement with the empirical results. The theoretical studies also revealed that optical differentiation between phytoplankton types may take into consideration the influence of substances other than phytoplankton. For example, dissolved organic matter may allow the distinction between phytoplankton under some conditions, but it can also lead to no identification or misidentification. Based on the theoretical analysis, it is now possible to evaluate the optimal conditions for application of the algorithm, based on the bio-optical properties of phytoplankton and other optical constituents in the water. Indeed, it is now recognised that differences between R_a depend on the relative contribution to reflectance from absorption by phytoplankton and coloured dissolved organic matter, and from backscattering by particles. The theoretical study confirmed that phytoplankton functional types are generally associated with a specific bio-optical environment, which allowed separation between groups in the majority of encountered cases (Alvain et al., 2012).

These recent theoretical results also highlight the necessity to consider the environmental conditions preferred by the different types of phytoplankton, to improve further the detection of phytoplankton types from space (see Section 5.5 below dealing with environmental algorithms). Finally, complementary studies, based on a large *in situ* database of IOP measurements for various phytoplankton species, will also be necessary to obtain a better agreement between the theoretical and empirical spectral anomalies of the different groups.

5.3 Differential Absorption-Based Method

It has been shown in the past (e.g., Bricaud et al. 2007) that differentiation of phytoplankton absorption spectra with respect to wavelength can be used to identify and quantify phytoplankton pigments and phytoplankton types from absorption spectra (see Chapter 2). But the use of such methods in a remote-sensing context has been limited because of the requirement for high-spectral resolution data (i.e., hyperspectral data); current space borne ocean-colour sensors have limited spectral resolution. Furthermore, in a remote-sensing context, appropriate non-linear optimization methods have to be developed to isolate the phytoplankton absorption signal from all other atmospheric and oceanographic constituents that contribute to the satellite signal.

These challenges have been addressed by Bracher et al. (2009) and Sadeghi et al. (2012a) who have developed and improved a method called PhytoDOAS, an adaptation of Differential Optical Absorption Spectroscopy (DOAS, developed by Perner and Platt, 1979) to detect phytoplankton types from hyperspectral satellite data. The method is designed for concurrent retrieval, at the global scale, of chlorophyll-a concentrations associated with different phytoplankton groups (diatoms, cyanobacteria, coccolithophores and dinoflagellates) from hyperspectral satellite data from the Scanning Imaging Absorption Spectrometer for Atmospheric Chartography (SCIAMACHY), which operated onboard the ENVISAT satellite from 2002 to 2012. This satellite sensor measured the direct solar and backscattered solar radiation in the UV-VIS-NIR spectral regions with a high spectral resolution (0.2 to 1.5 nm). Though SCIAMACHY was designed for the study of atmospheric chemical composition, the work by Bracher et al. (2009) and Sadeghi et al. (2012a) have successfully demonstrated its use as a hyperspectral ocean-colour satellite.

In the PhytoDOAS method, the ratio of the backscattered radiation at the top of the atmosphere to the direct solar radiation (both measured by SCIAMACHY) is computed. Using Levenberg-Marquardt least-square non-linear optimization, this spectrally-resolved ratio is fit to a modelled ratio that includes the contributions of all relevant absorption and scattering constituents in the ocean-atmosphere system, within the considered wavelength range. The analysis takes into account different phytoplankton groups, water vapour, water, and the atmospheric trace gases O_3, O_4, NO_2, glyoxal (CHOCHO) and iodine oxide (IO). In addition, Raman scattering of light by air (Ring effect) and by water molecules (vibrational Raman scattering), which causes the filling-in of Fraunhofer lines in the backscattered spectra, are treated as pseudo absorbers in the retrieval. The contributions of other substances with low levels of structure in the derivative spectra of inherent optical properties (e.g., absorption by coloured dissolved organic material and non-algal particles and scattering by air molecules and particles) are approximated by a second-order polynomial. The fit-factors of all relevant absorbing and scattering constituents with a high level of structure in the derivative spectra within the considered wavelength

range are the outputs of the retrieval. In the case of phytoplankton types, whose absorption coefficients are normalized to the chlorophyll-a concentration of each group, the units of the fit-factor are mg chlorophyll-a m^{-2}. This is the amount of chlorophyll associated with that group, and represents the concentration integrated over the depth range observed by the satellite. The average chlorophyll-a concentration (mg chl m^{-3}) for each satellite pixel is finally calculated by dividing the phytoplankton fit-factor for chlorophyll by the penetration depth for light derived from the fit-factor for the vibrational Raman scattering for water molecules, taken as a measure of water clarity, and hence, of the penetration depth of the satellite signal (Vountas et al., 2007). Note that the penetration depth at a particular wavelength is taken to be the inverse of the back-scattering coefficient for that wavelength according to Vountas et al. (2007), whereas conventionally, in optical oceanography, this quantity is taken to be the inverse of the diffuse attenuation coefficient, as in Gordon and McCluney (1975) and Gordon and Clark (1980).

Within the PhytoDOAS retrieval, the wavelength range considered is 429 to 495 nm in the single-target fit mode (only one phytoplankton type is retrieved at a time) as developed by Bracher et al. (2009), where diatoms and cyanobacteria fit-factors are retrieved in separate runs of the algorithm. The wavelength range has been extended to 529 nm for the multi-target fit mode developed by Sadeghi et al. (2012a) where diatom, coccolithophore and dinoflagellate fit-factors are retrieved simultaneously. The retrieval uses characteristic specific absorption spectra for the different phytoplankton groups measured on natural water samples collected during various research cruises in the Atlantic Ocean. The dominance of particular groups in samples were identified according to the composition and quantity of marker pigments measured using High-Performance Liquid Chromatography (HPLC), as described in Bracher et al. (2009) and Sadeghi et al. (2012a). The sample used to represent diatoms appeared to be made up of ~70% of diatoms. In the case of dinoflagellates, the value was ~90%, and for cyanobacteria it was 100%. Since none of the field samples available were identified as being dominated by coccolithophores, an absorption spectrum from a culture of *Emiliania huxleyi* was used to represent this phytoplankton type. The absorption spectra used for the four phytoplankton types and their corresponding differential spectra are shown in Figure 5.3.

The SCIAMACHY differential optical depth spectra (Figure 5.4) clearly show the distinct optical characteristics of different phytoplankton groups. In fact, the residuals of the optimization are much lower when differences in the absorption spectra of phytoplankton types are taken into consideration, compared with the case where these differences are not accounted for. Comparing the version of the retrieval that identifies a single dominant group with the version designed to retrieve multiple types simultaneously, it was found that the multi-type version diminished the residual in 80% of the cases (Sadeghi et al., 2012a).

The whole SCIAMACHY data set has been processed from July 2002 until the end of the ENVISAT mission in April 2012. Figure 5.5 shows, as an example, monthly
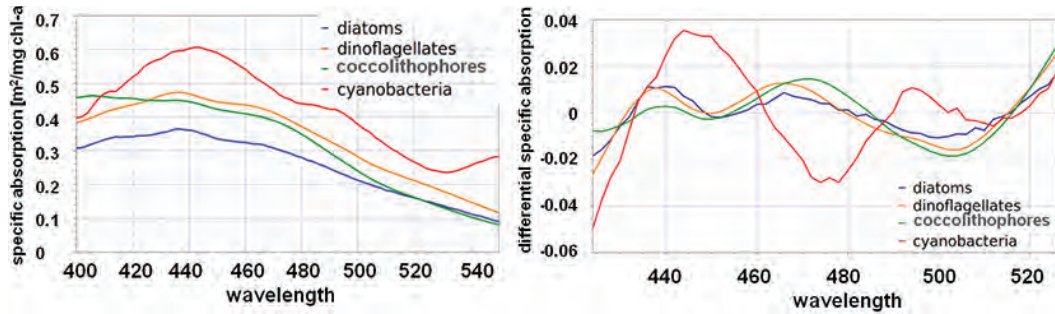
Figure 5.3 (Left) Specific absorption spectra of cyanobacteria (red), *E. huxleyi* (green), dinoflagellates (orange) and diatoms (blue) used in the PhytoDOAS fits of Bracher et al. (2009) and Sadeghi et al. (2012a). (Right) Differential specific absorption spectra of the left spectra. Each spectrum was derived by subtracting a second order polynomial fit from the corresponding specific absorption spectrum, shown in the left panel.
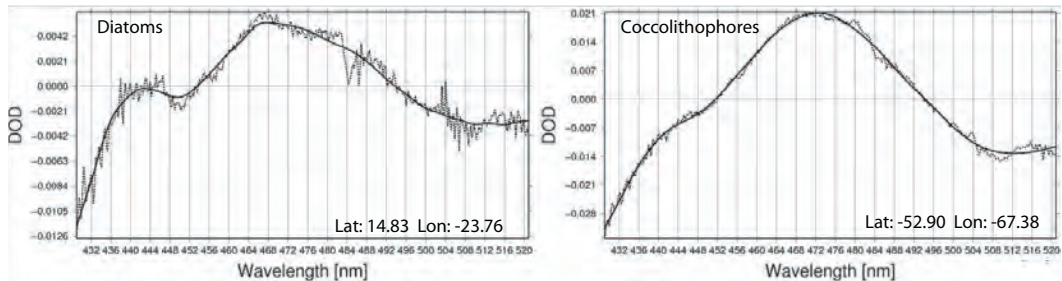
Figure 5.4 Spectral differential optical depth of SCIAMACHY data (dotted line) and the corresponding fit (straight line) for diatoms (left) and coccolithophores (right) using the specific differential absorption coefficients of each type scaled to match the observations according to the PhytoDOAS method described in Sadeghi et al. (2012a).

chlorophyll-a concentration for the four phytoplankton groups for October 2009 in the Western Pacific computed using the PhytoDOAS routine. Also plotted along a cruise track are the chlorophyll-a concentrations of the four types, derived from *in situ* HPLC pigment analysis obtained at the same time during the TransBrom Sonne cruise (Zindler et al., 2013). Both *in situ* and satellite results show similar ranges for this region. Preliminary validation by Bracher et al. (2009) indicated that satellite-derived information on cyanobacteria and diatom distributions matched well with corresponding *in situ* information based on pigment analyses of co-located water samples. Bracher et al. (2009) and Sadeghi et al. (2012a) also showed that the results from PhytoDOAS for diatoms, cyanobacteria and coccolithophores corresponded well with model results from the NASA Ocean Biogeochemical Model (Gregg and Casey, 2007). So far, no verification for the differential absorption method for dinoflagellates has been obtained. This method, applied to SCIAMACHY data, was used to study the development of coccolithophore blooms in three selected oceanic
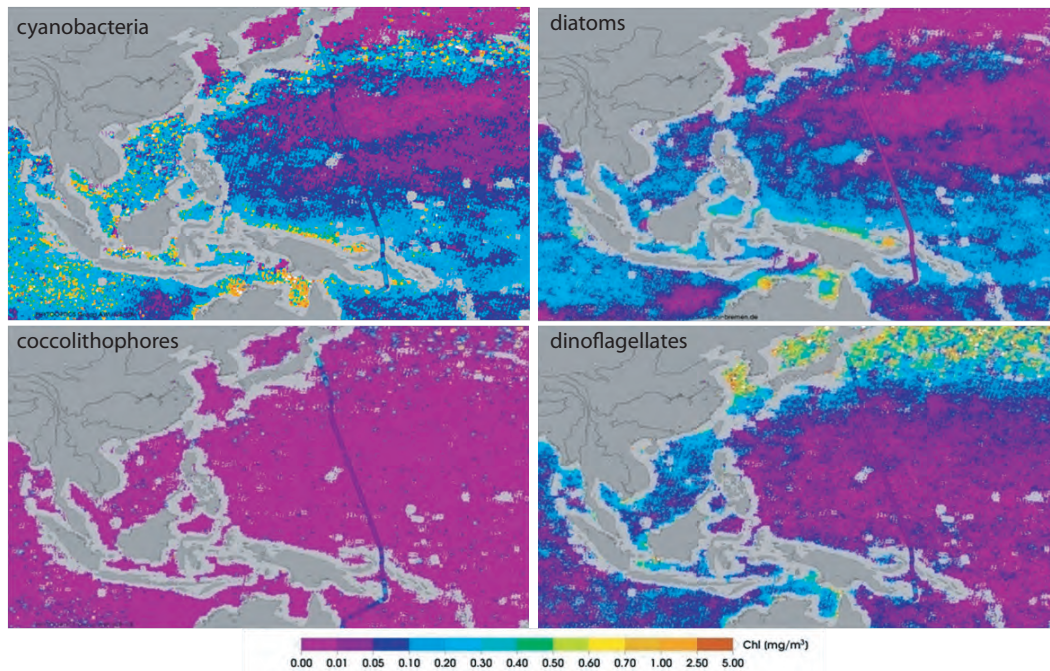
Figure 5.5 Colour coded chlorophyll-a concentration of cyanobacteria, diatoms, coccolithophores and dinoflagellates (in mg m^{-3}) as a monthly mean of October 2009 from PhytoDOAS retrieval. The coloured circles are the chlorophyll-a concentration of the respective groups derived from HPLC pigment concentration and further CHEMTAX analysis of *in situ* water samples taken during the TransBrom Sonne cruise (9–23 October 2009) at the specific locations.

regions from 2003 to 2010 (Sadeghi et al., 2012b). The results were compared with other satellite products: total chlorophyll-a from ESA's ocean-colour dataset, GlobColour (`http://www.globcolour.info/`; merged SeaWiFS-MODIS-MERIS data) and particulate inorganic carbon (PIC) from MODIS-Aqua. Results indicated that the seasonal patterns were consistent with the other ocean-colour products, especially with the PIC from MODIS-Aqua. Since PIC is a proxy for the abundance of coccolithophores in the open ocean, this agreement indicates that the PhytoDOAS method functions reasonably well with respect to retrieval of coccolithophores.

The spectral differential absorption method, as implemented in PhytoDOAS, exploits hyperspectral data in the blue-green domain to discriminate between different phytoplankton types according to their characteristic absorption properties, without assuming empirical relationships, as in the case of some other PFT methods (as for example, in abundance-based methods discussed in this chapter and elsewhere in the report). It is therefore possible, in principle, to use this method to detect changes in the distribution of phytoplankton types, which may be missed by empirical methods. The method presented here is based on *in situ* absorption spectra representative of particular types, measured in natural seawater samples (except

for coccolithophores). However, absorption spectra chosen to be representative of a certain group might also be vulnerable to change with the size of the population, which may vary with species or, to a smaller extent, with environmental conditions. Such changes are not accounted for in the present implementation of the method. Regional adaptations of the retrieval should be able to overcome this short-coming, at least to some extent.

Another limitation of the PhytoDOAS products is dictated by the relatively poor spatial and temporal resolution of the SCIAMACHY sensor: pixel resolution of 30×30 km at best, and a temporal resolution of about 6 days for global coverage. Since the absorption spectra used for diatoms and dinoflagellates in the PhytoDOAS method were not pure samples, these spectra were, in principle, influenced to a small extent by the other types of phytoplankton that were present in the samples. The similarity in the absorption spectra of many different types of phytoplankton limits the number of types that can be detected.

The inversion method, which treats separately the spectral signatures of sub-stances with a high level of structure in the derivative spectra (such as those of phytoplankton) from those that show a low level of structure, is relatively insensitive to atmospheric noise. One of the outputs from the retrieval is the penetration depth at the mean wavelength of the wavelength range. The PhytoDOAS biomass derived is the mean averaged over the penetration depth, assuming a uniform biomass distribution from the surface to the base of the penetration depth. PhytoDOAS phytoplankton group time series data have been used in various studies focusing on marine biogeochemistry, oceanic emissions and ecosystem dynamics (e.g., Sadeghi et al., 2012b; Ye et al., 2012).

The DOAS technique has potential for further improvements and extensions to derive PFTs of higher accuracy and higher temporal and spatial resolution from ocean-colour data, and also to derive new ocean-colour products. The atmospheric radiative transfer model, SCIATRAN (Rozanov et al., 2002), used in the algorithm to derive the pseudo-absorption of inelastic scattering, has been extended recently to account for coupled atmospheric-oceanic radiative transfer (Blum et al., 2012; Rozanov et al., 2014). Coupled radiative transfer models like SCIATRAN can be used to evaluate the sensitivity of the PhytoDOAS algorithm. This is done by simulating top-of-atmosphere spectra with varying phytoplankton compositions and concentrations which than can be used in the PhytoDOAS retrieval. The simulations can be used to verify whether additional phytoplankton groups, or even the effect of CDOM and chlorophyll fluorescence, which also cause filling-in of Fraunhofer lines, can be identified in hyperspectral satellite measurements. To derive DOAS ocean-colour products with higher temporal and spatial resolution, the method can be adapted (with the help of radiative transfer simulations) to other hyperspectral satellite sensors, i.e., the current OMI on AURA, the GOME-2 instruments on Metop-A and -B, and similar upcoming sensors (e.g., Sentinel-5-precursor, Sentinel-4 and Sentinel-5). All of these satellite sensors have improved spatial resolution and

temporal coverage. This will provide a long-term perspective of phytoplankton group products with reasonable temporal and spatial resolution.

5.4   Abundance-Based Methods

Abundance-based methods for mapping phytoplankton types are very similar in concept and implementation to abundance-based methods for mapping phytoplankton size classes, which were described in Chapter 4. The method is illustrated here using the work of Hirata et al. (2011).

In this method, Hirata et al. (2011) assembled a large data base of HPLC-based pigment data. Using the method of Uitz et al. (2006), contributions of the three phytoplankton size classes (micro, nano and picophytoplankton) to total chlorophyll concentration in each sample were computed on the basis of their diagnostic pigments. Next, the contribution to microplankton from diatoms is computed using the concentration of fucoxanthin, a diagnostic pigment for diatoms. Microplankton is assumed to be composed of diatoms and dinoflagellates, and the chlorophyll concentration associated with dinoflagellates is estimated by subtracting the diatom contribution from the microplankton concentration. Similarly, nanoplankton is subdivided into green algae and Prymnesiophytes, and picoplankton into prokaryotes and pico-eukaryotes and a separate class is assigned to *Prochlorococcus* sp.

Table 5.1   Equations used by Hirata et al. (2011) to estimate fractions (0.0 to 1.0) of phytoplankton size classes (micro-, nano and picoplankton) and some phytoplankton functional types. If a fraction is greater than 1, it is set to 1.0, and if it is less than zero, it is set to zero. *Note: a typo in the original paper for the *Prochlorococcus* formula has been corrected.

PSCs/PFTs	Formula	a_0	a_1	a_2	a_3	a_4	a_5	a_6
Microplankton	$[a_0 + \exp(a_1 x + a_2)]^{-1}$	0.91	-2.7	0.40				
Diatoms	$[a_0 + \exp(a_1 x + a_2)]^{-1}$	1.3	-4.0	0.20	—	—	—	—
Dinoflagellates	(= Micro – Diatoms)	—	—	—	—	—	—	—
Nanoplankton	(= 1 – Micro – Pico)	—	—	—	—	—	—	—
Green Algae	$(a_0/y)\exp[a_1(x + a_2)^2]$	0.25	-1.3	-0.55	—	—	—	—
Prymnesiophytes	($\simeq$ Nano – GreenAlgae)	—	—	—	—	—	—	—
Picoplankton	$-[a_0 + \exp(a_1 x + a_2)]^{-1}$ $+a_3 x + a_4$	0.15	1.0	-1.6	-1.9	3.0	—	—
Prokaryotes	$(a_0/a_1/y)\exp[a_2(x + a_3)^2/a_1^2]$ $+a_4 x^2 + a_5 x + a_6$	0.0067	0.62	-19	0.96	0.10	-0.12	0.063
*Prochlorococcus**	$(a_0/a_1/y)\exp[a_2(x + a_3)^2/a_1^2]$ $+a_4 x^2 + a_5 x + a_6$	0.0099	0.68	-8.6	0.97	0.0074	-0.16	0.044

$x = \log_{10}$(Chl-a); y =Chl-a

The partial contributions of each of these functional types is then plotted against the total chlorophyll concentration for all the samples, and empirical functions are fitted to each of the cases to capture the observed patterns. Once these empirical relationships are established, satellite-derived chlorophyll concentration is used to

compute and map the concentrations assigned to each of the phytoplankton types. The set of equations necessary for estimating the various phytoplankton types empirically, starting with satellite-derived chlorophyll-a concentration, is provided in Table 5.1, from Hirata et al. (2011). Examples of outputs from the Hirata et al. (2011) method are presented in Figure 5.6
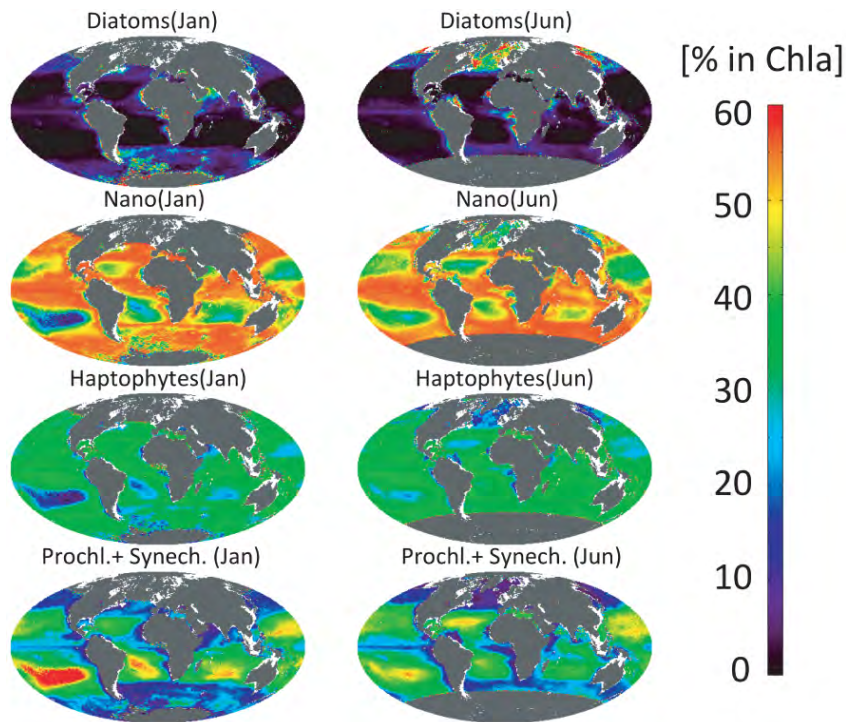
Figure 5.6   Partial contributions of diatoms, nanoplankton, haptophytes and *Synechococcus + Prochlorococcus* derived using the Hirata et al. (2011) method with SeaWiFS data from 1998 – 2010 to obtain the January and June climatologies, as in Figure 5.2.

5.5   Ecological Algorithms

Most of the algorithms presented and discussed in this report have been based exclusively on ocean-colour data. However, the possibility exists that improved and more robust algorithms might be possible by including additional information such as the physical, chemical and biological niches that favour different phytoplankton functional types.

The environments under which different types of phytoplankton thrive are reasonably well known, and we are learning more about them. For example, it is understood that diatoms do well in low-light, high-turbulence environments, and *Prochlorococcus* tends to dominate in high-light, low-nutrient, conditions. The

regional and ecological preferences of phytoplankton types are discussed at some length in Chapter 1. Information on many environmental factors is amenable to remote sensing, and if combined with the associated *in situ* information on the composition of phytoplankton community, it could form the basis for algorithm development. Note that such algorithms would fall under the category of indirect methods: the goal is not to detect the phytoplankton types directly. Instead, one searches for conditions that would favour one or another type of phytoplankton, and maps are then generated to indicate the probable distribution of phytoplankton types under a particular set of conditions. One might call such algorithms ecological algorithms, because the algorithms are based on ecological considerations.
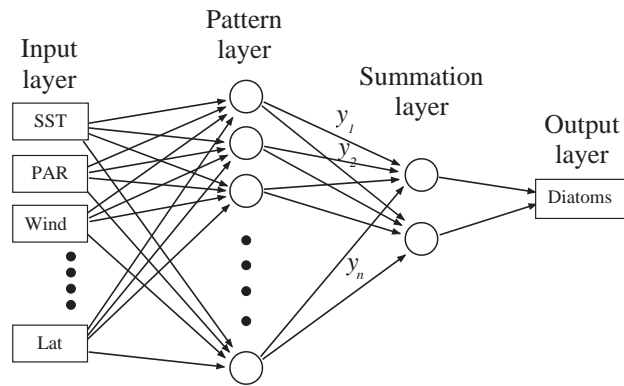
Figure 5.7 Schematic representation of the probabilistic neural network structure used to compute the probability of diatom occurrence.

One such method was implemented by Raitsos et al. (2008). They made use of a statistical approach known as Probabilistic Neural Network (PNN, see Figure 5.7), which is a type of Artificial Neural Network that employs Bayesian statistics (Specht, 1988; 1990). They used *in situ* data on phytoplankton composition and geographical location along with satellite-derived ocean-colour and physical variables. In particular, the variables that were used to identify the ecological "niches" of phytoplankton types were chlorophyll-a concentration, photosynthetically available radiation (PAR) at the sea surface, sea-surface temperature (SST), wind stress and normalised water-leaving radiances (L_{wN}); these were supplemented by geo-location information including longitude, latitude and season. The information on phytoplankton composition used to develop and train the PNN was derived from the Continuous Plankton Recorder (CPR), which is an upper-layer plankton monitoring programme in the North Atlantic Ocean and North Sea operating since 1931 (Reid et al., 2003b). Dominance of each phytoplankton type in the sample was estimated on the basis of cell counts (Raitsos et al., 2008). The total fraction of the functional types was correctly identified with an accuracy of >80%. The success in identification was not uniform across functional types. The order of performance was: silicoflagellates, coccolithophores, dinoflagellates, diatoms and no-dominance (93%, 91%, 83%,

81% and 80%, respectively). Additional details on the methodological approach as well as potential biases arising from the data used, or from the methodology, are identified in Raitsos et al. (2008).

In a somewhat similar approach, Palacz et al. (2013) used an Artificial Neural Network (ANN) to combine remotely-sensed and modelled data (SST, wind speed, PAR, Chl-a and Mixed Layer Depth) with biomass estimates of different phytoplankton types from the NASA Ocean Biogeochemical Model (NOBM) to compute distributions of four PFTs (diatoms, coccolithophores, cyanobacteria and chlorophytes) in key biogeochemical provinces, with a particular focus on resolving the diatom-coccolithophore coexistence in the sub-polar, high-nitrate, low-chlorophyll (HNLC) regions.

To some extent, the choice of predictive variables is dictated by data availability. It is, therefore, interesting to see which of the predictive variables have the most impact on the outcome. The importance of each predictor for the discrimination varied depending on whether the analysis is performed for the ensemble of functional types, or for individual functional types (in other words, some predictive variables were important to discriminate some functional types, but not necessarily all functional types). For instance, in the Raitsos et al. (2008) method, the relative impact of the eight predictors was assessed using the value of the smoothing function: the higher the value of the function associated with a particular variable, the higher is its importance as a discriminating factor. Spatio-temporal information such as longitude, month and latitude made an important contribution to the discrimination of the phytoplankton types. SST was found to be most important, followed by light intensity and wind stress. Chlorophyll-a and $L_{wN[555]}$ did contribute to the overall discrimination, but were of lesser importance compared with the other variables. Latitude, along with PAR and SST were the key factors for discriminating diatoms from other types. In addition, wind stress and chlorophyll-a play important discriminatory roles, whereas longitude had the lowest impact. Dinoflagellates were distinguished mostly on the basis of spatio-temporal information i.e., latitude, month and longitude, with PAR being the key physical property in the discrimination, followed by $L_{wN[555]}$ and wind stress. SST and chlorophyll-a contributed less to the dinoflagellate discrimination. For discrimination of coccolithophores, the influence of month, PAR, wind stress and $L_{wN[555]}$ appeared to be more important than SST. Longitude and $L_{wN[555]}$ had the highest impact for discriminating silicoflagellates, followed by month, SST and PAR; although chlorophyll-a and wind stress contributed to the final discrimination, their impacts appeared to be less significant. Finally, for the case of no-dominance, almost all predictors played important roles, but contributions of chlorophyll-a and $L_{wN[555]}$ were smaller.

Figure 5.8 illustrates a previously-unpublished example of diatom presence in the Northeast Atlantic derived using the Raitsos et al. (2008) method. The example denotes a monthly map of probability of diatom occurrence during May 2005. This example is independent of the period used for training the neural net (1997 –
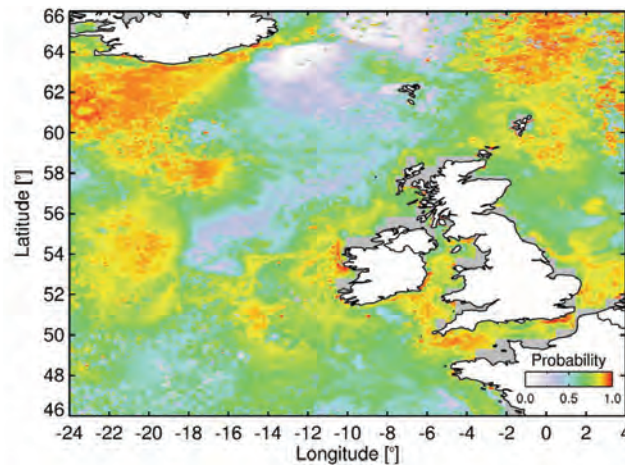
Figure 5.8 Map of diatoms presence for May 2005. May is an important month for diatom blooming in the study area. The scale of probability of diatom occurrence is from 0 (diatoms absent) to 1 (exclusively diatoms).

2003). This work demonstrated that neural networks are able to discriminate and identify four major functional types (diatoms, dinoflagellates, coccolithophores and silicoflagellates) with an accuracy of >80%. It is a first step towards an ecological approach, which would ideally be able to map phytoplankton types without geographical or seasonal information. As geographical information was considered during the training of the PNN, and since they appeared to be important, the resultant phytoplankton maps could only be produced for the North Atlantic Ocean. Once additional *in situ* data on the distribution of phytoplankton types becomes available, an attempt to exclude the geographical information could be made. Although this might decrease the accuracy of the model, it might lead to results that are more applicable globally. It is also noted that additional variables such as nutrients (known to be key regulators of phytoplankton abundance; Redfield et al., 1963) and the mixed-layer depth (responsible for the stratification and supply of nutrients; Estrada and Berdalet, 1997) were not used in the analysis because they are not available through remote sensing, and *in situ* data are not available either at sufficiently fine spatial and temporal resolution. However, wind stress (a measure of vertical mixing) was included as a discriminatory variable. Another possibility to broaden the list of variables used to define ecological niches might be to use outputs from ocean models, provided they are of sufficient accuracy and resolution (see Palacz et al., 2013).

Platt et al. (2005) argued that growth, as well as community and size structure of phytoplankton assemblages, are controlled by a number of physical factors that define the habitat of the epipelagic zone. Therefore, one factor alone was not sufficient to identify the PFTs. It has been argued (Alvain et al., 2005) that chlorophyll-a alone is insufficient to discriminate PFTs (notwithstanding the many

abundance-based methods that are available, and discussed in other parts of this report). At any rate, using chlorophyll-a concentration in combination with other variables may lead to significant improvement in the performance of satellite-based methods for mapping phytoplankton types, as the ecological approach presented here demonstrates.

As with any neural network, the results of PNN are influenced by the representativeness of the *in situ* and satellite match-up data used to train the network. In the approach illustrated here, the *in situ* data came from the Continuous Plankton Recorder, which might be biased towards larger cells, because of the nominal mesh size of the silk used for filtering the samples: the nominal mesh size is 270 *μ*m, though strands of silk that lie across the mesh help trap much smaller organisms, which are also enumerated during sample analysis. But is difficult to quantify any potential bias that might exist, compared with any other type of *in situ* method for enumeration of phytoplankton types. Abundance of a phytoplankton type was determined on the basis of cell counts in this approach, and the results might be very different if another measure of abundance (say chlorophyll-a concentration) was used in the analysis.

Overall, the results of Raitsos et al. (2008) and Palacz et al. (2013) highlight the benefits of using advanced statistical techniques to unravel complex and highly non-linear ecological interactions. The ecological approach has considerable potential for mapping spatial and temporal (seasonal cycle) trends in PFTs using remote sensing data alone, or together with outputs from physical and biological models.

5.6   Methods Based on Non-Linear Inversion of Ocean-Colour Models

In the context where the absorption (a) and backscattering (b_b) coefficients of seawater are known, irradiance reflectance R or remote-sensing reflectance R_{rs} at a particular wavelength λ can be expressed as functions of these inherent optical properties. For example, we have (see also Section 4.3 of Chapter 4):

$$R_{rs}(\lambda) \propto \frac{b_b(\lambda)}{a(\lambda) + b_b(\lambda)}. \tag{5.1}$$

The absorption coefficient can then be expressed as the sum of contributions from each component:

$$a(\lambda) = a_w(\lambda) + a_B(\lambda) + a_{dg}(\lambda), \tag{5.2}$$

where subscripts w, B and dg stand for water, phytoplankton biomass and combined detritus and gelbstoff (coloured dissolved organic matter). Similarly,

$$b_b(\lambda) = b_{bw} + b_{bp}, \tag{5.3}$$

where subscript p refers to particles. To be able to apply such models to remote-sensing of phytoplankton types, we have to subdivide phytoplankton absorption into its components:

$$a_B(\lambda) = \Sigma_{i=1}^N a_i(\lambda), \tag{5.4}$$

in which we consider the phytoplankton community to be composed of N components, each with absorption a_i, with i going from 1 to N. According to Beer's Law, the magnitudes of the absorption due to each component is related linearly to the concentration of the substance. To introduce the concentrations of the components into the equation, we make use of specific absorption coefficients, or absorption per unit concentration of phytoplankton. With chlorophyll biomass B_i representing concentration of component i, with corresponding specific absorption coefficient a_i^*, the above equation can be rewritten as:

$$a_B(\lambda) = \Sigma_{i=1}^N B_i a_i^*(\lambda). \tag{5.5}$$

Absorption by the combined detritus and dissolved matter (a_{dg}) that appears in the model (Eq. 5.2) is usually expressed as an exponential function:

$$a_{dg}(\lambda) = a_{dg}(\lambda_0) \exp\left(-S_{dg}(\lambda - \lambda_0)\right), \tag{5.6}$$

where $a_{dg}(\lambda_0)$ is the magnitude of the absorption at a reference wavelength (λ_0), and S_{dg} is the slope of the exponential function. Particle backscattering that appears in Eq. 5.3 is often approximated by a function of the form:

$$b_{bp}(\lambda) = b_{bp}(\lambda_0)\left(\frac{\lambda}{\lambda_0}\right)^n, \tag{5.7}$$

where $b_{bp}(\lambda_0)$ is the magnitude of the backscattering at the reference wavelength, and n determines the wavelength dependence in particle backscattering. Note that the reference wavelengths used in Eqs. 5.6 and 5.7 need not be the same. These two equations, together, introduce four more model parameters: $a_{dg}(\lambda_0)$, S_{dg}, $b_{bp}(\lambda_0)$, and n. Algorithms developers have to make a decision about whether some of these parameters (e.g., S_{dg} and n) can be held constant, or expressed as functions of other variables, or treated as unknowns in the model. Thus, if $a_i^*(\lambda)$ are known for each of the phytoplankton components of interest, then we have a non-linear system of equations (Eqs. 5.1 – 5.7) with at least N unknowns (the values of B_i). There may be up to four additional unknown parameters in the model associated with defining spectral variations in a_{dg} and b_{bp}, as we see from Eqs. 5.6 and 5.7. Then, if we have observations of R_{rs} at a number of wavebands equal to or greater than the number of unknown parameters, the set of R_{rs} values can be used along with non-linear optimisation techniques to solve for the concentrations of phytoplankton components. Such algorithms, which include a forward reflectance model and an inversion method are in routine use these days to retrieve in-water constituents

as represented, for example, in Eqs. 5.2 and 5.3. Many of them are described in IOCCG Report No. 5 (2006). What sets apart the algorithms examined in this section is the effort to take the models a step further, and partition the phytoplankton concentration into its components.

Roesler and Perry (1995) have pointed out that inversion methods that minimise the differences between observations and model may not yield satisfactory solutions for the unknowns: (a) if the model itself (Eq. 5.1) is a poor description of reality (errors in models may be related to how the proportionality between left and right-hands of the equation is defined, or from not including inelastic scattering processes such as Raman scattering or fluorescence); (b) if an incomplete set of components are assigned to absorption (Eq. 5.2) and back-scattering (Eq. 5.3); and if the optical properties of the components are poorly prescribed. Furthermore, technical choices such as the optimisation algorithm selected, the constraints applied and wavelengths used can impact the output from the inversion algorithm. The non-linearity in the system may be such that the uncertainty in the retrieved parameters is high. Poor precision and accuracy in the observations will further increase uncertainty. Clearly, it is essential that each of the model components have spectral optical characteristics that distinguish it from all other components, if the inversion is to be successful.

The feasibility of such approaches has been demonstrated by Gege (1998), who applied the method to quantify the components of the phytoplankton community of Lake Constance, using hyperspectral ship-based measurements of remote-sensing reflectance at 512 wavelengths. Phytoplankton belonging to the classes cryptophyta, diatoms, green algae and dinoflagellates were identified using this method. Roesler et al. (2004) used the reflectance model developed by Roesler and Perry (1995) with some modifications introduced by Roesler and Boss (2003) and a two-step inversion method (Roesler and Perry, 1995), to quantify phytoplankton components from *in situ* hyperspectral reflectance measurements in the southern Benguela region off South Africa. They showed that the method was successful in quantifying the concentrations of diatoms, the dinoflagellate *Dinophysis*, other dinoflagellates, *Mesodinium* and chlorophytes in absorption units and in chlorophyll units.

Though forward models and inverse algorithms have been used to estimate phytoplankton size classes from satellite data (e.g., Ciotti and Bricaud, 2006; Mouw and Yoder, 2010; Devred et al., 2011; see Chapter 4), they are yet to be used in a routine manner for mapping phytoplankton types (noting however, the overlap between size and type, as noted elsewhere in this report). No doubt, as hyperspectral data from satellites become more routinely available, it should become easier to implement such methods directly to satellite-derived reflectance spectra.

5.7   Discussion and Conclusion

This chapter has provided an overview of different types of methods that have been developed to map multiple types of phytoplankton from ocean-colour data simultaneously.

All the algorithms discussed here are similar in their requirement of a comprehensive database of *in situ* observations and match-up satellite data for their validation. The details of the requirements may, however, differ from one algorithm to another: for example, most of the algorithms discussed here are based on pigments as the measure of abundance of phytoplankton types, whereas the neural network approach of Raitsos et al. (2008) is based on cell counts. Ideally, the validation database would cover the full range of all possible concentrations of phytoplankton for which the method would be applied; it would cover a broad range of geographic locations and oceanographic conditions; and it would encompass many representative cases where different phytoplankton types dominate. Match-up databases are also required for validation of other, and perhaps simpler, algorithms, such as those for estimation of chlorophyll concentration or inherent optical properties. The present context merely highlights the value of including information on phytoplankton types in the database. Since the database should include match-ups for each sensor for which the algorithms are to be applied, the database should be maintained over a long time, and in a consistent manner. The paucity of *in situ* data limits the extent to which the algorithms can be validated or compared with each other.

In situ data are also required for algorithm development, but the different approaches presented here differ significantly from each other in their data requirements for model development. The method of Alvain and colleagues (2005; 2008) is developed using an extensive match-up database of *in situ* pigments and satellite-derived remote-sensing reflectance values. The abundance-based method of Hirata et al. (2011) is based on a database of diagnostic pigments and chlorophyll-a. The model-based approaches, such as the differential absorption method of Bracher et al. (2009) and the non-linear inversion methods (Gege, 1998; Roesler et al., 2004) require specific inherent optical properties of each of the phytoplankton types modelled. The ecological approaches (Raitsos et al., 2008; Palacz et al., 2013) use a variety of satellite and *in situ* observations along with modelled variables to train the algorithm. Of all these approaches, the one proposed by Palacz et al. (2013) is unique in that they side step the problem posed by paucity of *in situ* data by using modelled data on phytoplankton functional types to develop the algorithm. This of course, presupposes that the model used is sufficient for the requirements of the algorithm.

The ecological methods and the abundance-based methods discussed here are indirect methods, in the sense that the phytoplankton types are deduced from other satellite products, and no phytoplankton-type-specific satellite signal is used to

distinguish between phytoplankton types. Abundance-based methods make use of some measure of concentration of total phytoplankton concentration, whereas the ecological method accepts that total concentration of phytoplankton by itself may be insufficient to identify niches favoured by different types of phytoplankton. In the context of climate variability and climate change, it is important to ask whether adaptation to change would modify ecological relationships that exist at present, and which are used in indirect methods to map phytoplankton types.

Differential optical absorption spectroscopy is best implemented using hyper-spectral data, as discussed in Section 5.3. The method enhances, through differentiation with respect to wavelength, differences in the fine structure in phytoplankton absorption spectra that are associated with different types of phytoplankton. Torrecilla et al. (2011) also showed, using cluster analysis, that taking second derivative of hyperspectral remote-sensing reflectance spectra obtained under non-bloom conditions improved the possibility of differentiating between diagnostic pigments. Though second derivative with respect to wavelength of remote-sensing reflectance from MODIS-Aqua sensor has been applied (Simon and Shanmugam, 2012) to map some species of phytoplankton with unusual spectral signatures (*Trichodesmium erythareum*, *Noctiluca scintillans*, *Noctiluca miliaris*, and *Cochlodinium polykrikoides*) in coastal waters around India, limited spectral resolution in multi-spectral satellite data is bound to prevent the full exploitation of the power of the method. The model-based non-linear inversion techniques have also been tested in the field using hyperspectral data, and would be best implemented to hyperspectral satellite data. Such algorithms are likely to become more prevalent as hyperspectral ocean-colour data become more readily available.

The approach promulgated by Bracher et al. (2009) and Sadeghi et al. (2012a) also exploit the fine structure in the absorption spectra of different phytoplankton types to distinguish them from each other and from all other absorbing and scattering substances (such as aerosols, atmospheric molecules, pure seawater, non-algal particles and coloured dissolved organic matter) that contribute to the satellite signal at the top of the atmosphere, but have inherent optical properties varying slowly with wavelength in the blue and green parts of the spectral domain. The method thus targets absorption by phytoplankton, without having to go through a complex atmospheric correction procedure, and is unique in this respect, compared with the other methods discussed here. The price is the inability to distinguish well, in the coupled ocean-atmosphere system, between all the other components whose optical properties vary only slowly with wavelength. This raises an interesting and important question: is this novel approach, which deviates from the classical approach in ocean-colour remote sensing, yielding better results than previously possible? To address this question, and related questions regarding the relative performance of algorithms, we need to compare them in a systematic manner. But this is not a trivial task, as noted above with respect to the data required for validation, and for additional reasons outlined below.

Though all the algorithms presented here are designed with similar objectives in view, some differences between them make comparisons difficult (see Table 5.2).

Table 5.2 Key characteristics of various algorithms used to determine phytoplankton functional types.

Method	Key characteristics	Constraints
Method based on spectral anomalies.	Maps dominant types. Abundance measured in chlorophyll units. Designed for diatoms, dinoflagellates, *Synechococcus*-like cyanobacteria, *Phaeocystis*-like phytoplankton, *Prochlorococcus* and nano-eukaryotes. Implemented for SeaWiFS and MODIS sensors (multispectral).	Needs a large number of match-up *in situ* and satellite data covering a range of conditions for algorithm development; the reference spectra and the characteristic reflectance anomaly spectra for phytoplankton types have to be set up for each satellite sensor. Requires extremely clear-sky conditions.
Method based on differential absorption.	Maps abundance of diatoms, cyanobacteria, coccolithophores and dinoflagellates. Abundance measured in chlorophyll units. Implemented for the SCIAMACHY sensor (hyperspectral).	Does not account for within-type variability in the absorption characteristics of phytoplankton types. Designed for hyperspectral sensors. Low pixel resolution and low temporal coverage in products dictated by sensor characteristics.
Multi-sensor ecological approaches.	Indirect method. Maps abundance of silicoflagellates, diatoms, coccolithophores, dinoflagellates and non-dominance. Abundance measured in cell counts. Uses multiple satellite inputs for classification.	Need large database of multi-satellite (and possibly modelled) data and *in situ* data on phytoplankton types to develop algorithm as in Raitsos et al. (2008) method. *In situ* data availability was limited to North Atlantic. Palacz et al. (2013) model was trained using outputs from a biogeochemical model, and tested only for selected areas of the world ocean.
Abundance-based methods.	Indirect method. Hirata et al. (2011) have mapped abundance of diatoms, green algae, Prymnesiophytes, prokaryotes, pico-eukaryotes and *Prochlorococcus* sp. Applicable to any sensor which provides chlorophyll concentration.	Products should not be treated as independent of chlorophyll-a. Need a large and representative database of diagnostic pigments and chlorophyll-a for algorithm development.
Ocean-colour model-based inversion methods.	Products change with implementation. Possible to use different measures of abundance, such as absorption, pigment concentration or cell counts. Current methods based on hyperspectral data.	Yet to be implemented for routine operation from satellite sensors.

Not all of them are capable of quantifying proportions of different types present in a location simultaneously. The phytoplankton types that are studied change with methods. Different measures of abundance are used in different algorithms, with chlorophyll units, absorption coefficients and cell counts being in use. The methods have been implemented for different sensors, and consequently, not all methods yield products at the same time and at the same place.

In spite of these difficulties with comparisons, a standardized method has to be put in place to compare algorithms and evaluate their performance on a common basis, with the same criteria and the same input data, as was done, for example, by Brewin et al. (2013) for some other ocean-colour products. Such an activity would benefit greatly from the availability of a comprehensive database of the kind mentioned above. For the approaches that require and use extensive data on phytoplankton types for model development (e.g., methods based on spectral anomalies, ecological methods or abundance-based methods), it is even more difficult to obtain an equally comprehensive, but independent dataset for model validation.

There is an increasing requirement from the user community to characterise the errors in the satellite products. The descriptions of the approaches provided in this chapter, and the comparison in Table 5.2 show that each of the approaches has different sources of uncertainties and hence different error budgets from each other.

General Discussion and Conclusion

Shubha Sathyendranath, Robert J.W. Brewin, Chuanmin Hu, Heidi M. Sosik and Venetia Stuart

This monograph is being written at a time when the field of remote sensing of phytoplankton types is in a stage of dynamic growth. It is therefore not the intention of the authors of this report to suggest that what is described here represents the last word on the topic. Rather, we focus on a review of what has been attempted so far, with the full realization and even optimism that future developments will outperform what has been achieved to date. Hence the value of much of what is in this report may be transient, particularly when considering that the citations might not be complete and that new techniques are emerging. Still, in producing this report, our hope is twofold. For the would-be users of ocean-colour products related to phytoplankton types, we hope that the overview presented here helps guide choices from among the various options available. These users should be able to select solutions that best meet their particular requirements, with knowledge of both the capabilities and limitations of the products that they choose to use. For the would-be algorithm developers, we hope this report provides a starting point for identifying gaps and highlighting areas where effort should be focused to move the field forward.

As detailed in the preceding three chapters, a variety of algorithms are available for studying dominant phytoplankton functional types or community composition or size structure from space. They do not all provide the same information, and furthermore, their performance may vary with the criteria against which performance is evaluated, or it may vary with region or season. Therefore, it is important for the users to be aware of the principles that underlie the methods, their advantages and limitations, and the contexts in which a particular algorithm may be deemed suitable. This monograph is intended to help users choose the right algorithms or data products for their particular applications. In some instances, it may be important to exploit the complementarity of algorithms, and use more than one algorithm to obtain the information needed.

In this final chapter of the report, some issues that cut across chapters, and some thoughts on future directions are laid out.

6.1 Size and Community Structure

In this monograph, methods designed to retrieve community structure and size structure have been treated in separate chapters, but it should not be overlooked that it is often impossible in the ocean to disentangle the two completely: size change is typically accompanied by community change, since a given phytoplankton species has limited capacity to change its size. This inter-relationship between type and size influences the algorithms discussed in this monograph in many ways. For example, diatoms are mostly large-celled, and are treated as microplankton (cell size >20 μm), and the absorption spectra used for discrimination of diatoms from other populations display the flat absorption spectra characteristic of large-celled populations. But small-celled diatoms do exist, though they may not be abundant enough to dominate biomass and the optical signals exploited for both size-based and type-based models. Regional differences in the cell size of the diatom populations might be one of the reasons why the algorithms for discrimination of diatoms need regional tuning (Jackson et al., 2011).

6.2 Single-Variable and Multi-Variable Approaches

It has been shown by many authors (e.g., Yentsch and Phinney, 1989; Chisholm, 1992; Bricaud et al., 2004; Irigoien et al., 2004; Sathyendranath et al., 2005) that the phytoplankton size structure changes with chlorophyll concentration in open-ocean waters. The modifications in size are accompanied by shifts in community composition and in absorption properties (Sathyendranath et al., 2005), as summarized in Table 6.1. The dependence of phytoplankton absorption characteristics on size (or, concurrently, on community) is implicit in the many non-linear relationships that have been established between chlorophyll concentration and phytoplankton absorption (e.g., Bricaud et al., 2004), or between chlorophyll concentration and backscattering (Ulloa et al., 1994; Loisel and Morel, 1998). It also appears explicitly in some model-based relationships between absorption and chlorophyll concentration (e.g., Sathyendranath et al., 2001; Devred et al., 2006; 2011; Brewin et al., 2011a). Such trends in modulation of the inherent optical characteristics of phytoplankton with change in chlorophyll concentration is also implicit in the bio-optical algorithms that are used to retrieve chlorophyll concentration from reflectance ratios derived from ocean-colour data (see Figure 4.7).

It would be fair to say that abundance-based models for discrimination of size from satellite data attempt to render explicit and to quantify the general trends in size associated with changes in chlorophyll concentration. This is an advantage for abundance-based models (when applied to Case 1 waters) in the sense that chlorophyll concentration is the best validated of all ocean-colour products, and abundance-based models are based firmly on chlorophyll algorithms (or on other

Table 6.1 Typical changes in phytoplankton community structure that accompany changes in chlorophyll concentration in open-ocean waters.

Low Chlorophyll	High Chlorophyll
Small cells	Large cells
Picoplanktonic cyanobacteria, green algae	Diatoms, dinoflagellates, *Trichodesmium* and other large-celled cyanobacteria
High specific absorption	Low specific absorption
Pronounced peaks in absorption	Flat absorption spectrum
High ratio of blue peak to red peak in absorption spectrum	Low ratio of blue peak to red peak in absorption spectrum
High ratio of non-photosynthetic carotenoids to Chl-a	Low ratio of non-photosynthetic carotenoids to Chl-a
High ratio of Chl-b to Chl-a	Low ratio of Chl-b to Chl-a
Low ratio of Chl-c to Chl-a	High ratio of Chl-c to Chl-a
High negative slope of size spectrum	Low negative slope of size spectrum

related measures of phytoplankton abundance).

But it is important to acknowledge that abundance-based models do not yield information independent of chlorophyll concentration. As noted elsewhere in this report, these methods are therefore indirect methods. In fact, in these instances we are treating the waters very much as Case-1 waters, where a single variable, say chlorophyll-a concentration, dictates what might be inferred about the bio-optical characteristics and phytoplankton community structure. The community composition or size structure is not directly observed, but determined indirectly from a single measure of abundance, whether it be chlorophyll concentration or phytoplankton absorption at a single wavelength. The information on community structure should therefore not be treated as independent additional information, rather as a statistical derivation that brings to light some natural organization that underlies variability in the pelagic phytoplankton community. Remote sensing in this context is an extrapolation tool, to go from sparse *in situ* measurements to global-scale maps.

Following points made previously (Bricaud et al., 2004; Devred et al., 2006), we also have to acknowledge that there are regional differences around the general trends described above, such that a global model of abundance-based size retrievals may show systematic biases that are regionally delineated. This may explain at least partially why the differences between the three abundance-based models compared in Figure 4.4 show some regional structure, rather than white noise distributed uniformly across the regions. Even though all three of the models were parameterized from large databases with a global distribution, the datasets would have, inevitably, a non-uniform distribution across the different regions. One

potential solution to such regional biases would be to tune algorithms by season and by region, for example on the basis of the ecological provinces of the sea (Longhurst, 2006).

Abundance-based algorithms are empirical in nature, and the paucity of observations dictates that multi-year data be combined to establish the functional relationships between chlorophyll concentration and size structure. If, due to climate change, or extreme events, or long-term oscillations, the relationship between chlorophyll concentration and community structure shifts, abundance-based methods would be unable to detect those changes, unless there is auxiliary information. Particularly in the context of climate change, it is important to bear in mind that the relationships observed in the past may not be a reliable guide for predicting the future.

Methods based on spectral-inherent optical properties, such as some of the algorithms discussed in Chapters 3, 4 and 5, are multivariate approaches that use optical information at multiple wavebands to distinguish one phytoplankton type from the others, without relying on external information about the relationships between community structure and phytoplankton abundance. In this sense they are direct approaches, closer to the *in situ* methods, in that an optical signal from the target is used to identify and quantify the target. What sets these approaches apart from the *in situ* methods is that remote sensing deals with a highly non-linear and an especially noisy system, with optical signals from other substances in the water and in the intervening atmosphere being responsible for the noise. The better we learn to deal with the noise and the non-linearities in the system, the better the spectral methods may be expected to perform. But all direct methods require a unique optical signal that can be used to distinguish one type of phytoplankton from all other substances. In the absence of any such signal, our only recourse to their detection would be an indirect method, such as the abundance-based methods or an ecological approach, along the lines discussed in Chapter 5.

6.3   Uncertainties in Products and Limits of Detection

Many of the methods described in this monograph have been validated against *in situ* data, but not much effort has been made to inter-compare algorithms and to identify best algorithms for a particular application. A notable exception is the work of Brewin et al. (2011b) (see also Chapter 4) who made a systematic comparison of a number of algorithms designed to estimate phytoplankton size classes from remote sensing. Without a doubt, more work is needed along this direction. Furthermore, quantitative and qualitative criteria have to be used in a scoring system to evaluate which algorithm might be best suited for a particular application, as was done for example, in selecting in-water and atmospheric-correction algorithms for use in climate-change studies (Brewin et al., 2013; Müller et al., 2014).

With a combination of theoretical analyses and tests based on a practical implementation of the Equivalent Algal Population (EAP) inversion algorithm in the Benguela upwelling region, Evers-King et al. (2014) have suggested that size retrieval is highly dependent on algal biomass and that the error associated with radiometrically-derived size retrievals increases substantially below chlorophyll concentrations of around 10 mg m^{-3}. Their conclusions cannot be generalized for all algorithms and all regions, since many of the other algorithms discussed in this report are designed for application in open-ocean waters with concentrations typically much less than 10 mg m^{-3}. But at present, for most algorithms, we do not have a clear idea on the lowest concentrations at which phytoplankton types may be detected. Going forward, it would be extremely valuable if the limits of detection for each algorithm were clearly identified.

It is sometimes suggested that the phytoplankton community structure plays a secondary role to that of phytoplankton concentration in changing ocean colour. This is often taken to imply that detection of phytoplankton community structure is inherently more difficult than that of detecting phytoplankton concentration. But the problem is a bit more intricate than that. For example, in the extreme case of a picophytoplankton-dominated community changing completely to a microphytoplankton-dominated community, the phytoplankton specific absorption coefficient at 440 nm could be reduced by a factor of up to ten, which would be comparable to the effect of a ten-fold change in concentration. This is by no means a minor effect, as we can also infer from Figure 4.7. The problem is more that of being able to identify, unequivocally, whether a change in community or in concentration is responsible for a particular change in ocean-colour reflectance. Until algorithms reach that level of sophistication, we may anticipate uncertainties in algorithms for detection of both concentration and composition arising from our limited ability to distinguish between the two.

Moreover, it is known that the optical properties of particular types of phytoplankton are liable to change according to growth conditions (e.g., Stramski and Morel, 1990; Fujiki and Tagughi, 2002; Stramski et al., 2002; Nair et al. 2008). Such plasticity in optical properties of individual phytoplankton species or groups sets a limit on the precision with which we may be able to retrieve phytoplankton types, and we have yet to establish these limits.

In general, with the limited number of wavebands available for algorithm development from ocean-colour sensors, all algorithms designed for retrieval of multiple oceanic properties from remote sensing have to contend with the problem of having more unknown model parameters than the number of wavebands available. Furthermore, similarities in the spectral signatures of some of the other oceanic and atmospheric constituents (for example, the absorption spectra of detrital particles and coloured dissolved organic matter, the backscattering spectra of oceanic particles and aerosols) may limit our ability to distinguish among them, which in turn could introduce errors in the inferred phytoplankton absorption spectrum. This is

particularly true when residual errors from the imperfect atmospheric correction may represent a non-negligible portion of the surface reflectance (Hu et al., 2013). In the future, ocean-colour sensors with more spectral bands (e.g., Fishman et al., 2012) that operate over a larger spectral range would be able to help address some of these challenges.

6.4   Need for an *In Situ* Database

Comparison exercises would benefit from a concerted effort to collect and collate relevant *in situ* data from around the globe. The establishment of such a database should be a priority for the community. What should be included in such a database? Chapter 2 outlines the various *in situ* methods that are currently used to study phytoplankton community structure. Because different methods bring complementary information, and because different satellite algorithms match more or less with different *in situ* methods (see Table 2.3), it is important that the database carry information from a variety of *in situ* methods, so that each type of satellite algorithm may be compared against *in situ* data collected with the method that best matches the algorithm. Furthermore, we also have to consider the *in situ* data as bringing complementary information to what might never be accessible to remote sensing. Satellite and *in situ* data, taken together, would allow us to form a more complete picture of the phytoplankton community in the marine environment than would be possible by any method in isolation.

For further developments in algorithms for phytoplankton types, we have to rely, among other things, on improved information on the inherent optical properties of phytoplankton. We need to catalogue the optical properties of different types of phytoplankton, as well as to understand better the variability in the optical properties of particular types of phytoplankton. It is therefore important that the proposed *in situ* database also incorporates inherent optical properties of phytoplankton from the natural environment.

6.5   Harmful Algal Blooms

Harmful algal blooms may be considered as a group of phytoplankton functional types that are known to have deleterious effects. Some of the phytoplankton types, especially those discussed in Chapter 3, have a nuisance value, and some are known to be toxic, both to aquatic life and to humans. But detection of toxic blooms is particularly complicated, since some species of phytoplankton may be harmful or toxic only under some growth conditions. For example, *Pseudo-nitzchia pungens* is known to have toxic and non-toxic strains, with some strains producing the toxin only under certain growth conditions, such that remote sensing of such toxic events is particularly difficult (Sathyendranath et al., 1997). The particular problem of

detection of harmful algal blooms falls outside the scope of this report and is the subject of another IOCCG monograph that is currently being prepared.

6.6 Case-2 Waters

Whereas this report has focused on detection of phytoplankton types from ocean-colour radiometry, a parallel effort in the field is to solve the problem of remote sensing of ocean colour in the so-called Case-2 waters, where substances other than phytoplankton (including suspended sediments and coloured dissolved organic matter) also have a significant and independent effect on the ocean-colour signal. To the extent that algorithms for Case-2 waters and spectral-signature-based phyto-plankton functional type algorithms both attempt to retrieve multiple, independent oceanic components from the satellite data, the problems faced in the two fields are similar, from a mathematical point of view. There may be opportunities that can help advance both fields, which are yet to be exploited fully.

On the other hand, it has to be emphasized that most phytoplankton functional type algorithms currently available are designed largely for use in open-ocean waters where it might be safely assumed that the influence of substances other than phytoplankton co-vary in a predictable manner with phytoplankton. In other words, they are primarily meant for Case-1 waters. An exception is the algal blooms that float at the surface, which are discussed in Chapter 3, such as the blooms of *Ulva prolifera*, *Sargassum*, *Trichodesmium*, or other types of cyanobacteria that can also occur in optically-complex Case-2 waters. These blooms, however, often show distinctive spectral shapes in the NIR and visible, thus minimizing the impact of optical complexity on algorithm development and performance.

6.7 Directions for Future Work

The three preceding chapters of this book have outlined the various algorithms available for detecting phytoplankton types from satellite data, and identified the advantages and limitations of the various methods. These chapters, along with the previous sections of this chapter itself, are designed to help identify gaps in our knowledge, and point the way towards areas where further development is needed. Some additional points that may not have emerged yet are identified here.

An important point is that the field of detection of phytoplankton types from space cannot advance in isolation from other aspects of ocean-colour remote sensing. For example, errors in atmospheric correction or in instrument calibration could impact retrieval algorithms for phytoplankton types and are likely to add substantial uncertainty. Thus a prerequisite for improving algorithms for phytoplankton types is a well-calibrated instrument with high spectral resolution and high precision.

Undoubtedly, higher spectral resolution would be beneficial for improving algorithms for phytoplankton types. But what criteria could be used to select optimal wavebands for future sensors? One set of criteria could be provided by the locations of peaks in the *in vivo* absorption bands of diagnostic pigments of phytoplankton. But these may have to be refined on the basis of other criteria, for example aligning the wavebands with atmospheric transmission "windows" to reduce problems from atmospheric correction. Sathyendranath et al. (1989) and Lee et al. (2007) have examined the problem of optimal wavelengths for Case-2 waters, yet similar analyses for optimising wavebands for the detection of phytoplankton types are still to be undertaken.

These considerations may become irrelevant when ocean-colour sensors with hyperspectral capability become the norm, unless onboard spectral binning is required to increase signal-to-noise. Over time, we anticipate algorithms that exploit hyperspectral capabilities will become increasingly developed and used (for example algorithms that are based on derivative spectra, such as described in Section 5.3). With several missions currently being planned by various space agencies, for example, the PACE mission (NASA, 2010) and the GEO-CAPE mission (Fishman, 2012), it is possible to have hyperspectral sensors in the near future with sufficient spatial and temporal resolution that are best suited for aquatic applications.

Scientific advances will have to keep pace with such technological advances. As our understanding of the inherent optical properties of phytoplankton types improves over time, so will ocean-colour models. But there are other considerations as well: many of the models on which algorithms are based do not currently include trans-spectral processes such as Raman scattering or fluorescence by phytoplankton pigments and by coloured dissolved organic matter (though there are exceptions, such as the work of Bracher et al. (2009) which incorporates Raman scattering). Improving ocean-colour models should remain a target for future work.

Some algorithms for phytoplankton types have been developed that are based on the chlorophyll signal in the red part of the spectrum (e.g., Roy et al., 2013). However, a recent inter-comparison of in-water algorithms (Brewin et al., 2013) showed that those algorithms that attempted to provide independent information on phytoplankton absorption at 670 nm performed poorly. The difficulties likely arise from the remote-sensing reflectance signal being generally very low at 670 nm in the open ocean or possibly from fluorescence effects that were unaccounted for. Certainly, detection of phytoplankton types would benefit from reliable retrieval of phytoplankton absorption across the entire spectrum, rather than only at parts of the spectrum.

6.8   Serving the User Community

As noted in Chapter 1, the development of algorithms for detection of phytoplankton types parallels the interest in the biogeochemical and climate research communities to understand the role of different phytoplankton functional types in modulating and modifying biogeochemical cycles in the ocean as well as air-sea fluxes of climate-relevant gases. The algorithms and products should therefore be tailored to meet these research needs in several ways.

For ocean-colour products to be more useful for the biogeochemistry communities, we need to explore further the properties of the marine ecosystem at the boundary between biogeochemical models and remote sensing. The typical currency for measuring phytoplankton biomass in remote sensing is the chlorophyll concentration, and there are many practical applications for this measure of biomass, for example in primary production models. But the typical currency in ecosystem models is carbon or nitrogen biomass, and it is not straightforward to convert between these different measures of phytoplankton concentration. For example, the carbon-to-chlorophyll ratio in phytoplankton is known to vary over one to two orders of magnitude, and the variability may be related to the phytoplankton types present and to their growth conditions (e.g., Cloern et al., 1995; Sathyendranath et al., 2009). Modellers and remote sensing scientists have to work together to understand the causes of variability in these factors, to allow better comparison between models and observations.

It is also important to facilitate access to products. Unlike the "standard" ocean-colour data products such as chlorophyll concentration and diffuse attenuation that can be obtained and queried from several data portals (e.g., NASA GSFC, `http://oceancolor.gsfc.nasa.gov`), most of the products for phytoplankton types derived from the customized algorithms are often not available to the general user community. Future efforts should be dedicated to make these products available in user-friendly format to encourage more applications. In turn, results from applications of the PFT products in inter-disciplinary studies may serve as independent checks on the validity of the products, thus providing, feedback to help refine algorithms and products.

6.9   In Conclusion

Let us recall that it was stated in this report (Chapter 2) that a variety of *in situ* observations are needed to describe phytoplankton community structure. Similarly, it may require multiple algorithms to extract essential information on phytoplankton community from satellite data. Furthermore, we have to acknowledge that the oceans will always hide some secrets from a remote device, so that remote sensing by itself would always be insufficient to meet all our requirements. The challenge for the

oceanographer is to bring together various observation tools, whether they be *in situ* or remote, that complement each other, such that the whole picture of the world of phytoplankton can be pieced together.

References

Agustí, S. (2004) Viability and niche segregation of *Prochlorococcus* and *Synechococcus* cells across the Central Atlantic Ocean. Aquat. Microb. Ecol. 36: 53–59.

Aiken, J., Moore, G. (2000). Case 2 (S) Bright pixel atmospheric correction, MERIS ATBD 2.6, PO-TN-MEL-GS-0005, 6 pp.

Aiken, J., Fishwick, J., Lavender, S., Barlow, R., Moore, G., Sessions, H. et al. (2007). Validation of MERIS reflectance and chlorophyll during the BENCAL cruise October 2002: preliminary validation of new demonstration products for phytoplankton functional types and photosynthetic parameters. Int. J. Remote Sens. 28: 497–516.

Aiken, J., Hardman-Mountford, N.J., Barlow, R., Fishwick, J., Hirata, T., Smyth, T. (2008). Functional links between bioenergetics and bio-optical traits of phytoplankton taxonomic groups: an overarching hypothesis with applications for ocean colour remote sensing. J. Plankton Res. 30(2): 165–181.

Aiken, J., Pradhan, Y., Barlow, R., Lavender, S., Poulton, A., Holligan, P., Hardman-Mountford, N. (2009). Phytoplankton pigments and functional types in the Atlantic Ocean: A decadal assessment, 1995–2005. Deep-Sea Res. II 56: 899–917.

Allali, K., Bricaud, A., Claustre, H. (1997). Spatial variations in the chlorophyll-specific absorption coefficients of phytoplankton and photosynthetically active pigments in the equatorial Pacific. J. Geophys. Res. 102: 12,413–12,423.

Allen, J.I., Aiken, J., Anderson, T.R., Buitenhuis, E., Cornell, S., Geider, R. et al. (2010). Marine ecosystem models for Earth systems applications: the MarQUEST experience. J. Mar. Sys. 81: 19–33.

Alvain, S., Loisel, H., Dessailly, D. (2012). Theoretical analysis of ocean color radiances anomalies and implications for phytoplankton groups detection in case 1 waters. Opt. Express 20(2): 1070–1083.

Alvain, S., Le Quéré, C., Bopp, L., Racault, M.F., Beaugrand, G., Dessailly, D. Buitenhuis, E. (2013). Rapid climatic driven shifts of diatoms at high latitudes, Remote Sens. Environ. 132: 195–201.

Alvain, S., Moulin, C., Dandonneau, Y., Bréon, F. (2005). Remote sensing of phytoplankton groups in case 1 waters from global SeaWiFS imagery. Deep-Sea Res. Part I, 52: 1989–2004.

Alvain, S., Moulin, C., Dandonneau, Y., Loisel, H. (2008). Seasonal distribution and succession of dominant phytoplankton groups in the global ocean: A satellite view. Global Biogeochem. Cy. 22(GB3001), doi: 10.1029/2007GB003154.

Alvain, S., Moulin, C., Dandonneau, Y., Loisel, H., Bréon, B.M. (2006). A species-dependent bio-optical model of case 1 waters for global ocean color processing. Deep Sea Res. I 53: 917–925.

Amin, R., Zhou, J., Gilerson, A., Gross, B., Moshary, F., Ahmed, S. (2009). Novel optical techniques for detecting and classifying toxic dinoflagellate *Karenia brevis* blooms using satellite imagery. Opt. Express, 17: 9126–9144.

Anderson, D.M. (1995). Identification of harmful algal species using molecular probes: an emerging perspective. In: Harmful Marine Algal Blooms, Lassus, P., Arzul, G., Erard, E., Gentien, P., Marcaillou, C., (Eds.), Lavoisier.

Anderson, D.M. (2007). The ecology and oceanography of harmful algal blooms: multidisciplinary approaches to research and management. Anton Bruun Memorial Lecture, UNESCO, Paris.

Anderson, D.M., Hoagland, P., Kaoru, Y., White, A.W. (2000). Estimated annual economic impacts from harmful algal blooms (HABs) in the United States. Technical Report WHOI-2000-11, Woods Hole Oceanographic Institute, Woods Hole, Mass.

Anderson, D.M., Kulis, D.M., Keafer, B.A., Gribble, K.E., Marin, R., Scholin, C.A. (2005). Identification and enumeration of *Alexandrium* spp. from the Gulf of Maine using molecular probes. Deep-Sea Res. II 52: 2467–2490.

Anthony, E.J., Vanhee, S., Ruz, M.-H. (2006). Short-term beach-dune sand budgets on the north sea coast of France: Sand supply from shoreface to dunes, and the role of wind and fetch. Geomorphology, 81(3/4): 316.

Antoine, D., André, J.M., Morel , A. (1996). Oceanic primary production II. Estimation at global scale from satellite (Coastal Zone Color Scanner) chlorophyll. Global Biogeochem. Cy. 10: 57–69.

Archer, D., Aiken, J., Balch, W., Barber, D., Dunne, J., Flament, P. et al. (1997). A meeting place of great ocean currents: shipboard observations of a convergent front at 2°N in the Pacific, Deep Sea Res. Part II, 44: 1827–1849.

Armstrong, R. (1999). Stable model structures for representing biogeochemical diversity and size spectra in plankton communities. J. Plank. Res. 21: 445–464.

Arnold, S.R., Spracklen, D.V., Gebhardt, S., Alvain, S. (2010). Relationships between atmospheric organic compounds and air-mass exposure to marine biology, Env. Chem.7(3): 232–241.

Arrigo, K.R., Robinson, D.H., Worthen, D.L., Dunbar, R.B., DiTullio, G.R., VanWoert, M., Lizotte, M.P. (1999). Phytoplankton community structure and the drawdown of nutrients and CO_2 in the Southern Ocean. Science, 283: 365–367.

Aumont, O., Maier-Reimer, E., Blain, S., Monfray, P. (2003). An ecosystem model of the global ocean including Fe, Si, P colimitations. Global Biogeochem. Cy. 17(2): 1060.

Austin, R.W. (1974). The remote sensing of spectral radiance from below the ocean surface. In: Optical Aspects of Oceanography, Jerlov, N.G., Steenmann-Nielsen, E. (Eds.), London, Academic Press.

Babin, M. (2005). Phytoplankton fluorescence : theory, current literature and *in situ* measurement. In: Real-Time Observation Systems for Ecosystem Dynamics and Harmful Algal Blooms, Babin, M., Roesler, C.S., Cullen, J.J. (Eds.), UNESCO, Paris.

Babin, M., Morel, A., Claustre, H., Bricaud, A., Zolber, Z., Falkowski, P.G. (1996). Nitrogen- and irradiance-dependent variations of the maximum quantum yield of carbon fixation in eutrophic, mesotrophic and oligotrophic marine systems. Deep-Sea Res. 43: 1241–1272.

Balch, W.M., Eppley, R.W., Abbott, M.R., Reid, F.M.H. (1989). Bias in satellite-derived pigment measurements due to coccolithophores and dinoflagellates. J. Plank. Res. 11: 575–581.

Balch, W.M., Holligan, P.M., Ackleson, S.G., Voss, K.J. (1991). Biological and optical properties of mesoscale coccolithophore blooms in the Gulf of Maine, Limnol. Oceanogr. 36: 629–643.

Balch, W.M., Gordon, H.R., Bowler, B.C., Drapeau, D.T., Booth, E.S. (2005). Calcium carbonate measurements in the surface global ocean based on Moderate-Resolution Imaging Spectrometer data. J. Geophys. Res. 110(C07001), doi:10.1029/2004JC002560.

Barlow, R.G., Aiken, J., Moore, G.F., Holligan, P.M., Lavender, S. (2004). Pigment adaptations in surface phytoplankton along the eastern boundary of the Atlantic Ocean. Mar. Ecol. Prog. Ser. 281: 13–26.

Barnes, C., Irigoien, X., De Oliveira, J.A.A., Maxwell, D., Jennings, S. (2011). Predicting marine phytoplankton community size structure from empirical relationships with remotely sensed variables. J. Plankton Res. 33(1): 13–24.

Beaufort, L., Couapel, M., Buchet, N., Claustre, H., Goyet, C., (2008). Calcite production by coccolithophores in the south east Pacific Ocean. Biogeosciences, 5: 1101–1117.

Beaugrand, G. (2003). Plankton effect on cod recruitment in the North Sea. Nature 426: 661–664.

Beaugrand, G., Reid, P. (2003). Long-term changes in phytoplankton, zooplankton and salmon related to climate. Global Change Biol. 6: 801–817.

Behrenfeld, M.J., Randerson, J.T. , McClain, C.R. , Feldman, G.C. , Los, S.O. , Tucker, C.J. et al. (2001). Biospheric primary production during an ENSO transition. Science. 291: 2594–2597.

Belviso, S., Masotti, I., Tagliabue, A., Bopp, L., Brockman, P., Fichot, C., et al. (2012). DMS dynamics in the most oligotrophic subtropical zones of the global ocean. Biogeochem. doi:10.1007/s10533-011-9648-1.

Ben Mustapha, Z., Alvain, S., Jamet, C., Loisel, H., Dessailly, D. (2013). Automatic classification of water leaving radiance anomalies from global SeaWiFS imagery: Application to the detection of phytoplankton groups in open ocean waters. Remote Sens. Environ. doi:10.1016/j.rse.2013.08.046

Bernard, S., Probyn, T.A., Quirantes, A. (2009). Simulating the optical properties of phytoplankton cells using a two-layered spherical geometry. Biogeosciences Discuss. 6: 1497–1563.

Bernard, S., Shillington, F.A., Probyn, T.A. (2007). The use of equivalent size distributions of natural phytoplankton assemblages for optical modeling. Opt. Express 15(5): 1995–2007.

Beutler, M., Wiltshire, K.H., Meyer, B., Moldaenke, C., Lüring, C., Meyerhöfer, M. (2002). A fluorometric method for the differentiation of algal populations *in vivo* and *in situ*. Photosyn. Res. 72: 39–53.

Bidigare, R.R., Morrow, J.H., Kiefer, D.A. (1989). Derivative analysis of spectral absorption by photosynthetic pigments in the western Sargasso Sea. J. Mar. Res. 47: 323–341.

Bidigare, R.R., Ondrusek, M.E., Morrow, J.H., Kiefer, D. (1990). *In vivo* absorption properties of algal pigments. In SPIE vol. 1302 Ocean Optics X, Spinrad, R.W., (Ed.), pp. 290–302, SPIE.

Bidigare, R.R., Van Heukelem, L., Trees, C.C. (2002). HPLC phytoplankton pigments: sampling, laboratory methods, and quality assurance procedures. In: Ocean optics protocols for satellite ocean color sensor validation, Mueller, J.L., Fargion, G.S. (Eds.), pp. 258–268, NASA, Goddard Space Flight Center.

Biegala, I.C., Not, F., Vaulot, D., Simon, M. (2003). Quantitative assessment of picoeukaryotes in the natural environment by using taxon-specific oligonucleotide probes in association with tyramide signal amplification-fluorescence *in situ* hybridization and flow cytometry. Appl. Env. Microbiol. 69: 5519–5529.

Blackford, J.C., Allen, J.I., Gilbert, F.J. (2004). Ecosystem dynamics at six contrasting sites: a generic modelling study. J. Mar. Syst. 52(1-4): 191–215.

Blomster, J., Back, S., Fewer, P.D., Kiirikki,M., Lehvo, A., Maggs, A.C., Stanhope, M.J. (2002). Novel morphology in *Enteromorpha* (Ulvophyceae) forming green tides. Am. J. Botany 89(11): 1756–1763.

Blum, M., Rozanov V., Burrows, J.P., Bracher A. (2012). Coupled ocean-atmosphere radiative transfer model in framework of software package SCIATRAN: Selected comparisons to model and satellite data. Adv. Space Res. 49(12): 1728–1742.

Bohren, C.F., Singham, S.B. (1991). Backscattering by nonspherical particles – a review of methods and suggested new approaches. J. Geophys. Res. 96: 5269–5277.

Booth, B.C. (1993). Estimating cell concentration and biomass of autotrophic plankton using microscopy. In: Handbook of methods in aquatic microbial ecology, Kemp, P.F., Sherr, B.F., Sherr, E.B., Cole, J.J. (Eds.), pp. 199–206, CRC Press.

Bopp, L., Aumont, O., Cadule, P., Alvain, S., Gehlen, M. (2005). Response of diatoms distribution to global warming and potential implications: A global model study. Geophys. Res. Letters 32: L19606, doi: 10.1029/2005GL023653.

Borstad, G.A., Gower, J.F.R., Carpenter, E.J., Rueter, J.G. (1989). Development of algorithms for remote sensing of marine *Trichodesmium*. Int. Geosci. Remote Sens. Symposium (IGARSS'89), Vancouver, BC Canada.

Boss, E., Pegau, W.S., Gardner, W.D., Zaneveld, J.R.V., Barnard, A.H., Twardowski, M.S., Change, G.C., Dickey, T.D. (2001a). Spectral particulate attenuation and particle size distribution in the bottom boundary layer of a continental shelf. J. Geophys. Res. 106: 9509–9516.

Boss, E., Pegau, W.S., Lee, M., Twardowski, M., Shybanov, E., Korotaev, G., Baratange, F. (2004). Particulate backscattering ratio at LEO 15 and its use to study particle composition and distribution. J. Geophys. Res. 109: doi:10.1029/2002JC001415.

Boss, E., Twardowski, M.S., Herring, S. (2001b). Shape of the particulate beam attenuation spectrum and its inversion to obtain the shape of the particulate size distribution. Appl. Opt. 40: 4885–4893.

Bouman, H., Platt, T., Sathyendranath, S., Stuart, V. (2005). Dependence of light-saturated photosynthesis on temperature and community structure. Deep Sea Res. I, 52: 1284–1299.

Bowers, H.A., Tengs, T., Glasgow, H.B., Burkholder, J.M., Rublee, P.A., Oldach, D.W. (2000). Development of real-time PCR assay for rapid detection of *Pfiesteria piscicida* and related dinoflagellates. Appl. Env. Microbiol. 66: 4641–4648.

Bowers, H.A., Triceb, T.M., Magnien, R.E., Goshorn, D.A., Michael, B., Schaefer, E.F., Rublee, P.A., Oldacha, D.W. (2006). Detection of *Pfiesteria* spp. by PCR in surface sediments collected from Chesapeake Bay tributaries (Maryland). Harmful Algae 5: 342–351.

Boyd, P.W., Newton, P. (1999). Does planktonic community structure determine downward particulate organic carbon flux in different oceanic provinces? Deep Sea Res. I 46: 63–91.

Bracher, A., Vountas, M., Dinter, T., Burrows, J.P., Röttgers, R., Peeken, I. (2009). Quantitative observation of cyanobacteria and diatoms from space using PhytoDOAS on SCIAMACHY data. Biogeosciences 6: 751–764.

Brewin, R.J.W., Devred, E., Sathyendranath, S., Lavender, S.J., Hardman-Mountford, N.J., (2011a). Model of phytoplankton absorption based on three size classes. Appl. Optics 50(2): 4535–4549.

Brewin, R.J.W., Hardman-Mountford, N.J., Lavender, S., Raitsos, D.E., Hirata, T., Uitz, J. (2011b). An intercomparison of bio-optical techniques for detecting dominant phytoplankton size class from satellite remote sensing. Remote Sens. Environ. 115(2): 325–339.

Brewin, R.J.W., Hirata, T., Hardman-Mountford, N.J., Lavender, S., Sathyendranath, S., Barlow, R. (2012). The influence of the Indian Ocean Dipole on interannual variations in phytoplankton size structure as revealed by Earth Observation. Deep Sea Res. II 77-80: 117–127.

Brewin, R.J.W., Lavender, S.J., Hardman-Mountford, N.J. (2010b). Mapping size-specific phytoplankton primary production on a global scale. J. Maps 2010, 1–15.

Brewin, R.J.W., Lavender, S.J., Hardman-Mountford, N.J., Hirata, T. (2010c). A spectral response approach for detecting dominant phytoplankton size class from satellite remote sensing. Acta Oceanologica Sinica, 29: 14–32.

Brewin, R.J.W., Sathyendranath, S., Hirata, T., Lavender, S.J., Barciela, R., Hardman-Mountford, N.J. (2010a). A three-component model of phytoplankton size class for the Atlantic Ocean. Ecol. Model. 221: 1472–1483.

Brewin, R.J.W., Sathyendranath, S., Lange, P.K., Tilstone, G. (2014). Comparison of two methods to derive the size-structure of natural populations of phytoplankton. Deep-Sea Res. I 85: 72–79.

Brewin, R.J.W., Sathyendranath, S., Müller, D., Brockmann, C., Deschamps, P-Y., Devred, E., et al. (2013). The Ocean Colour Climate Change Initiative: III. A round-robin comparison on in-water bio-optical algorithms. Remote Sens. Environ. doi:10.1016/j.rse.2013.09.016.

Bricaud, A., Babin, M., Claustre, H., Ras, J., Tiéche, F. (2010). Light absorption properties and absorption budget of Southeast Pacific waters. J. Geophys. Res. 115: C08009.

Bricaud, A., Babin, M., Morel, A., Claustre, H. (1995). Variability in the chlorophyll specific absorption coefficients of natural phytoplankton: Analysis and parameterization. J. Geophys. Res. 100: 13,321–13,332.

Bricaud, A., Ciotti, A.M., Gentili, B. (2012). Spatial-temporal variations in phytoplankton size and colored detrital matter absorption at global and regional scales, as derived from twelve years of SeaWiFS data (1998-2009). Global Biogeochem. Cy. 26: GB1010.

Bricaud, A., Claustre, H., Ras, J., Oubelkheir, K. (2004). Natural variability of phytoplanktonic absorption in oceanic waters: Influence of the size structure of algal populations. J. Geophys. Res. 109: C11010.

Bricaud, A., Mejia, C., Biondeau-Patissier, D., Claustre, H., Crepon, M., Thiria, S. (2007). Retrieval of pigment concentrations and size structure of algal populations from their absorption spectra using multilayered perceptrons. Appl. Optics 46(8): 1251–1260.

Bricaud, A., Morel, A., Babin, M., Allali, K., Claustre, H. (1998). Variations of light absorption by suspended particles with the chlorophyll a concentration in oceanic (case 1) waters: Analysis and implications for bio-optical models. J. Geophys. Res. 103: 31,033–31,044.

Bricaud, A., Zaneveld, J.R.V., Kitchen, J.C. (1992). Backscattering efficiency of coccolithophorids: use of a three-layered sphere model. In: Ocean Optics XI, Gilbert, G.D. (Ed.), Proc. SPIE 1750, 27–33.

Broerse, A.T.C., Tyrell, T., Young, J.R., Poulton, A.J., Merico, A., Blaxch, W.M., et al. (2003). The cause of bright waters in the Bering Sea in winter. Continental Shelf Res. 23: 1579–1596.

Brotas, V., Brewin, R.J.W., Sá, C., Brito, A.C., Silva, A., Mendes, C.R. et al. (2013). Deriving phytoplankton size classes from satellite data: validation along a trophic gradient in the Eastern Atlantic Ocean. Remote Sens. Environ. 134: 66–77.

Brown, C.W. (2000). Spatial and temporal variability of *Emiliania huxleyi* blooms in SeaWiFS imagery. Proc. Am. Geophys. Soc. Ocean Sciences, 24–28.

Brown, C.W., Podesta, G.P. (1997). Remote sensing of coccolithophore blooms in the western South Atlantic Ocean. Remote Sens. Environ. 60: 83–91.

Brown, C.W., Yoder, J.A. (1994). Coccolithophorid blooms in the global ocean. J. Geophys. Res. 99: 7467–7482.

Brownlee, C., Taylor, A.R. (2002). Algal calcification and silification. In: Encyclopedia of life sciences. Macmillan Publishers Ltd, Nature Publishing Group. 1–6.

Bruggeman, J., Kooijman, S.A.L.M. (2007). A biodiversity-inspired approach to aquatic ecosystem modeling. Limnol. Oceanogr., 52(4): 1533–1544.

Bruland, K.W., Rue, E.L., Smith, G.J., DiTullio, G.R. (2005). Iron, macronutrients and diatom blooms in the Peru upwelling regime: brown and blue waters of Peru. Mar. Chem. 93: 81–103.

Bruland K.W., Rue, E.L., Smith, G.J. (2001). Iron and macronutrients in California coastal upwelling regimes: Implications for diatom blooms. Limnol. Oceanogr. 46: 1661–1674.

Budd, J.W., Drummer, T.D., Nalepa, T.F., Fahnenstiel, G.L. (2001a). Remote sensing of biotic effects: Zebra mussels (*Dreissena polymorpha*) influence on water clarity in Saginaw Bay, Lake Huron. Limnol. Oceanogr. 46(2): 213–223.

Budd, J.W., Beeton, A.M., Stumpf, R.P., Culver, D.A., Kerfoot, W.C. (2001b). Satellite observations of *Microcystis* blooms in western Lake Erie. Paper presented at the International Association of Theoretical and Applied Limnology, Verh. Internat. Verein. Limnol., Stuttgart.

Campbell, L., Hendrichs, D.W., Olson, R.J., Sosik, H.M. (2013). Continuous automated imaging-in-flow cytometry for detection and early warning of *Karenia brevis* blooms in the Gulf of Mexico. Environ. Sci. Pollut. doi:10.1007/s11356-012-1437-4.

Canadell, J.G., LeQuéré, C., Raupach, M.R., Field, C.B., Buitenhuis, E.T., Ciais, P. et al. (2007). Contributions to accelerating atmospheric CO_2 growth from economic activity, carbon intensity, and efficiency of natural sinks. PNAS, 104(47): 18,866–18,870.

Cannizzaro, J.P., Carder, K.L., Chen, F.R., Heil, C.A., Vargo, G.A. (2008). A novel technique for detection of the toxic dinoflagellate, *Karenia brevis*, in the Gulf of Mexico from remotely sensed ocean color data. Cont. Shelf Res. 28: 137–158.

Cannizzaro, J.P., Hu, C., English, D.C., Carder, K.L., Heil, C.A., Müller-Karger, F.E. (2009). Detection of *Karenia brevis* blooms on the west Florida shelf using *in situ* backscattering and fluorescence data. Harmful Algae, 8: 898–909, doi:10.1016/j.hal.2009.05.001.

Capone, D.G., Subramaniam, A., Montoya, J.P., Humborg, C., Voss, M., Pollehne, F., Carpenter, E.J. (1998). An extensive bloom of the diazotrophic cyanobacterium, *Trichodesmium*, in the Central Arabian Sea During the Spring Intermonsoon. Mar. Ecol. Prog. Series, 172: 281–292.

Capone, D.G., Zehr, J., Paerl, H., Bergman, B., Carpenter, E.J. (1997). *Trichodesmium*: A globally significant marine cyanobacterium. Science, 276: 1221–1229.

Carder, K.L., Steward, R. G. (1985). A remote-sensing reflectance model of a red-tide dinoflagellate off west Florida. Limnol. Oceanogr. 30: 286–298.

Carder, K.L., Hawes, S.K., Baker, K.A., Smith, R.C., Steward, R.G., Mitchell, B.G. (1991). Reflectance model for quantifying chlorophyll a in the presence of productivity degradation products. J. Geophys. Res. 96: 20,599–20,611.

Caron, D.A. (2013). Towards a molecular taxonomy for protists: benefits, risks, and applications in plankton ecology. J. Euk. Microbiol. 60: 407–413.

Carvalho, G.A., Minnett, P.J., Banzon, V.F., Baringer, W., Heil, C.A. (2011). Long-term evaluation of three satellite ocean color algorithms for identifying harmful algal blooms (*Karenia brevis*) along the west coast of Florida: A matchup assessment. Remote Sens. Environ. 115: 1–18, doi:10.1016/j.rse.2010.07.007.

Carvalho, G.A., Minnett, P.J., Fleming, L.E., Banzon, V.F., Baringer, W. (2010). Satellite remote sensing of harmful algal blooms: A new multi-algorithm method for detecting the Florida Red Tide (*Karenia brevis*). Harmful Algae, 9: 440–448, doi:10.1016/j.hal.2010.02.002.

Cavender-Bares, K.K., Frankel, S.L., Chisholm, S.W. (1998). A dual sheath flow cytometer for shipboard analyses of phytoplankton communities from the oligotrophic ocean. Limnol. Oceanogr. 43: 1383–1388.

Cavender-Bares, K.K., Karl, D.M., Chisholm, S.W. (2001). Nutrient gradients in the western North Atlantic Ocean: relationship to microbial community structure and comparison to patterns in the Pacific Ocean. Deep-Sea Res I, 48: 2373–2395.

Cavender-Bares K.K., Mann, E.L., Chisolm, S.W., Ondrusek, M.E., Bidigare R.L. (1999). Differential response of equatorial Pacific phytoplankton to iron fertilization, Limnol. Oceanogr., 44(2): 237–246.

Charleson, R. J., Lovelock, J.E., Andreae, M.O. and Warren, S.G. (1987). Oceanic phytoplankton, atmospheric sulphur, cloud albedo and climate. Nature 326: 655–661.

Chavez, F.P., Strutton, P.G., Friedrich, G.E., Feely, R.A., Feldman, G.C., Foley D.G., McPhaden, M.J. (1999). Biological and chemical response of the equatorial Pacific ocean to the 1997-98 El Niño. Science, 286: 2126–2131.

Chazottes, A., Bricaud, A., Crépon, M., Thiria, S. (2006). Statistical analysis of a database of absorption spectra of phytoplankton and pigment concentrations using self-organizing maps. Appl. Optics 45(31): 8102–8115.

Chazottes, A., Crépon, M., Bricaud, A., Ras, J., Thiria, S. (2007). Statistical analysis of absorption spectra of phytoplankton and of pigment concentrations observed during three POMME cruises using a neural network clustering method. Appl. Optics 46(18): 3790–3799.

Chekalyuk, A.M., Landry, M.R., Goericke, R., Taylor, A.G., Hafez, M.A. (2012). Laser fluorescence analysis of phytoplankton across a frontal zone in the California Current ecosystem. J. Plank. Res. 34: 761–777.

Chisholm, S.W. (1992). Phytoplankton size. In: Primary Productivity and Biogeochemical Cycles in the Sea, Falkowski, P.G., Woodhead, A.D. (Eds.), New York, Springer.

Chisholm, S.W., Olson, R.J., Zettler, E.R., Goericke, R., Waterbury, J.B., Welschmeyer, N.A. (1988). A novel free-living prochlorophyte abundant in the oceanic euphotic zone, Nature 334: 340–343.

Ciotti, A.M., Bricaud, A. (2006). Retrievals of a size parameter for phytoplankton and spectral light absorption by coloured detrital matter from water-leaving radiances at SeaWiFS channels in a continental shelf off Brazil. Limnol. Oceanogr. Methods 4: 237–253.

Ciotti, A.M., Cullen, J.J., Lewis, M.R. (1999). A semi-analytical model of the influence of phytoplankton community structure on the relationship between light attenuation and ocean color. J. Geophys. Res. 104: 1559–1578.

Ciotti, A.M., Lewis, M.R., Cullen, J.J. (2002). Assessment of the relationships between dominant cell size in natural phytoplankton communities and the spectral shape of the absorption coefficient. Limnol. Oceanogr. 47(2): 404–417.

Claustre, H. (1994). The trophic status of various oceanic provinces as revealed by phytoplankton pigment signatures. Limnol. Oceanogr. 39: 1206–1210.

Claustre, H., Hooker, S.B., Van Heukelem, L., Berthon, J.F., Barlow, R.G., Ras, J., Sessions, H., Targa, C., Thomas, C.S., van der Linde, D., Marty, J.C. (2004). An intercomparison of HPLC phytoplankton methods using *in situ* samples: Application to remote sensing and database activities. Mar. Chem. 85: 41–64.

Clavano, W.R., Boss, E., Karp-Boss, L. (2007). Inherent optical properties of non-spherical marine-like particles–from theory to observation. Oceanogr. Mar. Biol. 45: 1–38.

Cloern, J.E., Grenz, C., Vidergar-Lucas, L. (1995). An empirical model of the phytoplankton chlorophyll:carbon ratio – the conversion factor between productivity and growth rate. Limnol. Oceanogr. 40: 1313–1321.

Coelho, S.M., Simon, N., Ahmed, S., Cock, J.M., Partensky, F. (2013). Ecological and evolutionary genomics of marine photosynthetic organisms. Mol. Ecol. 22: 867–907.

Cokacar T., Kubilay, N., Oguz, T. (2001). Structure of *Emiliania huxleyi* blooms in the Black Sea surface waters as detected by SeaWiFS imagery. Geophys. Res. Lett., 28(24): 4607–4610.

Collier, J.L. (2000). Flow cytometry and the single cell in phycology. J. Phycol. 36: 628–644.

Colomb, A., Gros, V., Alvain, S., Sarda-Esteve, R., Bonsang, B., Moulin, C. et al. (2009). Variation of atmospheric volatile organic compounds over the Southern Indian Ocean (30-49° S). Environ. Chem. 6: 70-82.

Countway, P.D., Caron, D.A. (2006). Abundance and distribution of *Ostreococcus* sp. in the San Pedro Channel, California, as revealed by quantitative PCR. Appl. Env. Microbiol. 72: 2496–2506.

Cox, P.A., Banack, S.A., Murch, S.J., Rasmussen, U., Tien, G., Bidigare, R.R. et al. (2005). Diverse taxa of cyanobacteria produce beta-N-methylamino-L-alanine, a neurotoxic amino acid. Proc. Natl. Acad. Sci. USA, 102(27): 9734–9734.

Craig, S.E., Lohrenz, S.E., Lee, Z.P., Mahoney, K.L., Kirkpatrick, G.J., Schofield, O.M., Steward, R.G. (2006). Use of hyperspectral remote sensing reflectance for detection and assessment of the harmful alga, *Karenia brevis*. Appl. Optics, 45: 5414–5425.

Cullen, J.J. (1985). Diel vertical migration by dinoflagellates: roles of carbohydrate metabolism and behavioral flexibility. Contr. Mar. Sci. 27 (Suppl.): 135–152.

Cullen, J.J., Ciotti, A.M., Davis, R.F., Lewis, M.R. (1997). Optical detection and assessment of algal blooms. Limnol. Oceanogr. 42: 1223–1239.

Cullen, J.J., Franks, P.J.S., Karl, D.M., Longhurst, A. (2002). Physical influences on marine ecosystem dynamics, p. 297-336. In: The Sea, Robinson, A.R., McCarthy, J.J., Rothschild, B.J. (Eds.), Volume 12, John Wiley & Sons.

Cunningham, A. (1990). Fluorescence pulse shape as a morphological indicator in the analysis of colonial microalgae by flow cytometry. J. Microbiol. Meth. 11: 27–36.

Cury, P.M., Shin, Y.-J., Planque, B., Durant, J.M., Fromentin, J.-M., Kramer-Schadt, S. et al. (2008). Ecosystem oceanography for global change in fisheries. Trends Ecol. Evol. 23: 338–346.

Dall'Olmo, G., Westberry, T.K., Behrenfeld, M.J., Boss, E., Slade, W.H. (2009). Significant contribution of large particles to optical backscattering in the open ocean. Biogeosciences 6(6): 947–967.

Dandonneau, Y., Deschamps, P-Y., Nicolas, J-M., Loisel, H., Blanchot, J., Monteld, Y., Thieuleux, F., Bécu, G. (2004). Seasonal and interannual variability of ocean color and composition of phytoplankton communities in the North Atlantic, equatorial Pacific and South Pacific. Deep-Sea Res. II, 51: 303–318.

Davidson, K., Miller, P.I., Wilding, T., Shutler, J.D., Bresnan, E., Kennington, K., Swan, S. (2009). A large and prolonged bloom of *Karenia mikimotoi* in Scottish waters in 2006. Harmful Algae, 8(2): 349–361.

de Boyer Montégut, C., Madec, G., Fisher, A.S., Lazar, A., Iudicone, D., (2004). Mixed layer depth over the global ocean: An examination of profile data and a profile-based climatology. J. Geophys. Res. 109: C12003.

Demarcq, H., Reygondeau, G., Alvain, S., Vantrepotte, V. (2011). Monitoring marine phytoplankton seasonality from space. Remote Sens. Environ. 117: 211-222.

De Monte, S., Soccodato, A., Alvain, S., D'Ovidio, F. (2013). Can we detect oceanic biodiversity hotspots from space? ISME J. 1-3,doi:10.1038/ismej.2013.72.

Devassy, V.P., Bhattathiri, P.M.A., Qasim, S.Z. (1978). *Trichodesmium* phenomenon. Ind. J. Mar. Sci. 7(3): 168-186.

Devred, E., Sathyendranath, S., Stuart, V., Maas, H., Ulloa, O., Platt, T. (2006). A two-component model of phytoplankton absorption in the open ocean: Theory and applications. J. Geophys. Res. 111: C03011.

Devred, E., Sathyendranath, S., Stuart, V., Platt, T. (2011). A three component classification of phytoplankton absorption spectra: Applications to ocean-colour data. Remote Sens. Environ. 115(9): 2255-2266.

Dierssen, H.M. (2010). Perspectives on empirical approaches for ocean color remote sensing of chlorophyll in a changing climate. P. Natl. Acad. Sci. USA 107(40): 17,073-17,078.

Dierssen, H., Smith, R.C. (2000). ?Bio-Optical properties and remote sensing ocean color algorithms for Antarctic Peninsula Waters.? J. Geophys. Res. 105(C11): 26301-26312.

Doney, S.C. (2006). The dangers of ocean acidification. Scientific American 294: 58-65.

Doney, S.C., Balch, W.M., Fabry, V.J., Feely, R.A. (2009). Ocean acidification: A critical emerging problem for the ocean sciences. Oceanography 22(4): 16-25.

D'Ovidio, F., De Montec, S., Alvain, S., Dandonneau, Y., Lévy, M. (2010). Fluid dynamical niches of phytoplankton types. Proc. Natl. Acad. Sci. USA. 107(43): 18,366-18,370.

Dubelaar, G.B.J., Jonker, R.R. (2000). Flow cytometry as a tool for the study of phytoplankton. Sci. Mar. 64: 135-156.

Dubelaar, G.B.J., Gerritzen, P.L. (2000). CytoBuoy: a step forward towards using flow cytometry in operational oceanography. Sci. Mar. 64: 255-265.

Dubelaar, G.B.J., Groenewegen, A.C., Stokdijk, W., van den Engh, G.J., Visser, J.W.M. (1989). Optical Plankton Analyser: A flow cytometer for plankton analysis, II: Specifications. Cytometry 10: 529-539.

Duforêt-Gaurier, L., Loisel, H., Dessailly, D., Nordkvist, K., Alvain, S. (2010). Estimates of particulate organic carbon over the euphotic depth from *in situ* measurements. Application to satellite data over the global ocean. Deep Sea Res. I: 57(3): 351-367.

Dupouy, C., Benielli-Gary, D., Neveux, J., Dandonneau, Y., Westberry, T.K. (2011). An algorithm for detecting *Trichodesmium* surface blooms in the South Western Tropical Pacific. Biogeosci. Discuss, 8: 5653-5689.

Dupouy, C., Neveux, J., Subramaniam, A., Mulholland, M.R., Montoya, J.P., Campbell, L. et al. (2000). Satellite captures *Trichodesmium* blooms in the southwestern tropical Pacific, EOS Trans. 81(2): 13-16.

Dupouy, C., Petit, M., Dandonneau, Y. (1988). Satellite detected cyanobacteria bloom in the southwestern tropical Pacific: Implication for oceanic nitrogen fixation. Int. J. Remote Sens. 9: 389-396.

Duysens, L.N.M. (1956). The flattening of the absorption spectrum of suspensions as compared to that of solutions. Biochim. Biophys. Acta 19: 1-12.

Egeland, E.S., Guillard, R.R.L., Liaaen-Jensen, S. (1997). Additional carotenoid prototype representatives and a general chemosystematic evaluation of carotenoids in Prasinophyceae (Chlorophyta). Phytochem. 44: 1087-1097.

Eller, G., Töbe, K., Medlin, L.K. (2007). A set of hierarchical FISH probes for the Haptophyta and a division level probe for the Heterokonta. J. Plank. Res. 29: 629-640.

Eppley, R.W., Peterson, B.J. (1979). Paniculate organic matter flux and planktonic new production in the deep ocean. Nature 282: 677-680.

Eppley, R.W., Holm-Hansen, O., Strickland, J.D.H. (1968). Some observations on the vertical migration of dinoflagellates. J. Phycol. 4: 333-340.

Estrada, M., Berdalet, E. (1997). Phytoplankton in a turbulent world. Scientia Marina 61 (Supl. 1): 125-140.

Evers-King, H., Bernard, S., Robertson-Lain, L., Probyn, T.A. (2014). Sensitivity in reflectance attributed to phytoplankton cell size: forward and inverse modelling approaches. Optics Express, 22(10): 11,536-11,551.

Faust, M.A., Gulledge, R.A. (2002). Identifying harmful marine dinoflagellates. Contrib. U. S. Natl. Herb. 42: 1-144.

Faust, M.A., Norris, K.H. (1985). *In vivo* spectrophotometric analysis of photosynthetic pigments in natural populations of phyoplankton. Limnol. Oceanogr. 30: 1316-1322.

Field C., Behrenfeld, M., Randerson, J., Falkowski, P. (1998). Primary production of the biosphere: integrating terrestrial and oceanic components. Science 281: 237-240.

Fishman, J., Iraci, L.T. Al-Saadi, J., Change, K., Chavez, F., Chin, M. et al. (2012). The United States' next generation of atmospheric composition and coastal ecosystem measurement: NASA's Geostationary Coastal and Air Pollution Events (GEO-CAPE) Mission. BAMS, October 2012, 1547-1566, DOI:10.1175/BAMS-D-11-00201.1.

Fletcher, R.L. (1996). The occurrence of "green tides": a review. In: Marine benthic Vegetation: Recent Changes and the Effects of Eutrophication, Schramm, W., Nienhuis, P.H. (Eds.), Springer, Berlin, Germany. pp. 7-43.

Foster, R.A. Zehr, J.P. (2006). Characterization of diatom-cyanobacteria symbioses on the basis of nifH, hetR and 16S rRNA sequences. Environ Microbiol. 8: 1913-1925.

Frankel, S.L., Binder, B.B., Chisholm, S.W., Shapiro, H.M. (1990). A high-sensitivity flow cytometer for studying picoplankton. Limnol. Oceanogr. 35: 1164-1169.

Fujiki, T., Tagughi, S. (2002). Variability in chlorophyll a specific absorption coefficient in marine phytoplankton as a function of cell size and irradiance. J. Plank. Res. 24(9): 859–874 doi: 10.1093/plankt/24.9.859.

Fujiwara, M., Hirawake, T., Suzuki, K., Saitoh, S.I. (2011). Remote sensing of size structure of phytoplankton communities using optical properties of the Chukchi and Bering Sea shelf region. Biogeosci. 4: 817–835.

Galluzzi, L., Penna, A., Bertozzini, E., Vila, M., Garcés, E., Magnani, M. (2004). Development of Real-Time PCR assay for rapid detection and quantification of *A. minutum* (Dinoflagellate). Appl. Env. Microbiol. 70: 1199–1206.

Gardner, W.D., Mishonov, A.V., Richardson, M.J. (2006). Global POC concentrations from *in-situ* and satellite data. Deep-Sea Res. II 53: 718–740.

Garver, S.A., Siegel, D.A., Mitchell, B.G. (1994). Variability in near-surface particulate absorption spectra: What can a satellite ocean color imager see? Limnol. Oceanogr. 39: 1349–1367.

Gege, P. (1998). Characterization of the phytoplankton Lake Constance for classification by remote sensing. In: Lake Constance, Characterization of an ecosystem in transition, Bäuerle, E., Gaedke, U. (Eds.) Arch. Hydrobiol. Spec. Issues Advanc. Limnol. 53: 179–193.

Geider, R.J., Platt, T., Raven, J.A. (1986). Size dependence of growth and photosynthesis in diatoms: a synthesis. Mar. Ecol. Prog. Ser. 30: 93–104.

Gieskes, W.W.C., Kraay, G.W. (1983). Dominance of Cryptophyceae during phytoplankton spring bloom in the central North Sea detected by HPLC analysis of pigments. Mar. Biol. 75: 179–185.

Goericke, R., Montoya, J.P. (1998). Estimating the contribution of microalgal taxa to chlorophyll a in the field-variations of pigment ratios under nutrient- and light-limited growth. Mar. Ecol. Prog. Ser. 169: 87–95.

Goffart A., Catalano, G., Hecq, J.H. (2000). Factors controlling the distribution of diatoms and *Phaeocystis* in the Ross Sea. J. Mar. Sys. 27: 161–175.

Goldman, J.C., McCarthy, J.J., Peavey, D.G. (1979). Growth rate influence on the chemical composition of phytoplankton in oceanic waters. Nature, 279: 210–215.

Gordon, H.R., Balch, W.M. (1999). MODIS Detached Coccolith Concentration Algorithm, Theoretical Basis Document (ATBD) Version 4 (ATDB-MOD-23). MODIS Ocean Discipline Group. http://oceancolor.gsfc.nasa.gov/DOCS/MSL12/master_prodlist.html/#prod19.

Gordon, H.R., Clark, D.K. (1980). Remote sensing optical properties of a stratified ocean: an improved interpretation. Appl. Opt. 19: 3428–3430.

Gordon, H.R., McCluney, W.R. (1975). Estimation of the depth of sunlight penetration in the sea for remote sensing. Appl. Opt. 14: 413–416.

Gordon, H.R., Boynton, G.C., Balch, W.M., Groom, S.B., Harbour, D.S., Smyth, T.J. (2001). Retrieval of coccolithophore calcite concentration from SeaWiFS imagery. Geophys. Res. Lett. 28: 1587–1590.

Gordon, H.R., Brown, O.B., Evans, R.H., Brown, J., Smith, R.C., Baker, K.S., Clark, S.K. (1988). A semianalytic radiance model of ocean color. J. Geophys. Res. 93: 10,909–10,924.

Gordon, H.R., Clark, D.K. , Brown, J.W., Brown, O.B., Evans, R.H., Broenkow, W.W. (1983). Phytoplankton pigment concentrations in the Middle Atlantic Bight: Comparison of ship determinations and CZCS estimates. Appl. Opt. 22: 20–36.

Gordon, H.R., Clark, D.K., Muller, J.L., Hovis, W.A. (1980). Phytoplankton pigments from the Nimbus-7 Coastal Zone Color Scanner – Comparisons with surface measurements. Science, 210: 63–66.

Gower, J.F.R., King , S.A. (2011). Distribution of floating *Sargassum* in the Gulf of Mexico and the Atlantic Ocean mapped using MERIS. Int. J. Remote Sens. 32: 1917–1929.

Gower, J., King, S., Goncalves, P. (2008). Global monitoring of plankton blooms using MERIS MCI. Int. J. Remote Sens. 29(21): 6209–6216.

Gower, J., Young, E., King, S. (2013). Satellite images suggest a new *Sargassum* source region in 2011. Remote Sens. Lett. 4: 764–773.

Gower, J., King, S., Borstad, G., Brown, L. (2005). Detection of intense plankton blooms using the 709 nm band of the MERIS imaging spectrometer. Int. J. Remote Sens. 26: 2005–2012.

Gower, J., Hu, C., Borstad, G., King, S. (2006). Ocean color satellites show extensive lines of floating *Sargassum* in the Gulf of Mexico. IEEE Trans. Geosci. Remote Sens. 44: 3619–3625.

Green, R.E., Sosik, H.M., Olson, R.J. (2003). Contributions of phytoplankton and other particles to inherent optical properties in New England continental shelf waters. Limnol. Oceanogr. 48: 2377–2391.

Greene R.M., Geider R.J and Falkowski P.G. (1991). Effect of iron on photosynthesis in a marine diatom. Limnol. Oceanogr. 36: 1772–1782.

Gregg, W.W., Casey, N.W. (2007). Modeling coccolithophores in the global oceans. Deep Sea Res. II. 54(5-7): 447–477.

Gregg, W.W., Ginoux, P., Schopf, P.S., Casey, N.W. (2003). Phytoplankton and iron: validation of a global three-dimensional ocean biogeochemical model. Deep-Sea Res. II 50: 3143–3169.

Groom, S., Holligan, P.M. (1987). Remote sensing of coccolithophore blooms. Adv. Space Res. 7(2): 273–278.

Gruber, N., Sarmiento, J.L. (1997). Global patterns of marine fixation and denitrification. Global Biogeochem. Cy. 11: 235–266.

Guidi, L., Stemmann, L., Jackson, G.A., Ibanez, F., Claustre, H., Legendre, L., Picheral, M., Gorskya, G. (2009). Effects of phytoplankton community on production, size and export of large aggregates: A world-ocean analysis. Limnol. Oceanogr. 54(6): 1951–1963.

Hallegraeff, G.M. (1993). A review of harmful algal blooms and their apparent global increase. Phycologia 32: 79–99.

Hallegraeff, G.M., Jeffrey, S.W. (1984). Tropical phytoplankton species and pigments of continental shelf waters of North and North-West Australia. Mar. Ecol. Prog. Ser. 20: 59–74.

Harlay, J., Borges, A.V., Van Der Zee, C., Delille, B., Godoi, R.H.M., Schiettecatte, L.-S., et al. (2010). Biogeochemical study of a coccolithophorid bloom in the northern, Bay of Biscay (NE Atlantic Ocean) in June 2004. Prog. Oceanogr. 86: 317–336.

Haywood, A.J., Steidinger, K.A., Truby, E.W., Bergquist, P.R., Bergquist, P.L., Adamson, J., Mackenzie, L. (2004). Comparative morphology and molecular phylogenetic analysis of three new species of the genus *Karenia* (Dinophyceae) from New Zealand. J. Phycol., 40: 165–179.

He, M.-X., Liu, J., Yu, F., Li, D., Hu, C. (2011). Monitoring green tides in Chinese marginal seas. In: Handbook of Satellite Remote Sensing Image Interpretation: Applications for Marine Living Resources Conservation and Management, Morales, J., Stuart, V., Platt, T., Sathyendranath, S. (Eds.), EU PRESPO and IOCCG, Dartmouth, Canada. pp. 111 – 124.

Henderson, C. (2006). Paradise lost. New Scientist, August 5, 2006, 29–33.

Henriksen, P., Riemann, B., Kaas, H., Sorensen, H.M., Sorensen, H.L. (2002). Effects of nutrient-limitation and irradiance on marine phytoplankton pigments. J. Plank. Res. 24: 835–858.

Hirata, T., Brewin, R.J.W. (2009). Phytoplankton community structure from space. GLOBEC International Newsletter 15(1): 5–6.

Hirata, T., Hardman-Mountford, N.J., Brewin, R.J.W. (2012). Comparing satellite-based phytoplankton classification methods. EOS Trans. Am. Geophys. Union 93(6): 59–60.

Hirata, T., Aiken, J., Hardman-Mountford, N.J., Smyth, T.J., Barlow, R.G. (2008a). An absorption model to derive phytoplankton size classes from satellite ocean colour. Remote Sens. Environ. 112(6)P: 3153–3159.

Hirata, T., Hardman-Mountford, N.J., Aiken, J., Smyth, T., Barlow, R. et al. (2008b). Optical approach to derive phytoplankton size classes using ocean color remote sensing. In: Ocean Optics XIX. Castelvecchio Pascoli, Italy, 6-10 Oct. 2008, PDF No. oo080412 (CDROM).

Hirata, T., Hardman-Mountford, N.J., Barlow, R., Lamont, T., Brewin, R.J.W., Smyth, T., Aiken, J. (2009). An inherent optical property approach to the estimation of size-specific photosynthetic rates in eastern boundary upwelling zones from satellite ocean colour: an initial assessment. Prog. Oceanogr. 83: 393–397.

Hirata, T., Hardman-Mountford, N.J., Brewin, R.J.W., Aiken, J., Barlow, R., Suzuki, K. et al. (2011). Synoptic relationships between surface chlorophyll-a and diagnostic pigments specific to phytoplankton functional types. Biogeosciences 8: 311–327.

Hoepffner, N., Sathyendranath, S. (1991). Effect of pigment composition on absorption properties of phytoplankton. Mar. Ecol. Prog. Ser. 73: 11–23.

Hoepffner, N., Sathyendranath, S. (1993). Determination of the major groups of phytoplankton pigments from the absorption spectra of total particulate matter. J. Geophys. Res. 98: 22789–22803.

Holligan, P.M., Vollier, M., Harbour, D.S., Camus, P., Champagnephilippe, M. (1983). Satellite and ship studies of coccolithophore production along a continental-shelf edge. Nature, 304: 339–342.

Holligan, P., Fernandez, E., Aiken, J.A., Balch, W.M., Boyd, P., Burkill, P.H. et al. (1993). A biogeochemical study of the coccolithophore *Emiliania huxleyi* in the North Atlantic. Global Biogeochem. Cy. 7: 879–900.

Holm-Hansen, O., Lorenzen, C.J., Holmes, R.W., Strickland, J.D.H. (1965). Fluorometric determination of chlorophyll. J. Cons. Int. l'Exploration de al Mer 30: 3–15.

Hood, R.R., Laws, E.A., Armstrong, R.A., Bates, N.R., Brown, C.W., Carlson, C.A. et al. (2006). Pelagic functional group modeling: Progress, challenges and prospects. Deep-Sea Res. II 53: 459–512.

Hooker, S.B., Van Heukelem, L., Thomas, C.S., Claustre, H., Ras, J., Barlow, R. et al. (2005). The second SeaWiFS HPLC Analysis Round-Robin Experiment (SeaHARRE-2). Tech. Memo 2005-212787, NASA, Goddard Space Flight Center, Greenbelt, MD.

Hovis, W.A., Clark, D.K., Anderson, F. et al. (1980). Nimbus-7 Coastal Zone Color Scanner - System description and initial imagery. Science, 210: 60–63.

Hu, C. (2009). A novel ocean color index to detect floating algae in the global oceans. Remote Sens. Environ. 113: 2118–2129.

Hu, C., He, M-X. (2008). Origin and offshore extent of floating algae in Olympic sailing area. Eos. AGU Trans. 89(33): 302–303.

Hu, C., Feng, L., Lee, Z. (2013). Uncertainties of SeaWiFS and MODIS remote sensing reflectance: Implications from clear water measurements. Remote Sens. Environ. 133: 163–182.

Hu, C.M., Cannizzaro, J., Carder, K.L., Muller-Karger, F.E., Hardy, R. (2010a). Remote detection of *Trichodesmium* blooms in optically complex coastal waters: Examples with MODIS full-spectral data. Remote Sens. Environ. 114(9): 2048–2058.

Hu, C., Cannizzaro, J.P., Lee, Z.P., Muller-Karger, F.E., Soto, I. (2011). Red tide detection in the Eastern Guld of Mexico using MODIS imagery. In: Handbook of Satellite Remote Sensing Image Interpretation: Applications for Marine Living Resources Conservation Management, Morales, J., Stuart, V., Platt, T., Sathyendranath, S. (Eds.), EU PRESPO and IOCCG, p. 293.

Hu, C., Lee, Z., Ma, R., Yu, K., Li, D., Shang, S. (2010b). Moderate Resolution Imaging Spectroradiometer (MODIS) observations of cyanobacteria blooms in Taihu Lake, China. J. Geophys. Res. 115: C04002, doi:10.1029/2009JC005511.

Hu, C., Li, D., Chen, C., Ge, J., Muller-Karger, F.E., Liu,J., Yu, F., He, M.-X. (2010c). On the recurrent *Ulva prolifera* blooms in the Yellow Sea and East China Sea. J. Geophys. Res. 115, C05017, doi:10.1029/2009JC005561.

Hu, C., Luerssen, R., Muller-Karger, F.E., Carder, K.L., Heil, C.A. (2008). On the remote monitoring of *Karenia brevis* blooms of the west Florida shelf. Cont. Shelf Res. 28: 159–176.

Hu, C., Muller-Karger, F.E., Taylor, C., Carder, K.L., Kelble, C., Johns, E., Heil, C.A. (2005). Red tide detection and tracing using MODIS fluorescence data: A regional example in SW Florida coastal waters. Remote Sens. Environ. 97: 311–321.

Huot, Y., Babin, M. (2010). Overview of fluorescence protocols: Theory, basic concepts, and practice. In: Chlorophyll a Fluorescence in Aquatic Sciences: Methods and Applications, Suggett, D.J., Prášil, O., Borowitzka, M.A. (Eds.), pp. 31–74, Springer.

Huot, Y., Morel, A., Twardowski, M.S., Stramski, D., Reynolds, R.A. (2008). Particle optical backscattering along a chlorophyll gradient in the upper layer of the eastern South Pacific Ocean. Biogeosciences 5: 495–507.

Hutchinson, G.E. (1957). Concluding remarks. Cold Spring Harbor Symposia on Quantitative Biology 22: 415–427.

Iglesias-Rodríguez, M.D., Brown, C.W., Doney, S.C., Kleypas, J., Kolber, D., Kolber, Z. (2002). Representing key phytoplankton functional groups in ocean carbon cycle models: Coccolithophorids. Global Biogeochem. Cy. 16: doi:10.1029/2001GB001454.

IOCCG (1999). Status and plans for satellite ocean-colour missions: considerations for comeplementary missions. Reports of the International Ocean-Colour Coordinating Group, No. 2, Yoder, J.A. (Ed.), IOCCG, Dartmouth, Canada.

IOCCG (2006). Remote Sensing of Inherent Optical Properties: Fundamentals, Tests of Algorithms, and Applications. Reports of the International Ocean-Colour Coordinating Group, No. 5, Lee, Z.P. (Ed.), IOCCG, Dartmouth, Canada.

Irigoien, X., Meyer, B., Harris, R., Harbour, D. (2004). Using HPLC pigment analysis to investigate phytoplankton taxonomy: the importance of knowing your species. Helgoland Marine Research 58: 77–82.

Irwin, A.J., Finkel, Z.V., Schofield, O.M.E., Falkowski, P.G. (2006). Scaling-up from nutrient physiology to the size-structure of phytoplankton communities. J. Plank. Res. 28: 459–471.

Jackson, T., Bouman, H.A., Sathyendranath, S., Devred, E. (2011). Regional-scale change in diatom distribution in the Humboldt Current as revealed by remote sensing: implications for fisheries. ICES J. Mar. Sci. 68: 729–736, doi:10.1093/icesjms/fsq18.

Jeffrey, S.W., Vesk, M. (1997). Introduction to marine phytoplankton and their pigment signatures. In: Phytoplankton Pigments in Oceanography, Jeffrey, S.W., Mantoura, R.F.C., Wright, S.W. (Eds.), UNESCO Publishing, Paris.

Jeffrey, S.W., Mantoura, R.F.C., Wright, S.W. (Eds.) (1997). Phytoplankton pigments in oceanography: guidelines to modern methods, UNESCO, France.

Jin, X., Gruber, N., Dunne, J.P., Sarmiento, J.L., Armstrong, R.A. (2006). Diagnosing the contribution of phytoplankton functional groups to the production and export of particulate organic carbon, $CaCO_3$, and opal from global nutrient and alkalinity distributions. Global Biogeochem. Cycles 20. GB2015, doi:10.1029/2005GB002532.

Jochem F.J., Mathot, S., Quéguiner, B. (1995). Size fractionated primary production in the open Southern Ocean in austral spring. Polar Biol. 15: 381–392.

Johnsen, G., Nelson, N.B., Jovine, R.V.M., Prézelin, B.B. (1994). Chromoprotein- and pigment-dependent modelling of spectral light absorption in two dinoflagellates, *Prorocentrum minimum* and *Heterocapsa pygmaea*. Mar. Ecol. Prog. Ser. 114: 245–258.

Johnsen, G., Sakshaug, E. (2007). Bio-optical characteristics of PSII and PSI in 33 species (13 pigment groups) of marine phytoplankton, and the relevance for pulse-amplitude-modulated and fast-repetition-rate fluorometer. J. Phycol. 43: 1236–1251.

Johnson, Z.I., Zinser, E.R., Coe, A., McNulty, N.P., Woodward, E.M.S., Chisholm, S.W. (2006). Niche partitioning among *Prochlorococcus* ecotypes along ocean-scale environmental gradients. Science 311: 1737–1740.

Johnsen, G., Samset, O., Granskog, L., and Sakshaug, E. (1994). *In vivo* absorption characteristics in 10 classes of bloom-forming phytoplankton — Taxonomic characteristics and responses to photoadaptation by means of discriminant analysis. Mar. Ecol. Prog. Ser. 105: 149–157, 10.3354/meps105149.

Kahru, M., Leppanen, J.-M., Rud, O. (1993). Cyanobacterial blooms cause heating of the sea surface. Mar. Ecol. Prog. Ser. 191: 1–7.

Kahru, M., Leppanen, J.-M., Rud, O., Savchuk, O.P. (2000). Cyanobacteria blooms in the Gulf of Finland triggered by saltwater inflow into the Baltic Sea. Mar. Ecol. Prog. Ser. 207: 13–18.

Kameda, T., Ishizaka, J. (2005). Size-fractionated primary production estimated by a two-phytoplankton community model applicable to ocean color remote sensing. J. Oceanogr. 61: 663–672.

Karl, D.M., Letelier, R., Tupas, L., Dore, J., Christian, J., Hebel, D. (1997). The role of nitrogen fixation in biogeochemical cycling in the subtropical North Pacific Ocean. Nature 388: 533–538.

Keller, M.D. (1989). Dimethylsulfide production and marine phytoplankton: The importance of species composition and cell size. Biolog. Oceanogr. 6: 375–382.

Keller, M., Bellows, W.K., Guillard, R.R.L. (1989). Dimethyl sulfide production in marine phytoplankton. In: Biogenic Sulfur in the Environment, Saltzman, E.S., Cooper, W.J. (Eds.), American Chemical Society, Washington, D.C., pp. 183–200.

Kettle, A.J., Andreae, M.O. (2000). Flux of dimethylsulfide from the oceans: A comparison of updated data seas and flux models. J. Geophys. 105(D22): 26,793–26,808.

Kiefer, D. A. (1973). Fluorescence properties of natural phytoplankton populations. Mar. Biol. 22: 263–269.

Ki, J.-S., Han, M.-S. (2006). A low-density oligonucleotide array study for parallel detection of harmful algal species using hybridization of consensus PCR products of LSU rDNA D2 domain. Biosens Bioelectron 21: 1812–1821.

Kirk, J.T.O. (1975a). A theoretical analysis of the contribution of algal cells to the attenuation of light within natural waters I. General treatment of suspensions of pigmented cells. New Phytologist 75: 11–20.

Kirk, J.T.O. (1975b). A theoretical analysis of the contribution of algal cells to the attenuation of light within natural waters II. spherical cells. New Phytologist 75: 21–36.

Kirkpatrick, G.J., Millie, D.F., Moline, M.A., Schofield, O. (2000). Optical discrimination of a phytoplankton species in natural mixed populations. Limnol. Oceanogr. 45: 467–471.

Kishi, M.J., Kashiwai, M., Ware, D.M., Megrey, B.A., Eslinger, D.L., Werner, F.E. et al. (2007). NEMURO–a lower trophic level model for the North Pacific marine ecosystem. Ecol. Model. 202(1-2): 12–25.

Kitchen, J.C., Zaneveld, J.R.V. (1992). A 3-layered sphere model of the optical-properties of phytoplankton. Limnol. Oceanogr. 37: 1680–1690.

Kobayashi, F., Takahashi, K. (2002). Distribution along the equatorial transect in the western and central Pacific during the 1999 La Niña conditions. Deep Sea Res. II, 49: 2810–2821.

Kohenen, T. (1984). Self Organization and Associative Memory (2nd Ed.). Springer-Verlag Berlin, Heidelberg.

Kosakowska, A., Lewandowska, J., Stoń, J., Burkiewicz, K. (2004). Qualitative and quantitative composition of pigments in *Phaeodactylum tricornutum* (Bacillariophyceae) stressed by iron. BioMetals 17: 45–52.

Kostadinov, T.S., Siegel, D.A., Maritorena, S. (2009). Retrieval of the particle size distribution from satellite ocean color observations. J. Geophys. Res. 114: C09015.

Kostadinov, T.S., Siegel, D.A., Maritorena, S. (2010). Global variability of phytoplankton functional types from space: assessment via the particle size distribution. Biogeosciences 7: 3239–3257.

Krüger, O., Graßl, H. (2011). Southern Ocean phytoplankton increases cloud albedo and reduces precipitation. Geophys. Res. Lett. 38: L08809, doi:10.1029/2011GL047116.

Kuchler, D.A., Jupp, D.L.B. (1988). Shuttle photograph captures massive phytoplankton bloom in the Great Barrier Reef. Int. J. Remote Sens. 9(8): 1299–1301.

Kurekin, A.A., Miller, P.I., Van der Woerd, H.J. (2014). Satellite discrimination of *Karenia mikimotoi* and *Phaeocystis* harmful algal blooms in European coastal waters: Merged classification of ocean colour data. Harmful Algae, 31: 163–176. doi:10.1016/j.hal.2013.11.003.

Lana, A., Bell, T.G., Simó, R., Vallina, S.M., Ballabrera-Poy, J. Kettle, A.J. et al. (2010). An updated climatology of surface dimethylsulfide concentrations and emission fluxes in the global oceans. Global Biogeochem. Cy. 25(1): GB1004 doi:10.1029/2010GB003850.

Laney, S.R., Sosik, H.M. (2014). Phytoplankton assemblage structure in and around a massive under-ice bloom in the Chukchi Sea. Deep-Sea Res. II. http://dx.doi.org/10.1016/j.dsr2.2014.03.012.

Lapointe, B.E. (1995). A comparison of nutrient-limited productivity in *Sargassum natans* from neritic vs. oceanic waters of the western North Atlantic Ocean. Limnol. Oceanogr. 40: 625-633.

Laws, E.A., Falkowski, P.G., Smith Jr, W.O., Ducklow, H., McCarth, J.J. (2000). Temperature effects on export production in the open ocean. Global Biogeochem. Cy. 14: 1231–1246.

Lee, Z.P., Carder, K.L., and Arnone, R.A. (2002). Deriving inherent optical properties from water colour: a multiband quasi-analytical algorithm for optically deep waters. Appl. Optics 41: 5755–5772.

Lee, Z.P., Carder, K.L., Arnone, R., He, M-X. (2007). Determination of primary spectral bands for remote sensing of aquatic environments. Sensors, 7: 3428–3441.

Legendre, L., LeFevre, J. (1991). From individual plankton cells to pelagic marine ecosystems and to global biogeochemical cycles. In: Particle Analysis in Oceanography, Demers, S. (Ed.), Berlin, Springer.

Lelong, A., Hégaret, H., Soudant, P., Bates, S.S. (2012). *Pseudo-nitzschia* (Bacillariophyceae) species, domoic acid and amnesic shellfish poisoning: revisiting previous paradigms. Phycologia 51: 168–216.

Le Quéré, C., Harrison, S.P., Prentice, C.I., Buitenhuis, E.T., Aumont, O., Bopp, L., Claustre, H., et al. (2005). Ecosystem dynamics based on plankton functional types for global ocean biogeochemistry models. Global Change Biol. 11(11): 2016–2040, doi:10.1111/j.1365-2486.2005.1004.x.

Letelier, R.M., Abbott, M.R. (1996). An analysis of chlorophyll fluorescence algorithms for the Moderate Resolution Imaging Spectrometer (MODIS). Remote Sens. Environ. 58: 215–223.

Letelier, R.M., Bidigare, R.R., Hebel, D.V., Ondrusek, M.E., Winn, C.D., Karl, D.M. (1993). Temporal variability of phytoplankton community structure based on pigment analysis. Limnol. Oceanogr. 38: 1420–1437.

Lieberman, O.S., Shilo, M., van Rijn, J. (1994). The physiological ecology of a freshwater dinoflagellate bloom population: vertical migration, nitrogen limitation, and nutrient uptake kinetics. J. Phycol. 30: 964–971.

Lima, I.D., Doney, S.C. (2004). A three-dimensional, multinutrient, and size-structured ecosystem model for the North Atlantic. Global Biogeochemical Cy. 18: GB3019, doi:10.1029/2003GB002146.

Lima, I.D., Olson, D.B., Doney, S.C. (2002). Intrinsic dynamics and stability properties of size-structured pelagic ecosystem models. J. Plank. Res. 24: 533–556.

Liss, P.S., Hatton, A.D., Malin, G., Nightingale, P.D., Turner, S.M. (1997). Marine sulphur emissions. Phil. Trans. R. Soc. London, B352: 159–169.

Liu, D., Keesing, J.K., Xing, Q., Shi, P. (2009a). World's largest macroalgal bloom caused by expansion of seaweed aquaculture in China. Mar. Sci. Bull. doi:10.1016/j.marpolbul.2009.01.013.

Liu, H., Probert, I., Uitz, J., Claustre, H., Aris-Brossou, S., Frada, M., Not, F., de Vargas, C. (2009b). Haptophyta rule the waves: extreme oceanic biodiversity in non-calcifying haptophytes explains the 19-Hex paradox. Proc. Natl. Acad. Sci. USA. 106: 12803–12808.

Llewellyn, C.A., Fishwick, J.R., Blackford, J.C. (2005). Phytoplankton community assemblage in the English Channel: a comparison using chlorophyll a derived from HPLC-CHEMTAX and carbon derived from microscopy cell counts. J. Plank. Res. 27: 103–119.

Lohrenz, S.E., Weidemann, A.D., Tuel, M. (2003). Phytoplankton spectral absorption as influenced by community size structure and pigment composition. J. Plank. Res. 25: 35–61.

Loisel, H., Morel, A. (1998). Light scattering and chlorophyll concentration in case 1 waters: a reexamination. Limnol. Oceanogr. 43: 847-858.

Loisel, H., Poteau, A. (2006). Inversion of IOP based on R_{rs} and remotely retrieved K_d. In: Remote Sensing of Inherent Optical Properties: Fundamentals, Tests of Algorithms, and Applications, Lee, Z.P. (Ed.), Reports of the International Ocean Colour Coordinating Group, No. 5. IOCCG, Dartmouth, Canada, pp. 35–41.

Loisel, H., Stramski, D. (2000). Estimation of the inherent optical properties of natural waters from the irradiance attenuation coefficient and reflectance in the presence of Raman scattering. Appl. Optics 30(18): 3001–3011.

Loisel, H., Lubac, B., Dessailly, D., Duforêt-Gaurier, L., Vantrepotte, V. (2010). Effect of inherent optical properties variability on the chlorophyll retrieval from ocean color remote sensing: an *in situ* approach. Opt. Express 18(20): 20,949–20,959.

Loisel, H., Nicolas, J.-M., Deschamps, P.-Y., Frouin, R. (2002). Seasonal and inter-annual variability of particulate organic matter in the global ocean. Geophys. Res. Lett. 29: 49–52.

Loisel, H., Nicolas, J-M., Sciandra, A., Stramski, D., Poteau, A. (2006). Spectral dependency of optical backscattering by marine particles from satellite remote sensing of the global ocean. J. Geophys. Res. 111: C09024.

Longhurst, A. (2006). Ecological Geography of the Sea (2nd Edition). Elsevier, Amsterdam 543 p.

Longhurst, A.R., Sathyendranath, S., Platt, T., Caverhill, C. (1995). An estimate of global primary production in the ocean from satellite radiometer data. J. Plank. Res. 17: 1245–1271.

Lovelock, J. (2007). The Revenge of Gaia. Penguin Books Ltd. ISBN 0141025972.

Lü, X., Qiao, F. (2008). Distribution of sunken macroalgae against the background of tidal circulation in the coastal waters of Qingdao, China, in summer 2008. Geophys. Res. Lett., 35: L23614, doi:10.1029/2008GL036084.

Lubac, B., Loisel, H., Guiselin, N., Astoreca, R., Artigas, L.F., Mériaux, X. (2008). Hyperspectral versus multispectral remote sensing approach to detect phytoplankton blooms in coastal waters: application to a *Phaeocystis globosa* bloom. J. Geophys. Res. 113: C06026.

Lutz, V.A., Sathyendranath, S., Head, E.J., Li, W.K.W. (2001). Changes in the *in vivo* absorption and fluorescence excitation spectra with growth irradiance in three species of phytoplankton. J. Plankton Res. 23(6): 555–569.

MacIntyre, H.L., Lawrenz, E., Richardson, T.L. (2010). Taxonomic discrimination of phytoplankton by spectral fluorescence. In: Chlorophyll a fluorescence in aquatic sciences: Methods and applications, Suggett, D.J., Prášil, O., Borowitzka, M.A. (Eds.), pp. 129–169, Springer.

MacIsaac, E.A., Stockner, J.G. (1993). Enumeration of phototrophic picoplankton by autofluorescence microscopy. In: Handbook of Methods in Aquatic Microbial Ecology, Kemp, P.F., Sherr, B.F., Sherr, E.B., Cole, J.J. (Eds.), pp. 187–198, CRC Press.

Mackey, M.D., Mackey, D.J., Higgins, H.W., Wright, S.W. (1996). CHEMTAX - a program for estimating class abundances from chemical markers: Application to HPLC measurements of phytoplankton. Mar. Ecol. Prog. Ser. 144: 265–283.

Magaña, H.A., Contreras, C., and Villareal, T.A. (2003). A historical assessment of *Karenia brevis* in the western Gulf of Mexico. Harmful Algae 2: 163–171.

Mahoney, K.L. (2003). Backscattering of light by *Karenia brevis* and implications for optical detection and monitoring. Ph.D thesis, University of Southern Mississippi, Stennis Space Center, MS, USA, 116 p.

Maier-Reimer, E., Mikolajewicz, U., Winguth, A. (1996). Future ocean uptake of CO_2: interaction between ocean circulation and biology. Climate Dynamics, 12: 711–721.

Maloney, C.L., Field, J.G. (1991). The size-based dynamics of plankton food webs. I. A simulation model of carbon and nitrogen flows. J. Plankton Res. 13(5): 1003–1038.

Mangoni, O., Modigh, M., Conversano, F., Carrada, G.C., Saggiomo V. (2004). Effects of summer ice a coverage on phytoplankton assemblages in the Ross Sea, Antarctica. Deep. Sea Res. I, 51: 1601–1617.

Marandino, C.A., De Bruyn, W.J., Miller, S.D., Saltzman, E.S. (2008). DMS air/sea flux and gas transfer coefficients from the North Atlantic summertime coccolithophore bloom. Geophys. Res. Lett. 35: L23812, doi:10.1029/2008GL036370.

Marañón, E. (2009). Phytoplankton size structure. In: Encyclopedia of Ocean Sciences, Steele, J.H., Turekian, K., Thorpe, S.A. (Eds.), Oxford, Academic Press.

Marañón, E., Cermeno, P., Lopez-Sandoval, D.C., Rodriguez-Ramos, T., Sobrino, C., Huete-Ortega, M., Blanco, J.M., Rodriguez, J. (2013). Unimodal size-scaling of phytoplankton growth and the size dependence of nutrient uptake and use. Ecology Lett. 16: 371–379.

Margalef, R. (1967). Some concepts relative to the organization of plankton. Ann. Rev. Oceanogr. Mar. Biol., 5: 257–289.

Margalef, R. (1978). Life forms of phytoplankton as survival alternatives in an unstable environment. Oceanologica Acta 1: 439–509.

Margalef, R. (1994). Through the looking glass: how marine phytoplankton appears through the microscope when graded by size and taxonomically sorted. Sci. Mar. 58: 87–101.

Marie, D., Zhu, F., Balague, V., Ras, J., Vaulot, D. (2006). Eukaryotic picoplankton communities of the Mediterranean Sea in summer assess by molecular approaches (DGGE, TTGE, QPCR). FEMS Microb. Ecol. 55: 403–415.

Marinov, I., Doney, S.C., Lima, I.D. (2010). Response of ocean phytoplankton community structure to climate change over the 21st century: partitioning the effects of nutrients, temperature and light. Biogeosciences 7: 3941–3959.

Maritorena, S., Siegel, D.A., Peterson, A.R. (2002). Optimization of a semianalytical ocean color model for global-scale applications. Appl. Optics 41(15): 2705–2714.

Martinez-Vicente, V., Tilstone, G., Sathyendranath, S., Miller, P., Groom, S. (2012). Contributions of phytoplankton and bacteria to the optical backscattering coefficient over the mid-Atlantic ridge. Mar. Ecol. Prog. Ser. 445: 37–51.

Masotti, I., Moulin, C., Alvain, S., Bopp, L., Antoine, D. (2011). Large scale shifts in phytoplankton groups in the Equatorial Pacific during ENSO cycles. Biogeosci. 8: 539–550.

Mazard, S.L., Fuller, N.J., Orcutt, K.M., Bridle, O., Scanlan, D.J. (2004). PCR analysis of the distribution of unicellular cyanobacterial diazotrophs in the Arabian Sea. Appl. Env. Microbiol. 70: 7355–7364.

McCarthy, J.J. (2002). Biological responses to nutrients, In: The Sea, Robinson, A.R., McCarthy, J.J., Rothschild, B.J. (Eds.), Volume 12. John Wiley & Sons. pp. 219–244.

McCave, I.N. (1975). Vertical flux of particles in the ocean. Deep Sea Res. 22: 491–502.

McClain, C.R. (2009). A decade of satellite ocean color observation. Annu. Rev. Mar. Sci. 1: 19–42.

McGill, B.J., Enquist, B.J., Weiher, E., Westoby, M. (2006). Rebuilding community ecology from functional traits. Trends Ecol. Evol. 21(4): 178–185.

McKinna, L.I.W., Furnas, M.J., Ridd, P.V. (2011). A simple, binary classification algorithm for the detection of *Trichodesmium* spp. within the Great Barrier Reef using MODIS imagery. Limnol. Oceanogr. Methods 9: 50–66.

Medlin, L.K., Metfies, K. , Mehl, H., Wiltshire, K.H., Valentin, K. (2006). Picoeukaryotic plankton diversity at the Helgoland Time Series Site as assessed by three molecular methods. Microbial Ecol. 52: 53–71.

Medlin, L.K., Wiebe, H.C., Kooistra, H.C.F. (2010). Methods to estimate the diversity in the marine photosynthetic protist community with illustrations from case studies: a review. Diversity 2: 973–1014.

Merceron, M., Antoine, V., Auby, I., Morand, P. (2007). *In situ* growth potential of the subtidal part of green-tide forming *Ulva* spp. stocks. Sci. Total Environ. 384: 293–305.

Merico A., Tyrell, T. Brown, C.W., Groom S.B., Miller, P.I. (2003). Analysis of satellite imagery for *Emiliania huxleyi* blooms in the Bering Sea before 1997. Geophys. Res. Lett. 30(6): doi:10.1029/2002GL016648.

Metfies, K., Medlin, L.K. (2004). DNA microchips for phytoplankton: The fluorescent wave of the future. Nova Hedwigia 79: 321–327.

Metsamaa, L., Kutser, T., Strombeck, N. (2006). Recognising cyanobacterial blooms based on their optical signature: a modelling study. Boreal Environ. Res. 11(6): 493–506.

Michaels, A.F., Silver, M.W. (1988). Primary production, sinking fluxes and the microbial food web. Deep-Sea Res. I 35: 473–490.

Miller, P.I., Shutler, J.D, Moore, G.F., Groom, S.B. (2006). SeaWiFS discrimination of harmful algal bloom evolution. Int. J. Remote Sens. 27(11): 2287–2301.

Millie, D.F., Kirkpatrick, G.J., Vinyard, B.T. (1995). Relating photosynthetic pigments and *in vivo* optical density spectra to irradiance for the Florida red-tide dinoflagellate *Gymnodinium breve*, Mar. Ecol. Prog. Ser. 120: 65–75.

Millie, D.F., Schofield, O.M., Kirkpatrick, G.J., Johnsen, G., Tester, P.A., Vinyard, B.T. (1997). Detection of harmful algal blooms using photopigments and absorption signatures: A case study of the Florida red tide dinoflagellate, *Gymnodinium breve.* Limnol. Oceanogr. 42: 1240–1251.

Mitchell, B.G. (1994). Coastal zone color scanner retrospective. J. Geophys. Res. 99(C4): 7291–7292.

Moberg, E.A., Sosik, H.M. (2012). Distance maps to estimate cell volume from two-dimensional plankton images. Limnol. Oceanogr. Methods 10: 278–288.

Mobley, C.D. (1994). Light and Water: Radiative Transfer in Natural Waters. Academic Press, San Diego, California, 592 pp.

Mobley, C., Sundman, L. (2006). Hydrolight 4.4 technical documentation. Tech. rep., Sequoia Sci., Bellevue, Wash.

Moisan, T.A., Sathyendranath, S., Bouman, H.A. (2012). Ocean color remote sensing of phytoplankton functional types. Remote sensing of biomass-principles and applications. Intech, Rijeka, Croatia, 101–122.

Moisan, T.A., Moisan, J.R., Linkswiler, M.A., Steinhardt, R.A. (2013). Algorithm development for predicting biodiversity based on phytoplankton absorption. Cont. Shelf Res. 55: 17–28.

Moisander, P.H., Beinart, R.A., Hewson, I., White, A.E., Johnson, K.S., Carlson, C.A., Montoya, J.P., Zehr, J.P. (2010). Unicellular cyanobacterial distributions broaden the oceanic N_2 fixation domain. Science 327, doi: 1512-1514.10.1126/science.1185468

Moloney, C.L., Field, J.G. (1991). The size-based dynamics of plankton food webs. I. A simulation model of carbon and nitrogen flows. J. Plank. Res. 13: 1003–1038.

Moore, J.K., Doney, S.C., Lindsay, K. (2004). Upper ocean ecosystem dynamics and iron cycling in a global three-dimensional model. Global Biogeochem. Cy. 18. GB4028, doi:10.1029/2004GB002220.

Moore, L.R., Goericke, R.E., Chisholm, S.W. (1995). Comparative physiology of *Synechococcus* and *Prochlorococcus*: influence of light and temperature on growth, pigments, fluorescence and absorptive properties. Mar. Ecol. Prog. Ser. 116: 259–275.

Moore, L.R., Post, A.F., Rocap, G., Chisholm, S.W. (2002). Utilization of different nitrogen sources by the marine cyanobacteria *Prochlorococcus* and *Synechococcus*. Limnol. Oceanogr. 47: 989–996.

Moore, T.S., Campbell, J.W., Dowell, M.D. (2009). A class-based approach to characterizing and mapping the uncertainty of the MODIS ocean chlorophyll product. Remote Sens. Environ. 113: 2424–2430.

Moore, T.S., Dowell, M.D., Franz, B.A. (2012). Detection of coccolithophore blooms in ocean color satellite imagery: a generalized approach for use with multiple sensors. Remote Sens. Environ. 117: 249–263.

Morel, A. (1973). Diffusion de la lumiére par les eaux de mer. résultats expérimentaux et approche théorique. In: AGARD Lecture Series No. 61, Optics of the Sea (Interface and In-water Transmission and Imaging). London: North Atlantic Treaty Organisation.

Morel, A. (1988). Optical modeling of the upper ocean in relation to its biogenous matter content (case I waters). J. Geophys. Res. 93: 10,749–710,768.

Morel, A. (1997). Consequences of a *Synechococcus* bloom upon the optical properties of oceanic (case 1) waters. Limnol. Oceanogr. 42(8): 1746–1754.

Morel, A. (2009). Are the empirical relationships describing the bio-optical properties of case 1 waters consistent and internally compatible? J. Geophys. Res. 114: C01016.

Morel, A., Antoine, D. (2000). Pigment index retrieval in Case 1 waters. MERIS Level 2 algorithms theoretical basis document. European Space Agency.

Morel, A., Bricaud, A. (1981). Theoretical results concerning light absorption in a discrete medium, and application to specific absorption of phytoplankton. Deep-Sea Res. 28: 1375–1393.

Morel, A., Huot, Y., Gentili, B., Werdell, P.J., Hooker, S.B., Franz, B.A. (2007). Examining the consistency of products derived from various ocean color sensors in open ocean (case 1) waters in the perspective of a multi-sensor approach. Remote Sens. Environ. 111: 69–88.

Morel, A., Prieur, L. (1977). Analysis of variations in ocean color. Limnol. Oceanogr. 22: 709–722.

Mouw, C.B., Yoder, J. (2010). Optical determination of phytoplankton size composition from global SeaWiFS imagery. J. Geophys. Res. 115: C12018.

Mouw, C.B., Yoder, J., Doney, S.C. (2012). Impact of phytoplankton community size on a linked global ocean optical and ecosystem model. J. Marine Syst. 89: 61–75.

Müller, D., Krasemann, H., Brewin, R.J.W., Brockmann, C., Deschamps, P-Y., Doerffer, R. et al. (2014). The Ocean Colour Climate Change Initiative: I. A methodology for assessing atmospheric correction processors based on *in-situ* measurements. Remote Sens. Environ.

Nair, A., Sathyendranath, S., Platt, T., Morales, J., Stuart, V., Forget, M-H., Devred, E., Bouman, H. (2008). Remote sensing of phytoplankton functional types. Remote Sens. Environ. 112(8): 3366–3375.

NASA (2010). Responding to the Challenge of Climate and Environmental Change: NASA's Plan for a Climate-Centric Architecture for Earth Observations and Applications from Space. 48 pp. (http://science.nasa.gov/earth-science/).

Nelson, N.B., Siegel, D.A., Michaels, A. F. (1998). Seasonal dynamics of colored dissolved material in the Sargasso Sea. Deep-Sea Res. I 45: 931–957.

Nelson, T.A., Nelson, A.V., Tjoelker, M. (2003). Seasonal and spatial patterns of "Green Tides" (ulvoid algal blooms) and related water quality parameters in the coastal waters of Washington State, USA. Botanica Marina 46: 263–275.

NSSP (2011). Guide for the Control of Molluscan Shellfish 2011 Revision. http://www.fda.gov/downloads/Food/GuidanceRegulation/FederalStateFoodPrograms/UCM350344.pdf

Odum, E.P. (1959). Fundamentals of Ecology. Philadelphia: W.B. Saunders Co.

Olson, R.J., Chisholm, S.W. (1990). Flow cytometry: Applications and prospects. In: Photosynthesis in the Sea, Alberte, R., Barber, R. (Eds).

Olson, R.J., Chisholm, S.W., Zettler, E.R., Altabet, M.A., Dusenberry, J.A. (1990a). Spatial and temporal distributions of prochlorophyte picoplankton in the North Atlantic Ocean. Deep-Sea Res. 37: 1033–1051.

Olson, R.J., Chisholm, S.W., Zettler, E.R., Armbrust, E.V. (1990b). Pigments, size, and distribution of *Synechococcus* in the North Atlantic and Pacific Oceans. Limnol. Oceanogr. 35: 45–58.

Olson, R.J., Shalapyonok, A.A., Sosik, H.M. (2003). An automated submersible flow cytometer for pico- and nanophytoplankton: FlowCytobot. Deep-Sea Res. I 50: 301–315.

Olson, R.J., Sosik, H.M. (2007). A submersible imaging-in-flow instrument to analyze nano- and microplankton: Imaging FlowCytobot. Limnol. Oceanogr. Methods 5: 195–203.

Olson, R.J., Zettler, E.R., Anderson, O.K. (1989). Discrimination of eukaryotic phytoplankton cell types from light scatter and autofluorescence properties measured by flow cytometry. Cytometry 10: 636–643.

O'Reilly, J.E., Maritorena, S., Siegel, D.A., O'Brien, M.C., Toole, D., Mitchell, B.G., et al. (2000). Ocean color chlorophyll-a algorithms for SeaWiFS, OC2, and OC4: version 4. SeaWiFS postlaunch calibration and validation analyses, Part 3, NASA/TM 206892, 11, 9–23.

O'Reilly, J.E., Maritorena, S., Mitchell, B.G., Siegel, D.A., Carder, K.L., Garver, S.A., Kahru, M., McClain, C. (1998). Ocean chlorophyll algorithms for SeaWiFS. J. Geophys. Res. 103(C11): 24,937–24,953.

Organelli, E., Bricaud, A., Antoine, D., Uitz, J. (2013). Multivariate approach for the retrieval of phytoplankton size structure from measured light absorption spectra in the Mediterranean Sea (BOUSSOLE site). Appl. Opt. 52: 2257–2273.

Ornólfsdóttir, E.B., Pinckney, J.L., Tester, P.A. (2003). Quantification of the relative abundance of the toxic dinoflagellate, *Karenia brevis* (Dinophyta), using unique photopigments. J. Phycol. 39: 449-457.

Orr, J.C., Fabry, V.J. , Aumont, O., Bopp, L., Doney, S.C., Feely, R.A. et al. (2005). Anthropogenic ocean acidification over the twenty-first century and its impact on calcifying organisms. Nature 437: 681–686.

Palacz, A. P., John, M. A. St., Brewin, R. J. W., Hirata, T., and Gregg, W. W. (2013). Distribution of phytoplankton functional types in high-nitrate, low-chlorophyll waters in a new diagnostic ecological indicator model. Biogeosciences, 10: 7553-7574. doi:10.5194/bg-10-7553-2013.

Pan, X., Mannino, A., Marshall, H.G., Filippino, K.C., Mulholland, M.R. (2010a). Remote sensing of phytoplankton community composition along the northeast coast of the United States. Remote Sens. Environ. 115: 3731–3747.

Pan, X., Mannino, A., Russ, M.E., Hooker, S.B., Harding, L.W. (2010b). Remote sensing of phytoplankton pigment distribution in the United States northeast coast. Remote Sens. Environ. 114: 2403–2416.

Parsons, T.R., Lalli, C.M. (2002). Jellyfish populations explosions: Revisiting a hypothesis of possible causes. La Mer 40: 111–121.

Partensky, F., Hess, W.R., Vaulot, D. (1999). *Prochlorococcus*, a marine photosynthetic prokaryote of global significance. Microbiol. . Mol. Biol. R. 63: 106–127.

Pearl, M.R., Swanstrom, J.A., Bruckman, L.S., Richardson, T.L., Shaw, T.J., Sosik, H.M., Myrick, M.L. (2013). Taxonomic classification of phytoplankton with multivariate optical computing, Part III: Demonstration. Applied Spectroscopy 67: 640-647.

Perner, D., Platt, U. (1979). Detection of nitrious acid in the atmosphere by differential optical absorption. Geophy. Res. Lett. 93: 917 -920.

Platt, T., Bouman, H., Devred, E., Fuentes-Yaco, C., Sathyendranath, S. (2005). Physical forcing and phytoplankton distributions. Sci. Mar. 69: 55–73.

Platt, T., Denman, K.L. (1976). The relationship between photosynthesis and light for natural assemblages of coastal marine phytoplankton. J. Phycol. 12(4), 421–430.

Platt, T., Denman, K.L. (1977). Organisation in the pelagic ecosystem. Helgoänder wiss. Meeresunters. 30: 575–581.

Platt, T., Denman, K.L. (1978). The structure of pelagic marine ecosystems. Rapp. P.-v. Réun. Cons. perm. int. Explor. Mer: 60–65.

Pope, R., Fry, E. (1997). Absorption spectrum (380-700 nm) of pure water. II. Integrating cavity measurements. Appl. Optics 36(33): 8710–8723.

Popels, L.C., Cary, S.C., Hutchins, D.A., Forbes, R., Pustizzi, F., Gobler, C.J., Coyne, K.J. (2003). The use of quantitative polymerase chain reaction for the detection and enumeration of the harmful alga *Aureococcus* in environmental samples along the United States East Coast. Limnol. Oceanogr. Methods 1: 92–102.

Post, A.F. (2006). The genus *Prochlorococcus*. In: The Prokaryotes, Stackebrandt, E., Jones, D., Holzapfel, W. (Eds.), Springer. pp. 1099–1110.

Poulton, N.J., Martin, J.L. (2010). Imaging flow cytometry for quantitative phytoplankton analysis-FlowCAM. In: Microscopic and Molecular Methods for Quantitative Phytoplankton Analysis, Karlson, B., Cusack, C., Bresnan, E. (Eds.), IOC Manuals and Guides, No. 55, pp. 47–54, UNESCO, Paris.

Prieur, L., Sathyendranath, S. (1981). An optical classification of coastal and oceanic waters based on the specific spectral absorption curves of phytoplankton pigments, dissolved organic matter and other particulate materials. Limnol. Oceanogr. 26: 617–689.

Probyn, T.A. (1985). Nitrogen uptake by size-fractionated phytoplankton populations in the southern Benguela upwelling system. Mar. Ecol. Prog. Ser. 22: 249–258.

Quinn, P.K., Bates, T.S. (2011). The case against climate regulation via oceanic phytoplankton sulphur emissions. Nature 480: 52–56. doi:10.1038/nature10580.

Raimbault, P., Rodier, M., Taupier-Letage, I. (1988). Size fraction of phytoplankton in the Ligurian Sea and the Algerian Basin (Mediterranean Sea): Size distribution versus total concentration. Mar. Microb. Food Webs 3: 1–7.

Raitsos, D.E., Lavender, S.J., Maravelias, C.D., Haralambous, J., Richardson, A.J., Reid, P.C. (2008). Identifying four phytoplankton functional types from space: An ecological approach. Limnol. Oceanogr. 53(2): 605–613.

Raitsos, D.E., Lavender, A.J., Pradham, Y., Tyrell, T., Reid, P.C., Edwards, M. (2006). Coccolithophore bloom size and variation in response to the regional environment of the subarctic North Atlantic. Limnol. Oceanogr. 51(5): 2122–2130.

Ras, J., Claustre, H., Uitz, J. (2008). Spatial variability of phytoplankton pigment distributions in the subtropical South Pacific Ocean: Comparison between *in situ* and modelled data. Biogeosciences 5: 353–369.

Raven, J.A. (1998). Small is beautiful: The picophytoplankton. Funct. Ecol. 12: 503–513.

Raven, J. (Ed.) (2005). Ocean acidification due to increasing atmospheric carbon dioxide. The Royal Society, London, UK. Policy document 12/05.

Raymond, J.E.G. (1980). Plankton and Productivity in the Oceans. Vol. 1 – Phytoplankton, 2nd Ed. Pergamon Press, London.

Reckermann, M., Colijn, F. (Eds.) (2000). Aquatic flow cytometry: Achievements and prospects. Scientia Marina.

Redfield, A.C., Ketchum, B.H., Richards, F.A. (1963). The influence of organisms on the composition of sea water. In: The Sea, Hill, M.N. (Ed.), Wiley. p. 26–77.

Reid, P.C., Colebrook, J.M., Matthews, J.B.L., Aiken, J. (2003a). The Continuous Plankton Recorder: concepts and history, from plankton indicator to undulating recorders. Prog. Oceanog. 58(2–4): 117–175.

Reid, P.C., Matthews, J.B.L., Smith, M.A. (Eds.) (2003b). Achievements of the Continuous Plankton Recorder survey and a vision for its future. Prog. Oceanog. 58: 115–358.

Reynolds, C.S. (2006). The Ecology of Phytoplankton. Cambridge University Press, Cambridge, UK.

Reynolds, C.S., Huszar, V., Kruk, C., Naselli-Flores, L., Melo, S. (2002). Towards a functional classification of the freshwater phytoplankton. J. Plank. Res. 24: 417–428.

Reynolds, R.A., Stramski, D., Mitchell, B.G. (2001). A chlorophyll dependent semianalytical reflectance model derived from field measurements of absorption and backscattering coefficients within the Southern Ocean. J. Geophys. Res. 106: 7125–7138.

Rhodes, L., Haywood, A., Adamson, J., Ponikla, K., Scholin, C. (2004). DNA probes for the rapid detection of *Karenia* species in New Zealand's coastal waters. In: Harmful Algae 2002. Steidinger, K.A., Landsberg, J.H., Tomas, C.R., Vargo, G.A. (Eds.), St. Petersburg, FL: Florida Fish and Wildlife Conservation Commission, Florida Institute of Oceanography, and Intergovernmental Oceanographic Commission of UNESCO, pp. 273–275.

Rhodes, L., Scholin, C., Garthwaite, I. (1998). *Pseudo-nitzschia* in New Zealand and the role of DNA probes and immunoassays in refining marine biotoxin monitoring programmes. Natural Toxins 6: 105–111.

Richardson, A.J., Walne, A.W., John, A.W.G., Jonas, T.D., Lindley, J.A., Sims, D.W., Stevens, D., Witt, M. (2006). Using continuous plankton recorder data. Prog. Oceanogr. 68: 27–74.

Richardson, T.L., Lawrenz, E., Pinckney, J.L., Guajardo, R.C., Walker, E.A., Paerl, H.W., MacIntyre, H.L. (2010). Spectral fluorometric characterization of phytoplankton community composition using the Algae Online Analyser. Water Research 8: 2461–2472.

Riebesell ,U., Zondervan, I., Rost, B., Tortell ,P.D., Zeebe, R.E., Morel, F.M.M. (2000). Reduced calcification of marine plankton in response to increased atmospheric CO_2. Nature 407: 364–367.

Robbins, I.C., Kirkpatrick, G.J., Blackwell, S.M., Hillier, J., Knight, C.A., Moline, M.A. (2006). Improved monitoring of HABs using autonomous underwater vehicles (AUV). Harmful Algae 5: 749–761.

Rocap, G., Larimer, F.W., Lamerdin, J., Malfatti, S., Chain, P., Ahlgren, N.A. et al. (2003). Genome divergence in two *Prochlorococcus* ecotypes reflects oceanic niche differentiation. Nature 424: 1042–1047.

Roesler, C.S., Boss, E. (2003). Spectral beam attenuation coefficient retrieved from ocean color inversion. Geophys. Res. Letters 30: 1468–1472.

Roesler, C.S., Perry, M.J. (1995). *In situ* phytoplankton absorption, fluorescence emission, and particulate backscattering spectra determined from reflectance. J. Geophys. Res. 100(C7): 13,279–13,294.

Roesler, C.S., Etheridge, S.M., Pitcher, G.C. (2004). Application of an ocean color algal taxa detection model to red tides in the Southern Benguela, pp.303-305. In: Harmful Algae 2002, Steidinger, K. A., Lansdberg, J.H., Tomas, C.R., Vargo, G.A. (Eds.), Florida Fish and Wildlife Conservation Commission, Florida Institute of Oceanography, and Intergovernmental Oceanographic Commission of UNESCO.

Rooker, J., Turner, J., Holt, S. (2006). Trophic ecology of *Sargassum*-associated fishes in the Gulf of Mexico determined from stable isotopes and fatty acids. Mar. Eco. Prog. Ser. 313: 249–259.

Root, R.B. (1967). The niche exploitation pattern of the Blue-Gray Gnatcatcher. Ecological Monographs 37: 317–350.

Rost, B., Riebesell, U. (2004). Coccolithophores and the biological pump: responses to environmental changes. In: Coccolithophores, From Molecular Processes to Global Impact. Thierstein, H.R., Young, J.R. (Eds.), pp. 99–127.

Roy, S., Sathyendranath, S., Platt, T. (2010). Retrieval of phytoplankton size from bio-optical measurements: theory and applications. J. R. Soc. Interface 8(58): 650–660.

Roy, S., Llewellyn, C., Egeland, E.S., Johnsen, G. (Eds). (2011). Phytoplankton pigments: Characterization, chemotaxonomy and applications in oceanography, Cambridge University Press, Cambridge, UK.

Roy, S., Sathyendranath, S., Bouman, H., Platt, T. (2013). The global distribution of phytoplankton size spectrum and size classes from their light-absorption spectra derived from satellite data. Remote Sens. Env. 139: 185–197.

Rozanov, V.V., Buchwitz, M., Eichmann, K.-U., de Beek, R., Burrows, J.P. (2002). SCIATRAN - a new radiative transfer model for geophysical applications in the 240-2400 nm spectral region: the pseudo-spherical version. Adv. Space Res. 29: 1831–1835.

Rozanov, V.V., Rozanov, A., Kokhanovsky, A., Burrows, J.P. (2014). Radiative transfer through atmosphere and ocean: Software package SCIATRAN. J. Quant. Spectrosc. Rad. Transfer. 133: 13-71. doi: 10.1016/j.jqsrt.2013.7.004

Ryther, J.H. (1956). The Sargasso Sea. Scientific American 194: 98–104.

Sabine, C.L., Feely, R.A., Gruber, N., Key, R.M., Lee, K., Bullister, J.L. (2004) The ocean sink for anthropogenic CO_2. Science, 305(5682): 367–371 doi:10.1126/science.1097403.

Sadeghi, A., Dinter, T., Vountas, M., Taylor, B., Altenburg-Soppa M., Bracher, A. (2012b). Remote sensing of coccolithophore blooms in selected oceanic regions using the PhytoDOAS method applied to hyper-spectral satellite data. Biogeosci. 9: 2127–2143.

Sadeghi, A., Dinter, T., Vountas, M., Taylor, B., Peeken, I., Altenburg-Soppa M., Bracher, A. (2012a). Improvements to the PhytoDOAS method for identification of coccolithophores using hyper-spectral satellite data. Ocean Sciences 8: 1055–1070.

Sarmiento, J.L., Hughes, T.M.C. (1999). Anthropogenic CO_2 uptake in a warming ocean. Tellus, 51B: 560–561.

Satake, M., Tanaka, Y., Ishikura, Y., Oshima, Y., Naoki, H., Yasumoto, T. (2005). Gymnocin-B with the largest contiguous polyether rings from the red tide dinoflagellate, *Karenia* (formally *Gymnodinium*) *mikimotoi*, Tetrahedron Letters, 46.

Sathyendranath, S., Platt, T. (1997). Analytic model of ocean color. Appl. Optics 36: 2620–2629.

Sathyendranath, S., Platt, T. (1998). Ocean-color model incorporating transpectral processes. Appl. Optics 37: 2216–2226.

Sathyendranath, S. , Platt, T. (2007). Spectral effects in bio-optical control on the ocean system. Oceanologia, 49(1): 5–39.

Sathyendranath, S., Lazzara, L., Prieur, L. (1987). Variations in the spectral values of specific absorption of phytoplankton. Limnol. Oceanogr. 32: 403–415.

Sathyendranath, S., Prieur, L., Morel, A. (1989). A three-component model of ocean colour and its application to remote sensing of phytoplankton pigments in coastal waters. Int. J. Remote Sens. 10: 1373–1394.

Sathyendranath, S., Cota, G., Stuart, V., Maass, H., Platt, T. (2001). Remote sensing of phytoplankton pigments: a comparison of empirical and theoretical approaches. Int. J. Remote Sens. 22: 249–273.

Sathyendranath, S., Platt, T., Irwin, B., Horne, E., Borstad, G., Stuart, V., et al. (2004a). A multispectral remote sensing study of coastal waters off Vancouver Island. Int. J. Remote Sensing 25: 893–919.

Sathyendranath, S., Stuart, V., Nair, A., Oka, K., Nakane, T., Bouman, H., Forget, M.-H., Maass, H., Platt, T. (2009). Carbon-to-chlorophyll ratio and growth rate of phytoplankton in the sea. Mar. Ecol. Prog. Ser. 383: 73–84.

Sathyendranath, S., Stuart, V., Platt, T., Bouman, H., Ulloa, O., Maass, H. (2005). Remote sensing of ocean colour: Towards algorithms for retrieval of pigment composition. Indian J. Mar. Sci. 34: 333–340.

Sathyendranath, S., Subba Rao, D.V., Chen, Z., Stuart, V., Platt, T., Bugden, G.L., Jones, W., Vass, P. (1997). Aircraft remote sensing of toxic phytoplankton blooms: a case study from Cardigan River, Prince Edward Island. Can. J. Remote Sens. 23: 15–23.

Sathyendranath, S., Watts, L., Devred, E., Platt, T., Caverhill, C., Maass, H. (2004b). Discrimination of diatoms from other phytoplankton using ocean-colour data. Mar. Ecol. Prog. Ser. 272, 59–68.

Schena, M., Shalon, D., Davis, R.W., Brown, P.O. (1995). Quantitative monitoring of gene expression patterns with a complementary DNA microarray. Science 270: 467–470.

Schofield, O., Grzymski, J., Bissett, W.P., Kirkpatrick, G.J., Millie, D.F., Moline, M., and Roesler, C.S. (1999). Optical monitoring and forecasting systems for harmful algal blooms: Possibility or pipe dream? J. Phycol. 35: 1477–1496.

Schofield, O., Kerfoot, J., Mahoney, K., Moline, M., Oliver, M., Lohrenz, S.E., Kirkpatrick, G. (2006). Vertical migration of the toxic dinoflagellate *Karenia brevis* and the impact on ocean optical properties. J. Geophys. Res. 111: doi:10.1029/2005JC003115.

Scholin, C.A., Gulland, F., Doucette, G.J., Benson, S., Busman, M., Chavez, F.P. et al. (2000). Mortality of sea lions along the central California coast linked to a toxic diatom bloom. Nature 403: 80–84.

Shutler, J.D., Davidson, K., Miller, P.I., Swan, S.C., Grant, M.G., Bresnan, E. (2012). An adaptive approach to detect high-biomass algal blooms from EO chlorophyll-a data in support of harmful algal bloom monitoring. Remote Sens. Lett., 3(2): 101–110.

Shutler, J.D., Land, P.E., Brown, C.W., Findlay, H.S., Donlon, C.J., Medland, M., Snooke, R., Blackford, J.C. (2013). Coccolithophore surface distributions in the North Atlantic and their modulation of the air-sea flux of CO_2

from 10 years of satellite Earth observation data. Biogeosciences, 10: 2699–2709, doi:10.5194/bg-10-2699-2013.

Shutler, J.D., Grant, M.G., Miller, P.I., Rushton, E., Anderson, K. (2010). Coccolithophore bloom detection in the north east Atlantic using SeaWiFS: algorithm description, application and sensitivity analysis. Remote Sens. Environ. 114(5): 1008-1016, doi:10.1016/j.rse.2009.12.024.

Shutler, J.D., Miller, P.I., Groom, S.B., Aiken, J. (2005.) Automatic near-real time mapping of MERIS data in support of CASIX and as input to a phytoplankton classifier. Proc. ESA MERIS (A)ATSR Workshop 2005, (CD-ROM).

Sieburth, J.M., Smetacek, V., Lenz, J. (1978). Pelagic ecosystem structure: Heterotrophic compartments of the plankton and their relationship to plankton size fractions. Limnol. Oceanogr. 23, 1256–1263.

Siegel, D.A., Maritorena, S., Nelson, N.B., Behrenfeld, M. (2005). Independence and interdependencies among global ocean color properties: Reassessing the bio-optical assumption. J. Geophys. Res. 110: C07011.

Sieracki, C.K., Sieracki, M.E., Yentsch, C.S. (1998). An imaging-in-flow system for automated analysis of marine microplankton. Mar. Ecol. Prog. Ser. 168: 285–296.

Sieracki, M.E., Viles, C.L., Webb, K.L. (1989). Algorithm to estimate cell biovolume using image analyzed microscopy. Cytometry 10: 551–557.

Silió-Calzada, A., Bricaud, A., Uitz, J., Gentili, B. (2008). Estimation of new primary production in the Benguela upwelling area, using ENVISAT satellite data and a model dependent on the phytoplankton community size structure. J. Geophys. Res. 113: C11023.

Simis, S.G.H., Ruiz-Verdú, A., Domínguez-Gómez, J.A., Peña-Martinez, R., Peters, S.W.M, Gons, H.J. (2007). Influence of phytoplankton pigment composition on remote sensing of cyanobacterial biomass. Remote Sens. Environ. 106: 414–427.

Simó, R. (2001). Production of atmospheric sulfur by oceanic plankton: biogeochemical, ecological and evolutionary links. Trends Ecol. Evol. 16: 287–294.

Simon, A., Shanmugam, P. (2012.) Algorithm for classification of algal blooms using MOSIS-Aqua data in oceanic waters around India. Adv. Remote Sens. 1: 35–51.

Simon, N., Brenner, J., Edvardsen, B., Medlin, L.K. (1997). The identification of *Chrysochromulina* and *Prymnesium* species (Haptophyta, Prymnesiophyceae) using fluorescent or chemiluminescent oligonucleotide probes: a means of improving studies on toxic algae. Eur. J. Phycol. 32: 393–401.

Simon, N., LeBot, N., Marie, D., Partensky, F., Vaulot, D. (1995). Fluorescent *in situ* hybridization with rRNA-targeted oligonucleotide probes to identify small phytoplankton by flow cytometry. Appl. Environ. Microbiol. 61: 2506–2513.

Sivonen, K., Kononen, K., Carmichael, W., Dahlem, A., Rinehart, K., Kiviranta, J., Niemela, S. (1989). Occurrence of the hepatotoxic cyanobacterium *Nodularia spumigena* in the Baltic Sea and structure of the toxin. Appl. Environ. Microbiol., 55(8): 1990–1995.

Smayda, T.J. (1997). Harmful algal blooms: Their ecophysiology and general relevance to phytoplankton blooms in the sea. Limnol. Oceanogr. 42(5): 1137–1153.

Smayda, T.J. (1980). Species succession, In: The Physiological Ecology of Phytoplankton, Morris, I. (Ed.), Univ. Calif. Press, Berkeley, CA, pp. 493–570.

Smith, R.C., Baker, K.S. (1982). Oceanic chlorophyll concentrations as determined by satellite (Nimbus-7 Coastal Zone Color Scanner). Mar. Biol. 66: 269–279.

Smyth, T.J., Moore, G.F., Hirata, T., Aiken J. (2006). Semianalytical model for the derivation of ocean color inherent optical properties: description, implementation, and performance assessment. Appl. Opt. 45: 8116–8131.

Smyth, T.J., Tyrell, T., Tarrant, B. (2004). Time series of coccolithophore activity in the Barents Sea from twenty years of satellite imagery. Geophys. Res. Lett., 31 (L11302), doi:10.1029/2004GL019735.

Sosik, H.M. (2008). Characterizing seawater constituents from optical properties. In: Real-time coastal observing systems for ecosystem dynamics and harmful algal blooms, Babin, M., Roesler, C.S., Cullen, J.J. (Eds.), pp. 281–329, UNESCO, Paris.

Sosik, H.M., Mitchell, B.G. (1991). Absorption, fluorescence and quantum yield for growth in nitrogen limited *Dunaliella tertiolecta*. Limnol. Oceanogr. 36(5): 910–921.

Sosik, H.M., Olson, R.J. (2007). Automated taxonomic classification of phytoplankton sampled with imaging-in-flow cytometry. Limnol. Oceanogr. Methods 5: 204–216.

Sosik, H.M., Olson, R.J., Armbrust, E.V. (2010). Flow cytometry in phytoplankton research. In: Chlorophyll a fluorescence in aquatic sciences: Methods and applications, Suggett, D.J., Prasil, O., Borowitzka, M.A. (Eds.), pp. 171–185, Springer.

Sosik, H.M., Olson, R.J., Futrelle, J. (2011). Imaging FlowCytobot Data Dashboard, Woods Hole Oceanographic Institution. http://ifcb-data.whoi.edu/, accessed January 2014.

Sosik, H.M., Olson, R.J., Neubert, M.G., Shalapyonok, A.A., Solow, A.R. (2003). Growth rates of coastal phytoplankton from time-series measurements with a submersible flow cytometer. Limnol. Oceanogr. 48: 1756–1765.

Soto, I. (2013). Harmful algal blooms in the west Florida Shelf and Campeche Bank: Visualization and quantification using remote sensing methods. Ph.D., University of South Florida, Tampa, Flordia, 116 p.

Sournia, A., Chrétiennot-Dinet, M.-J., Ricard, M. (1991). Marine phytoplankton: how many species in the world ocean? J. Plank. Res. 13: 1093–1099.

South Atlantic Fishery Management Council. (2002). Fishery management plan for pelagic *Sargassum* habitat of the South Atlantic region. http://safmc.net/Library/pdf/SargFMP.pdf.

Specht, D.F. (1988). Probabilistic neural networks for classification, mapping, or associative memory (IEEE). Neural Networks 1: 525–532.

Specht, D.F. (1990). Probabilistic neural networks (IEEE). Neural Networks 3: 109–118.

Steele, J.H. (1991). Marine functional diversity. BioScience 41(7): 470–474.

Steidinger, K.A., Haddad, K. (1981). Biologic and hydrographic aspects of red tides. BioSci. 31: 814–819, 10.2307/1308678.

Steidinger, K A., Vargo, G.A., Tester, P.A., Tomas, C.R. (1998). Bloom dynamics and physiology of *Gymnodinium breve* with emphasis on the Gulf of Mexico. In: Physiological Ecology of Harmful Algal Blooms, Anderson, D.M., Cembella, A.D., Hallegraeff, G.M. (Eds.), Springer-Verlag, New York, 135-153.

Steidinger, K.A. (2009). Historical perspective on *Karenia brevis* red tide research in the Gulf of Mexico. Harmful Algae 8: 549-561, http://dx.doi.org/10.1016/j.hal.2008.11.009.

Steinke, M., Malin, G., Archer, S.D., Burkill, P.H., Liss, P.S. (2002). DMS production in a coccolithophorid bloom: evidence for the importance of dinoflagellate DMSP lyases. Aquatic Microb. Ecol. 26: 259–270.

Stramski, D., Kiefer, D.A. (1991). Light scattering by microorganisms in the open ocean. Prog. Oceanog. 28: 343–383.

Stramski, D., Mobley, C.D. (1997). Effects of microbial particles on oceanic optics: A database of single-particle optical properties. Limnol. Oceanogr. 42: 538–549.

Stramski, D., Morel, A. (1990). Optical properties of photosynthetic picoplankton in different physiological states as affected by growth irradiance. Deep-Sea Res. 37: 245–266.

Stramski, D., Sciandra, A., Claustre. H. (2002). Effects of temperature, nitrogen, and light limitation on the optical properties of the marine diatom *Thalassiosira pseudonana*. Limnol. Oceanogr. 47(2): 392–403.

Stramski, D., Reynolds, R.A., Kahru, M., Mitchell, B.G. (1999). Estimation of particulate organic carbon in the ocean from satellite remote sensing. Science 285: 239–242.

Stramski, D., Reynolds, R.A., Babin, M., Kaczmarek, S., Lewis, M.R., Röttgers, R. et al. (2008). Relationships between the surface concentration of particulate organic carbon and optical properties in the eastern South Pacific and eastern Atlantic Oceans. Biogeosciences 5: 171–201.

Stumpf, R.P. (2001). Applications of satellite ocean color sensors for monitoring and predicting harmful algal blooms. Human Ecol. Risk Assess. 7: 1363–1368.

Stumpf, R.P., Culver, M.E., Tester, P.A., Tomlinson, M., Kirkpatrick, G.J., Pederson, B. A., et al. (2003). Monitoring *Karenia brevis* blooms in the Gulf of Mexico using satellite ocean colour imagery and other data. Harmful Algae 2: 147–760.

Stumpf, R.P., Tomlinson, M.C., Calkins, J.A., Kirkpatrick, B., Fisher, K., Nierenberg, K. et al. (2009). Skill assessment for an operational algal bloom forecast system, J. Mar. Syst. 76: 151-161, http://dx.doi.org/10.1016/j.jmarsys.2008.05.016.

Subramaniam, A., Carpenter, E.J. (1994). An empirically derived protocol for the detection of blooms of the marine cyanobacterium *Trichodesmium* using CZCS imagery. Int. J. Remote Sens. 15: 1559–1569.

Subramaniam, A., Carpenter, E.J., Falkowski, P.G. (1999). Bio-optical properties of the marine diazotrophic cyanobacteria *Trichodesmium* spp. II. A reflectance model for remote sensing. Limnol. Oceanogr. 3: 618–627.

Subramaniam, A., Brown , C.W., Hood, R.R., Carpenter, E. , Capone, D.G. (2002). Detecting *Trichodesmium* blooms in SeaWiFS imagery. Deep-Sea Res. II 49: 107–121.

Sun, S., Wang, F., Li, C., Qin, S., Zhou, M., et al. (2008). Emerging challenges: Massive green algae blooms in the Yellow Sea. Nature Precedings, hdl:10101/npre.2008.2266.1.

Sunda, W., Kieber, D.J., Kiene, R.P., Huntsman, S. (2002). An antioxidant function for DMSP and DMS in marine algae. Nature, 418: 317–320.

Sunda, W.G., Huntsman, S.A. (1997). Interrelated influence of iron, light and cell size on marine phytoplankton growth. Nature 390: 389–392.

Tangen, K. (1977). Blooms of *Gyrodinium aureolum* (Dinophyceae) in north European waters, accompanied by mortality in marine organisms. Sarsia 63: 123–133.

Tassan, S. (1995). SeaWiFS potential for remote sensing of marine *Trichodesmium* at sub-bloom concentration. Int. J. Remote Sens. 16(18): 3619–3627.

Tester, P.A., Steidinger, K.A. (1997). *Gymnodinium breve* red tide blooms: Initiation, transport, and consequences of surface circulation. Limnol. Oceanogr. 42: 1039–1051.

Tester, P.A., Stumpf, R.P. (1998). Phytoplankton blooms and remote sensing: What is the potential for early warning. J. Shellfish Res., 17: 1469–1471.

Thyssen, M., Garcia, N., Denis, M. (2009). Sub-meso scale phytoplankton distribution in the north east Atlantic surface waters determined with an automated flow cytometer. Biogeosciences 8: 569–583.

Thyssen, M., Tarran, G.A., Zubkov, M.V., Holland, R.J., Gregori, G., Burkill, P.H., Denis, M. (2008). The emergence of automated high frequency flow cytometry: revealing temporal and spatial phytoplankton variability. J. Plank. Res. 30: 333–343.

Töbe, K., Eller, G., Medlin, L.K. (2006). Automated detection and enumeration of *Prymnesium parvum* (Haptophyta: Prymnesiophyceae) by solid-phase cytometry. J. Plank. Res. 28: 643–657.

Tomas, C.R. (1997). Identifying Marine Phytoplankton, Elsevier.

Tomlinson, M.C., Stumpf, R.P., Ranisbrahmanakul, V., Truby, E.W., Kirkpatrick, G.J., Pederson, B.A., et al. (2004). Evaluation of the use of SeaWiFS imagery for detecting *Karenia brevis* harmful algal blooms in the eastern Gulf of Mexico. Remote Sens. Environ. 91: 293–303.

Tomlinson, M.C., Wynne, T.T., Stumpf, R.P. (2009). An evaluation of remote sensing techniques for enhanced detection of the toxic dinoflagellate, *Karenia brevis* Remote Sens. Environ. 113: 598-609. http://dx.doi.org/10.1016/j.rse.2008.11.003.

Torrecilla, E., Stramski, D., Reynolds, R.A., Millán-Núñez, E., Piera, J. (2011). Cluster analysis of hyperspectral optical data for discriminating phytoplankton assemblages in the open ocean. Remote Sens. Environ. 115: 2578–2593.

Touzet, N., Keady, E., Raine, R., Maher, M. (2009). Evaluation of taxa-specific real-time PCR, whole-cell FISH and morphotaxonomy analyses for the detection and quantification of the toxic microalgae *Alexandrium minutum* (Dinophyceae), Global Clade ribotype. FEMS Microbiol. Ecol. 67: 329–341.

Trees, C.C., Aiken, J., Hirche, H-J. and Groom, S.B. (1992). Bio-optical variability across the Arctic front. Polar Biol. 12: 455–461.

Tsoar, H. (2005). Sand dunes mobility and stability in relation to climate. Physica A, 357(1): 50–56.

Tyrrell, T. (2008). Calcium carbonate cycling in future oceans and its influence on future climates. J. Plank. Res. 30(2): 141-156. 10.1093/plankt/fbm105.

Tyrrell, T., Holligan, P., Mobley, C.D. (1999). Optical impacts of oceanic coccolithophore blooms. J. Geophys. Res. 104: 3223–3241.

Tyrrell, T., Merico, A. (2004). *Emiliania huxleyi*: Bloom observations and the conditions that induce them., In: Coccolithophores: from Molecular Processes to Global Impact, Thiertein, H.R., Young, J.R. (Eds.), Springer-Verlag.

Uitz, J., Claustre, H., Griffiths, F.B., Ras, J., Garcia, N., Sandroni, V. (2009). A phytoplankton class-specific primary production model applied to the Kerguelen Islands region (Southern Ocean). Deep-Sea Res. I 56: 541–560.

Uitz, J., Claustre, H., Gentili, B., Stramski, D. (2010). Phytoplankton class-specific primary production in the world's oceans: Seasonal and interannual variability from satellite observations. Global Biogeochem. Cy. 24: GB3016.

Uitz, J., Claustre, H., Morel, A., Hooker, S.B. (2006). Vertical distribution of phytoplankton communities in open ocean: an assessment based on surface chlorophyll. J. Geophys. Res. 111: C08005.

Uitz, J., Huot, Y., Bruyant, F., Babin, M., Claustre, H. (2008). Relating phytoplankton photophysiological properties to community structure on large scales. Limnol. Oceanogr. 53(2): 614–630.

Uitz, J., Stramski, D., Gentili, B., D'Ortenzio, F., Claustre, H. (2012). Estimates of phytoplankton class-specific and total primary production in the Mediterranean Sea from satellite ocean color observations. Global Biogeochem. Cy. doi:10.1029/2011GB004055.

Ulloa, O., Sathyendranath, S., Platt, T. (1994). Effect of the particle-size distribution on the backscattering ratio in seawater. Appl. Optics 33: 7070–7077.

Utermöhl, H. (1931). Neue Wege in der quantitativen Erfassung des Planktons. (Mit besonderer Beriicksichtigung des Ultraplanktons.). Verh. Internat. Verein Limnol. 5: 567–595.

Uz, S.S., Brown, C.W., Heidinger, A.K., Smyth, T.J., Murtugudde, R. (2013). Monitoring a sentinel species from satellites: Detecting *Emiliania huxleyi* in 25 years of AVHRR imagery. In: Satellite Applications on Climate Change, Qu, J.J., Powell, A.M., Sivakumar, M.V.K. (Eds.), Springer, Dordrecht, pp. 277–288.

Vaillancourt, R.D., Brown, C.W., Guillard, R.R.L., Balch, W.M. (2004). Light backscattering properties of marine phytoplankton: relationships to cell size, chemical composition and taxonomy. J. Plankton Res. 26(2): 191–212.

Vaulot, D., Eikrem, E., Viprey, M., Moreau, M. (2008). The diversity of small eukaryotic phytoplankton (≤3μm) in marine ecosystems. FEMS Microbiol. Rev. 32: 795–820.

Veldhuis, M., De Baar, H.J.W. (2005). Iron resources and ocean nutrients: advancement of global environment simulations. J. Sea Res. 53: 1–6.

Vidussi, F., Claustre, H., Manca, B.B., Luchetta, A., Marty, J.C. (2001). Phytoplankton pigment distribution in relation to upper thermocline circulation in the eastern Mediterranean Sea during winter. J. Geophys. Res. 106(C9): 19,939-19,956.

Villareal, T.A., Carpenter, E.J. (2003). Buoyancy regulation and the potential for vertical migration in the oceanic cyanobacterium *Trichodesmium*. Microb. Ecol. 45: 1-10.

Vountas, M., Dinter, T., Bracher, A., Burrows, J.P., Sierk, B. (2007). Spectral studies of ocean water with space-borne sensor SCIAMACHY using differential optical absorption spectroscopy (DOAS), Ocean Sciences 3: 429–440.

Walsh, J.J., Steidinger, K.A. (2001). Saharan dust and Florida red tides: The cyanophyte connection. J. Geophys. Res. 106: 11,597–11,612.

Walsh, J.J., Jolliff, J.K., Darrow, B.P., Lenes, J.M., Milroy, S. P., Remsen, A., et al. (2006). Red tides in the Gulf of Mexico: Where, when and why? J. Geophys. Res. 111, C11003, doi:10.1029/2004JC002813.

Weber L.H., El-Sayed S. (1987). Contribution to the net, nano- and picoplankton flux in the Southern ocean from sediment trap data. J. Plankton Res. 9: 973–994.

Werdell, P.J., Bailey, S.W. (2005). An improved *in situ* bio-optical data set for ocean colour algorithm development and satellite data production validation. Remote Sens. Environ. 98: 122–140.

Westberry, T.K., Siegel, D.A., Subramaniam, A. (2005). An improved bio-optical model for the remote sensing of *Trichodesmium* spp. blooms. J. Geophys. Res. 110: C06012, doi:10.1029/2004JC002517.

Whitmire, A.L., Pegau, W.S., Karp-Boss, L., Boss, E., Cowles, T.J. (2010). Spectral backscattering properties of marine phytoplankton cultures. Opt. Express 18: 15073–15093.

WHO (2003). Guidelines for safe recreational water environments. 1: Coastal and Fresh Waters, World Health Organization, Geneva, pp. 136–158. http://whqlibdoc.who.int/publications/2003/9241545801.pdf

Winter, A., Hendericks, J., Beaufort, L., Rickaby, R.E.M., Brown, C.W. (2013). Poleward expansion of the coccolithophore *Emiliania huxleyi*. J. Plank. Res. doi:10.1093/plankt/fbt110.

Witherington B., Shigetomo, H., Hardy, R. (2012). Young sea turtles of the pelagic *Sargassum*-dominated drift community: habitat use, population density, and threats. Mar. Ecol. Prog. Ser. 463: 1–22.

Wozniak, S.B., Stramski, D. (2004). Modeling the optical properties of mineral particles suspended in seawater and their influence on ocean reflectance and chlorophyll estimation from remote sensing algorithms. Appl. Optics 43: 3489–3503.

Wright, S.W. (2005). Analysis of phytoplankton populations using pigment markers. Workshop on pigment analysis of Antarctic microorganisms : University of Malaya, June 29-July 1, 2005.

Ye, Y., Voelker, C., Bracher, A., Taylor, B., Wolf-Gladrow, D. (2012). Environmental controls on N_2 fixation by *Trichodesmium* in the tropical eastern North Atlantic. Deep Sea Res. I. 64: 104–117. doi:10.1016/j.dsr2011.12.008.

Yentsch, C.M., Horan, P.K. (1989). Cytometry in the aquatic sciences. Cytometry 10: 497–499.

Yentsch, C.S., Phinney, D.A. (1985). Spectral fluorescence: An ataxonomic tool for studying the structure of phytoplankton populations. J. Plank. Res. 7: 617–632.

Yentsch, C.S., Phinney, D.A. (1989). A bridge between ocean optics and microbial ecology. Limnol. Oceanogr. 34(8): 1694–1705.

Yentsch, C.S., Yentsch, C.M. (1979). Fluorescence spectral signatures: The characterization of phytoplankton populations by the use of excitation and emission spectra. J. Mar. Res. 37: 471–483.

Zapata, M., Jeffrey, S.W., Wright, S.W., Rodríguez, F., Garrido, J.L., Clementson, L. (2004). Photosynthetic pigments in 37 species (65 strains) of Haptophyta: Implications for oceanography and chemotaxonomy. Mar. Ecol. Prog. Ser. 270: 83–102.

Zehr, J.P., Waterbury, J.B., Turner, P.J., Montoya, J.P., Omoregie, E., Steward, G.F., Hansen, A., Karl, D.M. (2001). Unicellular cyanobacteria fix N_2 in the subtropical North Pacific Ocean. Nature 412: 635–638.

Zepp, R.G., Shank, G.C., Vähätalo, A., Bartels, E., Jones, R.P. (2008). Photobiogeochemistry of *Sargassum*: A potentially important source of chromophoric dissolved organic matter in the upper ocean. Ocean Science Meeting, 2-7 March 2008, Orlando, Florida, U.S.A.

Zhang, H. (2002). Detecting red tides on the west Florida Shelf by classification of SeaWiFs Satellite Imagery. M.Sc. Thesis, Department of Computer Science and Engineering, University of South Florida, 2002.

Zhang, X., Hu, L. (2009). Estimating scattering of pure water from density fluctuation of the refractive index. Opt. Express 17: 1671–1678.

Zhang, X., Hu, L., He, M-X. (2009). Scattering by pure seawater: Effect of salinity. Opt. Express 17: 5698–5710.

Zindler, C., Bracher, A., Marandino, C.A., Taylor, B., Torrecilla, E., Kock, A., Bange H.W. (2013). Sulphur compounds, methane and phytoplankton: interactions along a north-south transit in the western Pacific Ocean. Biogeosci. 10: 3297–3311.

Zubkov, M.V., Burkhill, P.H. (2006). Syringe pumped high speed flow cytometry of oceanic phytoplankton. Cytometry Part A 69A: 1010–1019.

Zwirglmaier, K., Heywood, J.L., Chamberlain, K., Woodward, E.M. S., Zubkov, M.V., Scanlan, D.J. (2007). Basin-scale distribution patterns of picocyanobacterial lineages in the Atlantic ocean. Environ. Microbiol. 9: 1278–1290.

Zwirglmaier, K., Jardillier, L., Ostrowski, M., Mazard, S., Garczarek, L., Vaulot, D., Not, F., Massana, R., Ulloa, O., Scanlan, D.J. (2008). Global phylogeography of marine *Synechococcus* and *Prochlorococcus* reveals a distinct partitioning of lineages among oceanic biomes. Environ. Microbiol. 10: 147–161

Acronyms and Abbreviations

AMT	Atlantic Meridional Transect
ANN	Artificial Neural Network
AVHRR	Advanced Very High Resolution Radiometer
BMAA	Beta Methyl Amino Alanine
$CaCO_3$	Calcium Carbonate
CCD	Charge-Coupled Device
CDOM	Coloured Dissolved Organic Matter
CO_2	Carbon Dioxide
CPR	Continuous Plankton Recorder
CTD	Conductivity, Temperature and Depth
CZCS	Coastal Zone Color Scanner
DMS	Dimethyl Sulphide
DMSP	Dimethyl Sulfoniopropionate
DOAS	Differential Optical Absorption Spectroscopy
EAP	Equivalent Algal Population
ENVISAT	Environmental Satellite (ESA)
EO	Earth Observation
ERBG	Enhanced RGB
ESA	European Space Agency
ETM	Enhanced Thematic Mapper
FAI	Floating Algae Index
FISH	Fluorescent In Situ Hybridization
FLH	Fluorescence Line Height
GEO-CAPE	GEOstationary Coastal and Air Pollution Events
GeP&CO	Geochemistry, Phytoplankton and Colour of the Ocean
GOCI	Geostationary Ocean Color Imager
GOM	Gulf of Mexico
HAB	Harmful Algal Bloom
HNLC	High-Nitrate, Low-Chlorophyll
HPLC	High Performance Liquid Chromatography
IOCCG	International Ocean-Colour Coordinating Group
IOP	Inherent Optical Properties
KBBI	*K. brevis* Bloom Index
L_{wN}	Normalised Water-leaving Radiance
LUT	Look-up Table

MCI	Maximum Chlorophyll Index
MERIS	Medium Resolution Imaging Spectrometer (ESA)
MODIS	Moderate Resolution Imaging Spectroradiometer (NASA)
NASA	National Aeronautics and Space Administration
NDVI	Normalized Difference Vegetation Index
NIR	Near-Infrared
NOAA	National Oceanic and Atmospheric Administration
NOBM	NASA Ocean Biogeochemical Model
NOMAD	NASA bio-Optical Marine Algorithm Data set
NPP	National Polar-orbiting Partnership
NPZ	Nitrogen-Phytoplankton-Zooplankton
OWT	Optical Water Type
PAR	Photosynthetically Available Radiation
PC	Phycocyanin
PEB	Phycoeryrthin
PFT	Phytoplankton Functional Type
PIC	Particulate Inorganic Carbon
PNN	Probabilistic Neural Network
PPC	Photoprotective Carotenoids
PSC	Photosynthetic Carotenoids
PSD	Particle Size Distribution
PUB	Phycourobilin
qPCR	Quantitative Polymerase Chain Reaction
RBD	Red Band Difference
RGB	Red, Green, Blue
SCIAMACHY	Scanning Imaging Absorption Spectrometer for Atmospheric Chartography
SeaBASS	SeaWiFS Bio-optical Archive and Storage System
SeaDAS	SeaWiFS Data Analysis System
SeaWiFS	Sea-viewing Wide Field-of-view Sensor
SI	Similarity Index
SLC	*Synechococcus*-Like Cyanobacteria
SNR	Signal-to-Noise Ratio
SOM	Self Organizing Maps
SST	Sea-Surface Temperature
TM	Thematic Mapper
UV	Ultra Violet
VIIRS	Visible Infrared Imaging Radiometer Suite
VIS	Visible
WFS	West Florida Shelf
WHO	World Health Organization